HIGH-GAIN AIRBORNE MICROPHONE

WINDSCREEN CHARACTERIZATION METHOD

USING MODIFIED RESEARCH WIND TUNNEL

By

JOSEPH ANDREW BANKS

Bachelor of Science in Mechanical and Aerospace

Engineering

Oklahoma State University

Stillwater, OK

2014

Submitted to the Faculty of the
Graduate College of the
Oklahoma State University
in partial fulfillment of
the requirements for
the Degree of
MASTER OF SCIENCE
May, 2017

HIGH GAIN AIRBORNE MICROPHONE

WINDSCREEN CHARACTERIZATION METHOD

USING MODIFIED RESEARCH WIND TUNNEL

Thesis Approved:

Dr. James Allan Kidd

Thesis Adviser

Dr. James Keith Good

Dr. Jamey Darin Jacob

ACKNOWLEDGEMENTS

I would like to thank Dr. R. Gaeta, Dr. J. Kidd and Dr. J. Callicoat for sharing their knowledge and experience with experimental acoustic and aerodynamic testing. I would also like to thank Mr. Christian Griffith for his assistance with fabrication and testing.

Name: JOSEPH ANDREW BANKS

Date of Degree: MAY, 2017

Title of Study: HIGH GAIN AIRBORNE MICROPHONE WINDSCREEN
            CHARACTERIZATION METHOD USING MODIFIED RESEARCH
            WIND TUNNEL

Major Field: MECHANICAL AND AEROSPACE ENGINEERING

Abstract: In recent years, UAS (unmanned aerial systems) have gained improved functionality by integrating advanced cameras, sensors, and hardware systems; however, UAS still lack effective means to detect and record audio signals. This is partially due to the physical scale of hardware and complexity of that hardware's integration into UAS. The current study is part of a larger research effort to integrate a high-gain parabolic microphone into a UAV (unmanned aerial vehicle) for use in acoustic surveying. Due to the aerodynamic interaction between a flush mounted parabolic antenna and the free-stream grazing flow, it is necessary to fair the antenna into the aircraft using a windscreen. The current study develops a characterization method by which various windscreen designs and configurations can be optimized. This method measures a candidate windscreen's normal incidence sound transmission loss (STL) as well as the increase of hydrodynamic noise generated by its installation at a range of flow speeds. A test apparatus was designed and installed on the Low Speed Wind Tunnel at Oklahoma State University. The test apparatus utilizes a "quiet box" attached to the wind tunnel test section floor. A pass-through window between the wind tunnel test section and the quiet box allows candidate wind screens to be mounted between the two environments. Microphones mounted both in the wind tunnel test section, and within the quiet box record the acoustic spectrum at various flow speeds, ranging between 36 and 81 feet per second. A tensioned Kevlar® wind screen validation specimen was fabricated to validate system performance. The STL spectrum is measured based on comparing the signal from microphones on either side of the Kevlar® membrane. The results for normal incidence STL for the flow off scenario are compared to results presented in other studies for the same material under tension. Flow-on transmission loss spectral data along with the increase in flow noise caused by the membrane is also measured at several flow speeds. The system has been shown to produce STL data consistent with the reference data for flow-on and flow-off test configurations, as well as being able to detect the increase in flow-induced noise generated by the validation specimen windscreen.

TABLE OF CONTENTS

Chapter   Page

LIST OF TABLES

LIST OF FIGURES

Figure   Page

CHAPTER I

INTRODUCTION

1.1. Background

Unmanned Aerial Vehicles (UAVs) have gained wide functionality in recent years as sensor, flight control hardware, and propulsion systems have becomes more miniaturized. This has resulted in rapid expansion of applications that can be performed from the air using these systems, airborne acoustic sensing being an exception to this trend. Acoustic sensing from an UAV requires advances to be made in more than one technological aspect. The airframe and propulsion noise generated by the aircraft must be minimized so that the target frequency range is not saturated by the background noise, a high-gain directional microphone system such as a parabolic antenna must be developed to maximize aircraft stand-off distance, and an effective windscreen provided to fair the microphone system installation into the fuselage to minimize flow-induced noise. This study develops an effective means by which candidate windscreens can be characterized for normal incidence sound transmission loss and grazing flow self-induced noise.

1.1.1. Project Motivation – Airborne Detection of Acoustic Sources

There are many applications for airborne acoustic sensors. A successful system could potentially be optimized to conduct search and rescue in hard to access environments, detect movement of troops, tanks, and other equipment on the battle field, conduct espionage missions, locate and detect wildfires, and many other possible applications which have yet to be considered. Counting the population of Greater Prairie-Chicken in a habitat is one example of a potential application for this technology, and an example followed throughout this study.

Land conservation is a highly regulated, important, and costly responsibility borne by land developers. This includes ecological protection for at-risk and endangered species. One such species commonly found in the great plains region of the United States is the Greater Prairie-Chicken (Tympanuchus Cupido Pinnatus), which the Partners in Flight (PIF) listed on their 2000 watch list of extremely high-priority species[1]. This species has been on the decline since the late 1800s, probably due to habitat loss. Lek (the location of avian mating rituals) surveys are accomplished to provide an index for avian populations within a region slated for development. The Traditional Lek Survey (TLS) is accomplished is accomplished by traversing a route, stopping on regular intervals, to listen for the "booming" calls created by male prairie-chickens during mating. The location of each lek is determined based on the location and direction of calls determined during the survey. Once the survey is complete, the birds are flushed and counted from each lek location. This procedure is repeated each day for as many days is required to flush and count each lek[1]. This is a time consuming and labor intensive process.

Figure 1. Male Greater Prairie-Chicken displaying on lek, Ft. Pierre National Grassland, SD, April 14, 2007[2].

The male Greater Prairie-Chicken creates a mating call known as "booming", which is a 3-syllable sound produced through the syrinx and amplified by the esophageal air sacs (brightly colored orange/yellow checks see in **Figure 1**). The primary booming frequency is between 280 and 310 Hz (as measured from audio recording provided by Cornell Laboratory of Ornithology) [2]. The low frequency nature of this call allows a greater detection range in air than that of a higher frequency call, thus making this species an ideal candidate to be detected from a UAV. Since UAV are already being developed and utilized for terrain mapping, there may be an opportunity to incorporate ecological impact surveys into the flights, thus further reducing development cost with this emerging technology.

A recent study[3] published by the American Ornithological Society confirmed the potential to count quantities of song birds from the air using a UAV. In this study, an off-the-shelf quad-rotor aircraft was equipped with a self-contained microphone and data recorder which was suspended eight meters below the aircraft using a thin cable. The aircraft was operated at a height of 28, 48,

and 68 meters above ground level. Standard bird counting methods were used on the area on the morning of the test so that the airborne detection method could be validated. It was determined that the number of bird detected from the air was reduced from that obtained using established standard count methods. A mean of 5.6 species per counting point detected by the UAV and a mean of 6.5 species per counting point detected with standard methods (when non-audible detections are omitted). The aircraft used in this study is not optimized for airborne detection or low noise emission which caused the call of certain species to be drowned out by aircraft noise. It was noted that avian behavior might be affected by the presence of the aircraft. This study indicates that airborne detection of birds is a possible, and might be a feasible method to reduce man-hours on the grounds.

1.1.2. Airborne Detection of Acoustic Signals

A challenge while recording natural acoustic signals is to maintain a sufficient stand-off distance between the observer and source such that the observer is undetectable by the source, but still able to resolve acoustic signals from the source. In the case of the Greater Prairie-Chicken, the presence of a loud UAV might frighten the birds and disrupt the production of mating calls or cause them to hide altogether. Research is ongoing at Oklahoma State University, and elsewhere, to reduce the amplitude and shift the frequency of noise generated by special purpose UAV platforms. The successes achieved in these studies will greatly affect the system performance of the system proposed herein.

An acoustic source's observed intensity level is a function of the distance from the source and the observer. For a monopole source (a spherical fluctuating pressure wave), the intensity, I, of the signal measured by the observer is a function of the inverse of the square of distance, r, between the source and observer, as seen in **Equation** (1)[4].

$$I = \frac{W}{4\pi r^2} \tag{1}$$

Where:
I = Intensity measured by the observer (W/m^2)
W = Acoustic power of the Source (W)
r = Distance from the source to the observer (m)

Sound propagation in a continuum such as air attenuates proportionally with frequency, i.e. a lower frequency source will attenuate less than a higher frequency source (reference **Equation** (2), (3), and **Figure 2**)[4]. **Figure 2** shows the attenuation in fully quiescent and isothermal standard air at various stand-off distances of an idealized broad band monopole source at an amplitude of 65 dB.

$$I_x = I(0)e^{-2\alpha x} \tag{2}$$

Where:
I_x = Acoustic intensity at distance x
$I(0)$ = Acoustic intensity at x = 0
α = Absorption Coefficient (nepers/m)

$$\alpha_c = \frac{\omega^2}{2\rho_0 c^3}\left[\frac{4}{3}\eta + (\gamma - 1)\frac{k}{c_p}\right] \tag{3}$$

Where:
ω = Frequency of the sound wave
ρ_0 = Density of the gas
c = Speed of sound in the gas
η = Shear viscosity coefficient
γ = Ratio of specific heats
c_p = Heat capacity of the gas at constant pressure
k = Thermal conductivity of the gas
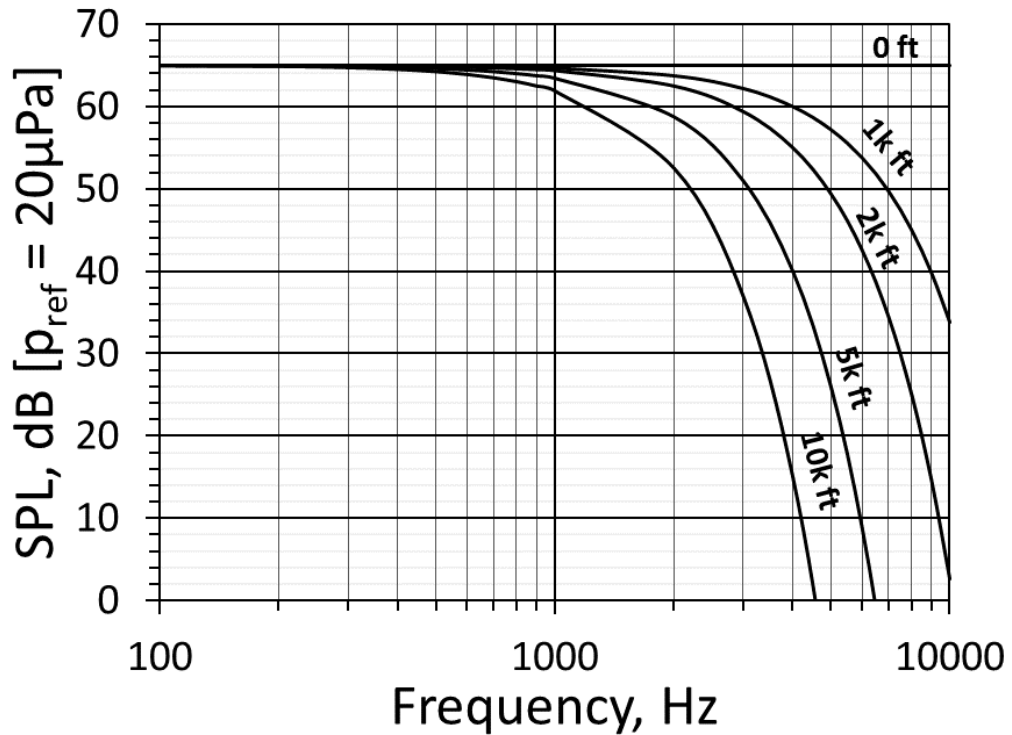
Figure 2. Sound attenuation spectrum for an idealized 65 dB broad band monopole source in fully quiescent isothermal standard atmosphere free from background noise at various stand-off distances calculated using **Equation (**3^4

This model suggests that if an aircraft's noise can be shifted up in frequency, the source intensity will drop off more rapidly than that of a lower frequency at the same amplitude. This also means target sources of higher frequencies will require detection from a shorter standoff distance, thus risking detection by the source. Sources such as the Greater Prairie-Chicken's "booming" call, having a frequency of 280-310 Hz, will propagate well through air. **Equation** (3) assumes a monopole source propagating through a fully quiescent and isothermal gaseous continuum.

Antenna gain is another factor that can affect required stand-off distance between a target source and the UAV. Parabolic antennae and phased array antennae offer good capability to collect sound energy from a broad area and focus it to a smaller area, in an effect similar to a magnifying glass. Phased array microphone antennas were not considered at this stage in the project due to the

number of microphones required, complexity of data processing, and cost of equipment. Acoustic parabolic antennas were chosen for this project because they function using a single microphone, and are relatively light weight, low cost, and simple to manufacture. The gain requirement for this project will be determined once further evaluation of the noise spectrum generated by the selected aircraft, as well as acoustic target detection thresholds are established.

Integration of a parabolic microphone antenna into a UAV is a challenge due to its relatively large size (12 to 24-inches in diameter, depending on lower frequency limit). If the system is to be used simultaneously with other sensors such as for photographic surveys, it makes sense to mount the antenna such that its primary reception lobe is pointed downward during steady level flight, and is therefore positioned with its opening parallel to the flow. This configuration requires an opening in the aircraft fuselage. If the opening is not screened, then separated flow is inevitable. Flow separation causes vortex shedding resulting in wide ranging eddy sizes within the flow (Reference **Figure 3**). Turbulent noise frequency is directly proportional to eddy size; therefore, it is useful to minimize the amount of large and medium size eddies present to minimize the ambient noise at the target frequency range. Reference **Figure 4** for conceptual schematic of the proposed acoustic sensing UAV.
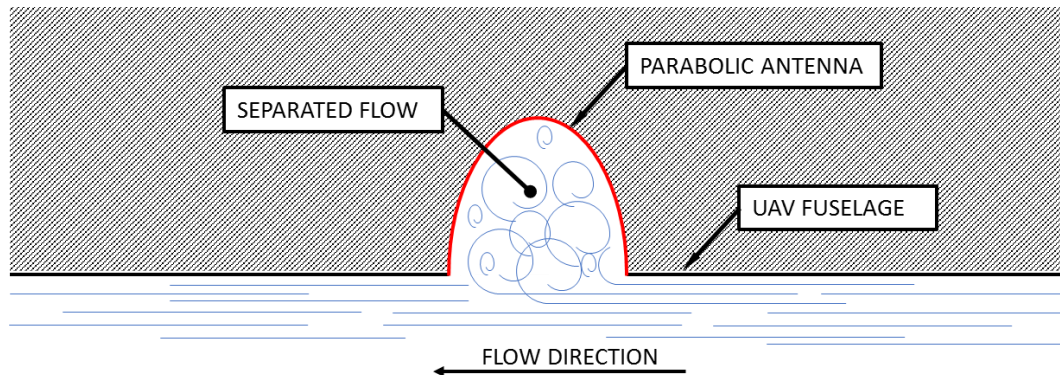
Figure 3. UAV cross-section showing flow separation resulting from a non-fared parabolic antenna installed flush into the outer fuselage surface
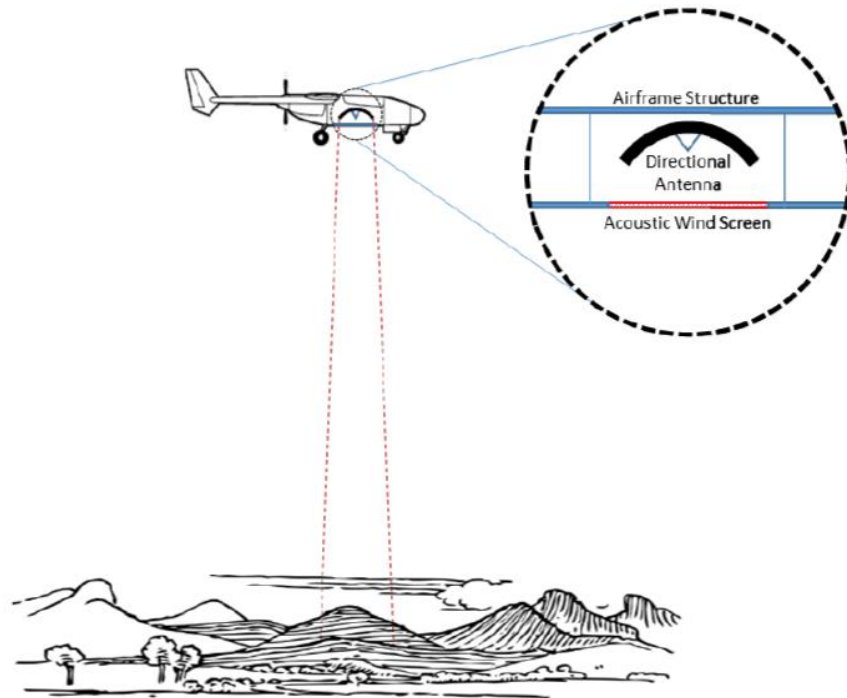
Figure 4. Conceptual high gain airborne acoustic system

Closed section aero-acoustic wind tunnels have been designed to address the flow separation problem using windscreens to maintain flow boundary layers. Previous research has shown light weight plain weave dry (i.e. non-epoxy impregnated) Kevlar® cloth held under bi-directional tension to be an effective means to control self-induced hydrodynamic noise with minimum attenuation across the membrane[5,6]. This approach shows promise for UAV applications; however, maintaining the windscreen tension, as done in the comparison studies, presents difficulty in small UAVs due to perimeter framing required to maintain high membrane tension. Ideally, the optimized windscreen will be sufficiently self-rigid without external tensioning, and possibly capable of carrying flight loads to avoid the need for added structural weight to redirect loads around the fuselage/antenna cutout.

CHAPTER II

REVIEW OF LITERATURE

2.1 Counting of Birds in an Environment

While remote sensing of the Greater Prairie-Chicken is only one of many examples for which airborne acoustic sensing may be used. Methods to improve the counting process of the Greater Prairie-Chicken were researched to provide insight on what challenges may face an acoustic sensing system on a UAV. Many methods exist by which to count the number and species of birds in an environment. Currently, most methods require personnel physically walking or driving transects to detect birds, or tagging and counting specific birds manually. This is a time consuming and labor intensive process which adds significant cost to development and conservation projects.

Table 1. Summary of selected studies on avian counting methods

Year	Author	Title and Reference Number	Publication	Significance of Study
2006	A. Clifton	Estimating Numbers of Greater Prairie-Chickens Using Mark-Resight Techniquies[1]	Journal of Wildlife Management 70(2): 479-484; 2006	Discusses reasons necessity to conserve habitat and current in-use methods to monitor populations
2017	A. Wilson	The Feasibility of Counting Songbirds Using Unmanned Aerial Vehicles[3]	American Ornithological Society AUK-16-216.1	Determines the effectiveness airborne detection of song birds compared to standard methods

According the Clifton, et. al.[1], the most common bird count method used to assess the GPC (Greater Prairie-Chicken) population size in a region is the TLS (Traditional Lek Survey). This TLS is conducted by manually listening for the "booming call" of GPC at 1.6 km intervals along a 16 km track. Once the track has been completed, the track is retraced, and the birds are flushed and counted manually counted by sight.

The uncertainty of the count is considered to estimate the total number of birds in the region. An improved method to estimate GPC populations is proposed in this study; however, it still requires manually catching, tagging (or marking), and eventually counting animals as they are re-sighted. While found to be more accurate than the TLS, this method is expected to be even more costly and labor intensive than the TLS method. An alternate method is desired.

With the commercialization of small affordable UAVs, many companies are looking for new and creative ways to utilize their capabilities. In the study conducted by Wilson, et. al.[3], the possibility of utilizing such technology to conduct avian counting from the air is proposed. In this study, a quad-rotor UAV is equipped with an acoustic sensing and recording equipment package which is dangled from the aircraft by a thin line. Various species of song birds were counted and the results compared to the standard counting methods. The detection technique employed by this study was based on the standard methods typically used where a recording was made a several points throughout an environment for 3 minutes at a time. The experiment was repeated at altitudes of 28, 48, and 68 meters to determine the impact of the count. It was determined that the UAV counting method resulted in a mean detection of 5.6 species per detection point compared to 6.5 species per detection point, as measured using standard manual methods (with non-audible detections omitted). It noted that the calls of certain bird species bird species are of a frequency which is completely dominated by aircraft self-induced noise. Also noted in this study is the possible impact the presence of recording UAV might have on avian behavior.

It is obvious from the results of this study that further work needs to be accomplished to reduce and/or optimize the frequency of the noise signature created by the observing UAV as

well as minimizing any effects the presence of the UAV may have on the detection methods. Increasing the stand-off distance from which a source can be detected will benefit the latter concern. Designing an airframe for low noise, with a self-induced noise signature sufficiently different from the frequency of the acoustic target source will serve both concerns. Additionally, it is necessary to improve the detection range of the system by increasing acoustic signal gain. This requires integration of a high-gain acoustic antenna which, as discussed in the introduction, will require fairing from a windscreen optimized for the specific application. The two acoustic parameters identified as critical for windscreen optimization are self-induced flow noise and normal incidence sound transmission loss.

2.2 Flow Noise Reduction Methods

Multiple methods were researched to determine the best approach to reduce the amount of self-induced flow noise detected by microphones in a flow, such as flush mounting a single microphone to a surface. Long range detection of acoustic sources requires signal amplification. A high gain antenna can be used to improve the detection range of a source. Parabolic antenna and microphone arrays are the preferred methods to improve signal gain; however, both methods have a large area which require aerodynamic fairings to prevent the signal from being dominated by self-induced hydrodynamic flow noise. Previously accomplished research has developed means by which large surface area microphone components can effectively be screened from a flow within a wind tunnel. These studies are listed in Error! Not a valid bookmark self-reference..

Table 2. Summary of design studies for acoustic wind tunnel windscreens

Year	Author	Title and Reference Number	Publication	Significance of Study
2000	S. Jaeger	Effect of Surface Treatment on Array Microphone Self-Noise.[5]	American Institute of Aeronautics and Astronautics, Inc. AIAA-2000-1937	Demonstrated the effectiveness of tensioned Kevlar® panels and provides transmission loss test data
2005	H.E. Carmargo	Evaluation and Calibration of a Prototype Acoustic Test Section for the Virginia Tech Stability Wind Tunnel[6]	Virginia Tech Internal Report VPI-AOE-294	Modification of closed section acoustic wind tunnel using Tensioned Kevlar® Panels and provides transmission loss and insertion noise test data

In 2000, Jaeger, et. al.[5] investigated the retrofit of the NASA Ames Research Center wind tunnel for use as an aero-acoustic facility. Modifications included a 70-element microphone array recessed into one of the test section walls. Several materials were tested, and a light weight plain weave Kevlar®, held under tension, was determined to show the best durability and acoustic properties. This study also proposed a semi-novel method to measure acoustic insertion loss by which an acoustic source is mounted in the wind tunnel test section and sound pressure measurements are taken on both sides of the windscreen membrane. The difference in intensity between the two environments is used to quantify the insertion loss. The tensioned Kevlar® membrane was reported to have an insertion loss of up to 2 dB across a frequency range of 50 Hz to 25k Hz.

In 2005, Carmargo, et. al.[6] published a report outlining the conversion of the stability wind tunnel at Virginia Polytechnic Institute at Blacksburg, VA to an aero-acoustics wind tunnel in a similar manner to the wind tunnel at NASA Ames Research Center. For this retrofit, two full-scale anechoic chambers were installed on opposite sides of the wind tunnel test section and are used to house acoustic measurement equipment such as microphone arrays. Tensioned Kevlar® windscreens replaced the original test section walls, and additional acoustic treatment was added

to the wind tunnel sections upstream and downstream of the test section. Special attention was paid to reducing the background noise and flow turbulence to improve the quality of acoustic measurement obtained by the modified wind tunnel. Carmargo, et. al.[6] validated the results obtained by Jaeger, et. al.[5] and reported on a method to measure the amount of flow induced noise caused by installation of the windscreens and other acoustic treatments. In this method, the overall sound pressure level (OASPL) generated by the flow noise is measured using a microphone equipped with a bullet nose cone. The OASPL is computed at multiple flow speeds, and for difference membrane configurations. The OASPL at each flow speed is plotted for each configuration, and the trend lines are compared (reference **Section 3.4.5** for more information on this test method).

Jaeger, et. al.[5] and Carmargo, et. al.[6] both concluded that tensioned light weight Kevlar® provides good STL and self-induced noise reduction; however, the tension required to prevent significant flow induced membrane deflection is prohibitive for light weight installation into UAV structures. Therefore, an alternate windscreen design is desirable, and it is necessary to be able to compare key characteristics of the novel windscreen designs. Methods to measure the key acoustic parameters were researched and are presented in the subsequent sections. The windscreen testing and evaluation procedures described in Jaeger, et. al.[5] and Carmargo, et. al.[6] were conducted in large and idealized facilities for acoustic testing. These facilities are cost prohibitive and out of reach for most research facilities. It is desirable to accomplish parabolic microphone windscreen characterization using a facility designed specifically for testing all acoustic parameters using a single full-scale sample with little-to-no configuration changes required.

2.3 Sound Transmission Loss Measurement Techniques

Of primary concern to screening a microphone is the amount of signal attenuated and reflected by the windscreen before it reaches the sensor. This is known as STL (sound transmission loss). Many standard measurement techniques exist to measure STL. The techniques addressed by the present work are listed in **Table 3**.

Table 3. Summary of standards and studies on the measurement of sound transmission loss

Year	Author	Title and Reference Number	Publication	Significance of Study
2009		ASTM E2611-09 Standard test Method for Measurement of Normal Incidence Sound Transmission of Acoustical Materials Based on the Transfer Matrix Method[7]	ASTM International	Impedance Tube governing standard
2010		SAE J1400: Laboratory Measurement of the Airborne Sound Barrier Performance of Flat Materials and Assemblies[8]	SAE Recommended Practice	Description of Two Room Method for Acoustic Transmission Loss Testing
2009	K.C. Vengala	Building a Modified Impedance Tube for Measurement of Sound Transmission Loss and Absorption Coefficients of Polymer Cross-Linked Aerogel Core Composites[9]	Master's Thesis, Oklahoma State University	Creation of Impedance Tube and math/physics behind it.
2016	J. Callicoat	Composite Materials Providing Improved Acoustic Transmission Loss for UAVs[10]	Doctoral Dissertation, Oklahoma State University	Development of Impedance Tube and Other OSU Resources

The American Society for Testing and Materials International (ASTM International) developed Standard E2611[7] which addresses the transfer matrix method for quantifying a material's tendency to reflect, absorb, or transmit an acoustic wave. This standard defines a test apparatus and procedure utilizing 4 microphones (2 mounted on each side of the test sample) mounted within a heavy walled tube. Acoustic plane waves are generated by a speaker at one end of the tube, and impinge on the test specimen. Two back walls are described, a solid backwall providing a reflected wave, and an anechoic backwall to be used on samples with symmetric acoustic properties for both faces. Reflected waves are detected by the microphone pair by monitoring the wave phase angle. This method provides a relatively simple bench-top method by which small material samples can be characterized.

In 2009, Vengala[9] developed and construction the 4-microphone impedance tube apparatus at Oklahoma State University. The MATLAB code developed by this study became the basis for the code used to operate the impedance tube for tested accomplished in the present work.

The impedance tube was determined to be a viable option to establish preliminary STL measurements for unstiffened scale samples of candidate windscreen components; however, the lack of ability to test at full-scale and with flow on prevents it from being viable option to compare STL between candidate windscreens. The Two-Room Method is an alternate to the impedance tube method allows full scale STL measurements and is presented in SAE J1400[8].

The International Society of Automotive Engineers (SAE International) published standard J1400[8] (originally published in 1982, most recently revised in 2010) which provides direction for testing full scale material samples using two adjoining chambers. A reverberant chamber containing an acoustic source and source room microphone(s) is connected by a pass-through window to an anechoic chamber which contains the receiving room microphone(s). The specimen under test is mounted in the pass-through window. A source signal is produced in the reverberant source room such that semi-omni-directional sound waves impinge on the specimen. The averaged signal from the reverberant source room is compared to the averaged signal from the receiving room. The difference between these two signals is corrected using a correction factor unique to each facility. The correction factor is obtained by measuring the STL a sample of known transmission loss such as PVC, vinyl, another limp mass material, or the suggested fiber material. The measured sample STL is compared to the previously established sample properties. The correction factor is the offset requirement to force each measured frequency bin match that of the established data. This correction factor is applied to every sample measured using the facility, and should be recalculated periodically, or any time major changes are made to the facility.

In 2016, J. Callicoat[10] published a study which developed and calibrated a two-room method facility at Oklahoma State University. This study also made use of the impedance tube, and developed the formalized impedance tube transfer matrix method MATLAB code that was used

for testing presented in the present work. The methods to measure transmission loss of a sample presented by Callicoat[10] are the basis for the apparatus developed herein.

The Two-Room Method is viable for STL characterization of full-scale parabolic microphone candidate windscreens; however, it provides no ability to measure STL with flow-on, nor does it provide any measurement of self-induced flow noise. It is desirable to develop a test apparatus which can compare all stated key acoustic parameters between candidate windscreen designs. This method will be similar to SAE J1400[8] in that an approximately anechoic environment will be attached to an approximately reverberant environment. The test sample will be placed in between, and STL measurements will be made on either side. The test section of the wind tunnel serve as the approximately reverberant environment, which will provide a means to measure STL with flow on and self-induced noise generation.

2.4 Design of Anechoic Environments

As discussed in SAE J1400[8], measurement of sound transmission loss of a material requires an anechoic environment to ensure all sound pressure recorded outside the source environment has passed through the sample material only. Anechoic chamber design is thoroughly understood and many textbooks and specifications have been written on the subject. Design of the anechoic environment required for the test apparatus utilized in the present study is based on these well-established theories and principles; however, due to the unusually small size of the anechoic environment, special accommodations had to be made to ensure the internal dimensions do not cause a buildup of standing waves at any location.

Table 4. Summary of standards and studies on design of anechoic environments

Year	Author	Title	Publication	Significance of Study
2012		ISO 3745: 2012: Acoustics - Determination of sound power levels and sound energy levels of noise sources using sound pressure - Precision methods for anechoic rooms and hemi-anechoic rooms[11]	BSI Standards Publications	Provides guidelines and requirements for anechoic chambers
2011	J. G. Rodrigues	Design and Implementation of Aspects of a Small Anechoic Room and Sound-Actuation System[12]	Thesis, Public University of Navarra Spain	Provides guidance for design of small anechoic environments.

The International Organization for Standards (ISO) developed ISO 3745[11] which provides many of the criteria for anechoic environments such as background noise limits, microphone placement, and theoretical information on sound measurement.

In 2011, J. Rodrigues[12] published research into the challenges with creating a small scale anechoic environment. These challenges include interaction with standing wave frequencies and inability to install sufficiently sized foam wedges. Rodrigues was a primary source for the design of the quiet box anechoic environment developed herein.

2.5 Gaps in Current Research

The measurement of STL has been standardized, and its processes are operational in industry. Experimental methods have also been developed to measure self-induced flow noise generated by the installation of a windscreen. Currently, no research has been conducted to combine STL and flow-induced noise generation measurement for parabolic microphone windscreens into a single test method. The current study develops this method with the focus on acoustic sensing UAV windscreens.

CHAPTER III

METHODOLOGY

3.1 Problem Statement

As established in the previous sections, creating a smooth surface to minimize boundary layer turbulence over the fuselage opening is required for proper integration of a parabolic microphone antenna; however, any membrane or barrier installed between the source and receiver will cause signal attenuation, as well as installation challenges. The focus of this study is the development of an apparatus and technique by which various windscreen materials and design configurations can be tested and characterized for key parameters. Sound Transmission Loss (STL), and overall self-induced hydrodynamic noise increase as a function of grazing flow speed have been chosen as the key controlling parameters. STL is defined as the reduction in Sound Pressure Level (SPL) across a membrane, or SPL on the source side of a membrane minus SPL on the receiver side of a membrane. The self-induced hydrodynamic noise increase is quantified by comparing the Overall Sound Pressure Level (OASPL) recorded near the windscreen turbulent boundary layer at a series of flow speeds.

3.1.1   Goal and Objectives

Aerial detection of the ground acoustic sources (the Greater Prairie-Chicken, for example) is the primary motivation of the overall research initiative to integrate high-gain acoustic sensing into UAV. There are many applications for this technology, all with unique target frequency ranges, aircraft speed requirements, and other requirements. Many methods exist by which the flow off sound transmission loss of a material sample can be measured.

Methods have also been developed which can determine the self-induced flow noise of a sample. All such methods require the use of high cost acoustic research facilities and equipment. No research has been conducted to combine these test methods into one simple apparatus and using common facilities and systems. The current research effort described herein is focused on the following goals:

- Modify the existing wind tunnel facility at Oklahoma State University to add capabilities to compare candidate windscreens.

- Allow for simultaneous characterization of STL and self-induced flow noise on full-scale candidate parabolic microphone windscreens using a single test apparatus.

3.2 Previously Developed Flow-Noise Reduction Techniques

Previous research conducted in the field of aero-acoustics wind tunnel development has led to many developments applicable the present study. Traditional aero-acoustic wind tunnel are open test section designs which utilizes a free jet and a collector located within an anechoic chamber. The microphone(s) are placed in the static air region of the anechoic chamber, outside the jet shear layer, to mitigate the problem of hydrodynamic noise generated by turbulence formed by the microphone itself. Reflection and refraction of sound waves will occur across the jet shear layer and must be corrected in accordance with Snell's law, as in the field of optics[13]
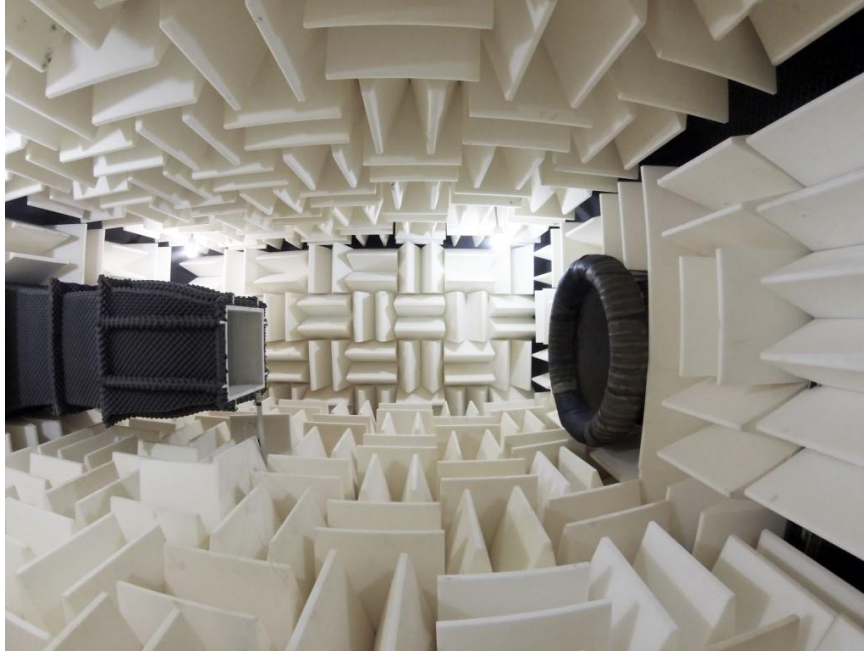
Figure 5. Open-section acoustic wind tunnel configuration showing the free jet plenum (left) and the collector (right), all housed within an anechoic environment from which acoustic measurements are made.[14]
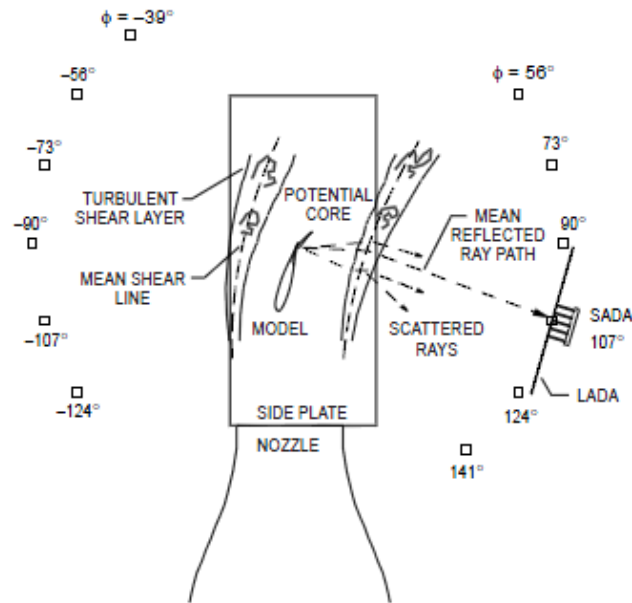
Figure 6. Shear layer noise ray paths distortion for boundary layer corrections required for effective operation of open section aero-acoustic wind tunnels[13]

This form of wind tunnel serves little use for UAV integrated applications as there exists no location to mount a microphone outside of the freestream airflow. An alternative method for acoustic wind tunnel design is the closed acoustic wind tunnel design. The test section of a closed acoustic wind tunnel is ideally constructed from an acoustically transparent, aerodynamically opaque material. Acoustic sensing equipment is located in an anechoic environment outside the flow field. The Virginia Tech Stability Wind Tunnel is a large-scale example of such a design. The test section of a previously constructed aerodynamic wind tunnel was retro-fitted to a tensioned Kevlar construction and acoustic absorbers were added to a length of the tunnel forward and aft of the tunnel test section. Phased array microphones are placed at a specified separation distance from the Kevlar windows in the anechoic chamber region outside the test section[6].
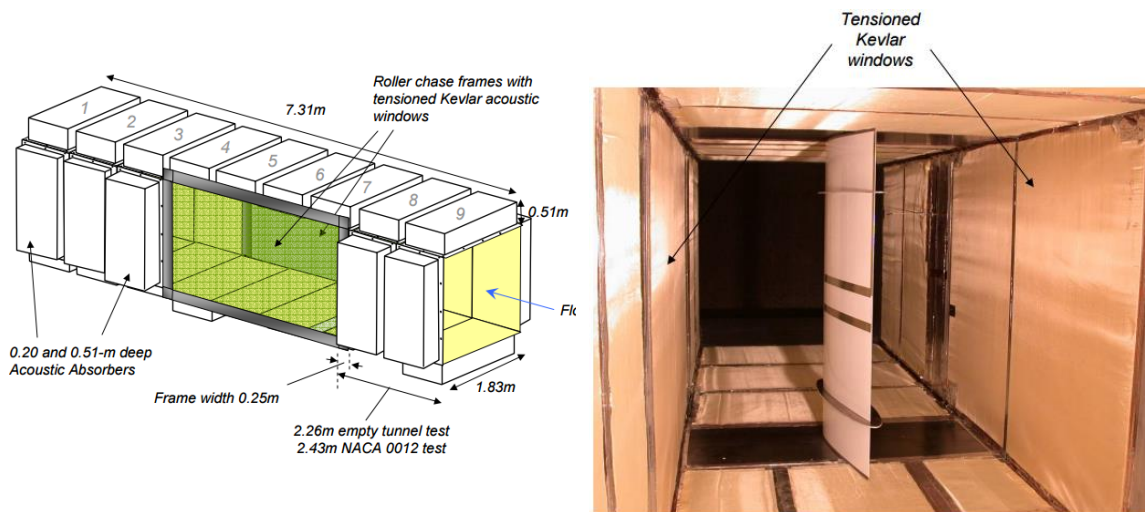
Figure 7. Schematic showing arrangement of acoustic absorbers and Kevlar® acoustic windows in Virginia Tech Stability Wind Tunnel[6]

Extensive modifications were required for the conversion from traditional aerodynamic to aero-acoustic wind tunnel which include significant acoustic treatment to regions up and down-stream of the test section, to reduce the overall background noise of the tunnel. These modifications include acoustic absorption panels and improved boundary layer control. Controlling the ambient

noise is less important for the current work of characterizing windscreens, provided that noise is consistent, and the tones used to determine STL of a candidate windscreen can be generated at an amplitude sufficiently above the background.

3.3 Impedance Tube Testing

Preliminary STL transmission loss testing was accomplished for light weight Kevlar woven fabrics, similar to those used in close section acoustic wind tunnels. This is accomplished with the use of an acoustic Impedance Tube configured to conduct transmission loss measurements for this specimen. The impedance tube's only application to this study is for measuring no grazing flow sound transmission loss. Furthermore, the limited size of samples which can be mounted in the impedance tube available for this testing will result in errors caused by critical frequency affects (natural vibrational frequencies of the membrane) for any stiff specimen. Impedance tube testing serves only as a means to generate preliminary STL data for a material prior to investing in a full-scale test specimen

3.3.1   Impedance Tube Apparatus

An impedance tube consists of a circular or rectangular straight tube constructed from a sufficiently massive material so sound transmission through the tube wall is negligible compared to the sample. A sound generating source is connected to one end and a test specimen mounted in the tube. For transmission loss measurements, as were conducted in this preliminary experiment, two microphones are mounted on each side of the test specimen (four microphones total) so that the diaphragms are flush with the inside surface of the tube. Plane waves are generated in the tube via the source driver, generating broadband white noise. The resulting wave pattern is decomposed into transmitted, reflected, and absorbed components from signal acquired by each microphone and examining their relative amplitude and phase angle[7].
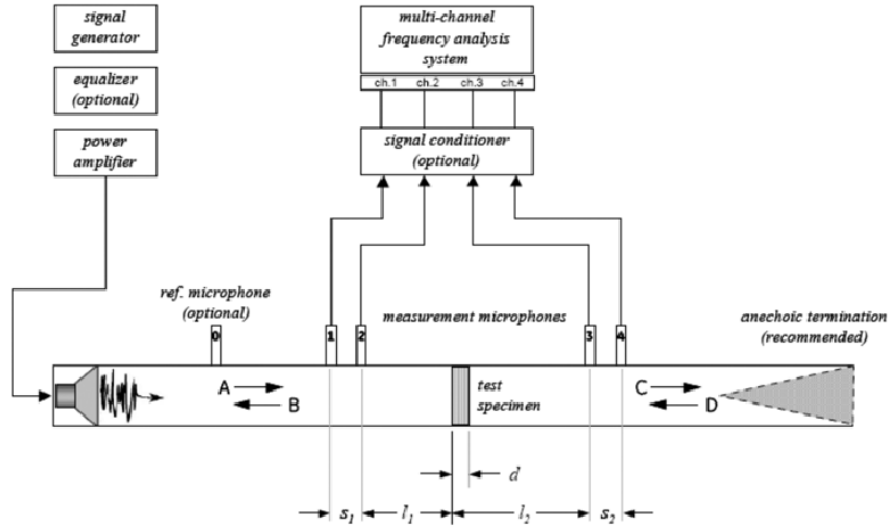
Figure 8. ASTM E2611-09 impedance tube, configured to acquire transmission loss coefficient for a sample, as utilized in the preliminary experiment[7]

The impedance tube at Oklahoma State University has multiple configurations allowing for transmission and reflection testing to be accomplished. For this study, only transmission testing was accomplished. The impedance tube was constructed to ASTM E2611-09 standards for the 4-microphone method and has a square internal cross section measuring 2.50 by 2.50 inches. The apparatus consists of two equal volume rectangular tubes which hold the test sample in between. The Impedance Tube used in this study is limited to measurements ranging from 80 to 2500 Hz. The upper boundary of the measurement range is determined by **Equation** (4)**.**

$$f_u < \frac{K\,c}{d} \tag{4}$$

The lower frequency limit of the Impedance Tube is limited by the spacing of the microphones and the accuracy of the analysis system. The microphone spacing is greater than 1% of the wave length of the lower frequency limit[7]. According to Callicoat[10], the impedance tube apparatus at Oklahoma State University has a measurement uncertainty of ±3 dB, as established by testing. It was noted that only 4 sample data sets were compared to determine this uncertainty

interval; therefore, it is likely that uncertainty interval is actually less than the stated ±3 dB, but additional testing is required for further refinement.

3.3.2 Impedance Tube Sample Fabrication

A 5.0 oz. plain weave Kevlar® was selected for the test specimen since comparison results for this weight were presented in Jaeger, et. al.[5]. This study indicated that Kevlar® was found to have superior durability when exposed to air flow compared to the other materials tested. Wire mesh was observed to fail rapidly in fatigue, and fiberglass was observed to fail in shear due to turbulence in the boundary layer. For the impedance tube testing conducted herein, three test specimens were fabricated to gain insight about the effects of epoxy impregnation weight on STL. One sample was left dry, one was lightly impregnated, and one was heavily impregnated. The minimum amount of epoxy to wet the sample was used for the lightly impregnated sample, and the epoxy was added until the cloth was saturated, then the excess was removed for the heavily impregnated sample (impregnation levels were not quantitatively measure). Material specifications and cure cycle information are presented below:

Table 5. Impedance tube test specimen fabrication material and processing information

Fabric	Resin	Hardener	Cure Method	Cure Time
Kevlar, 5.0 oz. Plain Weave, 17 x 17 Thread Count, 0.010 Inch thick	Resin Services Inc. WB-400	Resin Services Inc. SC-150-NB	Room Temp Vacuum Bag 23 in-Hg	12 hours
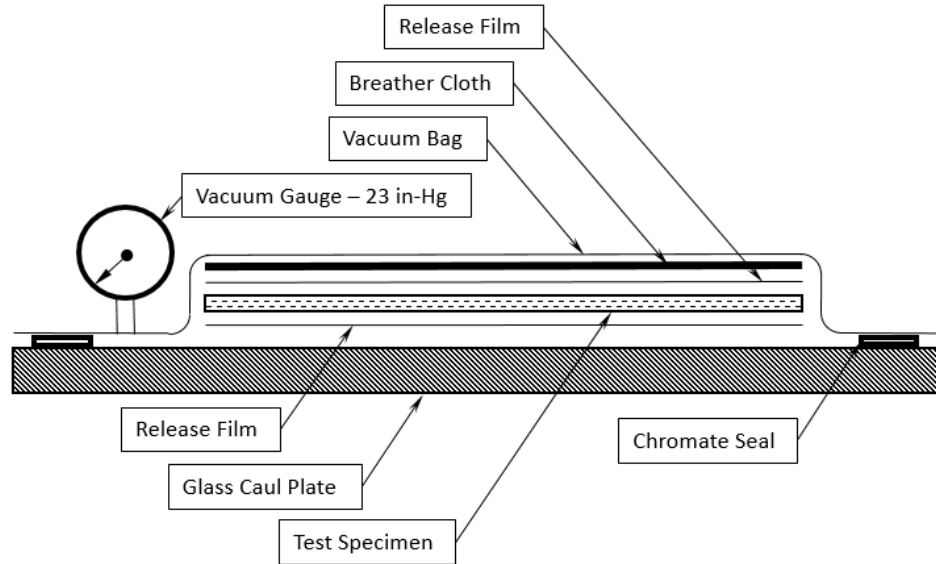
Figure 9. Impedance tube test specimen fabrication vacuum bag configuration diagram

3.3.3 Specimen Fixture and Signal Generation for Impedance Tube

Holding the test specimen securely in the impedance tube is critical to the fidelity of transmission loss testing. If a consistent level tension cannot be maintained between tests, or a non-negligible amount of acoustic energy escapes the impedance tube, test results will be erroneous. A specimen holder was designed and fabricated for use in this experiment. The specimen holder was printed from Acrylonitrile Butadiene Styrene (ABS) plastic on an Airwolf single head 3D printer. The specimen holder was designed to apply a slight, but consistent tension to the membrane. This is accomplished by stretching the membrane tightly over the aft surface of the outer ring, then forcing the inner ring in place. This causes a small amount of strain in the membrane is forced into against the fixture. Petroleum jelly was used on the interface between specimen holder assembly and the impedance tube to ensure an air tight seal. Reference **Figure 10** for CAD three-view (top), manufacturing photo on 3D printer (left), and test installed in fixture on impedance tube (right). Note that the bluish green tint present on the Kevlar® test specimen is a result of epoxy impregnation.

24
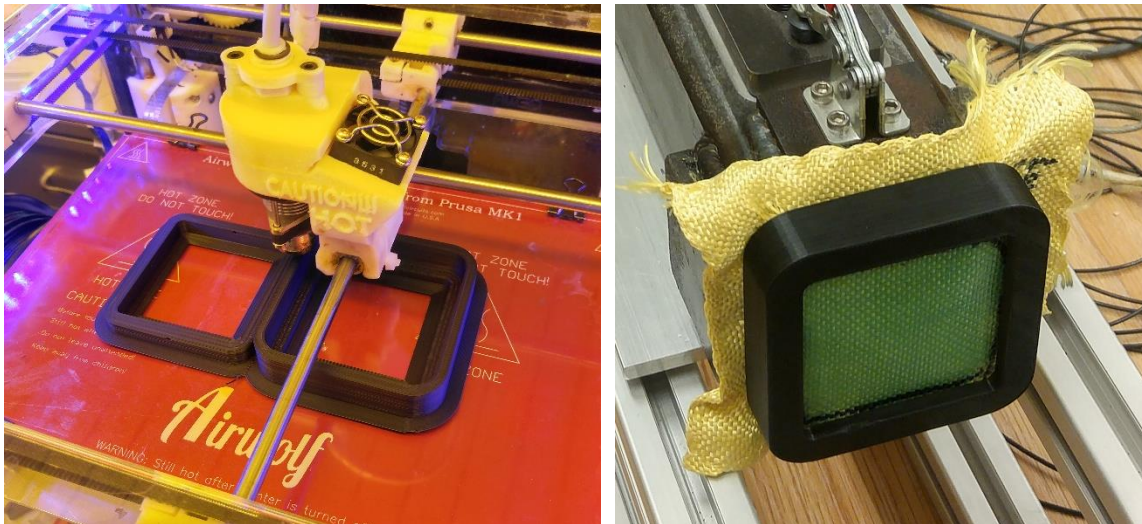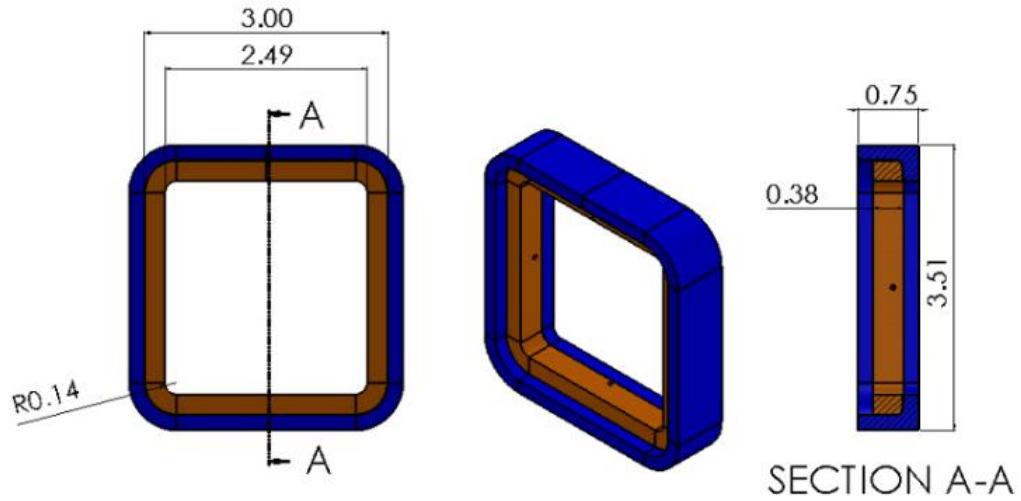
Figure 10. Mounting fixture for use with Kevlar® impedance tube test specimen (all dimensions shown are in inches)

A signal generator was set to 250 mV in white noise mode. This signal was fed into an amplifier then into a Kicker 4 Ohm coaxial speaker (Model 41KSC44) installed in an enclosure attached to the transmission end of the impedance tube. Data were collected over a period of 60 seconds for each run. Three consecutive and identical tests were accomplished for each specimen. Additional tests were conducted using the specimen fixture, but without a specimen installed, and also with the two halves of the impedance tube joined together with no specimen or fixture. This was done to assess the effect of installing the specimen fixture. The change in transmission loss for

the no specimen, no fixture configuration and the fixture only configuration was determined by averaging the transmission loss spectral data for all three data sets for each configuration, then subtracting the no fixture configuration data from the fixture only configuration data. Reference **Figure 11** for plotted data.

(a)

(b)
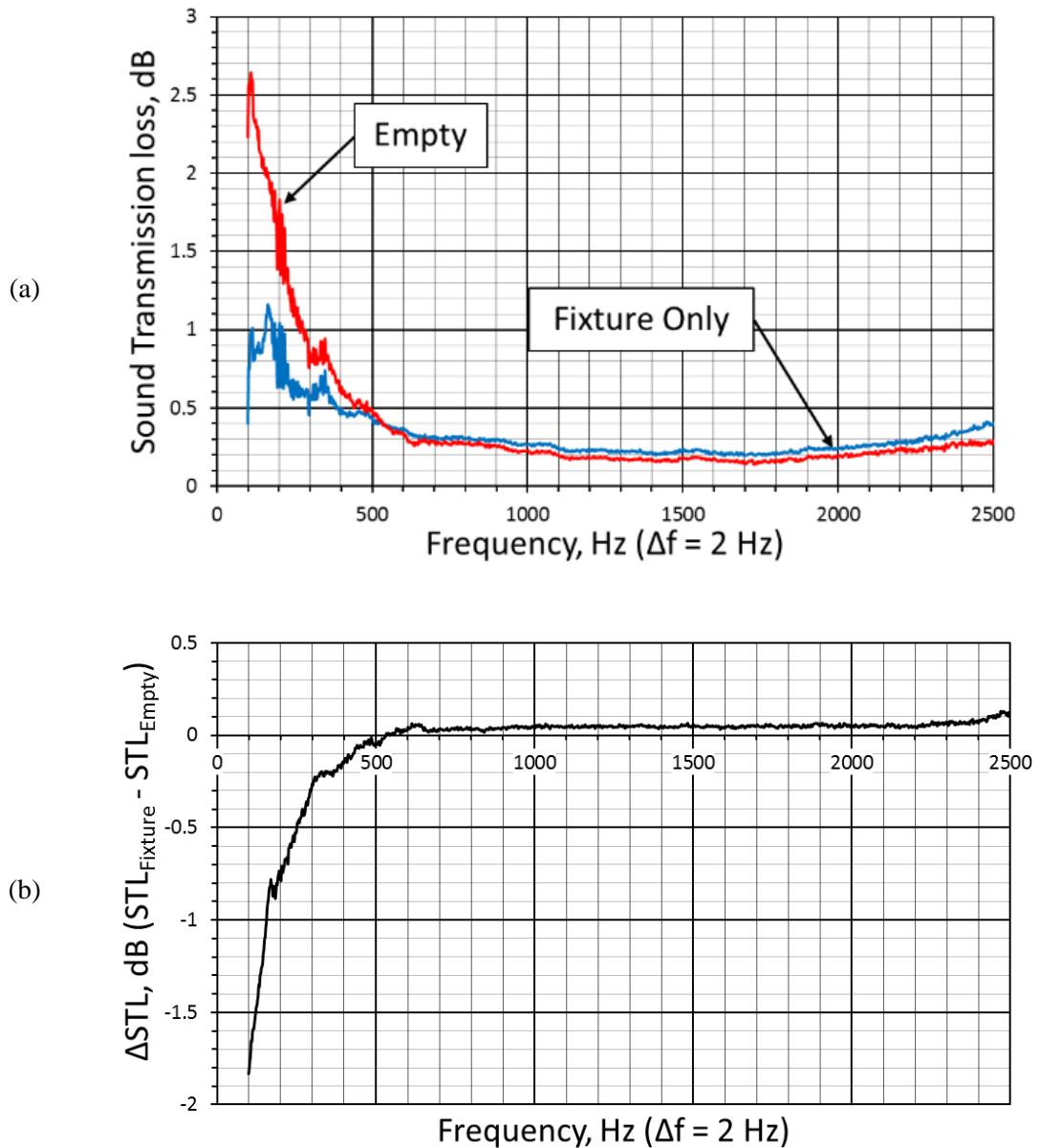
Figure 11. Impedance tube testing error induced by addition 3D printed ABS specimen fixture. (a) – Measured sound transmission loss for fixture only and empty tube. (b) – Transmission loss difference between both configurations ($STL_{Fixture\ Only} - STL_{Empty\ Tube}$)

The maximum variation between the configurations over the impedance tube operating spectrum is 1.9 dB; however, the majority of the spectrum has a difference of less than 0.05 dB. This indicates only a small amount of error is introduced into the system as a result of fixture installation. Note that the variation for microphone spacing due to removal of the specimen fixture was factored into data analysis for each method, as is required for proper use of the transfer matrix method used in this analysis. It should be noted that the data below 500 Hz contains more error. The cause of this variation is not fully investigated herein, as impedance tube testing is not the primary means for windscreen characterization. However, it should be noted that that theoretical lower cutoff frequency of the anechoic backwall, facilitated by an 18-inch foam wedge, is 186 Hz. Also, the heavy walled steel tube is expected to attenuate more effectively at high frequencies; therefore, it is possible that sound energy is more capable of transmission (or "leakage") across the tube walls at the lower limit of the spectrum, which would appear as an increased transmission loss

3.3.4   Data Processing for Impedance Tube Testing

Signal from all four microphones was collected in a data acquisition device (DAQ) then converted from electrical signal to acoustic spectral data using Labview Sound and Vibrations Suite. The acoustic data collected is saved in an excel format which is later analyzed a MatLab based Transmission Loss Code. The code utilized the One-Load Method for Transfer Matrix. This method is a simplified version of the Two-Load method and is adequate since it is assumed that the test specimen should have symmetric acoustic properties on each face. Additionally, anechoic termination was used for all test cases[7, 9, 10]. The Normal Incidence Transfer Matrix is calculated as shown below[7]. Note: Reference **Figure 8** for wave direction and spatial annotations used in the following derivation.

Derivation of the transfer matrix is based on the Two-Load method where a reflecting and anechoic termination are both utilized. At the termination of type "a", the acoustic pressure and particle velocity transfer matrix is given **Equation (5**.

$$\begin{bmatrix} p_a \\ u_a \end{bmatrix}_{x=0} = \begin{bmatrix} T_{11} & T_{12} \\ T_{21} & T_{22} \end{bmatrix} \begin{bmatrix} p_a \\ u_a \end{bmatrix}_{x=d} \tag{5}$$

At the termination of type "b", the transfer matrix is given by:

$$\begin{bmatrix} p_b \\ u_b \end{bmatrix}_{x=0} = \begin{bmatrix} T_{11} & T_{12} \\ T_{21} & T_{22} \end{bmatrix} \begin{bmatrix} p_b \\ u_b \end{bmatrix}_{x=d} \tag{6}$$

The decomposed forward and backward traveling waves are represented by the following (reference **Figure 8**):

$$A = j \frac{H_{1,ref} e^{-jkl_1} - H_{2,ref} e^{-jk(l_1 - s_1)}}{2 \sin(ks_1)}$$

$$B = j \frac{H_{2,ref} e^{+jk(l_1 + s_1)} - H_{1,ref} e^{+jkl_1}}{2 \sin(ks_1)}$$

$$\tag{7}$$

$$C = j \frac{H_{3,ref} e^{+jk(l_2 + s_2)} - H_{4,ref} e^{+jkl_2}}{2 \sin(ks_2)}$$

$$D = j \frac{H_{4,ref} e^{-jkl_2} - H_{3,ref} e^{-jk(l_2 - s_2)}}{2 \sin(ks_2)}$$

$H_{x, ref}$ = corrected transfer function of microphone x relative to a reference signal

Acoustic pressure and particle velocity on both faces of the specimen are calculated as follows:

$$p_0 = A + B \qquad\qquad\qquad p_d = C e^{-jkd} + D e^{+jkd} \tag{8}$$

$$u_0 = \frac{(A - B)}{\rho c} \qquad u_d = \frac{\left(Ce^{-jkd} - De^{+jkd}\right)}{\rho c}$$

The Two-Load transfer matrix is calculated as follows:

$$T = \begin{bmatrix} \dfrac{p_{0a}u_{db} - p_{b0}u_{da}}{p_{da}u_{db} - p_{db}u_{da}} & \dfrac{p_{0b}p_{da} - p_{0a}p_{db}}{p_{da}u_{db} - p_{db}u_{da}} \\[2ex] \dfrac{u_{0a}u_{db} - u_{0b}u_{da}}{p_{da}u_{db} - p_{db}u_{da}} & \dfrac{p_{da}u_{0b} - p_{db}u_{0a}}{p_{da}u_{db} - p_{db}u_{da}} \end{bmatrix} \tag{9}$$

For the One-Load Method, reciprocity places the following constraints on the transfer matrix

$$T_{11} = T_{22} \; and \; T_{11}T_{22} - T_{12}T_{21} = 1 \tag{10}$$

This allows the elements of the matrix to be determined by a measurement of the microphone transfer function with a single termination case. In this study, an anechoic termination was utilized.

$$T = \begin{bmatrix} \dfrac{p_d u_d + p_0 u_0}{p_0 u_d + p_d u_0} & \dfrac{p_0^2 - p_d^2}{p_0 u_d + p_d u_0} \\[2ex] \dfrac{u_0^2 - u_d^2}{p_0 u_d + p_d u_0} & \dfrac{p_d u_d + p_0 u_0}{p_0 u_d + p_d u_0} \end{bmatrix} \tag{11}$$

The transmission coefficient, τ, for the anechoic backed case is as follows:

$$\tau = \frac{2e^{jkd}}{T_{11} + (T_{12}/\rho c) + \rho c T_{21} + T_{22}} \tag{12}$$

The normal Incidence Transmission Loss, TL, is therefore computed as follows:

$$TL = 20 \log_{10} \left| \frac{1}{\tau} \right| \tag{13}$$

3.3.5   Significant Findings from Impedance Tube Testing

The output from the Transfer Matrix method was plotted and is presented below in **Figure 12**. As expected, there exists a trend between epoxy saturation level and the harmonic characteristic of transmission loss variation. As the mass fraction of epoxy impregnated into the specimen

increases, its transmission loss characteristic becomes dominated by its bending stiffness. Rigid structures deflect the most while under cyclic loading at the structures natural frequency and its associated harmonic frequencies. This deflection results in a reduction of sound energy absorbed at those frequencies causing a reduction in acoustic transmission loss. The high epoxy saturation specimen is observably more stiff than the low epoxy saturation and dry samples. As expected for stiffness dominated transmission loss characteristics, the first observable "valley" or local minimum in the STL curve is shifted to a lower frequency than the first "valley" observed for the low saturation sample. The dry specimen is not epoxy stiffened, and therefore, does not exhibit resonant behavior as was seen for the epoxy impregnated stiffened samples.
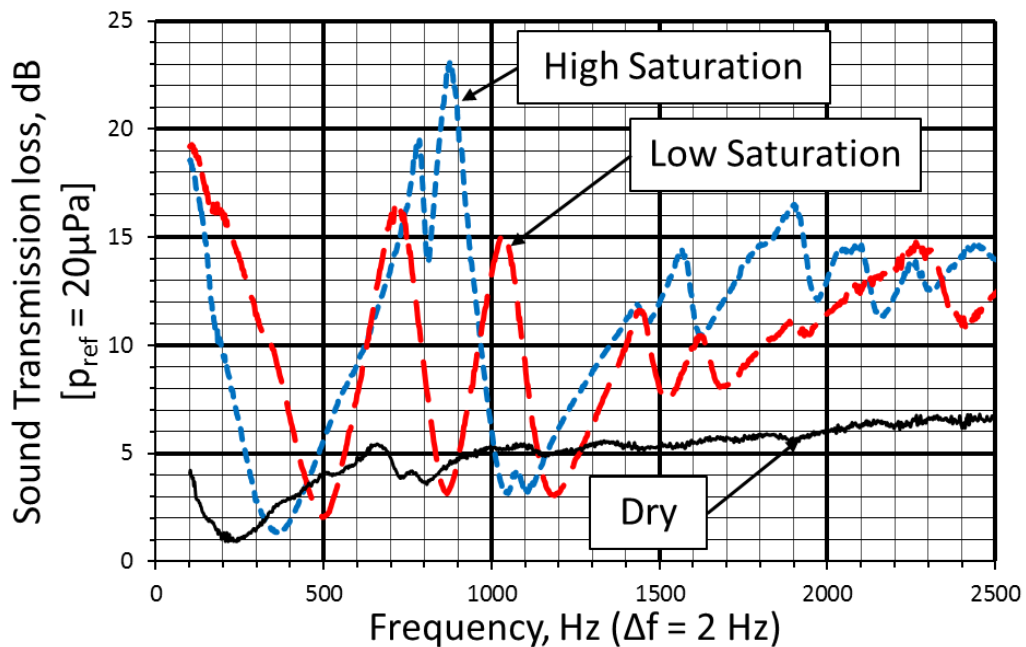
Figure 12. Impedance Tube derived transmission loss spectrum for lightly tensioned 5.0 oz. plain weave dry, low epoxy saturation, and high epoxy saturation Kevlar® samples tested using a white noise source

The dry test specimen was included in this study to produce validation results to be compared with the results obtained during evaluation of a windscreen used to cover a large

microphone array embedded in the wall of the large section wind tunnel at NASA Ames Research Center[5]. The dry Kevlar® sample tested in the current impedance tube is not identical in style or specimen mounting tension to that used for the NASA Ames sample. Additionally, the experimental method used at NASA Ames varies significantly; therefore, they are not expected to be an exact match. The STL data obtained for the dry sample and a portion of the results obtained for the "thick sample" 5.0 oz. Kevlar® material tested at NASA Ames Research Center are presented in **Figure 13**.The full data set obtained by the NASA experiment is presented in **Figure 14**[5].
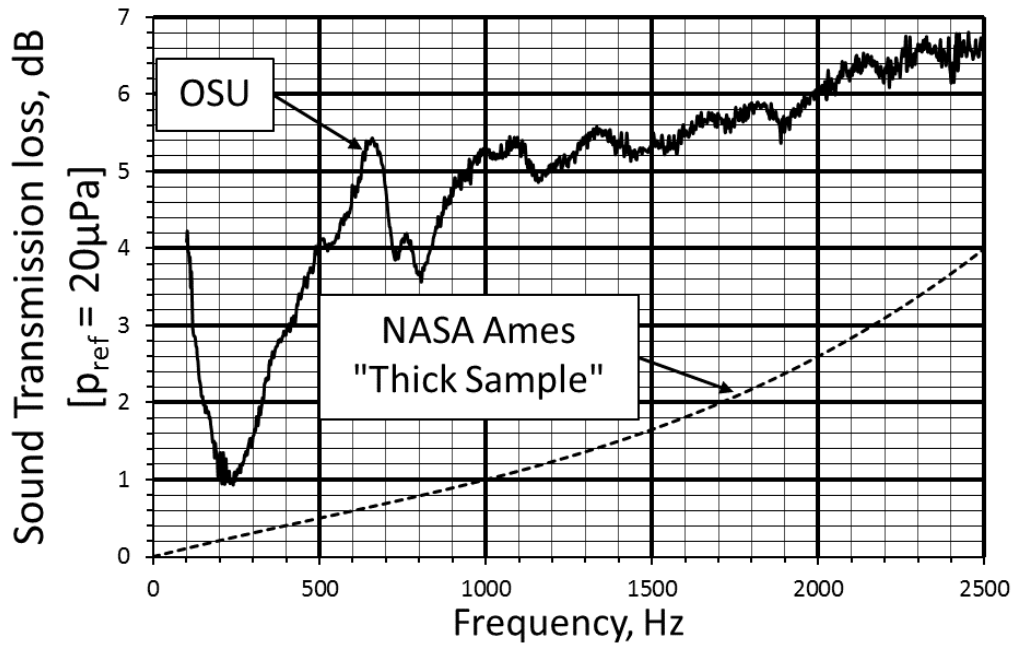
Figure 13. Comparison between data obtained at NASA Ames Research Center[5] using 5.0 oz. Kevlar® sample tested in large test section wind tunnel at a frequency resolution of $\Delta f = 62.5$ Hz[3] and data obtained at Oklahoma State University using 5.0 oz. Kevlar® sample tested in ASTM E2611-09[7] impedance tube at a sampling rate of $\Delta f = 2$ Hz.
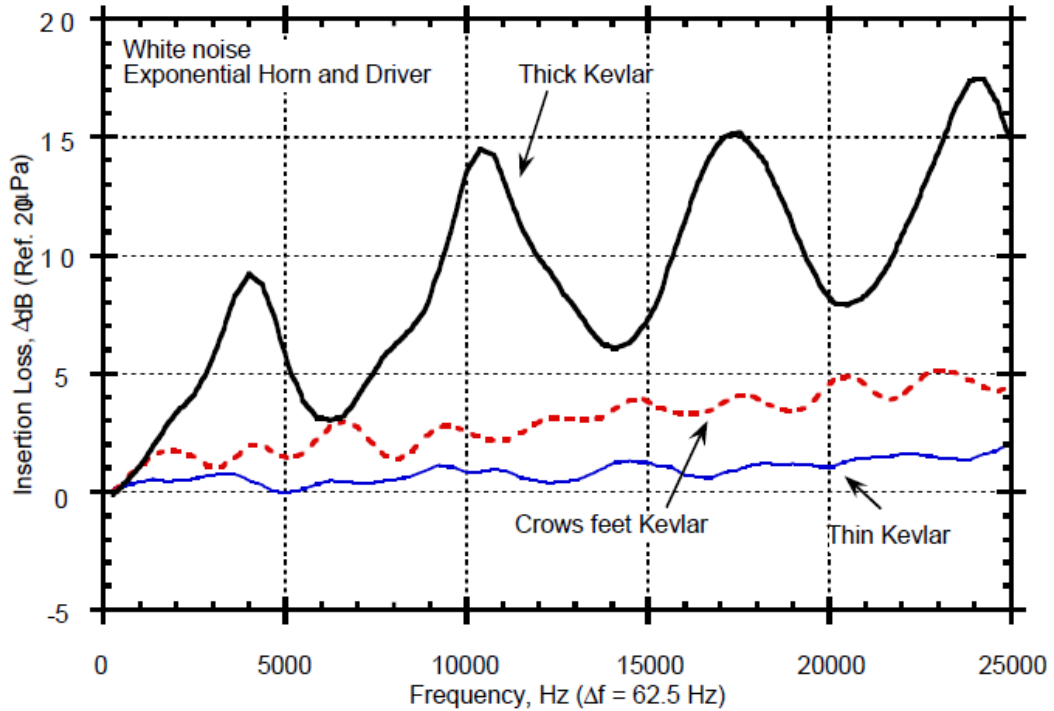
Figure 14. Anechoic chamber incretion loss testing results for three weights of Kevlar® obtained at NASA Ames Research Center during study the effects of surface treatment on microphone array self-noise as presented in Jaeger, et. al.[5]

It is also noteworthy that the previous study[5] was conducted using a method similar to the Two-Room Method rather than in an impedance tube and over a much larger frequency spectrum than the OSU impedance tube is capable of measuring. Comparing the data presented in **Figure 13**, both experiments achieved similar results, although the transmission loss observed by the previous experiment is lower than that observed for the data obtained herein. This is possibly the result of a difference in sample mounting tension to that used for the NASA Ames experiment[5], variations in error associated with the different test methods used, or the difference in sample size used. Additionally, the frequency resolution collected in the NASA Ames experiment is 62.5 Hz between data points whereas this study used a 2 Hz resolution. This can account for some small differences in plotting accuracy; however, is not likely responsible for the variation observed. Another noteworthy observation from **Figure 14** is that a frequency dependent harmonic effect was

observed for a non-epoxy-impregnated test specimen, although at frequencies much higher than can be observed using the equipment available for the current study[3]. It is expected that the Kevlar® samples without epoxy impregnation would still exhibit the same vibrational harmonic tendencies as the samples which were impregnated; however, the significantly reduced stiffness will cause the first natural frequency to be shifted lower in the frequency spectrum, below the lower cutoff frequency of the test equipment. Information gained through impedance tube testing is valuable for the future design of candidate windscreens; however, due to the dominance of the effects of sample stiffness in transmission loss testing, a full scale (or near full scale) test system is desired.

3.4   Wind Tunnel Test System Apparatus

The characterization method developed herein involves modification to the wind tunnel facility at Oklahoma State University. The Low Speed Wind Tunnel at OSU's School of Mechanical and Aerospace Engineering was originally configured to conduct aerodynamic testing on small aircraft and models, with little consideration for sound mitigation. The tunnel is housed in facility having concrete walls, floors, and ceilings and exposed HVAC equipment. Additionally, the tunnel and test section are constructed from hard materials such as fiberglass, acrylic plastic, and wood (**Figure 15** shows the original configuration of wind tunnel prior to any modifications for acoustic testing). The result is a relatively high background noise level in the room of 60.3 dB OASPL and in the tunnel of 57.1 dB OASPL with the flow off (OASPL integrated from 200 to 8000 Hz).
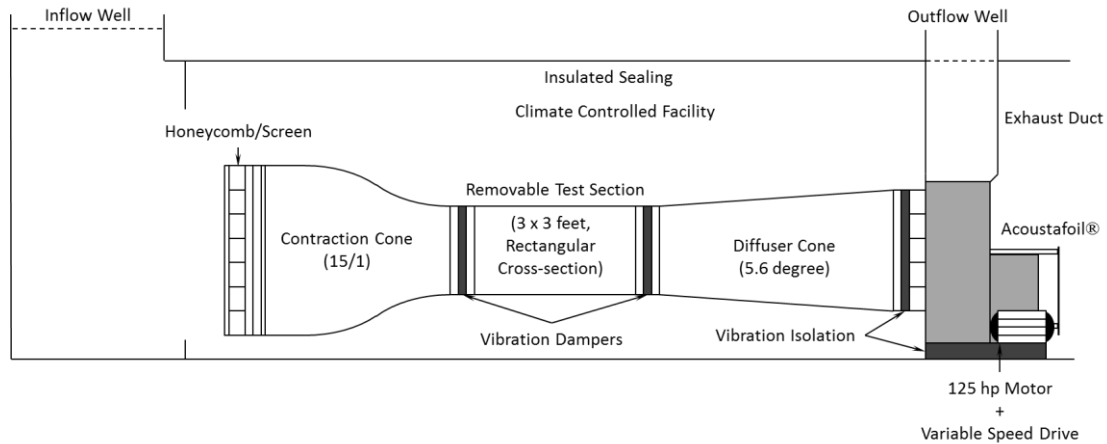
Figure 15. Configuration of OSU's low speed wind tunnel prior to modifications for acoustic testing[15]

When an acoustic pressure wave interacts with a discontinuity in a continuum, the wave's energy will be reflected, transmitted, and absorbed. The amount of energy allotted to each of these three possibilities is dependent of the nature of the discontinuity. STL characterization is focused on measuring only the energy that is transmitted. Characterizing a windscreen's STL requires measuring the spectra on both sides of the membrane and comparing the difference to determine how much of an acoustic pressure wave has been transmitted. To do this accurately, no acoustic energy can be allowed to "leak" around the membrane boundaries; therefore, it is necessary to create an environment with boundaries that outside acoustic energy cannot penetrate except through the transmission loss measurement specimen. For the current study, this environment was provided by a "quiet box" which has specially designed walls which provide a high level of acoustic attenuation. The quiet box was installed on the bottom side of the wind tunnel test section. A schematic of the modifications to the wind tunnel test section are shown in **Figure 16**. The quiet box extends from the lower surface of the test section with a specimen window open to the wind tunnel test section. The quiet box houses the primary microphone used recording signals transmitted through candidate windscreens. Additional information about the design and construction of the quiet box can be found subsequent chapters. The OSU wind tunnel was already equipped with closed-cell-foam vibration isolators at key segment junctions; however, it was

34

decided to further isolate the quiet box/acoustic test section to reduce vibrations generated by the fan motor and drive assembly. The sections were separated, creating a thin air gap between the section junctions. The gap was then sealed with aluminum tape. A controlled acoustic source driver was flush mounted in the test section upper panel and is used to generate noise which can be used to raise the ambient noise level, and to generate specific tones used in testing. A flush mounted reference microphone equipped with a bullet fairing nose cone is mounted in the flow on a pylon above the specimen window, and is used to compare the sound pressure with that recorded by the microphone contained within the quiet box. A 4-channel data acquisition card is connected to the microphones and data fed into a computer for analysis. Detailed discussion about system design, testing procedures, and signal analysis are contained in subsequent chapters.
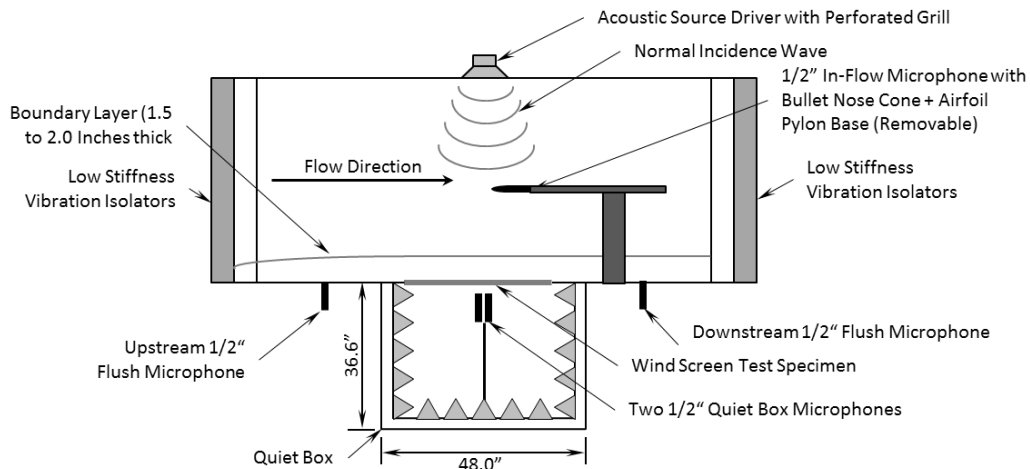
Figure 16. Modifications to OSU wind tunnel test section for UAV windscreen acoustic characterization (schematic not drawn to scale)

Previous studies on modification of aerodynamic wind tunnels into closed section aero-acoustic wind tunnels[5, 6] have been conducted which suggest that tensioned light weight plain weave Kevlar® fabrics effectively produce windscreens with a low STL (ranging from 0 to 7 dB from 0 to 20k Hz) compared to other weights and weaves of tensioned Kevlar®. These studies provide STL data which is used as a validation comparison to the STL data achieved using the test apparatus developed herein.

3.4.1   Quiet Box Design
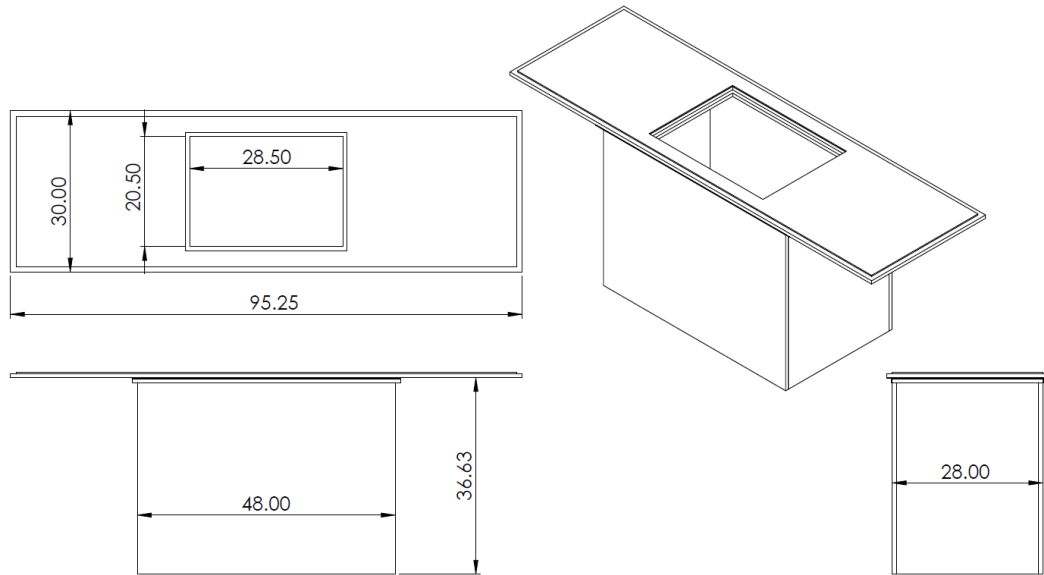
Figure 17. Wind tunnel test section quiet box environment pass-through window and external dimensions

The quiet box designed and constructed for this study utilizes sound attenuation techniques similar to those used in large scale anechoic and semi-anechoic chambers; however, due to the relatively small volume available for this installation, consideration must be given avoid the standing wave phenomenon. The Rayleigh formula (**Equation (**14)) is used to estimate Eigen-modes for standing waves based on the internal dimensions of the chamber[12]. The distribution of the Eigen-mode frequencies was found to be sufficiently well distributed using the internal dimensions (without foam) of L = 42.00 inches, W = 22.00 inches, and H = 32.88 inches, which results in an internal volume of 17.6 square feet. The box dimensions are also limited by the space available within the wind tunnel test section support frame.

$$f_{k,m,n} = \sqrt{\left(\frac{k}{L_x}\right)^2 + \left(\frac{m}{L_y}\right)^2 + \left(\frac{n}{L_z}\right)^2} \qquad (14)$$

Where
f = Standing wave frequency
k, m, n = integer values 1, 2, 3, ..., i
L_x , L_y, L_z *= x, y, z dimensions of chamber interior*

An ideal quiet box would rely primarily on acoustic foam wedges to attenuate all environmental and reverberant noise which is present, across the entire test frequency band. The wedge shape foam wedge is used to minimized normal incidence surfaces which can reflect a pressure wave directly back at the sensors and increase the amplitude of any standing waves that may exist in the system. By providing angled surfaces for pressure waves to impinge on, the wave is reflected towards the base of the foam where it is attenuated. Reference **Figure 18** for schematic of the reflected wave vector resulting from foam angles[12].
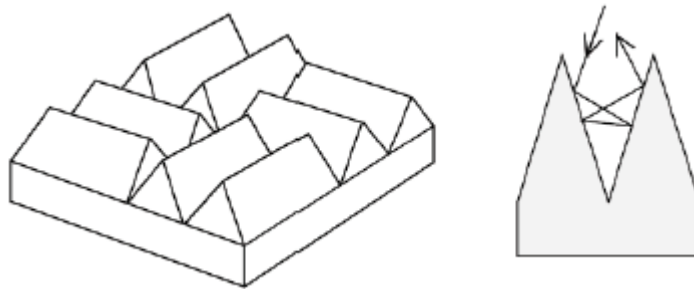
Figure 18. Schematic of open-cell foam wedges used in quiet box design demonstrating beneficial reflected wave vector resulting from foam angles[12]

The thickness of foam wedges is directly proportional to the quarter wave length of the lowest frequency which will be attenuated by the foam[12]. The relationship is given by **Equation (15.** As an example, in order to achieve a theoretical lower cutoff frequency of 200 Hz, a foam wedge of at least 1.4 feet thick would be needed for every reflective surface within an environment.

This presents an obvious problem considering the size restrictions associated with installing the chamber within the existing wind tunnel support frame.

$$f = \frac{c}{\lambda} = \frac{c}{4 * l_c}, \qquad l_c \geq \frac{\lambda}{4} \tag{15}$$

$Where$:
$f = frequency$
$c = Speed\ of\ Sound$
$\lambda = Wave\ Length$
$l_c = Wedge\ Length$

A commercially available 4-inch-thick open cell polyurethane foam wedge material was chosen as the largest practical for the available volume (a datasheet for the foam is provided in **Appendix A: Add Foam Factory 4" wedge data sheet**). This foam provides a theoretical minimum lower cutoff frequency of 840 Hz, which is well above the desired lower frequency range for this system.
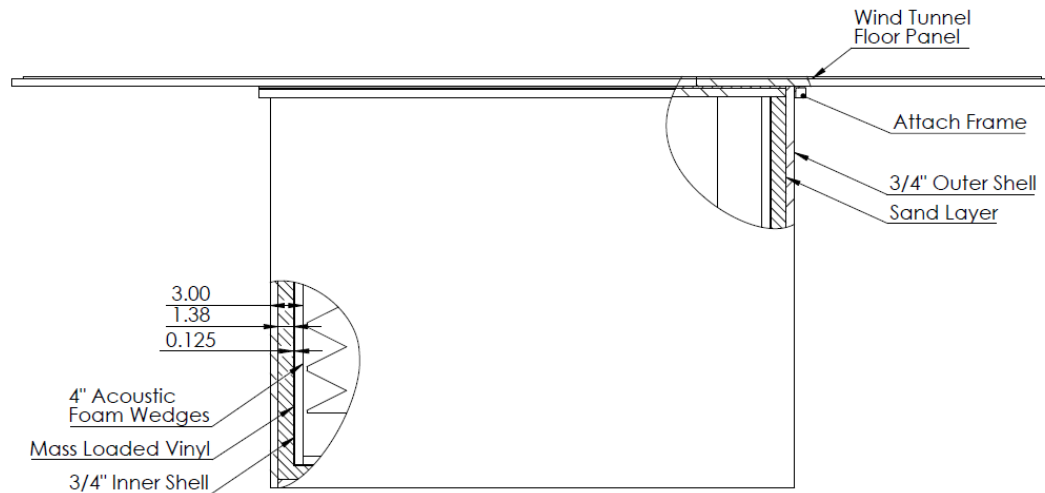
Figure 19. Quiet box environment cutaway schematic showing double wall configuration details and dimensions

To further reduce the low frequency attenuation of the chamber, a high mass, double wall design was used. The chamber wall is constructed from two layers of 3/4-inch medium density fiberboard (MDF), with a 1/8-inch-thick, 1.0 pound per square foot mass loaded vinyl bonded to

the outer surface of the inner wall. On the sides and bottom of the chamber, a 1-3/8-inch-thick layer of fine grain sand was also included. This limp mass layer reduces the amount of low frequency sound energy which can pass through. A conceptual understanding of this method of attenuation is similar to Hook's law for spring deflection, where a reduced stiffness and an increased mass result in a reduced acceleration. This tends to be more effective at lower frequencies than high. The "mass law" can be used as an analytical model to predict transmission loss caused by this phenomenon[16]. The chamber was constructed using lap joints, bonded in place with wood glue and screwed with countersunk drywall screws. After assembly, all joints on the inner and outer walls of the chamber were sealed with a silicon based adhesive to prevent air leakage. The foam wedges and mass loaded vinyl were bonded in place using the same silicon based adhesive. Two RG6 coaxial cables were installed in the box by creating slip fit holes through both walls and the sand layer. BNC connectors were attached to the wires once they were passed through the box walls, and their continuity was tested. Finally, signal from a microphone attached to the data cables installed through the box was compared to that of a known good wire to ensure a good connection exists.

A soft pine wood was chosen to construct the base stand of the chamber to provide a reduced compressive stiffness over that of a metal base. This was intended to reduce the effects of any vibrations transmitted by the concrete floor. A layer of vinyl mat was placed between the base stand and the concrete floor as a moisture barrier and additional vibration isolator. The base stand was designed such that a standard pallet jack can be used to position and transport the quiet box. This is important considering that once full of sand, the quiet box assembly weighs roughly 900 pounds.

Initial quiescent testing of the installed chamber using a single ½ inch condenser microphone (reference **Section 3.4.2** for description of sound measurement equipment used) inside the box sealed quiet box revealed a high amplitude response in the low frequencies region (between 60 and 70 dB with peaks ranging from 100 to 1000 Hz) when chamber sides were tapped. The

frequencies are well-below those expected to be attenuated viscoelastically by the foam wedges (below 800 Hz). This response was induced by tapping on one of the large side panels of the outer wall using a fingertip. This response is believed to have been associated with the panel's natural vibrational frequencies, and associated harmonics. This appeared to result in a "drum head" effect whereby deflection of the outer chamber wall causes an increased pressure within the sealed chamber. The wall vibrates at its natural frequency and the tones and their harmonics are detected by the box microphones.

Aluminum extrusions were added to stiffen the outer wall of the chamber and reduce the size of the free-vibrating panels. This stiffening shifted the natural frequencies of the chamber walls higher in the spectrum towards a frequency range that could be more effectively attenuated by the foam wedges. Replicating the tapping input on the various chamber wall panels after installation of the stiffeners shows a much lower response. Direct stimulation of the side walls at their respective natural frequencies causes a clear increase in sound pressure level within the quiet box; however, this phenomenon has not been shown to present a problem during testing since the deflection of the chamber walls is minimal without directly tapping on them, and tapping does not occur during testing. There is a clear correlation between the spike at approximately 200 Hz caused by tapping and the spike at the same frequency observed during the white noise test. This is likely a natural vibrational frequency or its harmonic; however, that has not been confirmed. Note that testing with the specimen door in place revealed the same spike in amplitude at 200 Hz, which further supports the theory that it is caused by a natural vibrational frequency of the box structure. Additional testing using a vibrometer could be used to validate this theory.

Figure 20. Photographs of quiet box after addition of aluminum angle stiffeners on outer wall panels shift natural frequency for better attenuation
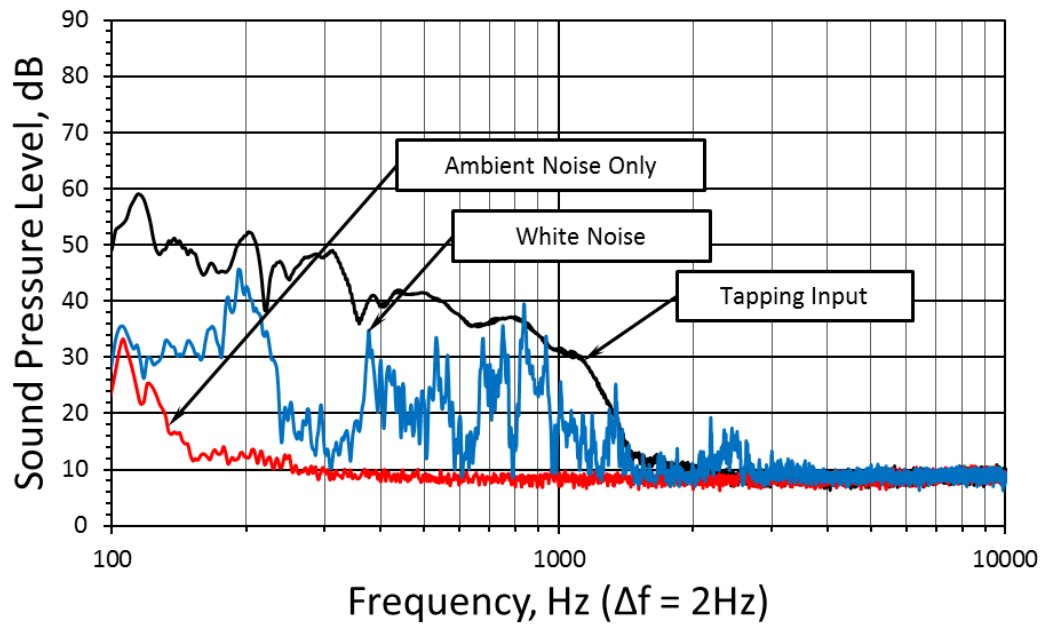
Figure 21. Frequency spectrum inside sealed box with plug door installed demonstrating effect of fingertip tapping on to side panel compared to ambient background noise and white noise

3.4.2 Experimental Acoustic Equipment

Acoustic measurements were accomplished using four Type 40AD GRAS 1/2-inch diaphragm pre-polarized pressure microphones, each attached to a Type 26CA GRAS 1/2-inch CCP preamplifier, connected to a National Instruments NI USB-4432 24-Bit data acquisition card using RG6 coaxial cables and BNC connectors. During some testing, a RA0020 GRAS 1/2-inch nose cone was installed on the in-flow microphone. Recording and data processing was accomplished using National Instruments LabVIEW, Sound and Vibrations Assistant. Acoustic signal was generated using computer from a MATLAB code for tonal signals and .wav file for white noise. A Technical Pro LZ 4200 Watt amplifier was connected to a Kicker DSC693 360 Watt (peak) 4Ω 6-inch by 9-inch coaxial speaker mounted in a sealed MDF enclosure and connected through a 20 Hz high pass filer. See **Figure 22** for a photograph of recording equipment, example microphone, and source amplifier. See **Figure 23** for photo of Kicker 6-inch by 9-inch acoustic driver mounted in top of wind tunnel test section used to generate normal incidence sound waves for transmission loss testing.
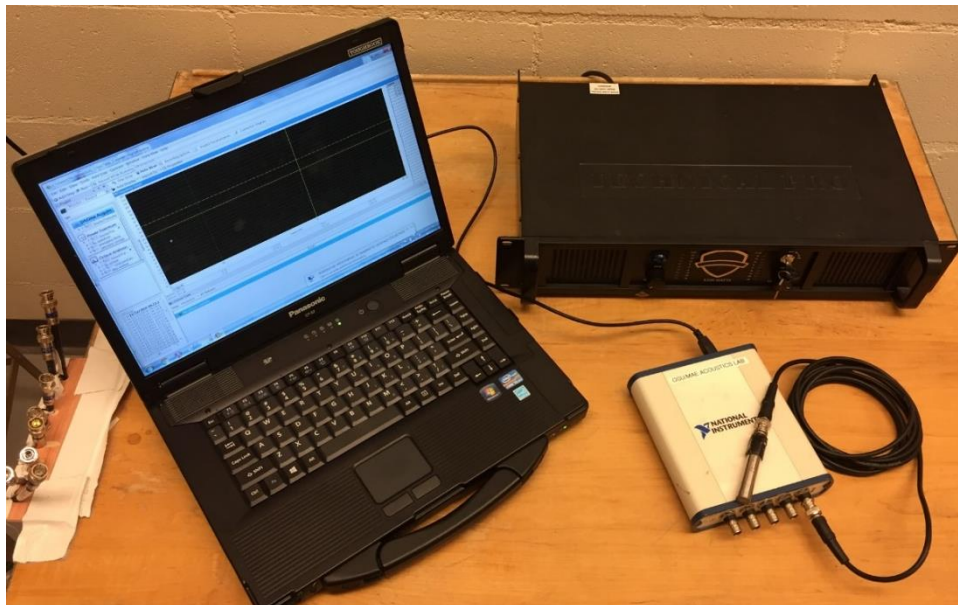
Figure 22. Acoustic recording and sound generation equipment used in testing

Figure 23. Kicker DSC693 6-inch by 9-inch 4Ω woofer used as acoustic source driver mounted in top of wind tunnel test section to provide normal incidence sound waves for transmission loss testing.

The microphones used in this study are dynamically calibrated from the factory, and a calibration curve is provided with each one. Microphone voltage is generated by deforming the microphone's diaphragm, which generates a voltage. This voltage is converted to pressure a pressure reading by use of a calibration factor (typically between 45 and 55 mV/Pa for the microphones used in this study). The calibration factor is dependent on the resistance of any cables, connectors, and recording equipment. The calibration factor is determined at the beginning of each series of testing by using a controlled acoustic source. For this testing, a piston phone was used. This piston phone seals around each microphone and generates controlled 1000 Hz signal at 114 dB. The microphone sensitivity is adjusted until the recording device measures 114 dB at 1000 Hz. This procedure is repeated for each microphone. Varying conditions can

cause this calibration to drift; therefore, the calibration procedure is repeated anytime a system change is made (such as removing a microphone), and at the start of each test series. It was noted that the calibration factor for each microphone typically drifted less than ±0.1 dB from day-to-day.

The Kline and McClintock single test method[17] to determine the uncertainty of the measurement system was used for this study. In this method, the sum of uncertainty of all constituent components is computed. This method requires that the uncertainty of all the constituent components is known. The equations used to determine the 95th percentile (or 20:1 odds) uncertainty intervals of the acoustic measurement equipment used for this study are shown in **Equations** (16) and (*17*)[17].

$$R = \hat{R}(measured) \pm \delta R \quad (20{:}1) \tag{16}$$

$$\delta R = \left\{ \sum_{i=1}^{N} \left(\frac{\partial R}{\partial X_i} \delta X_i \right)^2 \right\}^{1/2} \tag{17}$$

According to the equipment manufacturer's datasheets (reference **Appendix C**), the microphones have an uncertainty of ±0.06 dB, the preamplifiers have an uncertainty of ±0.20 dB, and the DAQ has an output noise of ±200 µV, and an input noise of ±240 µV. The SPL variation as a function of voltage uncertainty was calculated using the average calibrated microphone sensitivity (50 mV/Pa). The results of this analysis area shown in **Table 6**. Based on the method developed by Kline & McClintock[17], the theoretical measurement uncertainty of the test equipment used in this study is ±0.21 dB. This calculated theoretical maximum uncertainty is consistent with the ±0.1 dB "drift" observed while calibrating the microphone systems at the beginning of each test. All sound pressure levels reported herein are assumed to maintain a maximum uncertainty of ±0.21 dB. This uncertainty is considered for all calculations accomplished using SPL measurements.

Table 6. Acoustic measurement uncertainties for theoretical uncertainty calculation

System Detail	Uncertainty	$\partial R/\partial X_i$	$(\partial R/\partial X_i)\, \delta X_i$ [dB]
Microphone	± 0.06 dB	1	± 0.06
Preamplifier	± 0.20 dB	1	± 0.2
DAQ Input Noise	$\pm 240\ \mu V$	12.0×10^{-5} dB-μV^{-1}	$\pm 2.00 \times 10^{-6}$
DAQ Output Noise	$\pm 200\ \mu V$	12.0×10^{-5} dB-μV^{-1}	$\pm 1.67 \times 10^{-6}$
Total $\delta R = \pm 0.21$ dB			

3.4.3 Validation of Anechoic Properties

Effective transmission loss measurements require the receiving room microphone to be house in an environment sufficiently free from ambient noise. Per ISO 3745:2012[11], this noise threshold for sufficiently low ambient noise requires that the signal of interest be at least 6 dB above any background noise, and 10 dB for all 1/3 octave frequencies with mid-range frequencies ranging from 250 to 5000 Hz[11]. It is required that the quiet box environment be able to maintain this level of ambient noise attenuation throughout the frequency spectrum when subjected to wind tunnel flow noise.

3.4.3.1 Validation Method

To validate the performance of the quiet box environment, baseline measurements were needed to determine the level of sound being transmitted into the box. These measurements were tested with and without the wind tunnel motor running and with and without speaker signal tones. Flow-on testing was used to determine if vibrations generated by the fan motor and transmitted through the floor and wind tunnel segments stimulate natural vibrations frequencies of the structure. Flow off testing was accomplished to ensure that the level of noise recorded by the in-flow microphone is not artificially high due to hydrodynamic noise. The testing was accomplished using three microphones. A boom mounted microphone was located between 15 and 16 inches above the test section floor, 8.5 to 9.5 inches aft of the quiet box center point, and centered in the test section from right to left. A microphone was mounted at the center of the box with the diaphragm between 5 and 6 inches below the upper surface of the wind tunnel. An additional "ambient" microphone

was placed outside the wind tunnel test section next to the operator's station with its diaphragm located between 3 and 4 feet from the test section wall. The ambient microphone was used to compare the noise spectrum inside the tunnel with the noise spectrum outside the tunnel. The box was completely sealed for the baseline testing using a plug door was constructed to seal the pass-through window opening.

3.4.3.2 Plug Door Design and Fabrication

The quiet box was designed to have interchangeable doors in the interface window to facilitate installation of various test specimen. For the baseline validation testing, this window needs to be sealed. A plug door was fabricated to mimic the acoustic attenuation properties of the top of the box. The plug door is constructed from two layers of 3/4-inch-thick MDF bonded and screwed together in the same manner as the quiet box structure. A layer of mass loaded vinyl was bonded to the interior surface, and the 4-inch foam wedges used to line the box were bonded to the vinyl. All vinyl bonding was accomplished utilizing the same silicon based adhesive used to seal the box seams (see **Figure 24.** for a schematic of the plug door). The doors are sealed by a strip of chromate vacuum bag seal which is compressed by the attaching fasteners. Aluminum foil tape is used to create a smooth aerodynamic transition over the edges of the door, and as an additional air-tight seal.
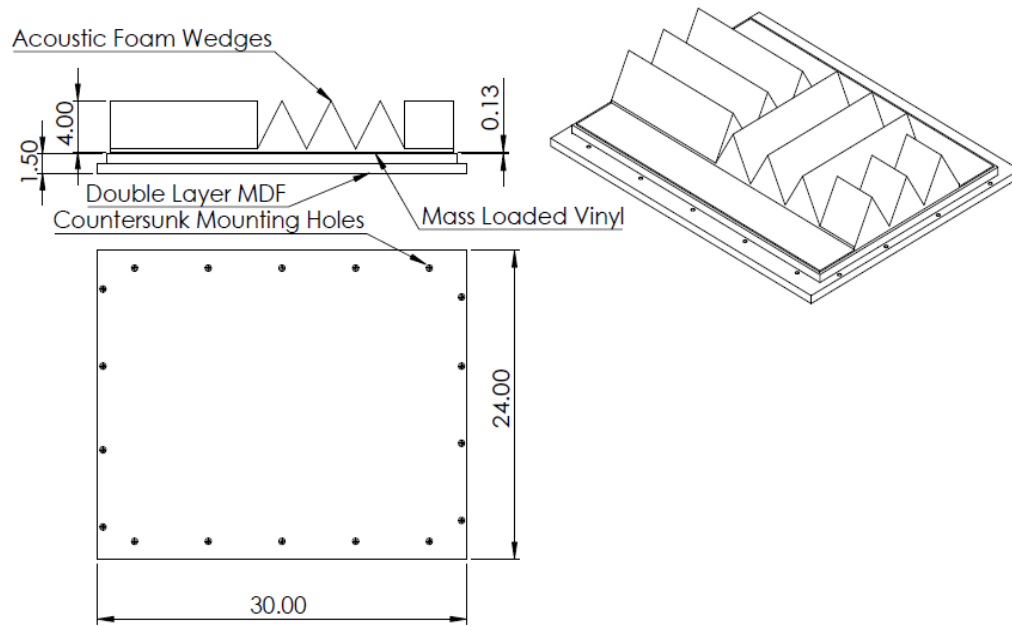
Figure 24. Schematic of plug door installed in pass-through window for testing and evaluation of quiet box sound attenuation characteristics

3.4.3.3 Quiet Box Anechoic Properties

It is necessary to accomplish testing to determine the background noise present within the quiet box when exposed to white noise signal and with the wind tunnel motor running. Two microphones were placed in the quiet box and the plug door was installed in the pass-through window. The bullet nose cone microphone was located on the pylon in the position used for flow-on testing. The signal from the two microphones within the quiet box was averaged. **Figure 25** shows the recorded narrow band signal from the averaged quiet box microphones and the in-flow bullet nose cone microphone. The white noise source was generated at an amplitude more than 10 dB above the flow noise. The wind tunnel flow was held steady at 0.8 in-H_2O (59 ft/s) for this test. **Figure 26** shows the signal attenuation spectrum for the box. This data is calculated by subtracting the sound pressure spectrum recorded by the internal quiet box microphones from the sound pressure level recorded by the bullet nose microphone. The minimum narrow band attenuation

recorded is 23 dB with an average of 45 dB. The industry accepted minimum noise reduction for acoustic testing is 10 dB[11]. Based on this information, the quiet box is shown to provide a sufficient acoustic attenuation to conduct STL measurements.
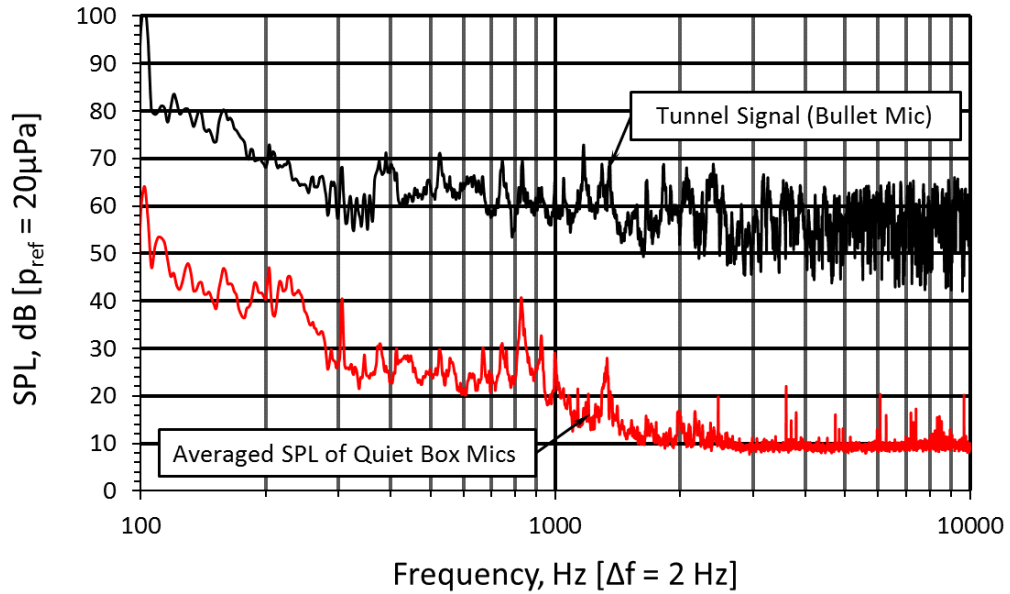
Figure 25. Quiet box signal with plug door installed, white noise source, and wind tunnel flow at 59 ft/s.
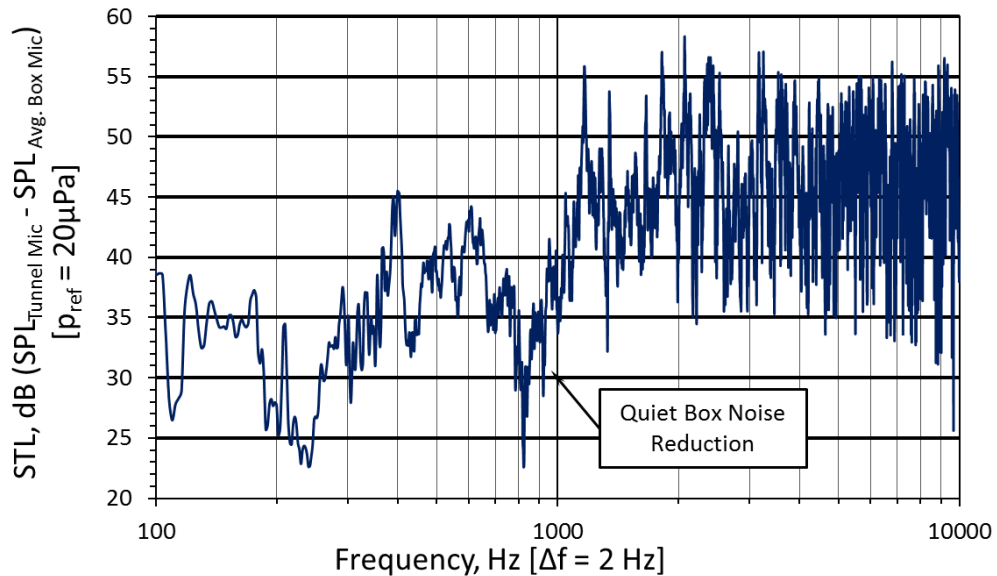
Figure 26. Quiet box noise attenuation (sound level in tunnel minus sound level in quiet box) measured with plug door installed, white noise source, and wind tunnel flow at 59 ft/s.

3.4.3.4 Specimen Door Design and Fabrication

The validation test specimen door was created using the same style, weave, weight, and material used by the comparison study[3]. The comparison study[5] found that tensioned 1.8 oz. Style-120 plain weave Kevlar® fabric perform better in acoustic transmission loss than heavier weight and crow's foot weave fabrics. The comparison study also tested fiberglass and metallic fabrics which were found to fail rapidly due to the shear loading and fatigue caused by turbulence in the boundary layer[5]. An elliptical specimen shape was chosen to avoid any unnecessary vibrational harmonics associated with square or rectangular membranes, and to most closely mimic a cutout window that would be used in an aircraft for a parabolic antenna which has capability to pan. The specimen was created using two layers of 3/4 inch MDF cut to fit the pass-through window (reference **Figure 27** for specimen door dimensions). The two layers of MDF were assembled in a jig to maintain proper alignment. The layers were bonded together using standard wood glue, then screwed together using counter-sunk screws to hold the assembly in position during the cure. Once cured, the elliptic opening was cut out using a CNC controlled router. This ensured precision of the elliptical profile. After machining, the upper faying surface of the door panel was prepared for bonding. The Kevlar® material was tensioned using a custom-built tension frame (see **Section 3.3.3.5** for description of the tension device). The material was tensioned, and a comparative tension measurement was taken (See **Section 3.3.3.6** for description of comparative tension measurement). The upper faying surface of the specimen door panel was coated in a general purpose two-part epoxy (see **Appendix B** for epoxy system datasheet). Due to the nearly 400 in^2 surface area available to bond the tensioned specimen material in place, a high strength resin system is not needed. A smooth, flat glass caul sheet was prepared and covered in release film. The loaded tension frame was placed on the glass caul sheet with the outer surface of the material specimen against the tool surface. The epoxy coated specimen door panel assembly upper faying surface was placed against the inner surface of the specimen material and layer of perforated release film and

breather cloth were placed within the elliptical cutout of the specimen door panel assembly to draw any excess epoxy away from the area of the specimen material that is to remain dry (not epoxy impregnated). The tension frame and specimen door panel assembly were covered with a vacuum bag, and a chromate seal was placed around the edge. A vacuum fitting medallion was installed in a non-critical area, and the specimen was allowed to cure for 12 hours under 22 in-HG of vacuum and at room temperature, as recommended by the epoxy manufacturer (see **Figure 28** for layup template and **Figure 29** for photograph of curing assembly). Once cured, the bagging material was removed and the excess Kevlar® was cut along the outer edge of the specimen door panel assembly using a razor blade.
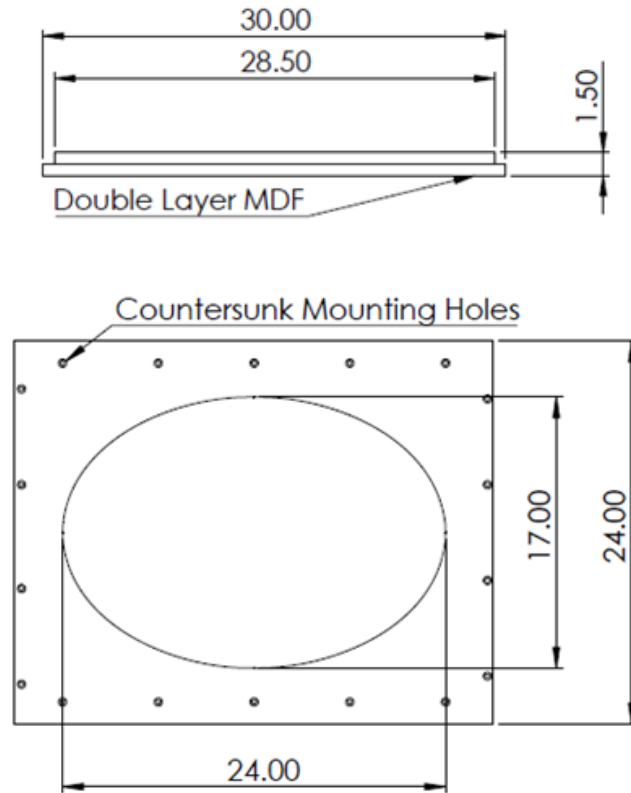
Figure 27. Quiet box specimen door panel assembly construction schematic (all dimensions are shown in inches)
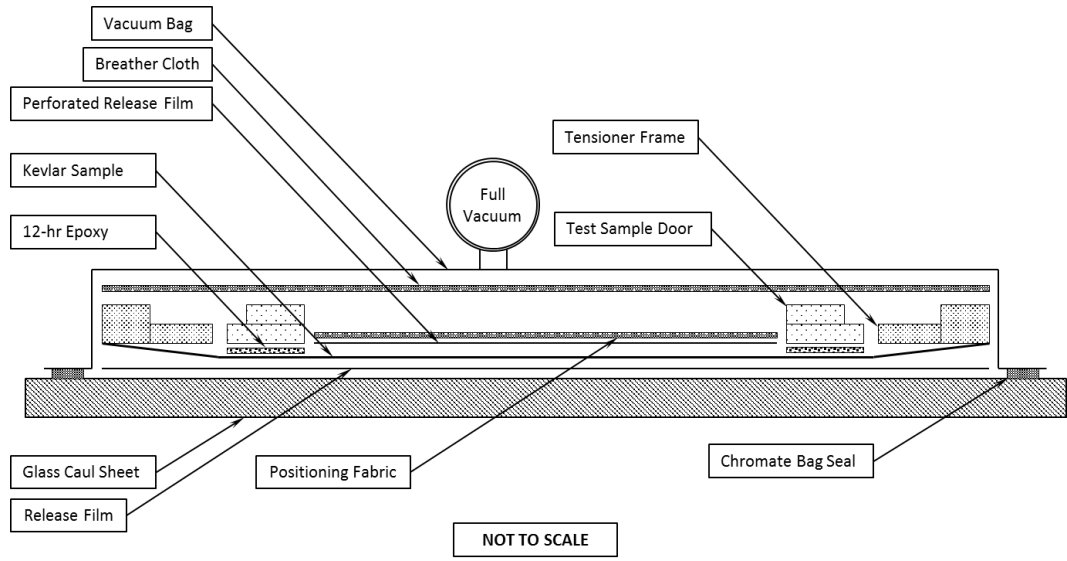
Figure 28. Layup template for bonding tensioned Kevlar® sample specimen door panel assembly using general purpose epoxy cured under 22 in-HG of vacuum at room temperature
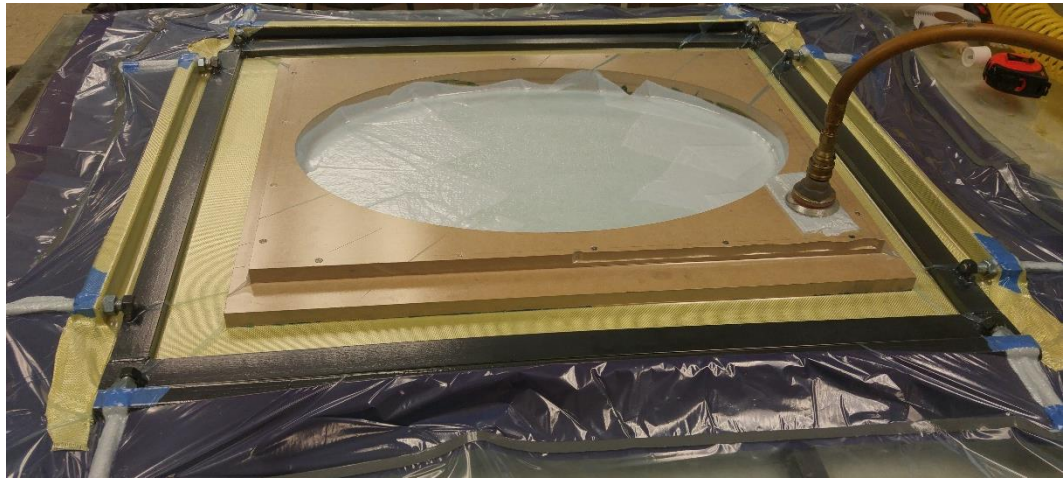
Figure 29. Validation specimen under tension during bonding procedure

3.4.3.5 Specimen Tension Device

Specimen tension for the Kevlar® panels used in the NASA Ames[5] and Virginia Tech[6] wind tunnel conversion projects was maintained using a tension device integral to the tunnel wall. This design requires significant design consideration to house and fair the tension frame device during wind tunnel operation. Since the final windscreen design for UAV acoustic sensing will ideally not require high tension, it is not desired to incorporate a tensioning device into the quiet box apparatus. Instead of the integrated tension frame device, the validation specimen door was designed to have the specimen bonded to the specimen door panel under tension. The adhesive system and door panel bear the tension loads from the specimen material. To achieve the required tension in the material, a tension frame was constructed. The frame utilizes ridged steel extrusions to minimize mid-span deflection while loaded. The fame is constructed from 1-inch by 0.5-inch "C" extrusions which are butt-joint welded at the junctions. 1/2 -13 threaded nuts were welded to the lower surface of the frame and 6-inch-long sections of threaded rod were inserted, which serve as lead screws for tensioning of the sample. Heavy walled (0.13-inch-thick walls) square tubing was used to create the sample attachment points. A heavy wall was necessary to reduce the amount of mid-span deflection generated while the sample is under tension to reduce the amount of non-uniform strain in the sample. An additional tensioning nut was added to each lead screw to adjust the sample tension. Sample attachment is accomplished by using heavy duty adhesive tape to secure the material to the bar, then rolling the sample over on itself several times. Reference **Figure 30** for tension frame schematic.
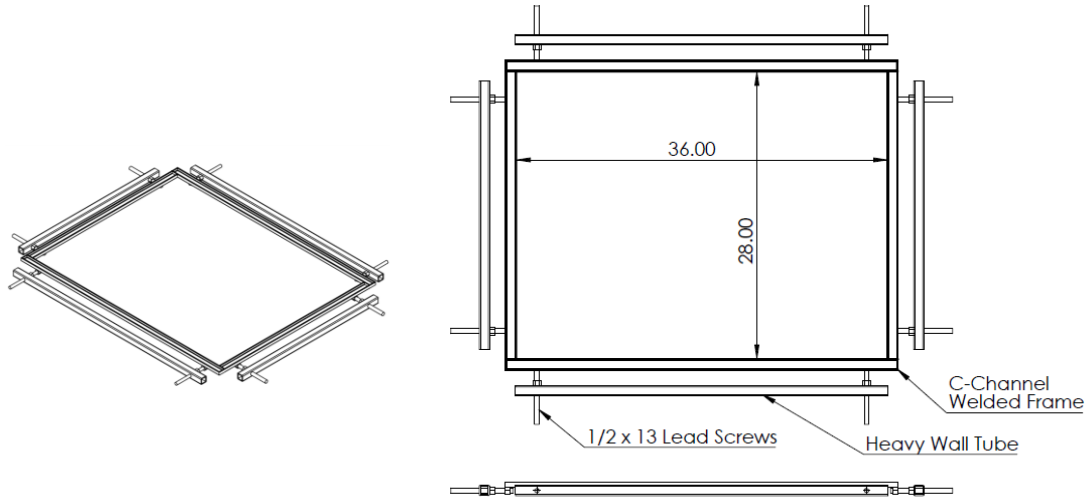
Figure 30. Kevlar® test specimen tension frame schematic used in fabrication of validation specimen door (all dimensions are shown in inches)

It is ideal to maintain a uniform strain in the Kevlar® membrane. Since the specimen length is greater than its width, it is necessary to deflect the membrane more along its length than its width by a ratio of 9:7. The specimen's short sides were mounted to the frame first, and the slack was taken up using the lead screws. The screws were tightened one half turn at a time, alternated between the four screws that control tension along the specimen's short side, until the membrane appeared sufficiently well tensioned to prevent flapping in turbulent flow. The number of turns of the lead screws were counted. After the short side had been fully tensioned, the long side was attached to the tension bars. This was done to prevent the membrane from bunching up along the long side tension bars while the short side was tensioned. The long side was tensioned in the same way as the long side, alternating between lead screws, except that the long side was deflected less to maintain bi-directionally symmetric strain, as discussed above. Reference **Figure 31** for photographs of tensioned Kevlar® specimen held by tension frame.
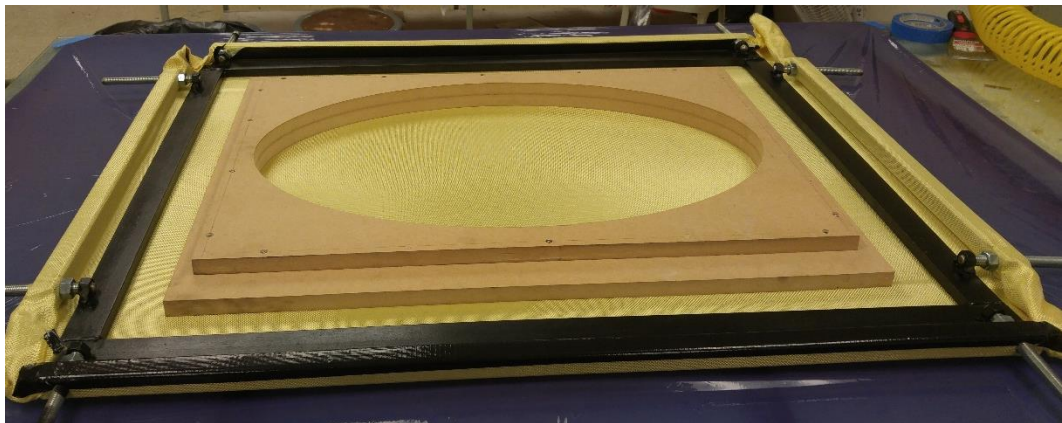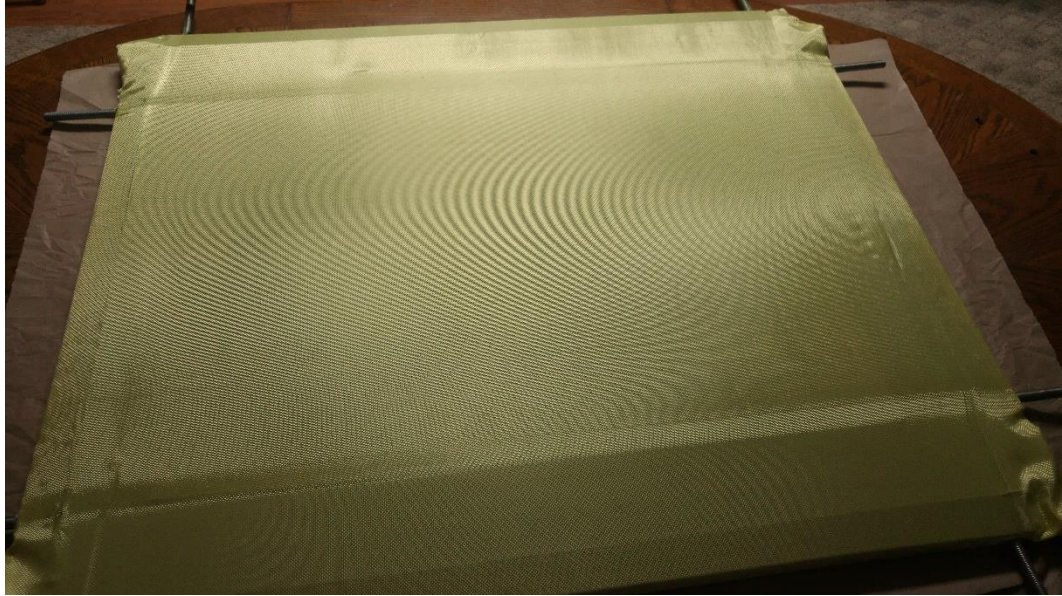
Figure 31. Photograph of tension frame with Kevlar® specimen mounted under tension (top) and specimen door assembly test fitted prior to bonding (bottom)

3.4.3.6 Comparative Tension Measurement

To achieve a degree of repeatability for the experiments conducted herein, it is necessary to verify any new validation samples created are tensioned to the same level as the original sample. Since no direct membrane tension levels are provided by the comparison study[5], the specimen membrane used in the current study was tensioned sufficiently to maintain a stable aerodynamic surface. Direct tension measurements were not captured. Instead, a comparative tension measurement system was devised. This method utilizes a measurement fixture to locate seventeen (17) locations where a weighted rod is used to deflect the tensioned membrane. The center deflection measurement is located at the center point of the elliptical membrane, and measurement locations 1, 3, 5, 9, 13, 15, and 17 align with the ellipse long axis centerline (reference **Figure 32**). The weighted rod passed through the measurement fixture and deflects the membrane below. The deflection is measured at each location to an accuracy of at least ±0.005 inches. The weighted rod is fabricated from 0.25-inch-diameter steel bar which has a 0.25-inch radius on one end. A 2.0-pound weight is balanced on the top of the rod. The weight of the rod assembly was adjusted to provide a measurable amount of membrane deflection. The total weight of the rod assembly is 2.240 pounds (combined weight of the rod, adapter, and weight). Reference **Figure 32** for measurement fixture and deflector rod schematics.
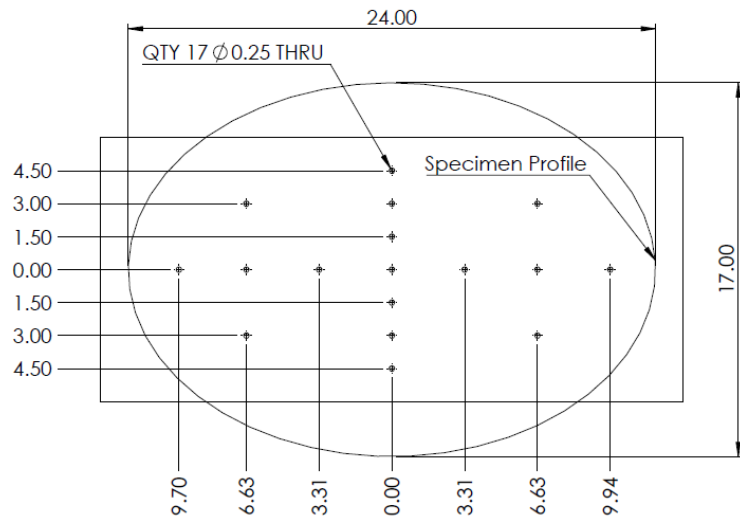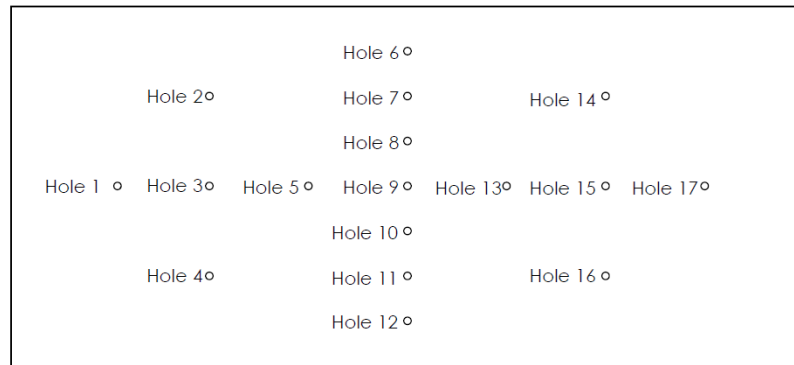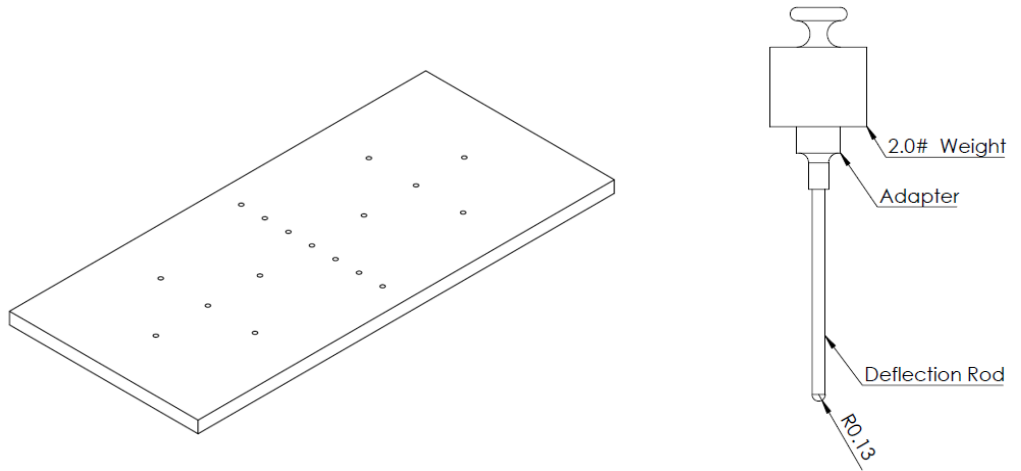
Figure 32. Specimen door membrane comparative tension measurement system

In the un-bonded state, the tensioned specimen deflection will be the result of strain over a distance spanning the length of the tension frame. The deflection induced strain will not be spread over the same distance after the specimen has been bonded to the specimen door panel which will cause the deflection measurement should vary between the bonded and un-bonded conditions. Therefore, deflection measurements are recorded before and after bonding. The recorded deflection measurements for the pre-cure and post-cure conditions are presented in **Table 7**. A mistake in the bagging procedure occurred during the cure of the specimen which caused the specimen membrane to be temporarily unsupported while under direct vacuum. This caused the membrane to strain more on one side than the other, resulting in asymmetric tension on the bonded sample. While this defect may affect test results, the effects are believed to be negligible. The sample was used for testing and no additional material was available for fabrication of a new sample.

Table 7. Pre-bond and post-bond specimen door deflection measurement data

Hole No.		1	2	3	4	5	6	7	8	9	10	11	12	13	14	15	16	17
Pre-Bond	Calibrated Deflection (Inch)	0.27	0.28	0.32	0.32	0.31	0.09	0.17	0.27	0.34	0.34	0.31	0.23	0.25	0.23	0.22	0.24	0.18
Post-Bond		0.41	0.22	0.48	0.56	0.50	1.15	0.23	0.36	0.45	0.53	0.58	0.50	0.43	0.19	0.38	0.45	0.30

3.4.4   Method to Characterize STL of Candidate Windscreen

The goal of the test procedure developed herein is to establish a reasonably simple means to characterize a candidate windscreen's ability to transmit normal incidence sound while assessing the level of noise generated by a grazing flow over the windscreen material. Transmission loss is measured in a manner similar to the two-room method addressed in SAE J1400[8]. This method utilizes a full scale anechoic chamber adjacent to a full scale reverberant chamber. A sample is mounted in a pass-through window between the two chambers. An acoustic source is placed in the reverberant chamber so that semi-omni-directional sound will impinge on the test sample. Microphones are placed in the reverberant chamber and in the anechoic chamber (reference **Figure 33** for two-room method facility schematic).
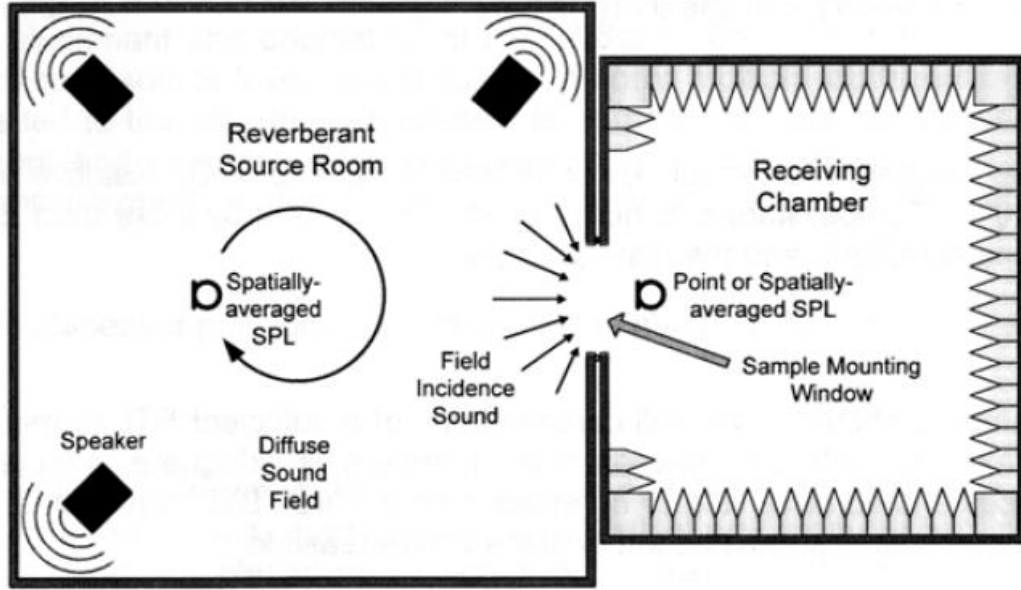
Figure 33. Two-Room method schematic presented in SAE J1400 for facility to measure STL of a material sample[8]

A correction for background noise is applied to the signals from each chamber in accordance with(18[8].

$$L_S = 10 \log_{10} \left(10^{\frac{L_C}{10}} - 10^{\frac{L_B}{10}} \right)$$

(18)

$Where$:
$L_S = corrected\ SPL\ of\ the\ signal, dB$
L_C
$= SPL\ of\ the\ signal\ and\ background\ noise\ combined, dB$
$L_B = SPL\ of\ the\ background\ noise\ alone, dB$

Corrections are only applied when the difference between the combined background noise and signal and the background noise only signal (L_C-L_B) at each frequency is less than 15 dB. If the difference is less than 5 dB, a constant reduction of 1.3 dB is used instead. For the test method developed herein, the background noise only signal is measured with the validation specimen door in place, but no tunnel flow or acoustic signal generated by the tunnel source speaker. The combined signal is measured with tunnel flow on and/or acoustic source signal generated. The MNR

(Measured Noise Reduction) of the specimen under test is computed using **Equation (**19 where SPL$_f$(source room) is the background noise corrected signal, as computed by **(18)**, from the ½-inch pylon mounted in-flow microphone with the bullet nose cone installed, and SPL$_f$ (receiving room) is the averaged and background noise corrected signal obtained by the two adjacent 1/2-inch condenser microphones mounted within the quiet box environment.

$$MNR_f = SPL_f(source\ room) - SPL_f(recieving\ room) \tag{19}$$

The specification outlines the fabrication of a reference standard sample which is installed in the pass-through window and used to calibrate the system. A statistically robust sample pool of STL test data for the reference standard based on testing at multiple laboratories is provided in the specification as well. To calibrate a new STL test facility, the reference standard sample is fabricated and tested. A calibration factor is computed per **Equation (**20 by subtracting the provided reference STL$_f$ for the calibration standard from the MNR$_f$ measured for the calibration standard. An acceptable correction factors range is specified as +10/-0 dB for a well-implemented system and +15/-0 dB for a typical system. If the correction factor exceeds +15/-5 dB, steps should be taken to improve the facility. This calibration factor is then applied to all future STL measurements performed using the facility.

$$C_f = MNR_f(reference) - STL_f(reference) \tag{20}$$

This calibration factor is applied to future MNR spectrum measured using the facility per **Equation (**21. This calibration procedure should be accomplished periodically, and any time significant modifications are made to the facility.

$$STL_f(sample) = MNR_f(sample) - CF_f \tag{21}$$

The power spectrum is compared between the microphone(s) located in the reverberant chamber and those located in the anechoic chamber. The difference in sound pressure level (SPL)

from the source room (reverberant chamber) and the receiving room (anechoic chamber) is the uncorrected sound transmission loss (STL) [8].

The STL measurement method presented in this study is similar to that presented in SAE J1400[8], except with the following variations. The chamber volume available for both the source and receiving rooms are significantly smaller than recommended. Additionally, the wind tunnel test section is hard walled and reflects sound well; however, the environment is not truly reverberant due to the sharp corners and non-uniform construction materials. The result is an environment that likely has highly varied local sound pressure levels caused by standing wave nodes and anti-nodes. Optimization of microphone placement within the source room (wind tunnel test section) is critical to the integrity of this system. This is addressed in detail in a subsequent section.

The purpose of this study is not to accurately measure STL of a windscreen, but rather to generate qualitative and comparative data by which candidate windscreens can be evaluated. It is not necessary to the current scope of work to invest effort in accurate calibration; therefore, reference data generated in a study conducted in a large wind tunnel is used in place of the reference standard suggested in SAE J1400[8]. The reference data used herein was generated in the large wind tunnel at the NASA Ames Research Center[5]. This study used a 1.8 oz./yd^2 Style-120 plain weave Kevlar® tensioned over a large window between the wind tunnel test section and an anechoic environment used to house a microphone array. No data is provided regarding the level of tension of the sample during the test. It should also be noted that differences in the sizes of the chambers available at NASA Ames and those available for the present study will impact the STL measured for the samples. As a result, the data presented in Jaeger, et. al.[5] is used only as a comparison rather than a statistically robust reference standard to calibrate the proposed system. The reference data was extracted from Jaeger, et. al. [5] is presented in **Figure 34**.
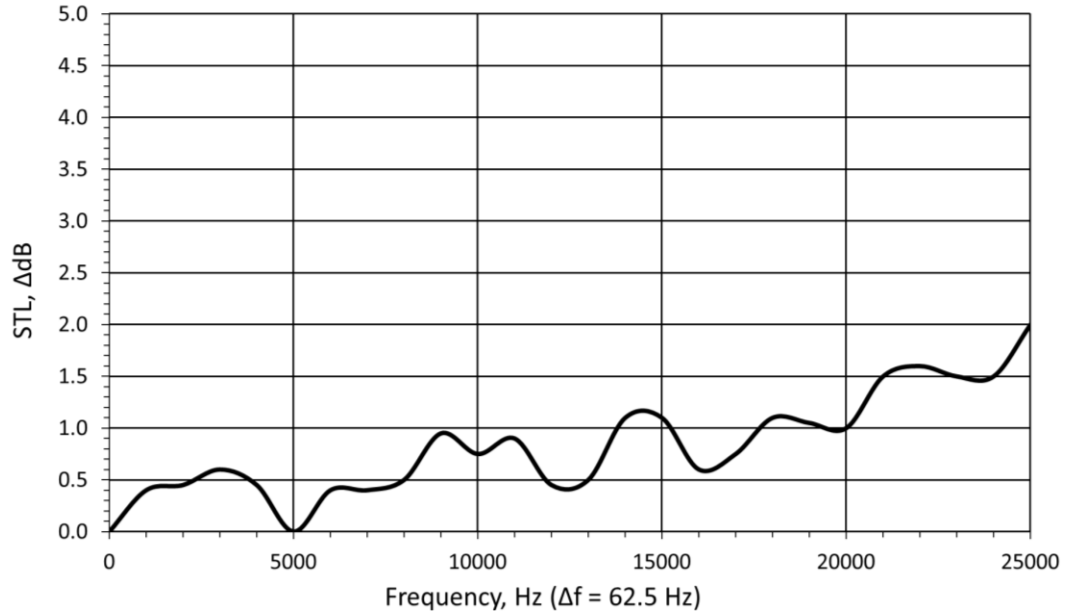
Figure 34. Reference sound transmission loss data for tensioned 1.8 oz./yd^2 Style-120 plain weave Kevlar® measured at NASA Ames Research Center as presented in Jaeger, et. al. [5]

3.4.5 Method to Characterize Self-Induced Hydro-dynamic Noise Increase

Virginia Polytechnic Institute retro-fitted the Blacksburg stability wind tunnel facility into an aero-acoustic test facility in a similar manner to the conversion at NASA Ames Research Center, as presented in Jaeger, et. al.[5] This test facility is intended to take accurate acoustic measurements of objects in the flow; therefore, a comparison of various wall treatments was made by testing each treatment over multiple flow speeds. The overall A-weighted sound pressure level was computed at each flow speed, then plotted against data provided from other established acoustic wind tunnels. The results presented in Carmargo, et. al.[6] are shown in **Figure 35**. Note that some of the acoustic wind tunnels shown in **Figure 35** are open section acoustic tunnels and do not include acoustically transparent test section walls[6].
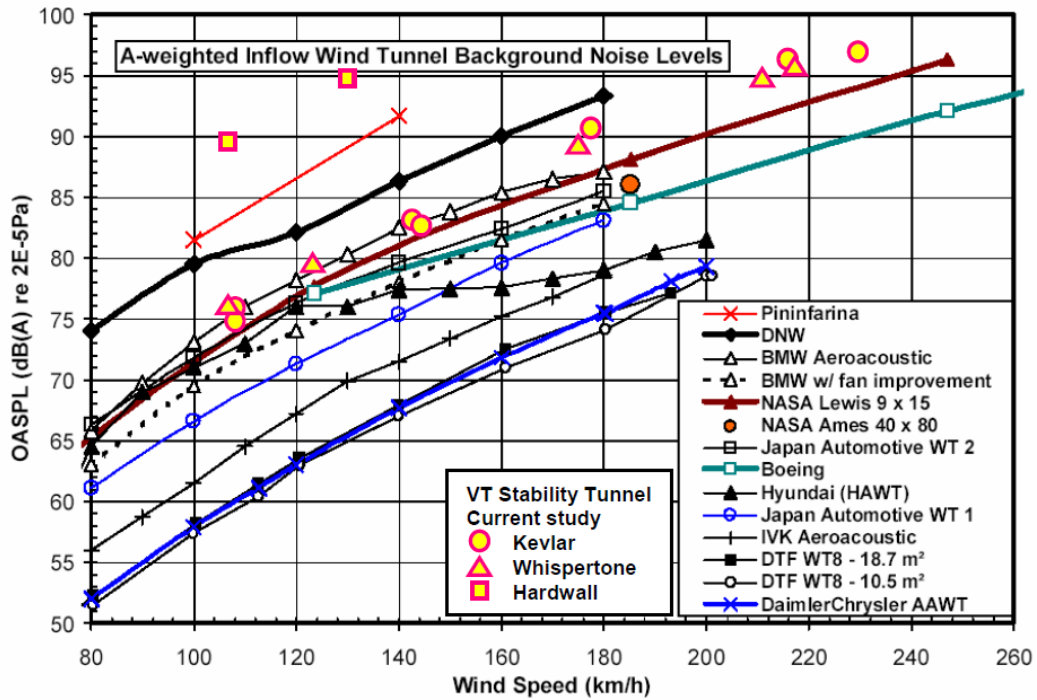
Figure 35. A-weighted in-flow noise levels as a function of flow speed for various acoustic wind tunnel facilities including Virginia Tech, as presented in Carmargo, et. al. [6]

The measurement method described in Carmargo, et. al.[6] utilizes an in-flow microphone placed close to the tunnel treatment being studied. The characterization procedures under development make measurements using two different methods and compares the results to determine which method shows the most resolution. The first flow-induced noise measurement method is similar to that presented by Carmargo, et. al.[6] in that the OASPL noise increase caused by flow over the candidate wind screen is measured by an in-flow, pylon mounted microphone as seen in **Figure 36**. The OASPL is computed for the entire spectrum at four wind tunnel flow speeds. Each OASPL data point is plotted versus flow speed, then compared to the measurements for the "clean" or plug door configuration. The results are compared to determine the increase in self-induced hydrodynamic flow noise. The method presented herein varies from that of Carmargo, et. al.[6] by omitting the application of the A-weighting filter. A-weighting is a method of filtering which gives preference to tones favorable to human hearing. Since comparison to previous test data is not

relevant to making qualitative measurements of candidate windscreens, there is no need to apply this filter to data collected in this test. The second method uses two microphones installed flush in the wind tunnel test section floor (reference **Figure 37**). One is located upstream, and the other downstream of the specimen door. Since these microphones are placed on the tunnel floor and within the boundary layer, hydrodynamic pressure fluctuations detected more readily than with the bullet microphone. Comparing the signals between the upstream and downstream microphones will provide a qualitative measurement of the increase in flow turbulence intensity created by the presence of the windscreen. Both methods are tested and compared to determine which can more effectively detect changes in self-induced flow noise. Note that the pylon microphone assembly used for other test procedures is removed during the flush mounted microphone tests.
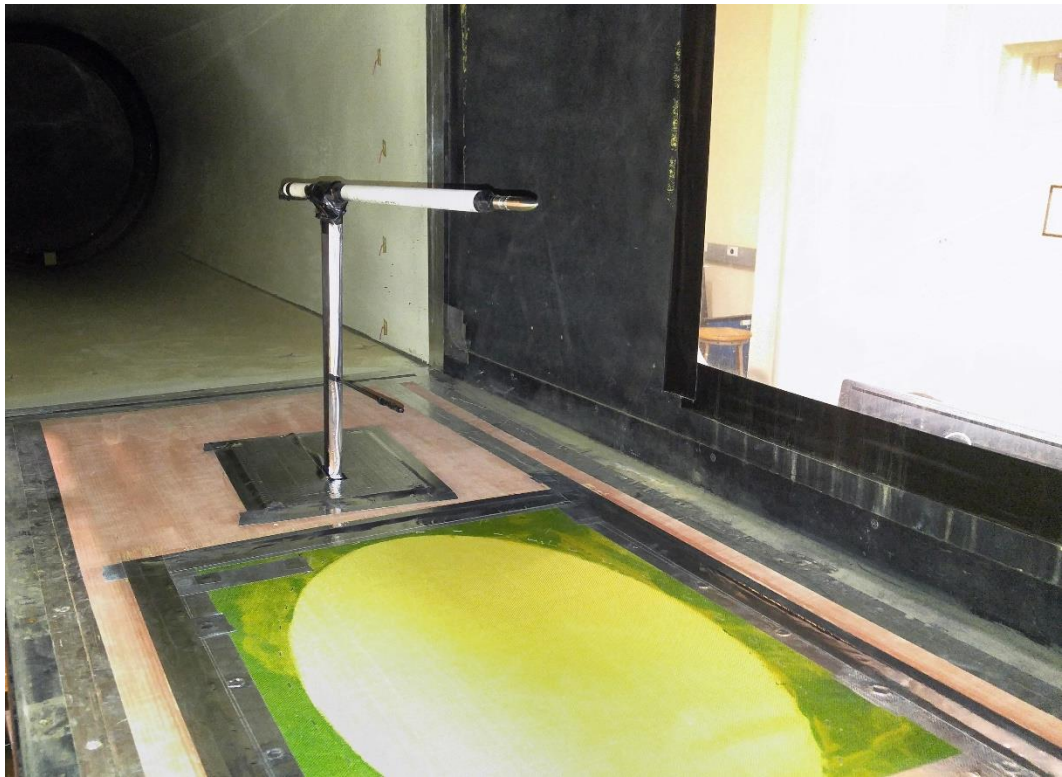
Figure 36. Pylon mounted microphone with bullet nose cone fairing used in flow-on wind tunnel OASPL testing

Figure 37. Forward and aft flush mounted microphone locations in wind tunnel test section floor used for boundary layer turbulence increase measurements

3.4.5.1 Bullet Nose Cone Validation

Originally, testing was accomplished with a 1/4-inch GRAS flush microphone. Upon reviewing the preliminary results, it was determined that the noise floor of this microphone was not sufficiently low to provide adequate spectral data. As an alternative, a 1/2-inch condenser microphone was flush-mounted into the test section floor ahead of the test specimen. This system provided better results; however, it was suspected that a large portion of the signal recorded by the microphone was caused by hydrodynamic pressure fluctuations in the boundary layer and wake shedding caused by the microphone's protective grill. A GRAS brand 1/2-inch bullet nose cone (reference **Appendix C:Microphone Equipment Datasheets** for microphone and nose cone datasheets) was obtained, and a pylon mount was fabricated. The pylon consists of a symmetric airfoil wood pylon mounted to a metal plate base. A length of PVC pipe forms a hollow boom to hold the microphone at the proper location. A flow-on test was conducted with both a 1/2-inch flush mounted condenser microphone located directly upstream from the test specimen and a 1/2-inch condenser microphone equipped with the bullet nose cone mounted on the pylon at 9 inches aft of the test specimen center point, and 9 inches above the floor plane of the test section. The frequency spectrum recorded during this test for both microphones is shown in **Figure 38**. It can

be seen that the signal amplitude measured by the flush mounted condenser microphone is higher than that of the pylon mounted bullet nose microphone. It is assumed that this difference is caused by the increased hydrodynamic noise detected by flush mounted condenser microphone; therefore, the bullet microphone was used as the primary tunnel microphone for this study.
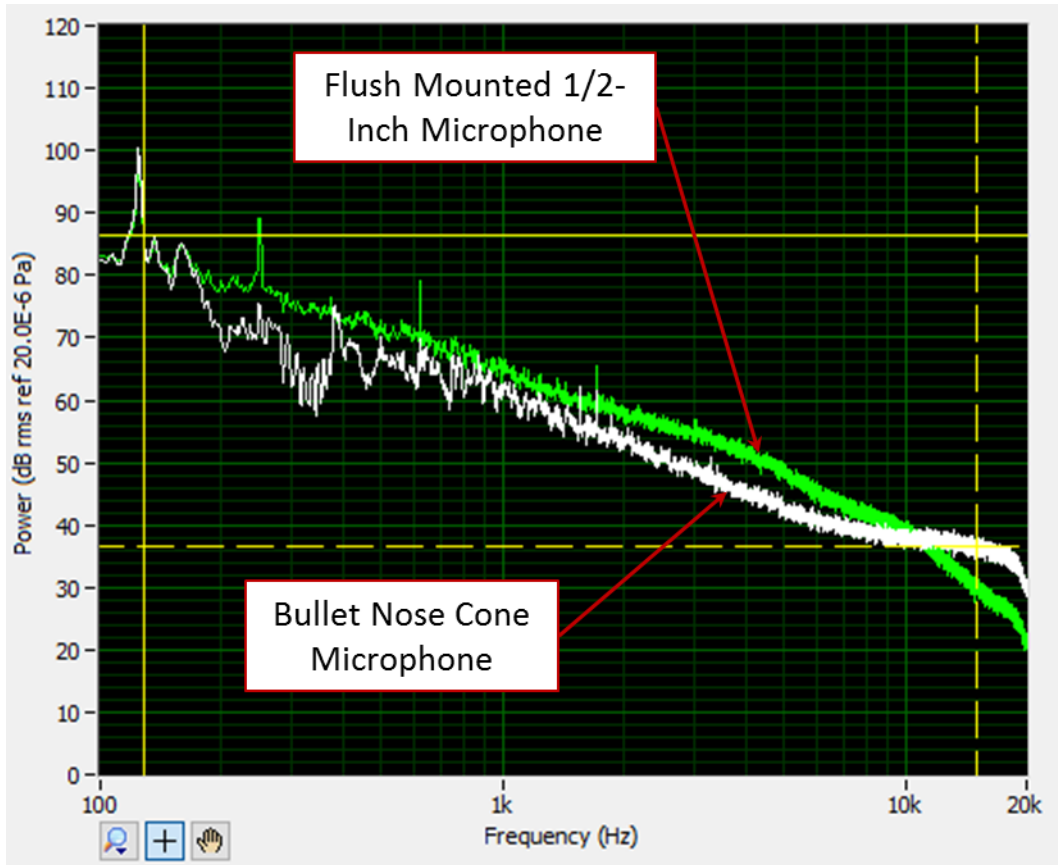
Figure 38. Flow-on (81 ft/s free-stream velocity) frequency spectrum comparison between flush mounted 1/2-inch condenser microphone and pylon mounted 1/2-inch condenser microphone equipped with bullet nose cone (Plug door installed in pass-through window)

3.4.5.2 Microphone Position Optimization

As mentioned previously, the poor reverberant quality of the wind tunnel test section is likely to cause a standing wave phenomenon where nodes and anti-nosed exist in close proximity. Preliminary testing revealed a high, possibly periodic variation in amplitude of STL as a function of frequency (reference **Figure 39** for plot showing STL amplitude variation). The STL of

unstiffened light weight Kevlar® does not exhibit this periodic trait in any of the previous studies (Jaeger, et. al.[5], and Carmargo, et. al.[6]) used as reference for this study; therefore, this phenomenon is assumed to be a condition caused by a physical attribute of the testing apparatus. In an attempt to reduce this variation, the position of the test section in-flow microphone was optimized. This optimization was accomplished by stretching a single monofilament fishing line in the wind tunnel test section over the quiet box pass-through window. A forward-facing microphone with bullet nose cone installed was attached to the fishing line and a single microphone was placed on a stand in the center of the quiet box. The specimen door was installed for this test. Microphone signal was recorded while white noise was generated from the tunnel speaker. Wind tunnel flow was not on for this test. Data was collected at 11 locations ranging from 15 inches ahead and 15 inches aft of the center of the specimen at 3 inch intervals. The sound transmission loss was calculated at each tunnel microphone location by subtracting the tunnel microphone signal from the quiet box microphone signal. The STL spectra for each wind tunnel microphone location were to the STL provided in Jaeger, et. al.[5]. The locations where these data points were closest to the reference spectrum occurred at locations 3, 6, and 9 inches aft of the specimen center point. The STL spectrum for these three locations was plotted. Trend lines computed based on a 100-point moving average were reviewed in lieu of the full narrow band data for better plot clarity. From these trend lines, it was observed that the location 9 inches aft of the specimen center point shows a reduced periodic tendency compared to the other locations (reference **Figure 39**).
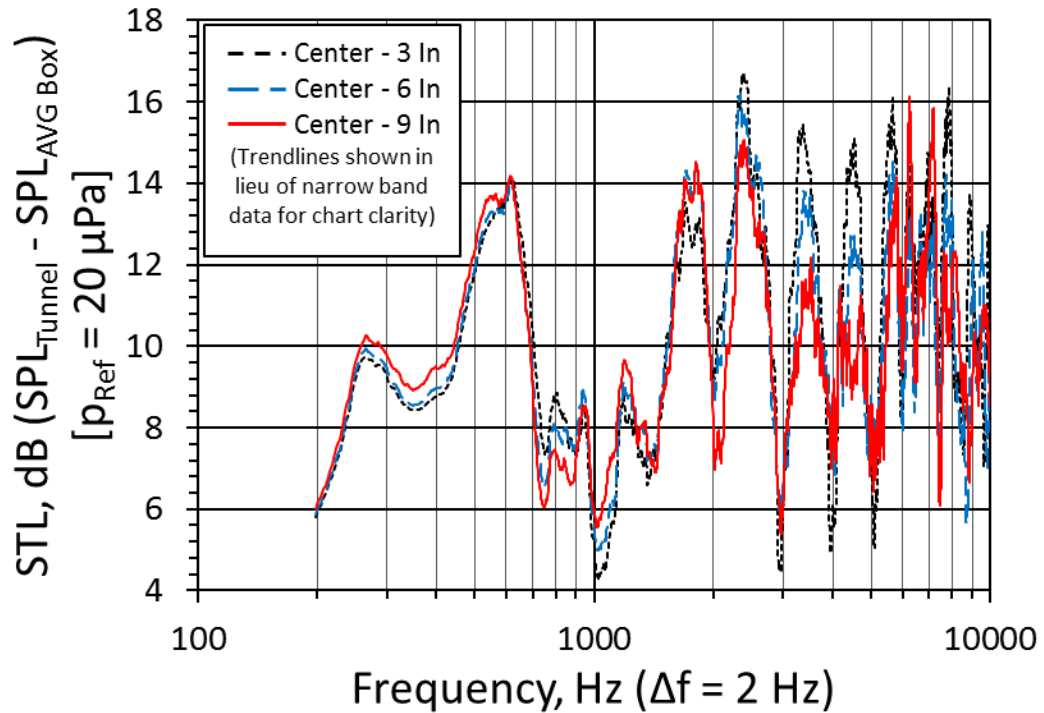
Figure 39. STL plot used to optimize position of tunnel microphone (with bullet nose cone installed). Testing performed white noise source, flow-off, and specimen door installed in pass-through window. 100 point moving average trendlines shown in lieu of narrow band data for clarity purposes.

3.4.5.3 Quiet Box Microphone Signal Variation

As seen in **Figure 39**, optimizing the position of the tunnel microphone alone did not sufficiently reduce the frequency dependent variation in the STL spectrum. To further reduce this phenomenon, the microphone placement within the quiet box was examined. Two microphones were installed to determine the effect of microphone directionality. However, it was noted that with both microphones diaphragms at the same angle and position, a variation between the two SPL spectra of up to 40 dB was occurring, even when only exposed to ambient noise. This difference in amplitude is extremely high, and seems unrealistic for two microphones in such close proximity. Both microphones were single point calibrated at the start of testing; therefore, diaphragm contamination and/or damage was initially suspected to play a role in the assumed faulty signal.

This possibility was ruled out by relocating all the test equipment (excluding microphone cables) to the full scale anechoic chamber at Oklahoma State University. The white noise test in the full scale anechoic chamber revealed a variation of less than 5 dB consistently across the spectrum, without the apparently periodic tendencies observed during identical testing within the quiet box (reference **Figure 40** for anechoic chamber microphone variation spectrum). The variation is assumed to be electronic background noise present within the measurement equipment since the variation is the same amplitude with, and without microphones attached to the cables.

Figure 40. Screenshot of variation between two identical microphones mounted with approximately 1/2 inch separation and coplanar diaphragms. Testing conducted in full-scale anechoic chamber measured with the same equipment and white noise source used for quiet box measurements (excluding microphone cables).

The findings in the anechoic chamber ruled out a possible fault with equipment so it was reinstalled in the quiet box and further testing was accomplished. Peaks in the variation signal were noted at 60 Hz and 120 Hz, which is the alternating frequency and first harmonic of wall power (reference **Figure 41** for screenshot of signal interference without acoustic source). Investigation of the signal conductors used to connect the microphones to the data acquisition card revealed that one cable had become entangled with a recently installed laptop charger attached to unrelated equipment in the lab.

Figure 41. Screenshot of variation between two identical microphones mounted with approximately 1/2 inch separation and coplanar diaphragms. Testing conducted within quiet box environment with flow-off, ambient acoustic noise only, specimen door installed, and unintentional electronic interference with signal cable and intermittently faulty BNC cable connector.

The electro-magnetic interference from the laptop charger was resolved, and a faulty BNC type connecter was discovered and repaired in the quiet box. The tests were repeated without an acoustic source, and the results were found to be within the suspected electronic system noise range of ±5 dB observed in the full scale anechoic chamber testing. The microphone variation results are shown in **Figure 42**. This variation is considered to be acceptable for testing. Note that the wind tunnel test section microphone position optimization study was conducted prior to installation of the laptop charger which caused the EMI interference. Additionally, the quiet box microphone cable found to have a faulty connector was not utilized for that testing; therefore, it is assumed the wind tunnel test section microphone position optimization study was unaffected by these conditions.

Figure 42. Variation between two identical microphones mounted with approximately 1/2 inch separation and coplanar diaphragms. Testing conducted within quiet box environment with flow-off, ambient acoustic noise only, specimen door installed after unintentional electronic interference with signal cable and intermittently faulty BNC cable connector were corrected.

A white noise acoustic source was broadcast from the test section driver. With the specimen door installed, a seemingly periodic variation was observed between the two microphones. The cause of this variation is not fully understood, but is expected to be caused by the standing wave phenomenon resulting in frequency dependent nodes and anti-nodes located in close proximity, causing each microphone to read a difference signal amplitude. Microphone position was adjusted, but little change was noted. Reference **Figure 43** for signal variation under a white noise source with the specimen door installed, and the two quiet box microphones centered forward to aft, and left to right, at a height found to result in the least variation and mounted approximately 1/2 inches apart with their diaphragms coplanar. It should also be noted that the variation within the quiet box with the plug door installed was consistent with that measured in the full-scale anechoic chamber, further lending to the theory that the variation is a result of the direct impingement of the normal incidence source waves.
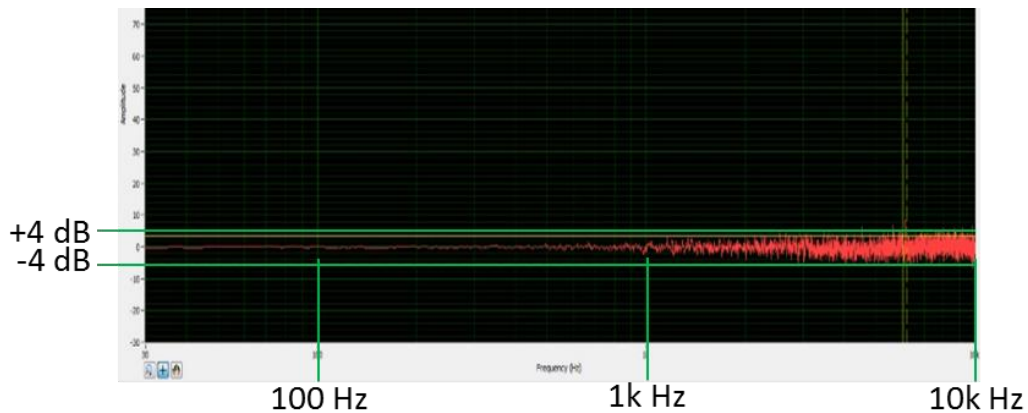
Figure 43. Variation between two identical microphones mounted with approximately 1/2 inch separation and coplanar diaphragms. Testing conducted within quiet box environment with flow-off, white noise acoustic source, specimen door installed.

The microphone variation for the no acoustic source, flow-on case was investigated since it appeared that the normal incidence source was common to all testing where a high level of microphone variation was observed. The highest speed case (59 ft/s) was chosen as the most extreme example. The microphone variation for the flow-on, acoustic source off case is shown in **Figure 44**. It is observed that the variation without the normal incidence source is insignificant, even with a significant level of flow noise.
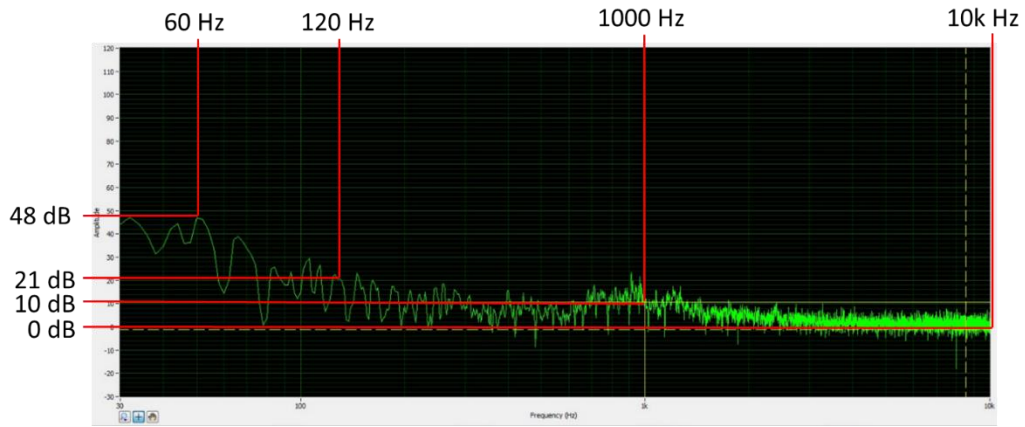
Figure 44. Variation between two identical microphones mounted with approximately 1/2 inch separation and coplanar diaphragms. Testing conducted within quiet box environment with flow-on at 59 ft/s, ambient acoustic noise only, specimen door installed after unintentional electronic interference with signal cable and intermittently faulty BNC cable connector were corrected.

Since it is suspected that the microphone variation is a direct result of normal incidence sound waves impinging on the quiet box, additional tests were conducted to determine if the source amplitude has an effect on the microphone variation. Two tests were conducted with identical setups, except the low amplitude test was conducted with the white noise source amplitude measured at the driver cables measuring 1.50 Volts (AC), and the high amplitude test was conducted at an amplitude measuring 1.9 Volts (AC). The frequency of predominant spikes was noted vary; however, the amplitude of variation remained approximately the same. It was concluded that the amplitude of the white noise has little effect on the level of variation between the two microphones. The low amplitude (1.5 VAC) microphone variation and spectrum measured in the wind tunnel by the bullet microphone are shown **Figure 45**, and the high amplitude microphone variation and spectrum measured in the wind tunnel by the bullet microphone are shown in **Figure 46**.
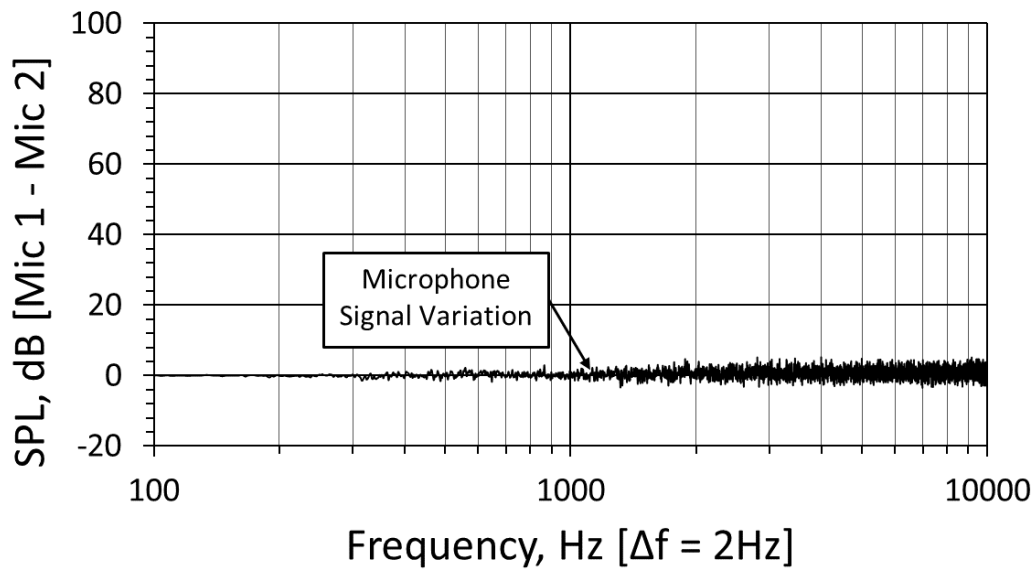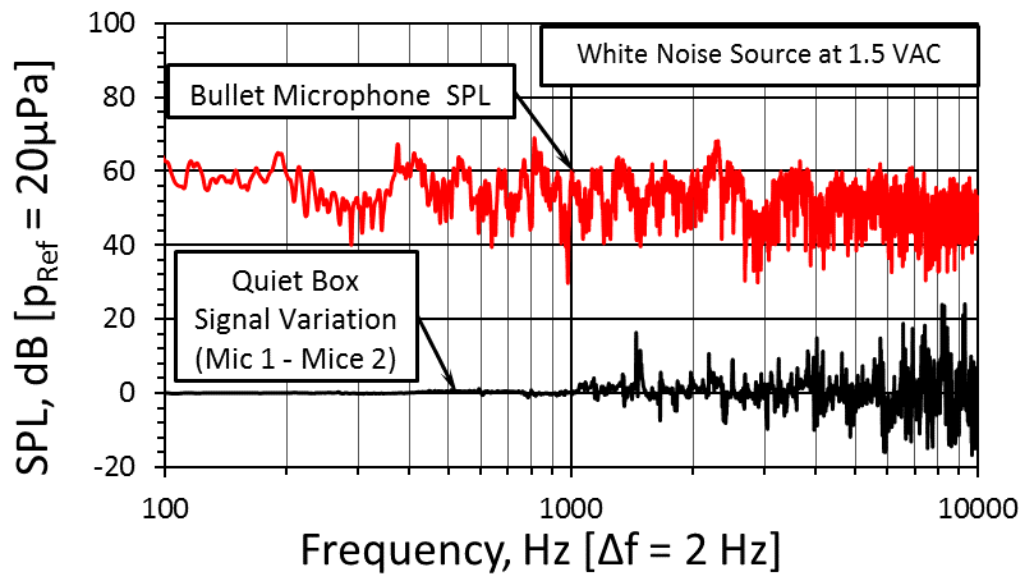
Figure 45. Variation between two identical microphones mounted with approximately 1/2 inch separation and coplanar diaphragms. Testing conducted within quiet box environment with flow-off, white noise source at 1.5 VAC, and specimen door installed.
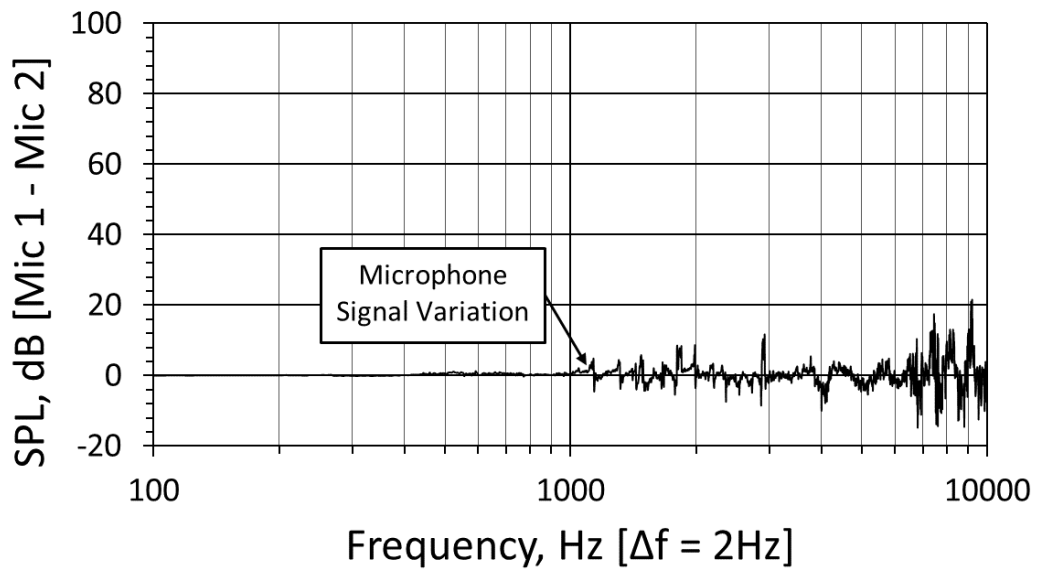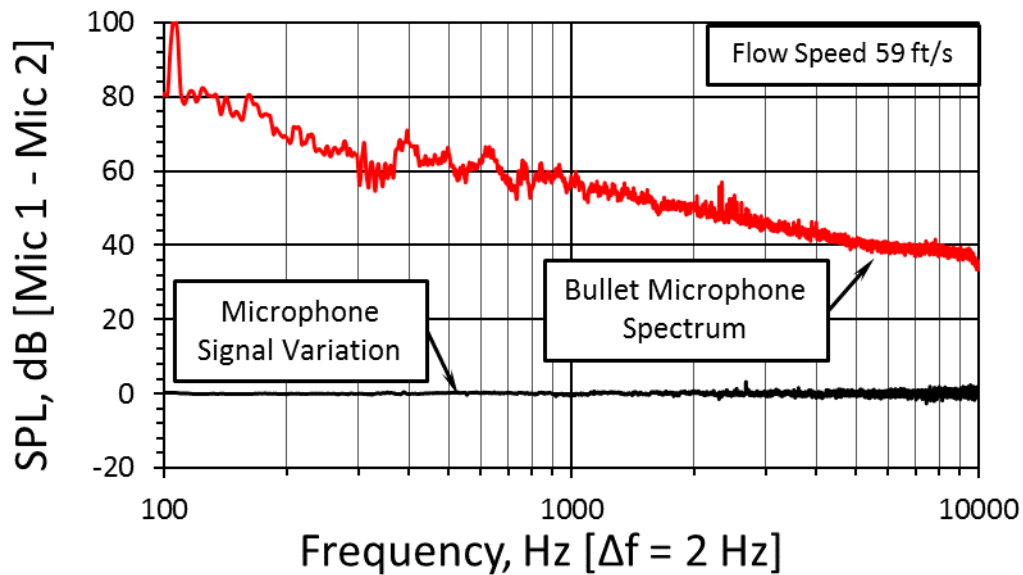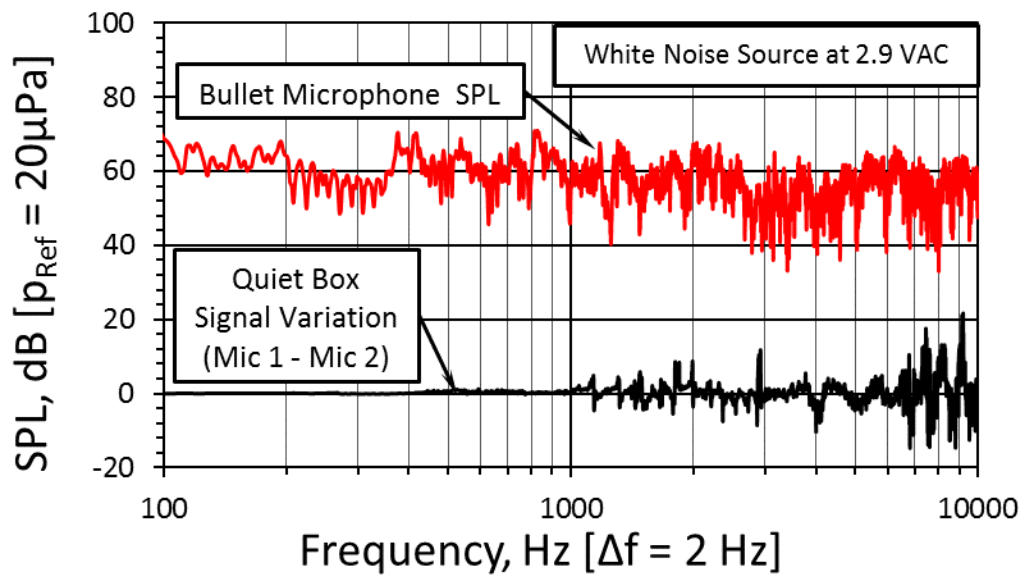

Figure 46. Variation between two identical microphones mounted with approximately 1/2 inch separation and coplanar diaphragms. Testing conducted within quiet box environment with flow-off, white noise source at 2.9 VAC, and specimen door installed.

For final testing, two microphones were used in the quiet box, and their signals were averaged. The white noise acoustic source was held a 2.0 Volts (AC), as measured between the speaker cables. The upper cutoff frequency for the testing was be reduced 1500 Hz to avoid any areas where signal variation is observed at an amplitude exceeding the ±5 dB electronic noise limit typical throughout the measurements. This revised upper cutoff frequency is acceptable since high frequency signals attenuate more in air than lower frequency signals. It is not likely that any naturally occurring avian or human generated source above 1500 Hz will have sufficient range to be detected from the air at a reasonable stand-off distance (reference **Figure 2** for plot of sound attenuation spectrum in standard atmosphere various stand-off distances).

3.4.6   Wind Tunnel Boundary Layer Survey

A boundary layer survey was conducted on the wind tunnel to determine boundary layer height and flow regime. A 1/4-inch traversing Pitot tube attached to an inclined water manometer was used to measure centerline flow velocity at multiple heights above the wind tunnel floor. The Pitot tube was located approximately 3-feet ahead of the leading edge of the quiet box pass-through window.

The traversing Pitot tube was used to set the wind tunnel flow speed instead of the permanently installed free-stream Pitot tube. This was done to avoid conducting a calibration of the free-stream Pitot tube and manometer. Once the flow speed was established and stabilized, the traversing Pitot tube was retracted to its lowest obtainable position (0.369 inches from the wind tunnel test section floor to the centerline of the pitot tube). Flow was measured accurate to 0.001 inches using a calibrated high-precision inclined water manometer. The traverse leadscrew was rotated one-quarter turn between each measurement point, resulting in a height increase of 0.25 inches. Measurements were taken on one-quarter inch intervals until free-stream velocity was achieved. At that point, several more data points were measured at one-half inch intervals, then one inch intervals until thoroughly out of the boundary layer. This procedure was repeated at four

different flow speeds, approaching the maximum tunnel speed. Note that the maximum tunnel speed achievable during the boundary layer survey is reduced compared to the flow-on acoustic testing due to an artificial fan speed limits applied at the time. Tests were conducted at 36.5, 41.3, 46.7, and 51.0 ft/s (corresponding to 0.30, 0.40, 0.50, and 0.60 in-H_2O). The boundary layer was measured to be between 1.60 and 1.90 inches thick throughout the flow speeds tested. The shape of the velocity profile exhibits characteristics of a laminar flow regime, as presented in Barlow, et. al.[18] Reference **Figure 47** for velocity profile of a laminar and turbulent boundary layer.
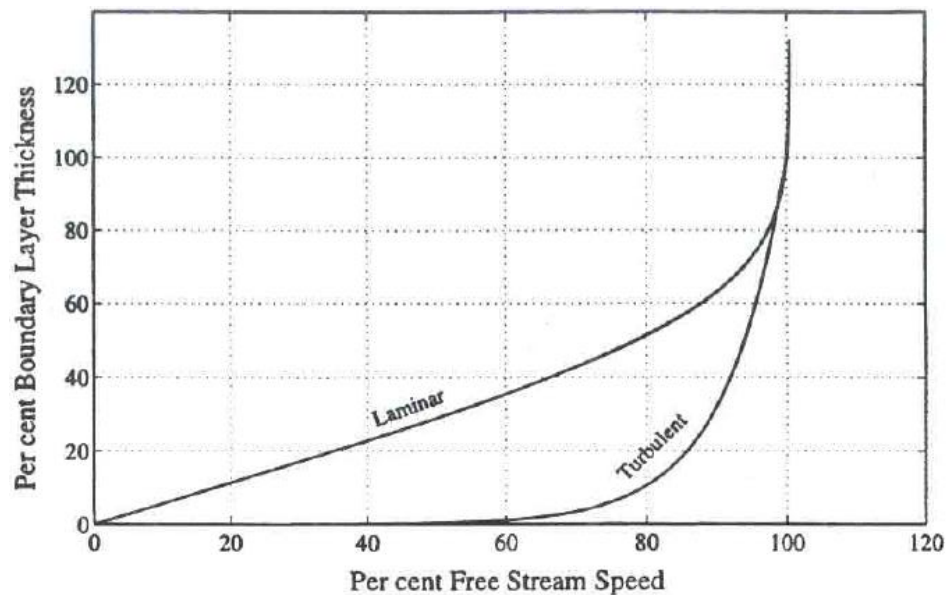
Figure 47. Velocity distribution in laminar and turbulent boundary layers, Barlow, et. al.[18]

The velocity profiles measured at free-stream velocities of 36.5 ft/s (denoted in the plot as "Low Speed") and 51.0 ft/s (denoted in the plot as "High Speed") are charted and shown in **Figure 48**. The laminar and turbulent boundary layer velocity profiles extracted from Barlow, et. al.[18] are superimposed with the measured velocity profiles for the speed extremes. The velocity profiles measured at each flow speed appear to more closely match the laminar velocity profile; however, it is not clear whether the boundary layer exists in laminar or turbulent state. The ambiguity between laminar and turbulent boundary layers could be the result of high levels of

free stream turbulence caused by obstacles in the flow path between the wind tunnel inflow well

and the wind tunnel collector section. Full graphical results from the boundary layer test are

resented in **Appendix E:**   **Boundary Layer Survey Results**.
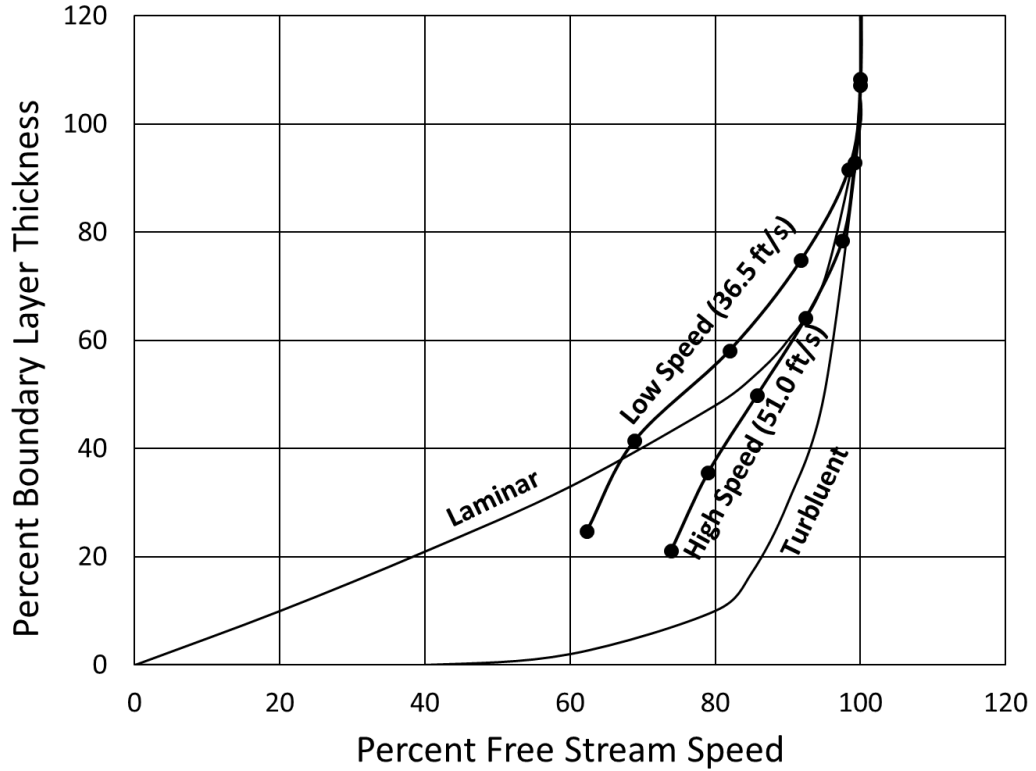
Figure 48. Velocity distribution of minimum and maximum flow speeds tested in boundary
layer survey of Oklahoma State University Low Speed Wind Tunnel with laminar and
turbulent boundary layer profiles extracted from Barlow, et. al.[18] superimposed.

CHAPTER IV

FINDINGS

The test procedures described in the preceding sections are designed to validate the experimental apparatus developed in this study and determine its usefulness for creating comparative data to evaluate candidate windscreen designs for applications in UAV acoustic measurements. Flow-off sound transmission loss (STL) testing results for the tensioned Kevlar® validation specimen door measurements are compared to data generated in a previous study[5], although the results are not expected to be an exact match due to variations in testing methods. The flow-on testing is expected to show a trend of increasing STL with flow speed due to increased boundary layer turbulence. Two methods are evaluated to measure the self-induced grazing flow noise generated by the installation of the tensioned Kevlar® validation specimen. The superior method will be recommended for use in comparing candidate windscreen designs.

4.1   Flow-Off Transmission Loss of Kevlar® Validation Sample

Flow-off testing is used to validate the test system apparatus constructed in this study by comparing the results to data for tensioned Kevlar® panels reported in Jaeger, et. al.[5]. For this testing, the specimen door was installed in the box and white noise was generated using the source driver installed in the upper wall of the wind tunnel test section at an amplitude of approximately 20 dB above the ambient (2.0 VAC, as measured on the at the amplifier output). The recording equipment used was as reported in **Section 3.4.2**. A recording was made for a duration of 30 seconds,

77

with 300 data point averages made. As required for noise reduction data processing procedure of SAE J1400[8] shown in **Equation** (18, a data recording was also made without the white noise. The ambient noise-only recording spectrum, as measured by the pylon mounted bullet nose cone microphone, is shown in **Figure 49**, and the white noise source recording spectrum is shown in **Figure 50**. A 30-point moving average trend line (approximating a sampling rate of $\Delta f = 60$ Hz) is also shown due to the high level of data scatter observed while exposed to the white noise source. It should be noted that the comparison STL data provided in Jaeger, et. al.[5] was recorded with a frequency resolution of $\Delta f = 62.5$ Hz; therefore, it is appropriate to use the 30 point moving average trend line for comparison. The white noise source shown in **Figure 50** has been corrected for background noise in accordance with the method presented in **Equation** (18.

Figure 49. Sound pressure level of averaged quiet box microphones and pylon mounted bullet nose cone microphone mounted in tunnel test section configured with Kevlar® specimen door and ambient tunnel noise only. (a) – Narrow band data, (b) – 30 data point moving average trendlines for chart clarity

The ambient noise only test shows a low level of scatter compared to the white noise source test. Note that the lowest sound pressure level that can be detected by the microphones used in this experiment is approximately 10 dB; therefore, any measurements below 10 dB will not be measured. The quiet box noise level reaches this minimum electronic noise floor SPL at approximately 1500 Hz, and the wind tunnel test section reaches it at approximately 3000 Hz. The

flow-off ambient environmental noise level in the wind tunnel cannot be detected beyond 3000 Hz

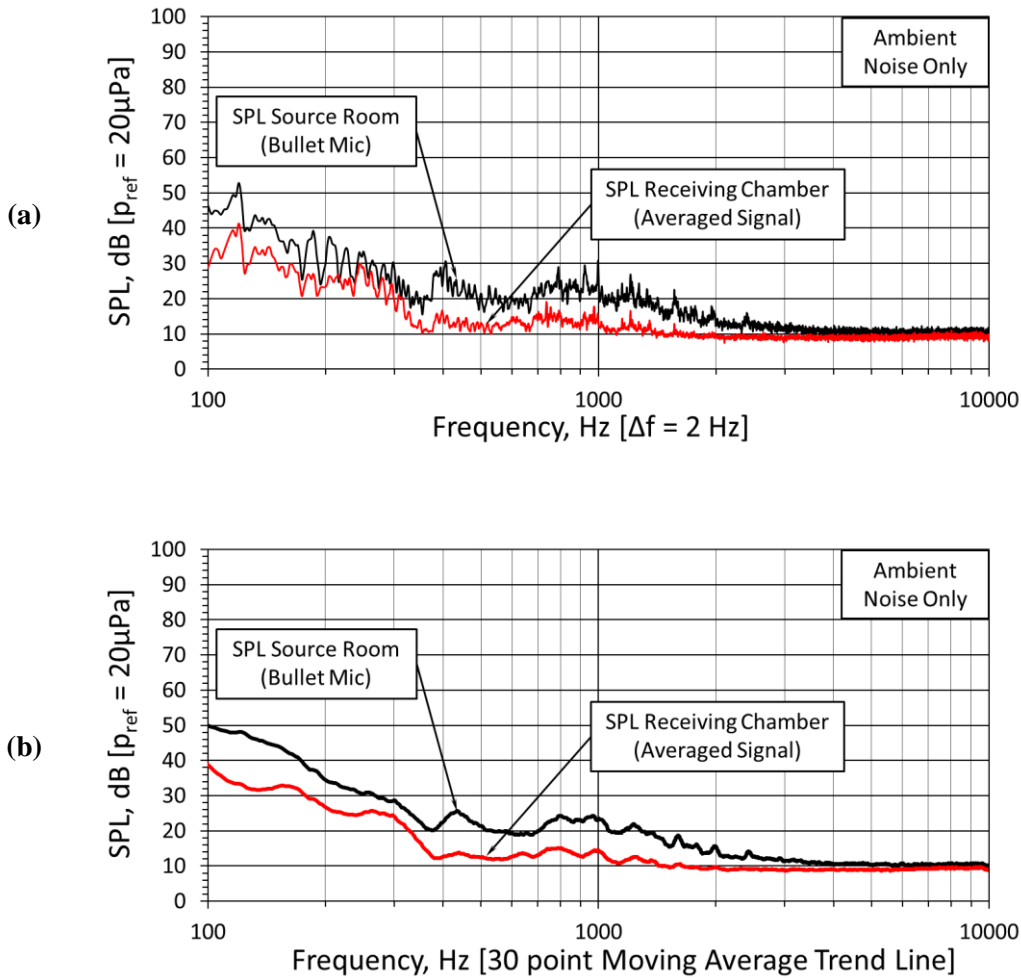without using more sensitive, and probably larger diaphragm microphones.
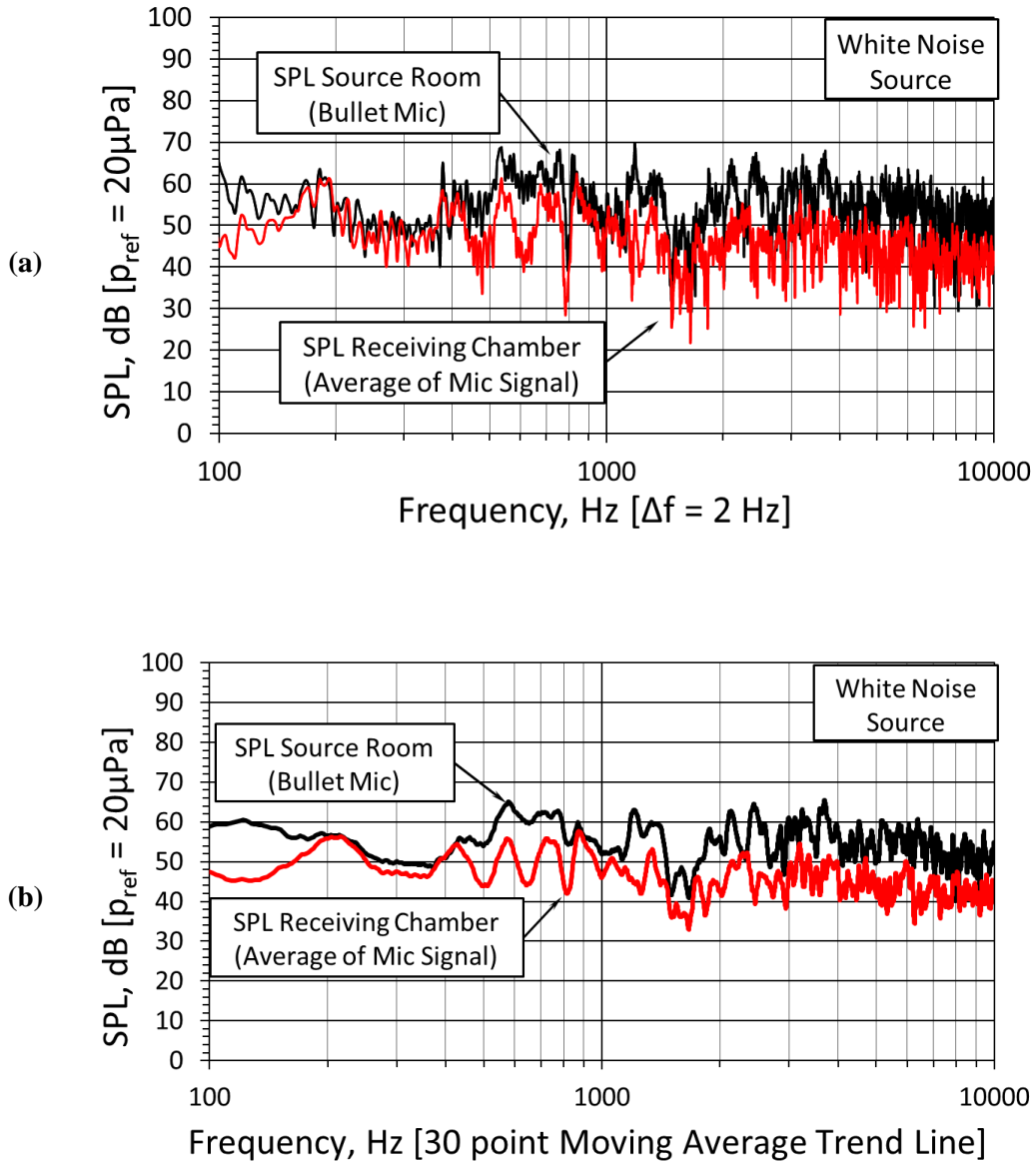
Figure 50. Sound pressure level with of averaged quiet box microphones and pylon mounted bullet nose cone microphone mounted in tunnel test section configured with Kevlar® specimen door and white noise source. (a) – Narrow band data, (b) – 30 data point moving average trendlines for chart clarity

Recalling the quiet box microphone variation shown in **Figure 42** and **Figure 43**, the ambient noise only test shows little variation throughout the entire spectrum. The white noise source test shows significant variation between the quiet box microphones at frequencies higher than 1500 Hz. The presence of significant STL variation above 1500 Hz in the white noise source test (**Figure 49**) is likely due to the quiet box microphone variation. The lack of this STL variation on the ambient noise-only test (**Figure 50**) is further evidence to this point. The spectrum measured in the quiet box and in the wind tunnel test section both show an increased SPL between 400 and 900 Hz. Using **Equation (14)**, the first 16 standing wave modes were calculated, and the frequencies were collected into 2 Hz bins. The bins were totaled and plotted, and it was noted that the highest concentrations of standing wave frequencies exist between 300 and 600 Hz. This analysis is based on a perfectly sealed, perfectly rigid and hard walled chamber, which is different than the test configuration as measured. The Kevlar® covered opening, compliant walls, and the foam wedges will cause the measured data to diverge from the analytical model. It is suspected that this concentration of standing wave frequencies could be partially responsible for the observed rise in measured SPL between 400 and 900 Hz.

The MNR$_f$ (Measured Noise Reduction as a function of frequency) was calculated using the noise reduction formula presented **Equation** (18)[8]. This is calculated by measuring the spectrum in the source room and the receiving room without the noise source (background noise only), then repeating the test with the noise source (combined background noise and source noise). The background noise only amplitude is subtracted from the combined background noise for each frequency bin. No correction is necessary for frequencies where the background noise is 15 dB or less below the source noise amplitude. Due to the amplitude of white noise used for this test, most bins do not require noise correction. Reference **Figure 51** for MNR$_f$ of tensioned Kevlar® specimen door.
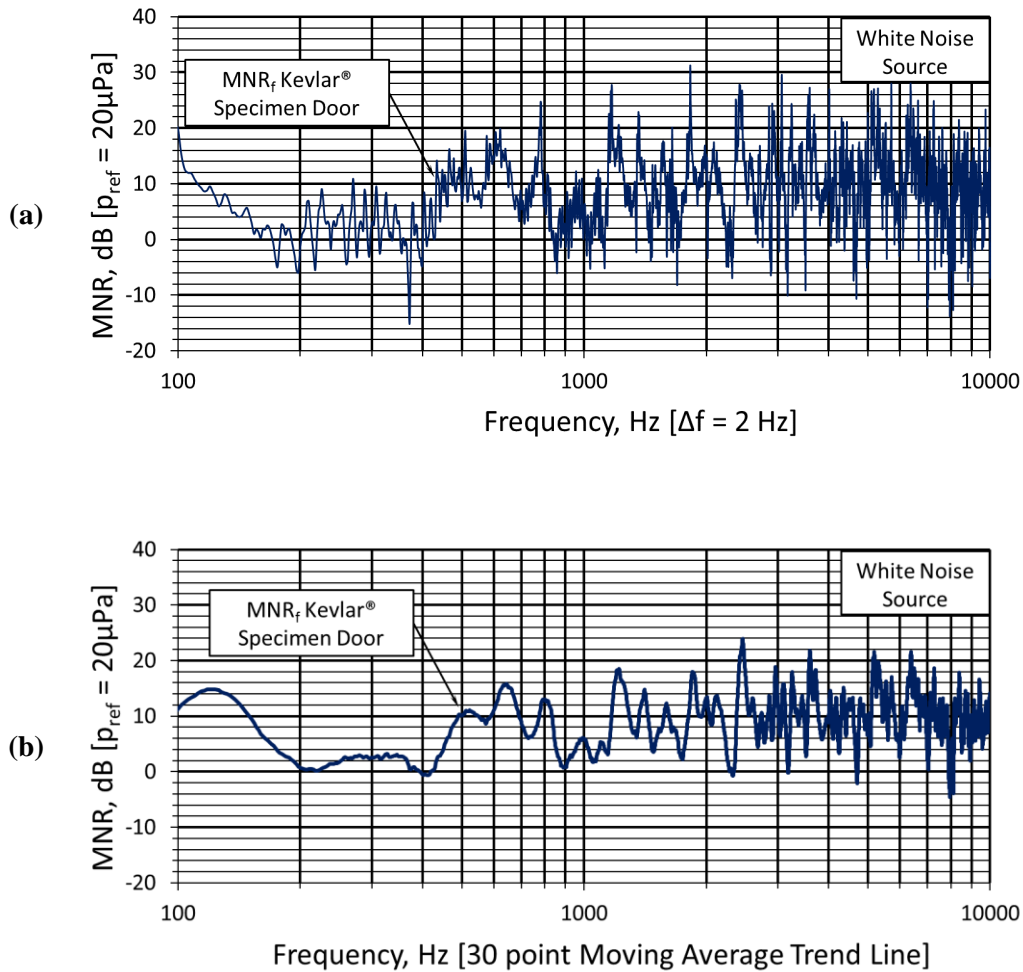
Figure 51. Measured Noise Reduction (MNR) of Kevlar® specimen door with white noise source. (a) – Narrow Band Δf = 2 Hz. (b) – 30 point moving average trend line

The STL (Sound Transmission Loss) spectrum for the ambient noise only case is shown in **Figure 52**. As with the SPL spectrum for the test section and the quiet box, the 30-point moving average trend line is presented in addition to the narrow band. For the test frequency range of 200 to 1500 Hz, the STL of the Kevlar® sample with ambient noise only ranges between 5 dB and 15 dB for the narrow band data. The trend line spectrum, which approximates a 60 Hz resolution, ranges from -1 dB to 10 dB. This is well within the correctable limits of +15/-5 dB established SAE J1400[8], when compared to the data for STL of a tensioned Kevlar® panel.
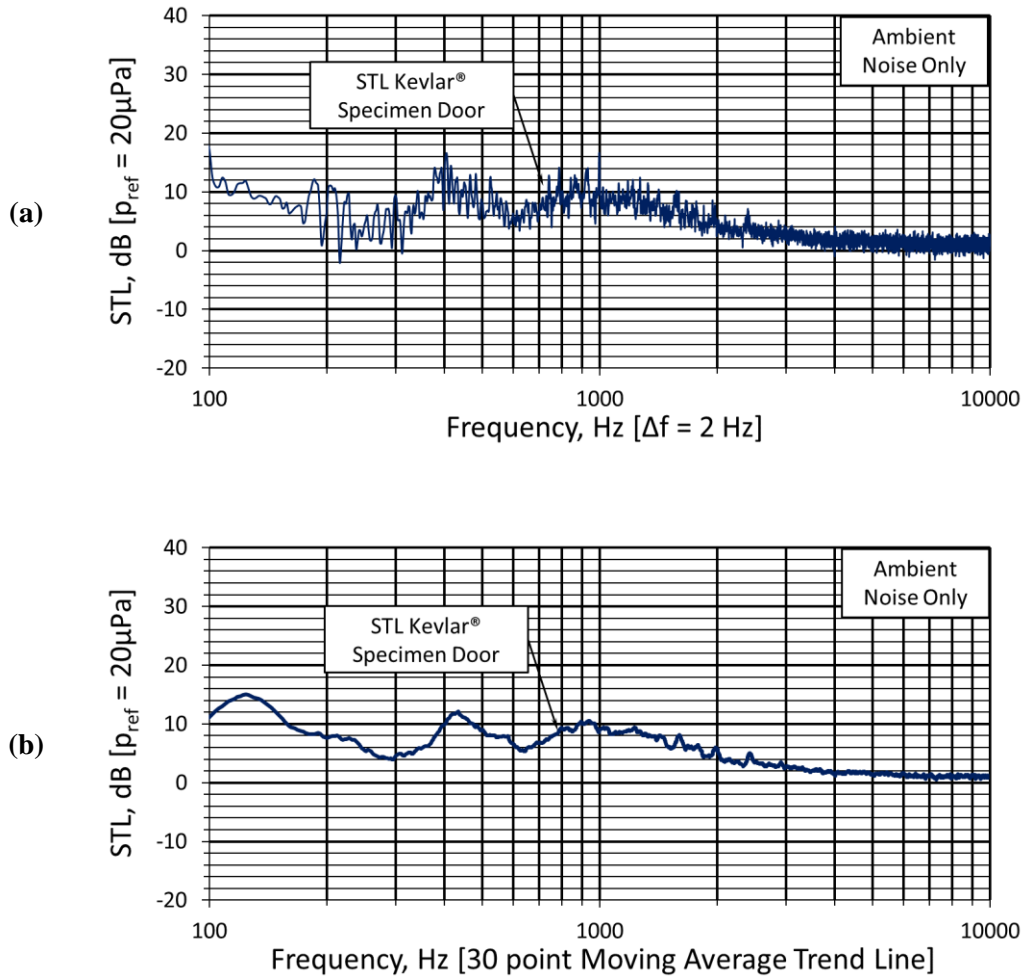
Figure 52. Sound transmission loss (SPL$_{Tunnel}$ – SPL$_{Quiet\ Box}$) of Kevlar® specimen door with ambient noise only. (a) – Narrow Band Δf = 2 Hz. (b) – 30 point moving average trend line

The MNR$_f$ of the tensioned Kevlar® specimen door was measured to range from -15 dB to +28 dB for the narrow band data (Δf = 2 Hz) and -1 dB to +19 dB for the 30-point moving average trendline (approximating Δf = 60 Hz) within the test frequency range of 200 to 1500 Hz. This data is outside of the correctable limits of +15/-5 dB specified in SAE J1400[8] when compared to the STL data for a tensioned Kevlar® panel provided in Jaeger, et. al.[5] (reference **Figure 34** for tensioned Kevlar® STL data); however, the considerable differences in the setup, size of test chambers, and undoubtedly superior reverberant environment provided by the large test section

available at NASA Ames Research Center, these tests are not likely to compare well. Furthermore, the purpose of this study is to provide a comparative test method to optimize candidate windscreens. Exact STL data for a windscreen is not currently in the scope of this study. To calibrate this STL measurement facility, another STL specimen should be constructed from a limp mass material such as a PVC vinyl sheet having geometry for which a closed form analytical solution for sound transmission loss is known.

4.2   Flow-On Transmission Loss of Kevlar® Validation Sample

For the flow-on test case, it is desirable to be able to simultaneously interrogate both sound transmission loss and flow-induced noise caused by the windscreen. The flow induced noise characterization results are addressed in subsequent sections. In order to discern flow noise from the normal incidence acoustic source, tones were generated using a MATLAB code (reference **Appendix G**) and the amplifier and speaker system installed in the wind tunnel. The MATLAB code generates tones at 200, 300, 400, 500, 600, 700, 800, 900, 1000, and 1500 Hz, which fully encompass the frequency range of interest. The code is written such that the amplitude can be adjusted for each tone, thus providing a source at least 10 dB above the flow-induced background noise, except for the 400 Hz tone at the highest flow speed. This tone was only 9 dB above the background flow noise. Data were collected at free-stream velocities of 36.3, 46.8, 55.4, and 59.2 ft/s (corresponding to 0.30, 0.50, 0.70, and 0.80 in-H_2O). Additional higher frequency tones are seen in the spectrum at a lower amplitude than the primary tone frequencies. These harmonic frequencies are an artifact of having multiple primary frequencies generated simultaneously. These harmonic frequencies are not included in the sample noise reduction calculations. Reference **Figure 53** for wind tunnel spectra showing flow noise only and flow noise + source tones measurements demonstrating amplitude of tones above the flow noise. The spectra measured for each flow speed are shown in **Appendix F: Acoustic Test Data**. Note that the "Source Room", as references

in SAE J1400[8], is the wind tunnel test section and the "Receiving Chamber" is the quiet box internal volume.

(a)

(b)
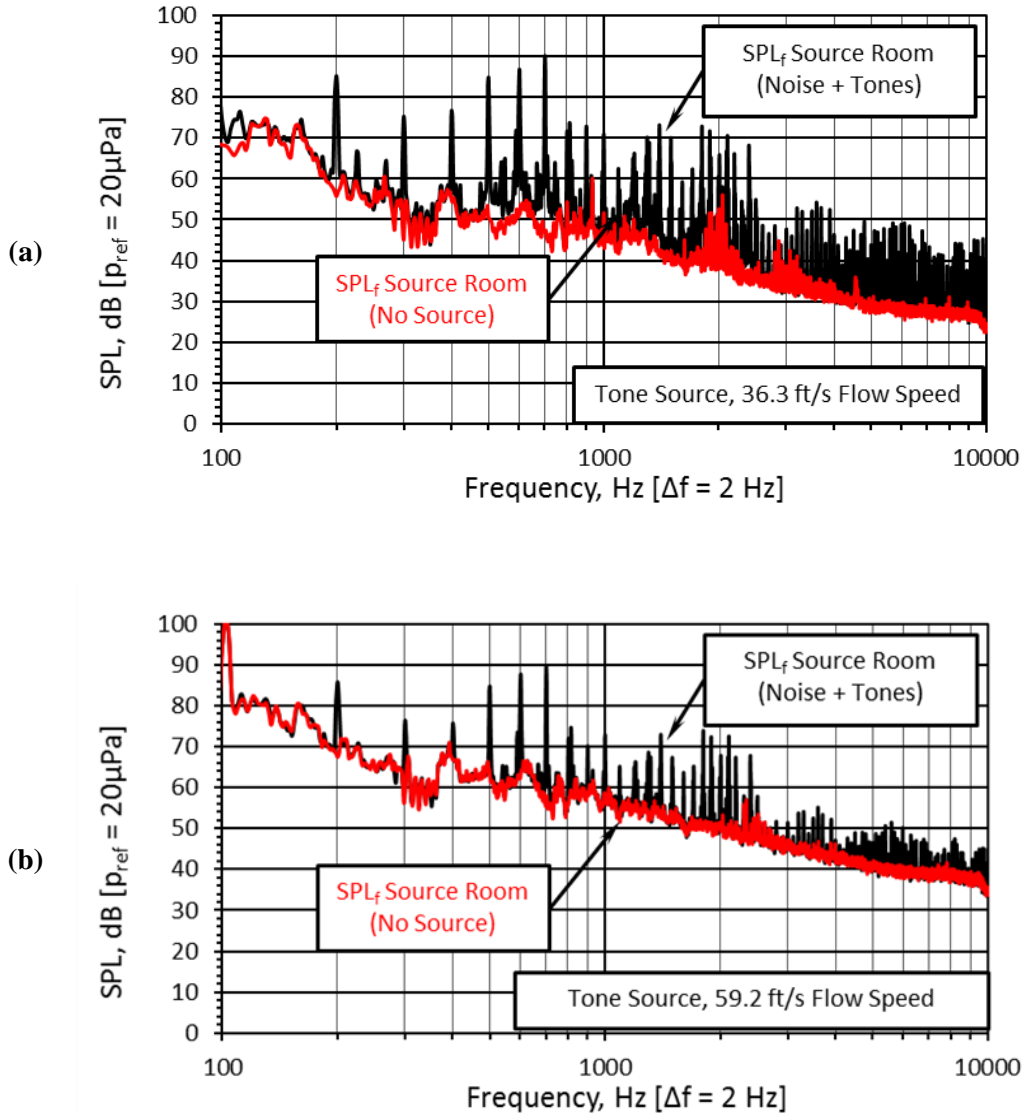
Figure 53. Bullet Mic measured tunnel noise spectrum contrasting flow noise only from flow noise + source tones recordings. Tones generated at 200, 300, 400, 500, 600, 700, 800, 900, 1000, and 1500 Hz. (a) – Minimum free-stream flow velocity test (36.3 ft/s), (b) – Maximum free-stream flow velocity test (59.2 ft/s).

The noise reduction method of **Equation** (18) was utilized for the wind tunnel source room and the quiet box receiving chamber, as done for the flow-off transmission loss case[8]. The wind

tunnel and quiet box spectra at the highest and lowest flow speeds are shown in **Figure 54**. The full

spectral data for all flow speeds are shown in **Appendix F**. As expected, the spectrum amplitude

tends to increase with increased flow speeds due to increases in flow noise. The variation between

quiet box microphones was observed to be nearly undetectable across the test frequency spectrum

of 200 to 1500 Hz. The microphone variation is shown in **Figure 55**. The absence of wide spectrum

white noise is expected to be partially responsible for the decreased microphone variation.

(a)

(b)
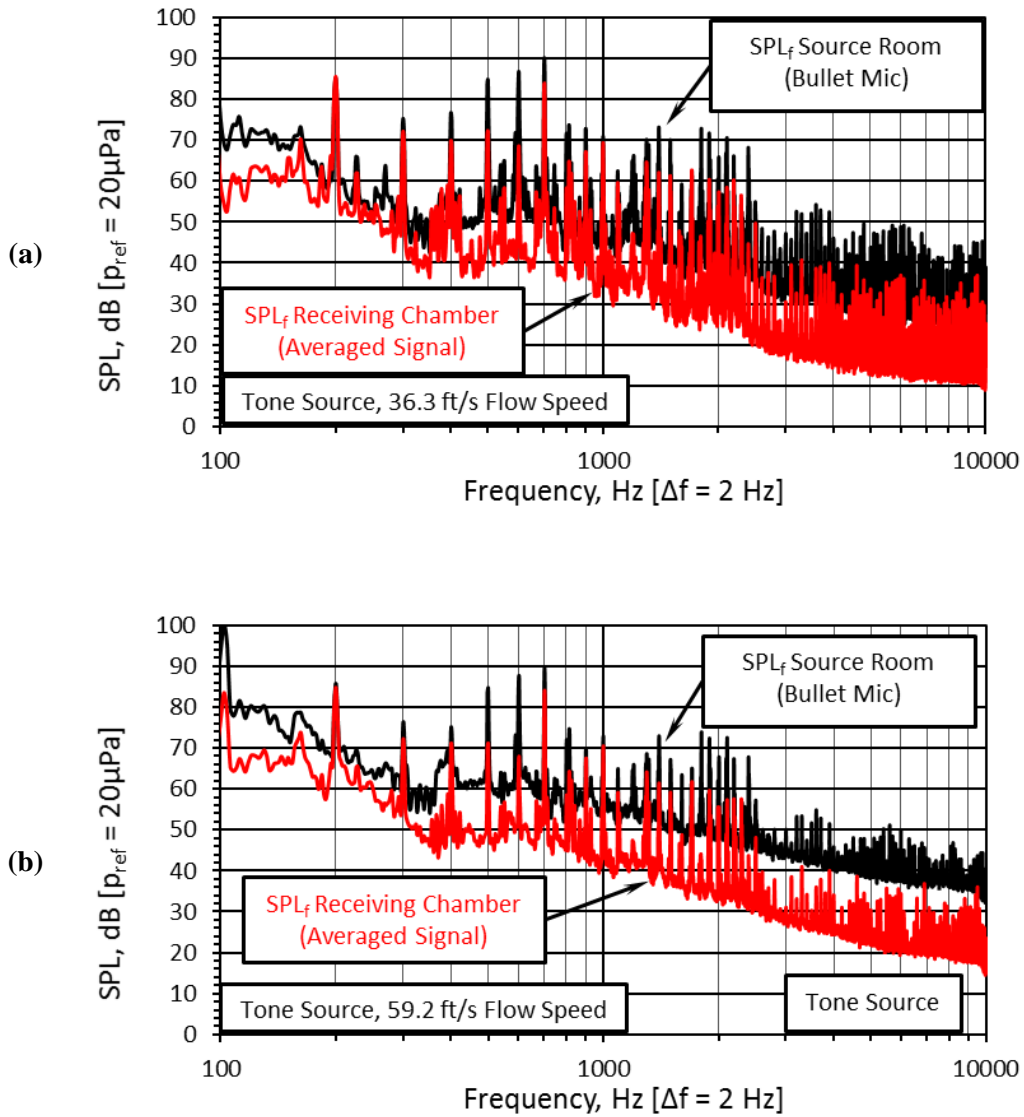
Figure 54. Bullet Mic measured tunnel noise and quiet box averaged microphone spectra with Kevlar® validation specimen flow noise + source tones testing. (a) – Minimum free-stream flow velocity test (36.3 ft/s), (b) – Maximum free-stream flow velocity test (59.2 ft/s).
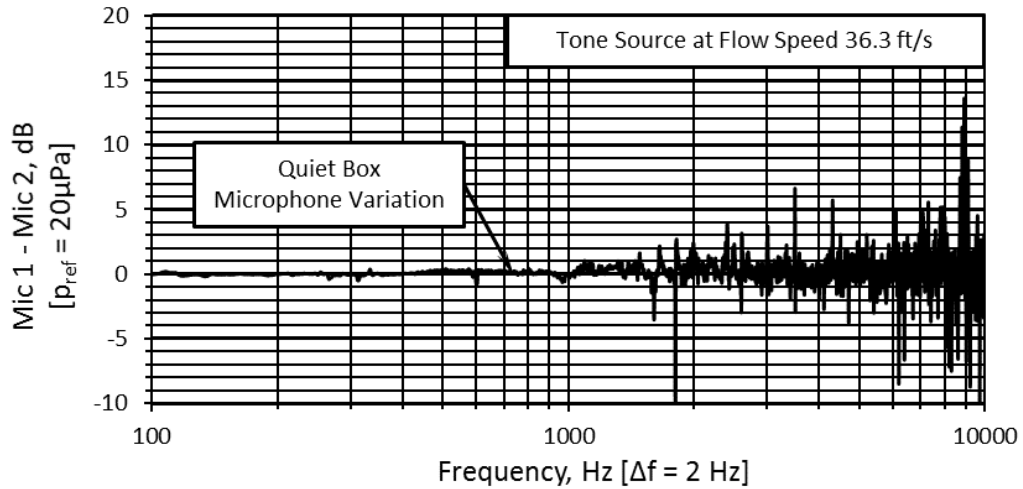
Figure 55. Quiet box microphone variation during flow-on tone source testing at 36.2 ft/s free-stream velocity

The MNR_f was calculated using **Equation** (19) at each primary tone, for each flow speed. No reference data for flow-on sound transmission loss is currently available for tensioned Kevlar® panels; therefore, no conclusions can be made about calibration limits. The minimum observed MNR of -0.6 dB was measured with a free-stream flow velocity of 46.8 ft/s, and the maximum observed MNR of 19.9 dB was measured with a free-stream velocity of 59.2 ft/s. Reference **Figure 56** for tone source MNR for the Kevlar® validation specimen.
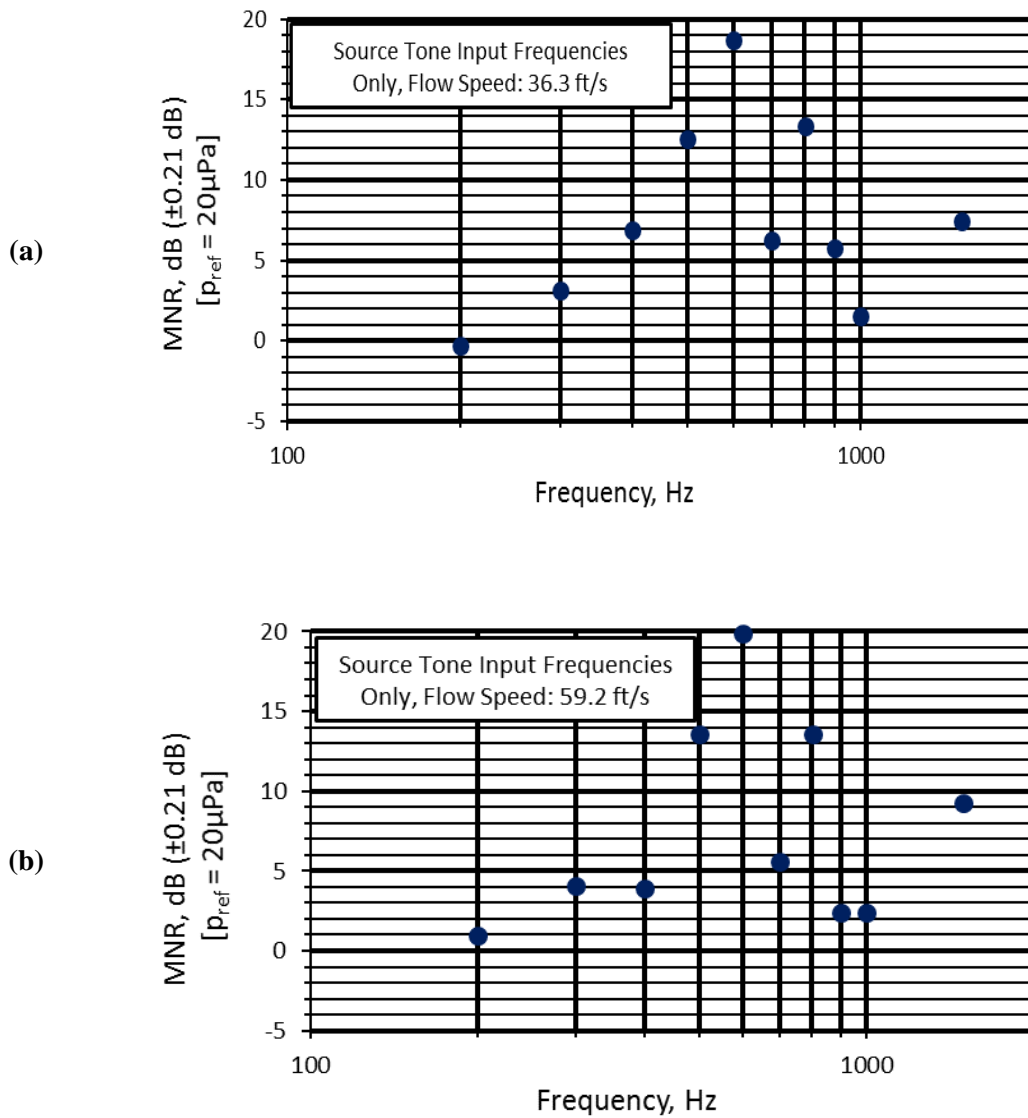
Figure 56. Source tone-only, flow on, specimen door configuration Measured Noise Reduction specturm (MNR) measured by correcting for background noise then subtracting receiving chamber SPL from source room SPL_f. (a) – Free-stream flow velocity of 36.3 ft/s, (b) – Free stream flow velocity of 59.2 ft/s (Note: MNR for all measured flow speeds shown in **Appendix F**)

It is noted that the sample's sound transmission loss amplitude tends to increase with increased flow velocity. The overall integrated sound pressure level, maximum STL, and minimum STL for all flow speeds are shown in **Table 8**. This is the expected result. As flow speed increases, so does boundary layer turbulence intensity. When sound propagating through a continuum

interacts with a discontinuity, portions of its energy will be transmitted, reflected, and absorbed. The portion of the energy to undergo each of these three possibilities is dependent on the intensity of the discontinuity in the continuum[19]. When sound waves interact with flow turbulence, it is expected that waves will tend to be scattered and absorbed in a similar manner to an open cell foam; therefore, increasing the absorption component of the energy transfer and decreasing the energy available to be transmitted[4]. Full spectral results for flow-on testing are provided in **Appendix F**.

Table 8. Flow-on OASPL measurements for all tested free-stream flow velocities over the frequency range of 200 to 1500 Hz with a tone

Flow Speed [ft/s]	OASPL [dB]
36.3	21.3
46.8	21.6
55.4	21.8
59.2	22.2

4.3   Bullet Microphone Method for Overall Flow-Induced Noise Increase for Kevlar® Validation Sample

Any candidate windscreen must be optimized to have minimum normal incidence transmission loss and minimum flow-induced noise generation over it surface. The test apparatus developed in this study can be utilized to provide comparative flow-induced noise generation data. Two methods were proposed to measure this characteristic, and both were tested on the tensioned Kevlar® validation specimen door. The first method utilizes the same pylon mounted bullet microphone utilized in the transmission loss testing. The results for testing with this method are addressed in this section. The second method installs two 1/2-inch condenser microphones flush mounted in the wind tunnel test section floor. One forward, and one aft of the specimen door. The results for testing with this method are addressed in the next section.

The pylon mounted bullet nose cone microphone is located along the wind tunnel test section centerline, mounted 9 inches aft of specimen door center point. The boundary layer survey

89

accomplished for the wind tunnel in its current configuration concluded that this microphone is well out of any boundary layer turbulence. The wind tunnel acoustic spectrum was measured with the smooth plug door installed using this microphone at the same four flow speeds (36.2, 46.8, 55.4, and 59.2 ft/s). This test was repeated with the tensioned Kevlar® specimen door installed as well. Special attention was paid to ensure the smoothest aerodynamic transitions possible, using aluminum foil tape to blend any steps and/or gaps between the test section floor and the quiet box door panels. The spectrum for flow speed of 36.3 for both pass-through door panels are presented in **Figure 57**. The spectra for all flow velocities are shown in **Appendix F**.
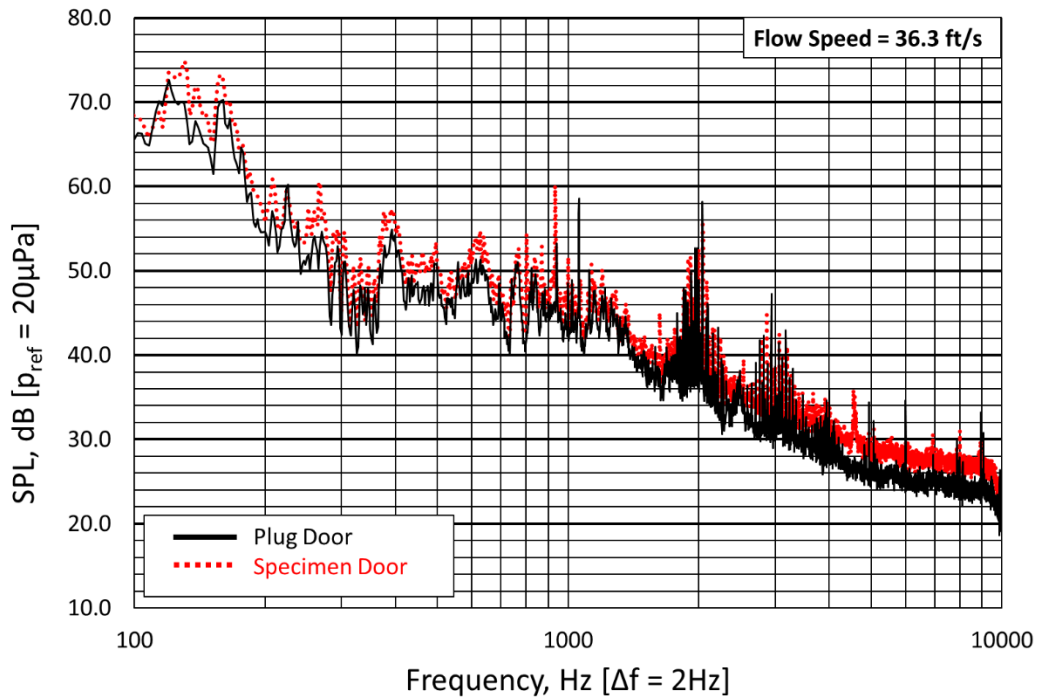
Figure 57. Typical sound pressure spectrum measured in wind tunnel test section by pylon mounted bullet nose cone microphone for plug door and specimen door configurations, free-stream velocity shown: 36.3 ft/s free-stream velocity (spectrum for all flow velocities shown in **Appendix F**)

It was noticed that most amplitude difference between the flush (plug door) and tensioned Kevlar® validation specimen door configurations occurs between 100 and 1000 Hz. Note that previously defined test frequency range for quiet box testing does not apply to this test since the attenuation factors driving the lower cutoff frequency and the microphone variation phenomenon are both dependent on measuring spectra within the quiet box. No quiet box measurements are made during this test procedure. Extreme effort was placed into ensuring no difference occurred in ambient noise and other variable factors except the pass-through door configuration between test runs. Assuming no other variations exist, it is reasonable to attribute any increase in acoustic amplitude levels between the plug door and specimen door to either increased hydro-dynamic pressure fluctuations or turbulence induced flow noise increase. Either cause is likely the result of the increased surface roughness of the tensioned Kevlar® specimen door, compared to the smooth surface of the plug door; therefore, it is reasonable to assess the OASPL integration over only the frequencies showing the highest variations, 100 to 1000 Hz.

It was noted that a broad increase in amplitude of 8 to 20 dB, at 2000 to 2500 Hz was present throughout all flow speeds, and both pass-through door configurations. The cause of this spike is not known, although it is suspected to be electronic interference with the test equipment. This spike does not affect the results of the OASPL integration since it is outside the frequency region of interest (100 to 1000 Hz).

The OASPL was calculated for the above-mentioned frequency range for each flow speed and pass-through door configuration. The results were plotted and a trend line computed. The results are shown in **Figure 58**.
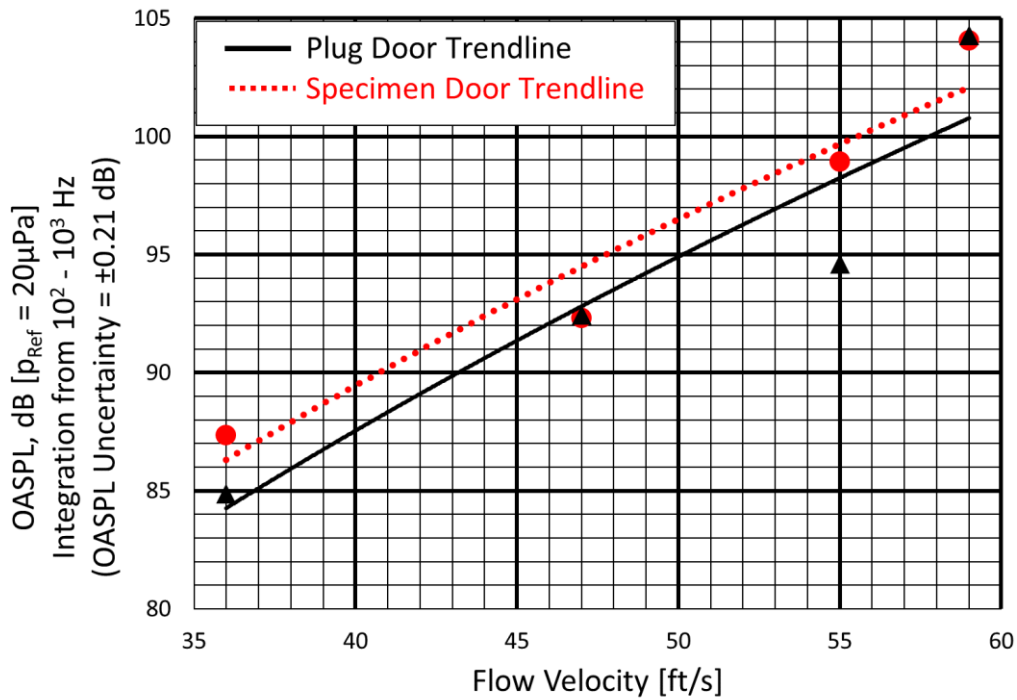
Figure 58. Overall sound pressure level integration from 100 to 1000 Hz for bullet microphone method at various flow speeds for the plug door and tensioned Kevlar® specimen door configurations with trend lines shown

The difference in OASPL between the plug door and specimen door is low, but not statistically insignificant. The 36.3 ft/s free-stream velocity run resulted in a difference of 2.5 dB, and the 55.2 ft/s free-stream velocity run resulted in a difference of 4.4 dB, the other two flow speeds resulted in OASPLs within 0.2 dB between the two configurations, which is below the test equipment's ability to discern. The test equipment has been theoretically determined to have an OASPL uncertainty of 0.21 dB (uncertainty analysis covered in **Section 3.4.2**), which proves that the 36.3 and 55.2 ft/s data points are statistically different, and the 46.8 and 55.4 are not statistically different. The resulting trend lines are separated by approximately 2.5 dB, which is sufficient to conclude a measurable increase in OASPL for the specimen door. It is also worth noting that the surface roughness of the tensioned Kevlar® specimen door does not significantly higher than that of the plug door (quantitative roughness measurements not currently available for either surface).

It is assumed that future candidate windscreen designs will either be significantly more porous than the Kevlar® panel, or the parameter will be irrelevant, and other factors such as normal incidence transmission loss or ease of structural integration will dominate the decision.

4.4   Flush Microphone Method for Turbulence Increase for Kevlar® Validation Sample

Based on the microphone comparison data obtained during the testing described in **Section 3.3.5.1**, it is suspected that pressure fluctuations detected by the microphone flush-mounted on the wind tunnel test section floor are likely caused, at least in part, by boundary layer turbulence-induced hydro-dynamic, rather than acoustically induced, pressure fluctuations. This idea is the basis for the method to quantify self-induced hydro-dynamic noise presented in this section.

For this test, two 1/2-inch condenser microphones with standard protective grill installed were mounted so that the top of the microphone grills were flush with the wind tunnel test section floor surface (reference **Figure 37** for a photograph of the installation). One microphone was mounted 13.5 inches upstream of the leading edge of the quiet box pass-through window, and the other was mounted 13.5 inches downstream of the trailing edge of the quiet box pass-through window. Measurements were made for the flow-on, acoustic source off configuration at flow speeds of 36.3, 46.8, 55.4, and 59.2 ft/s. The spectra were compared for the upstream and downstream microphones for plug door configuration and for the specimen door configuration at each flow speed with the hope of seeing a measurable difference between the upstream and downstream microphones, indicative of changes in the boundary layer caused by the specimen door configurations. Reference **Figure 59** for upstream and downstream microphone SPL for plug door configuration at flow speed extremes and **Figure 60** for upstream and downstream microphone SPL for specimen door configuration at flow speed extremes. The spectra for all tested flow speeds are shown in **Appendix F**.
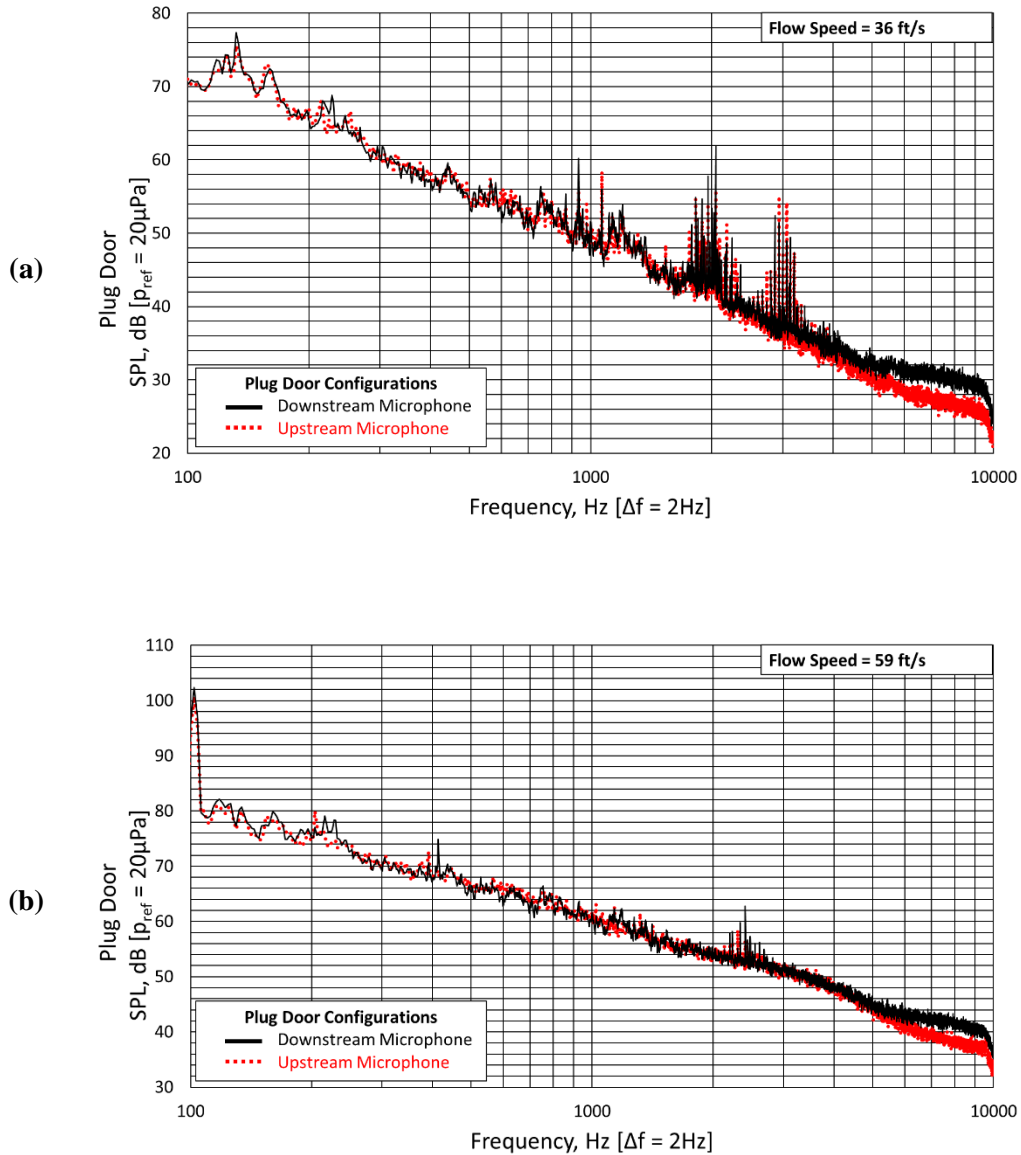
Figure 59. Sound pressure spectrum measured by flush mounted downstream microphones in wind tunnel test section for plug door configuration. (a) – 36 ft/s free-stream velocity, (b) – 59 ft/s free-stream velocity (spectra for all flow speeds shown in **Appendix F**)
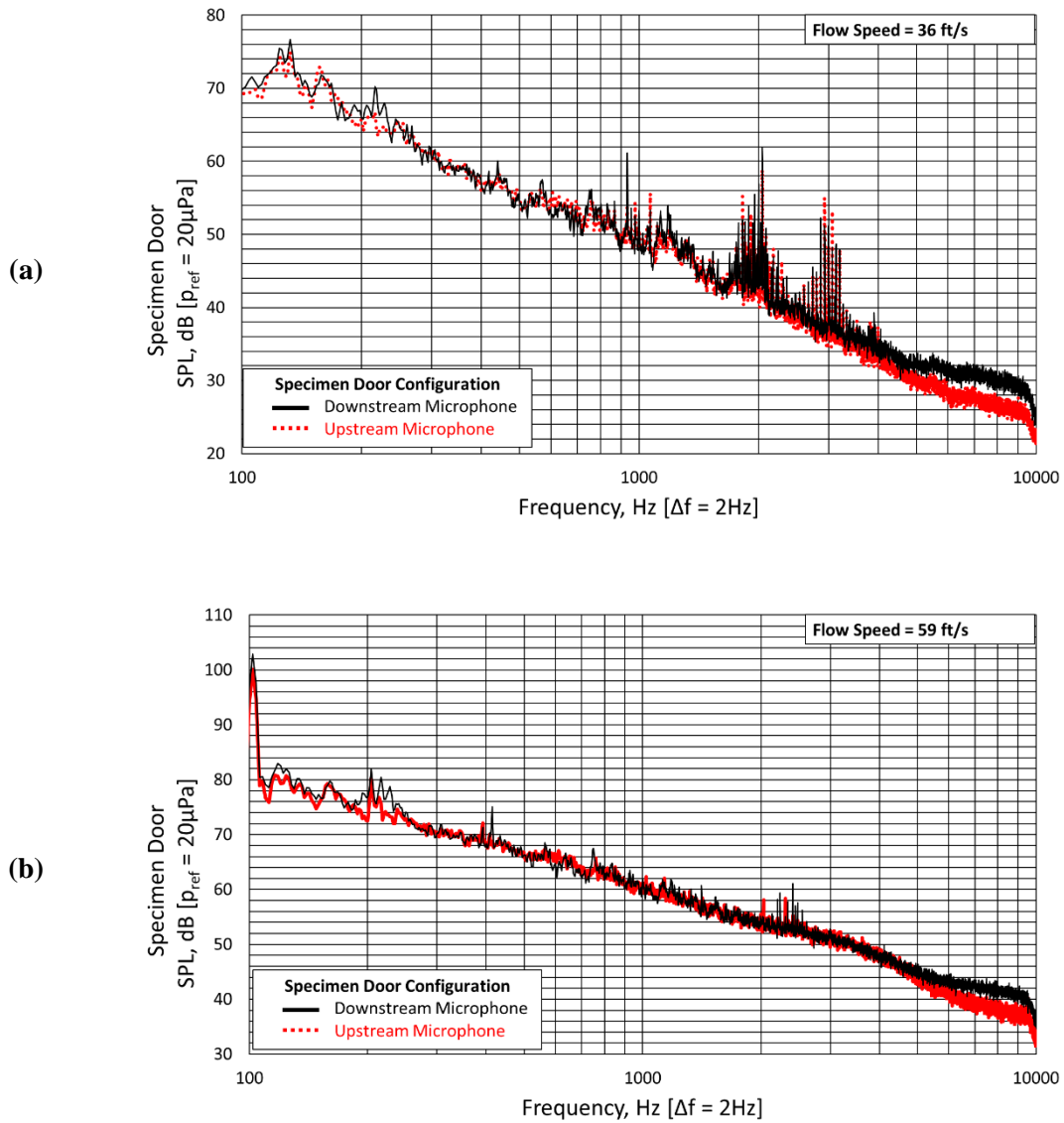
Figure 60. Sound pressure spectrum measured by flush mounted downstream microphones in wind tunnel test section for specimen door configuration. (a) – 36 ft/s free-stream velocity, (b) – 59 ft/s free-stream velocity (spectra for all flow speeds shown in **Appendix F**)

Unlike the bullet microphone method discussed in the preceding section, there appears to be no measurable difference between the signal recorded for each configuration. To further validate this point, the difference between the upstream microphone SPL was subtracted from the downstream microphone SPL. There exist two notable spikes in these spectra, one at approximately 195 to 225 Hz and another at 2000 to 2500 Hz; however, these spikes do not appear to be caused

by detection of turbulence increase due to the spikes having amplitudes which are equally positive and negative. A true hydro-dynamic pressure fluctuation frequency would likely span more than one frequency bin. It would also be expected that if the downstream microphone were detecting a signal different from that of the upstream, the amplitude variation would be positive only when subtracting the upstream from the downstream microphone. Another notable feature in the data is a gradual rise in the difference between the upstream and downstream mics between 5000 and 8000 Hz, resulting in a 4-dB average difference. This is also not believed to be a result of added turbulence caused by the specimen door configuration since both the plug door and specimen door configurations show this spectral feature at the same frequency and amplitude for their respective flow speeds. It is likely this variation is the result of a difference in dynamic response between the microphones at high frequencies. Reference **Figure 61** for the difference between the downstream and upstream microphones for the flow velocity extremes (spectra for all flow speeds shown in **Appendix F**).
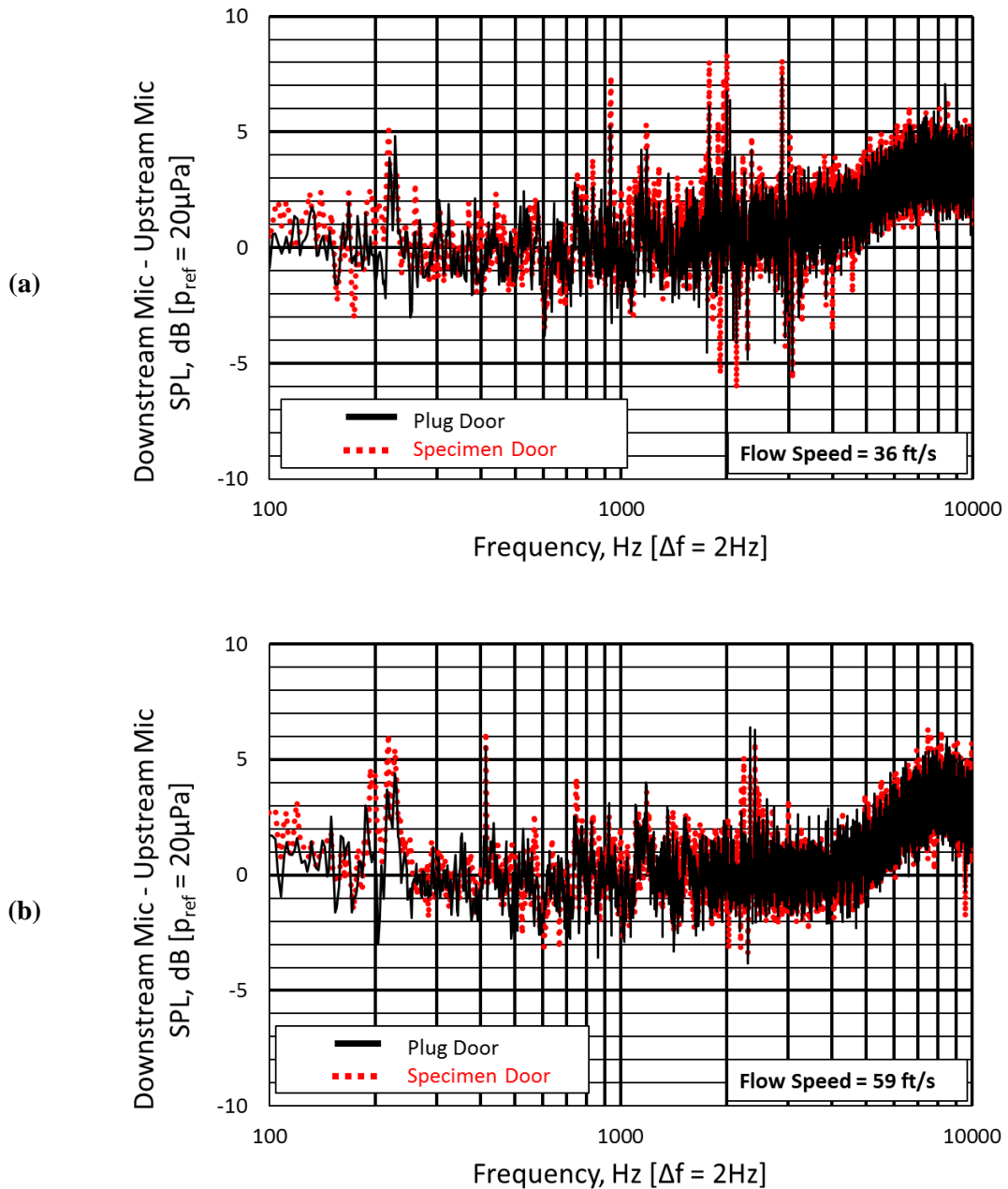
Figure 61. Difference between flush mounted microphones (downstream mic – upstream mic) for plug door and specimen door configurations. (a) – 36 ft/s free-stream velocity, (b) – 59 ft/s free-stream velocity (spectra for all flow speeds shown in **Appendix F**)

Figure 62 shows the difference between two spectra presented in **Figure 61** (specimen door – plug door) for the flow extremes (spectra for all flow speeds shown in **Appendix F**). This difference

demonstrates that no significant variation exists between the two spectra for any of the unexplained frequency spikes addressed above.
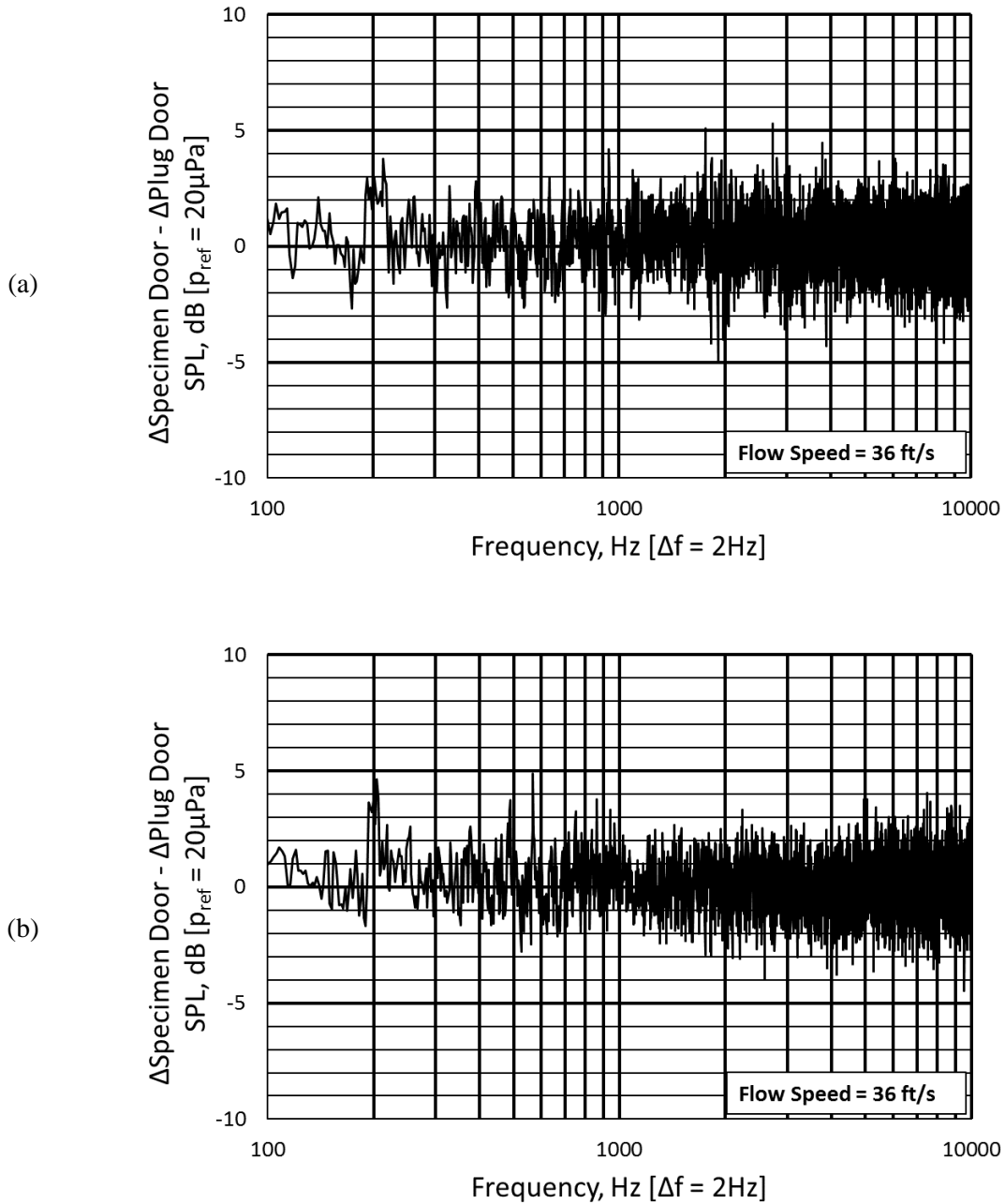
Figure 62. Downstream – upstream microphone SPL for specimen door configuration subtracted from downstream – upstream microphones SPL for plug door configuration. (a) – 36 ft/s free-stream velocity, (b) – 59 ft/s free-stream velocity (spectra for all flow speeds shown in **Appendix F**)

No clear and/or measurable turbulence frequencies were shown to exist between the plug door and specimen door configurations. Since the downstream microphone is located where any added turbulence due to the specimen door would be present, the overall sound pressure level (OASPL) integration for the downstream microphone was computed at each flow speed for both door configurations. The integration was accomplished from 100 to 1000 Hz since this is the frequency range determined to predominately change as a result of changing between the plug door and specimen door configurations in the bullet microphone method discussed in the preceding section. The OASPL values are shown in **Figure 60**. The separation between the OASPL data points for each configuration are observed to be within the theoretical ±0.21 dB uncertainty limit of the test equipment, with the exception of the 36 ft/s flow speed which has a difference just outside the theoretical uncertainty limits at 0.7 dB. Therefore, it is concluded that this method does not provide useful and statistically different data regarding turbulence increase for the test specimen. While it is worth noting that the tensioned Kevlar® validation specimen is not particularly rough compared to the wind tunnel test section floor or other surfaces exposed to the flow (quantitative surface roughness measurements for the Kevlar® specimen or the plug door are currently available), and a difference should be measurable. One possibility is that any hydro-dynamic pressure fluctuation differences detected by the microphones are the result of flow shedding caused by the microphone grills. This would depend on the installation angle, and other highly sensitive factors. This method for measuring turbulence increase would be better accomplished by measuring boundary layer turbulence intensity with a hot wire probe to determine any changes in boundary layer thickness caused by the specimen door.
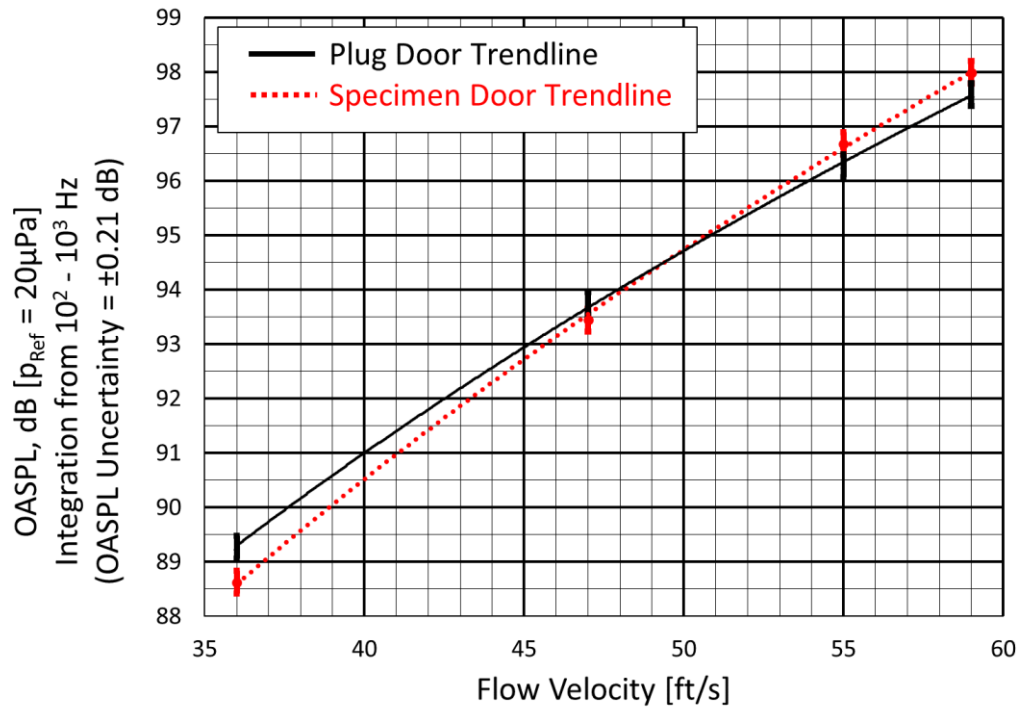
Figure 63. Overall sound pressure level integration from 100 to 1000 Hz for downstream flush mounted microphone at various flow speeds for the plug door and tensioned Kevlar® specimen door configurations with trend lines shown

CHAPTER V

CONCLUSIONS AND RECOMMENDATIONS

The purpose of this study is to develop and validate a method by which candidate windscreen designs can be compared. The quiet box apparatus constructed for this study was found to be capable of sufficient sound attenuation for quality acoustic testing. The STL measurement method was used to generate uncalibrated STL measurements for the tensioned Kevlar® validation specimen, which were determined to be sufficiently accurate for comparative evaluation of candidate windscreen designs. The flow-on testing showed the expected trend of increasing sample STL with flow speed. The bullet microphone method to compare flow-induced noise increase was shown to have sufficient resolution to measure the difference between the plug door and specimen door configurations. The flush mounted added turbulence method to compare flow-induced noise increase was not shown to be able to resolve the difference between the plug door and specimen door configurations.

5.1   Impedance Tube Testing

Impedance tube testing provides good reference data for material samples despite its short-comings for application in the scope of the current study. Obviously, the impedance tube cannot provide any insight in to flow-on transmission loss or grazing flow self-induced noise generation and any stiffened samples will have their normal incidence sound transmission loss affected by natural resonance frequencies that will not translate directly to the full scale. However, the impedance tube has been shown to generate accurate results, and its ease of use makes it an attractive option for first pass evaluation of material samples prior to more involved development and testing. The samples tested as part of this study proved that standard methods of epoxy impregnation result in stiffened structures which have undesirable acoustic transmission loss characteristics. Future work should avoid stiffening and sealing membrane materials in this manner. A more robust mounting fixture could be developed with the capability to tension samples for improved testing versatility as well.

5.2   Quiet Box Design and Installation

The quiet box environment designed and build as part of this study proved to be a cost-effective means of reducing ambient sound for high precision acoustic testing. The materials cost between $500 and $700 to purchase, and the construction methods are sufficiently easy such that a person with reasonable skill could replicate the fabrication. The available volume was not sufficient to provide attenuation through foam wedges alone; therefore, a high-density double wall design was used in addition to 4-inch open-cell polyurethane foam wedges. Qualification testing resulted in a sealed box attenuation of 25 to 45 dB from 100-10000 Hz, which is well above the minimum requirements of ISO 3745: 2012[11]. It was determined upon initial installation and testing that any deflection of the outer wall would be transmitted directly into the chamber where it would be detected as a pressure wave. Stiffeners were added to the quiet box walls; however, this was a

reactive solution. A better solution may be to an additional wall layer and airgap to further decouple outer wall vibrations from the air volume internal to the quiet box environment. The quiet box internal volume is small compared to the guidelines set forth in ISO 3745:2012[11] and SAE J1400[8], which was expected to create challenges for accurate testing. It is believed that the high level of variation observed between adjacent microphone locations within the quiet box is a result of this reduced volume. The observed variation resulted in a reduction of the test range upper cutoff frequency to 1500 Hz. If a full re-design were to be undertaken, it would be advisable to maximize the internal volume to separate standing wave locations as much as possible.

The reverberant behavior of the wind tunnel test section is also an area which should undergo improvement if a redesign/rebuild were attempted. The MDF, which comprises most of the test section construction material, provides a relatively hard boundary for acoustic reflection; however, this material does provide some level of acoustic absorption. Cox, et. al.[20] reports an absorption coefficient of up to 0.3 for fiberboard material. To achieve the more effective reverberant environment recommended for testing, the test section walls could be lined with sheet metal or similar very low absorption material. Sharp corners are also problematic for reverberant environments, and should probably be addressed for any future rework. Addressing corner reflections by changing corner geometry will affect airflow characteristics in the test section. The impact these changes have on flow noise and other wind tunnel testing operations should be considered. As an alternate to improving reverberant chamber qualities of the test section, the test section could be modified to improve anechoic properties instead. This is the approach used by Virginia Tech while modifying their stability wind tunnel into an aero-acoustic facility[6]. For this modification, test section walls and the section walls immediately upstream and downstream from the test section were replaced with large panels filled with a sound absorbent batting material such as fiberglass insulation. These panels were streamlined to the airflow with tensioned Kevlar® windscreens similar to those used on the test section[6].

5.3   Wind Tunnel Flow-Off STL Measurement

The test method developed herein has been shown to produce comparative data which can be used to optimize windscreen design. This comparative data does not require the system calibration outlined in SAE J1400[8]. If quantitative STL data is desired for a candidate windscreen, a reference sample with known STL characteristics would need to be constructed and tested, then the difference between the measured noise reduction (MNR) and the theoretical STL would be determined and used as the calibration factor. This calibration factor would be applied for any STL testing.

The no acoustic source test configuration of the tensioned Kevlar® validation specimen resulted in sound transmission loss values within the calibration limits (+15/-5 dB) provided in SAE J1400[8] when compared to the STL data for tensioned Kevlar® provided by Jaeger, et. al.[5]. The white noise source STL data showed more frequency dependent variation than the no source configuration. This is believed to be a function of standing was frequencies caused by the normal incidence white noise. Reducing the frequency resolution of the test data provides a smoother curve with less variation. It was noted that the STL data provided in Jaeger, et, al.[5] was recorded with a frequency resolution of $\Delta f = 62.5$ Hz. When comparing both spectra at this resolution, the STL data measured for tensioned Kevlar® validation specimen constructed herein is only just outside the calibration limits prescribed in SAE J1400[8] over the target frequency of 200 to 1500 Hz. There is reason to suspect the measurement method used in Jaeger, et. al.[5] will produce a notably different tensioned Kevlar® STL spectrum due to differences in source and receiving chamber size and an increased number of microphones. Also, minimum data is available on how the STL values were determined and how the system was calibrated.

5.4   Wind Tunnel Flow-On STL Measurement

As expected, the flow-on transmission loss measurements showed a tendency of slightly increased STL with higher flow speeds for the tensioned Kevlar® validation sample. This is believed to be caused by increased boundary layer turbulence intensity as a result of higher flow energy over the sample. This increased turbulence will cause greater absorption and reflection of sound waves, resulting in higher STL amplitude.

Tones generated by the normal incidence acoustic source driver in the top of the wind tunnel test section were shown to provide results consistent with those obtained testing with white noise. Use of specific tones allows higher signal amplitudes compared to a white noise source by providing the full available power to specific frequencies. This allows measurements to be made in the presence of higher background noise. Furthermore, the use of source tones in lieu of white noise allows STL and self-induced flow noise to be measured simultaneously by focusing only on the generated tones for STL measurement and the frequency regimes where tones are not present for self-induced flow noise measurements. One drawback to testing with multiple tones is presence of secondary harmonic tone created by the combination of multiple primary tones. The number of these secondary tones can be reduced by reducing the number of primary tones; however, this will cause a reduced STL frequency resolution. The tone source method also resulted in a reduced microphone variation within the quiet box. This is likely caused by the lack of normal incidence frequency saturation which occurs during testing with a white noise source.

The test results obtained for flow on testing revealed a minimum Measured Noise Reduction (MNR) of -0.6 dB, and a maximum MNR of 19.9 dB across all test frequencies. No calibration method for flow on testing currently exists. Development of a calibration reference standard would require a statistically robust sample set of test data from multiple well established testing facilities since no closed form analytical solution for any material currently exists. It is not

necessary to calibrate the test apparatus developed herein since comparative data is sufficient for evaluating and comparing candidate windscreens.

5.5   Bullet Microphone Method for Flow-On OASPL Increase

The bullet microphone method was shown to be viable for detecting changes in self-induced noise caused by the installation of the test specimen. The spectrum generated for each test configuration was measured and studied. It was noted that most of the variation between the spectra for the two configurations was contained between 100 and 1000 Hz; therefore, the OASPL integration was performed on this frequency region. This reduced frequency band also prevented inclusion of an amplitude spike occurring between 2000 and 2500 Hz, depending on flow speed. The source of this spike is not known; however, it is expected to be the result of some form of electrical interference on the test system. This spike was observed in other flow-on test spectra; however, it is outside the test frequency range so it was not included in the OASPL integration.

The OASPL as a function of flow speed showed measurable and statistically unique differences between the test configurations for tests conducted at the free-stream velocities of 36 and 55 ft/s. This level of resolution is believed to be sufficient for windscreen comparison purposes during the design phase of a project. It is also noted that the tensioned Kevlar® validation specimen is likely to have a low surface roughness compared to future candidate windscreen designs. A candidate windscreen with an increased surface roughness should result in a higher level of noise generation by the windscreen, which will be more easily detectable.

5.6   Flush Mounted Microphone Added Turbulence Method

Flush mounting microphones has not been shown to provide a clear detection of surface differences in self noise generation between the plug and specimen door configurations. The spectra generated for each flow speed indicated a difference between the two door configurations which

falls within the measurement uncertainty limits of the system. OASPL integration was accomplished from 100 to 1000 Hz, which was found to be the frequency range most influenced by the configuration change in the bullet microphone testing. The OASPL values were plotted versus flow speed for the aft microphone only since this is the location the most change was expected. The variation between the configurations was measured at less than 0.5 dB decibel at each flow speed except for the 36 ft/s flow speed which was measured to have a difference of 0.7 dB. These variations are fall within the theoretical uncertainty limits of the acoustic test equipment; therefore, the data points cannot be deemed statistically different. It is likely that the pressure fluctuations recorded by the flush mounted microphones are dominated by flow over the microphone grills. If this method of measurement is to be viable for future testing, work should be done to protect the microphone diaphragms without minimal effect on flow over them. In its present state, this method should not be favored over the bullet microphone method for flow noise measurement. Any future work towards characterizing the boundary later turbulence intensity caused by the windscreen should probably focus on hot wire flow speed measurements rather than hydrodynamic pressure fluctuation measurement.

5.7   Overall Conclusions and Recommendations

The test apparatus developed herein has proven to be a viable means by which comparative data can be generated to compare candidate windscreen designs for use in UAV acoustic sensing applications across frequency spectrum expected to be desirable for airborne detection. No attempt has been made to generate a calibration curve to be used for sound transmission loss testing. This calibration is not necessary to generate comparative data between candidate windscreens tested in the same facility. The test facility has been shown fully qualified, using the methods developed herein, to characterize windscreen designs. Future work will focus on windscreen design. The tensioned Kevlar® membrane has been shown by this study and others[5,6] to be an effective option; however, the structure required to maintain the membrane tension is prohibitive for its installation

in small aircraft. The goal of this research will be to develop a light-weight windscreen with sufficient strength to be self-rigid without the need for a tensioning mechanism, minimized normal incidence sound transmission loss, and minimized grazing-flow-induced self-generated turbulence noise. Consideration has been given to a structure using a shallow non-metallic honeycomb core material bonded to a light weight dry PEEK® cloth outer skin, with a possible open weave carbon, fiberglass, or Kevlar® inner skin. An open weave inner skin should be used to reduce any resonator effect that may be caused by partially closing the honeycomb core cells.

Once a candidate windscreen is shown to be sufficiently optimized for the specific application, further research will be required to optimize the aircraft itself. It is necessary to understand how an acoustic source is most likely to detect the aircraft. Most biological target sources are capable of optically and acoustically detecting the aircraft. For the example of the Greater Prairie-Chicken, if the UAV resembles one of bird's natural predator, it is likely to hide or change its behavior which would impact the accuracy of the population count. Proper camouflage such as painted patterns on the aircraft's lower surface could be used to disrupt any hawk-like shape a fixed-wing aircraft might have. The frequency response of the Greater Prairie-Chicken's hearing is another area that warrants further investigation. It would be ideal that any airframe used for counting this species would avoid frequencies of high hearing sensitivity.

REFERENCES

[1]   A. Clifton, "Estimating Numbers of Greater Prairie-Chickens Using Mark-Resight Techniques," *The Journal of Wildlife Management, Vol. 70, No. 2,* 2006.

[2]   J. Johnson, "Greater Prairie Chicken (Tympanuchus Cupido)," 2011. [Online]. Available: https://birdsna.org/Species-Account/bna/species/grpchi.

[3]   A. Wilson, "The Feasibility of Counting Songbirds Using Unmanned Aerial Vehicles," *American Ornithological Society,* vol. 134, no. AUK-16-216.1, pp. 350-362, 2017.

[4]   J. A. Klepp, Engineering Applications of Acoustics, Norwood, MA: Artech Hourse, Inc., 1989.

[5]   S. Jaeger, "Effect of Surface Treatment on Array Microphone Self-Noise," *American Institute of Aeronautics and Astronautics, Inc.,* 2000.

[6]   H. E. Carmargo, "Evaluation and Calibration of a Prototype Acoustic Test Section for the Virginia Tech Stability Wind Tunnel," Virginia Polytechnic Institute and State University, Blacksburg, VA, 2005.

[7]   ASTM E2611-09, "Standard Test Method for Measurement of Normal Incidence Sound Transmission of Acoustical Materials Based on the Transfer Matrix Method," ASTM International, 2009.

[8]   SAE Standard J1400, "Laboratory Measurement of the Airborne Sound Barrier Performance of Flat Materials and Assemblies," SAE International, Warrendale, PA, 2010

[9]   K. C. Vengala, "Building a Modified Impedance Tube for Measurement of Sound Transmission Loss and Absorption Coefficients of Polymer Cross-Linked Aerogel Core Composites," Oklahoma State University, Stillwater, 2007.

[10]   J. R. Callicoat, "Composite Materials Providing Improved Acoustic Transmission Loss for UAVs," Oklahoma State University, Stillwater, 2016.

[11] ISO 3745:2012, "Acoustics - Determination of sound power levels and sound energy levels of noise sources using sound pressure - Precision methods for anechoic rooms and hemi-anechoic rooms," BSI Standards Publication, 2012.

[12] J. G. Rodrigues, "Design and Implementation of Aspects of a Small Anechoic Room and Sound-Actuation System," 2011.

[13] Brooks et. al.: NASA Langely Research Center, "Effect of Directional Array Size on the Measurement of AIrframe Noise Components," in *Fifth AIAA/CEA Aeroacoustics Conference*, Bellevue, 1999.

[14] Applied Fluid Dynamics Inc., "Wind Tunnel Information Sheet," 2015. [Online]. Available: http://appliedfluiddynamics.ca/facilities/. [Accessed 2017].

[15] J. Cates, "Construction and Operation of the MAE Flexible Use Wind Tunnel Facility," Oklahoma State University, Stillwater, 1996.

[16] M. Möser, Engineering Acoustics, An Introduction Into Noise Control, Berlin: Springer-Verlag Berlin Heidelberg NewYork, 2004

[17] R. Moffat, "Describing the Uncertainties in Experimental Results," Elsevier Science Publishing Co., Inc., 1988

[18] J. Barlow, Low-Speed Wind Tunnel Testing, Third Edition, New York: John Wiley & Sons, INC., 1999.

[19] Schlinker, "Refraction and Scattering of Sound by a Shear Layer," NASA Langley Research Center, 1980.

[20] Cox, Acoustic Absorbers and Diffusers, SAGE Publications, 2005.

[21] J. A. Banks, "AIAA-2017-0931 Windscreen Design for UAV Mounted Airborne Acoustic Sensing," *AIAA,* 2017.

[22] D. Kobilinsky, "Drone Successfully Capture Bird Sounds," 17 March 2017. [Online]. Available: http://wildlife.org/drones-successfully-capture-bird-sounds/. [Accessed 14 April 2017].

APPENDICES

Appendix A: Add Foam Factory 4" wedge data sheet

RIVERBANK ACOUSTICAL LABORATORIES

1512 S. BATAVIA AVENUE
GENEVA, ILLINOIS 60134

Alion Science and Technology

TEST REPORT

630/232-0104
FOUNDED 1918 BY
WALLACE CLEMENT SABINE

FOR: Foam Factory Inc.
Clinton Township, MI

Sound Absorption Test
RAL™-A11-146

ON: Foam Factory 4" Wedge Foam

Page 1 of 4

CONDUCTED: 13 July 2011

TEST METHOD

The test method conformed explicitly with the requirements of the ASTM Standard Test Method for Sound Absorption and Sound Absorption Coefficients by the Reverberation Room Method: ASTM C423-09a and E795-05. Riverbank Acoustical Laboratories has been accredited by the U.S. Department of Commerce, National Institute of Standards and Technology (NIST) under the National Voluntary Laboratory Accreditation Program (NVLAP) for this test procedure (NVLAP Lab Code: 100227-0). A description of the measuring procedure and room qualifications is available separately.

DESCRIPTION OF THE SPECIMEN

The test specimen was designated by the manufacturer as Foam Factory 4" Wedge Foam. The overall dimensions of the specimen as measured were nominally 2.74 m (108 in.) wide by 2.44 m (96 in.) long and 102 mm (4 in.) thick. The specimen consisted of twelve (12) pieces. Eight (8) pieces were nominally 610 mm (24 in.) wide by 1.22 m (48 in.) long. Four (4) pieces were nominally 305 mm (12 in.) wide by 610 mm (24 in.) long. Valley Depth: 3.25"; Base Thickness: 0.625"; Peak to Peak: 3.875". The specimen was tested in the laboratory's 292 m^3 (10,311 ft^3) test chamber.

The manufacturer's description of the specimen was as follows: Open Cell Polyurethane Foam Rubber; Fire Retardant. A visual inspection verified the manufacturer's description of the specimen.

The weight of the entire specimen as measured was 7.6 kg (16.75 lbs), an average of 1.1 kg/m^2 (0.23 lbs/ft^2). The area used in the calculations was 6.7 m^2 (72 ft^2). The room temperature at the time of the test was 22°C (71°F) and 62±1% relative humidity.

MOUNTING A

The test specimen was laid directly against the test surface. The perimeter was sealed using metal framing.

RIVERBANK ACOUSTICAL LABORATORIES

TEST REPORT

Foam Factory Inc.

RAL™-A11-146

13 July 2011

Page 2 of 4

TEST RESULTS

1/3 Octave Center Frequency (Hz)	Absorption Coefficient	Total Absorption In Sabins
100	0.38	27.55
** 125	0.39	27.75
160	0.39	27.73
200	0.48	34.68
** 250	0.61	43.65
315	0.77	55.63
400	0.88	63.56
** 500	0.91	65.24
630	0.86	62.13
800	0.82	59.06
** 1000	0.79	56.72
1250	0.81	58.56
1600	0.84	60.71
** 2000	0.95	68.53
2500	1.03	74.37
3150	1.04	75.04
** 4000	1.03	74.09
5000	1.07	76.99

SAA = 0.81
NRC = 0.80

RIVERBANK ACOUSTICAL LABORATORIES

**1512 S. BATAVIA AVENUE
GENEVA, ILLINOIS 60134**

Alion Science and Technology

TEST REPORT

Foam Factory Inc.

13 July 2011

RAL™-A11-146

Page 3 of 4

TEST RESULTS (Continued)

The sound absorption average (SAA) is defined as a single number rating, the average, rounded to the nearest 0.01, of the sound absorption coefficient of a material for the twelve one-third octave bands from 200 through 2500 Hz, inclusive.

The noise reduction coefficient (NRC) is defined from previous versions of this same test method as the average of the coefficients at 250, 500, 1000, and 2000 Hz, expressed to the nearest integral multiple of 0.05.

Tested by _____

Dean Victor
Senior Experimentalist

Approved by _____

David L. Moyer
Laboratory Manager

RIVERBANK ACOUSTICAL LABORATORIES

1512 S. BATAVIA AVENUE
GENEVA, ILLINOIS 60134

Alion Science and Technology

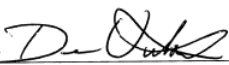630/232-0104
FOUNDED 1918 BY
WALLACE CLEMENT SABINE
Page 4 of 4

TEST REPORT
SOUND ABSORPTION REPORT
RAL-A11-146

SAA=0.81
NRC=0.80

This report shall not be reproduced except in full, without the written approval of RAL.
THE RESULTS REPORTED ABOVE APPLY ONLY TO THE SPECIFIC SAMPLE SUBMITTED FOR MEASUREMENT. NO RESPONSIBILITY IS ASSUMED FOR PERFORMANCE OF ANY OTHER SPECIMEN.

ACCREDITED BY DEPARTMENT OF COMMERCE, NATIONAL VOLUNTARY LABORATORY
ACCREDITATION PROGRAM FOR SELECTED TEST METHODS FOR ACOUSTICS.
THE LABORATORY'S ACCREDITATION OR ANY OF ITS TEST REPORTS IN NO WAY CONSTITUTES
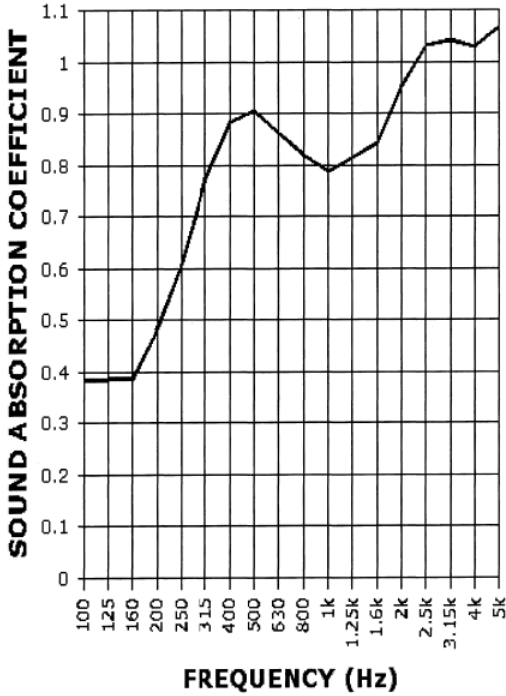OR IMPLIES PRODUCT CERTIFICATION, APPROVAL, OR ENDORSEMENT BY NIST.

NVLAP Lab Code 100227-0

115

Appendix B: Laminating resin system used to fabricate samples

Resin Services, Inc.

Home | About Us | F.A.Q. | News | Testimonials | Products

Room Temperature Laminating – WB-400

Category: Laminating
Ratio: 100pbw to 50pbw
Hardener: SC-150N
Description: WB-400 is an unfilled, clean epoxy resin system with virtually no blush on surface or back. WB-400 is a tough, strong impact-resistant resin with good chemical resistance. It has excellent wetting quality on Kevlar, Carbon Graphite and Fiberglass.
Ratio By Weight: 100pbw to 50pbw
Pot Life (454 Gram Mass): 30 minutes
Pot Life at 72° F (200 Gram Mass): 50 mins.
Viscosity CPS: 2,500
Cure Time: 30 hours
Shore "D": 82
Shore "D" Room Temperature: 78
Flexural Strength: 14,000
Compressive Yield_PSI: 15,000
Izod Impact, Ft-Lb_Inch Notch: 0.46
Tensile Elongation at Break, %: 6.0
Tensile Strength @25C: 8,500
Flexural Strength @25C: 8,900
Heat Distortion: 160°F
Density Resin: 9.4
Density Hardener: 8.5
Density Mixed: 9.18
Specific Gravity Resin: 1.14
Specific Gravity Hardener: 1.03
Specific Gravity Mixed: 1.11
Shelf Life Resin_Hardener: 1 year

« Back To Product Listings

Contact Us

5959 18 ½ Mile Road
Sterling Heights, MI 48314
586.254.6770
[Map]
resinservices@aol.com

© Copyright 2017 Resin Services Inc.
Website Design & Development By 3Sixty Interactive

Appendix C: Microphone Equipment Datasheets
C.1   GRAS 1/2-Inch Condenser Microphone Typical Datasheet

Calibration Chart
½" Prepolarized Pressure Microphone
Type 40AD

G.R.A.S.
SOUND & VIBRATION

Microphone Type 40AD: **Serial No. 145170**

Calibration Date: 05 April, 2011
Operator: HM

Enviromental Calibration Conditions:
Temperature: 23 °C
Relative humidity: 32 %
Barometric pressure: 1010 hPa

Open Circuit Sensitivity
The calibration is performed by comparison with a Reference Microphone Cartridge Type 40AG and is traceable to the National Physical Laboratory, UK.
The stated sensitivity for the microphone cartridge is the open circuit sensitivity. When used with a typical preamplifier, like the G.R.A.S. Type 26AH, the sensitivity will be 0.2 dB lower.

Test Frequency [Hz]	Measured Level [mV/Pa]	Measured Level [dB re. 1V/Pa]	Uncertanty [dB]
250	52.86	-25.54	±0.06
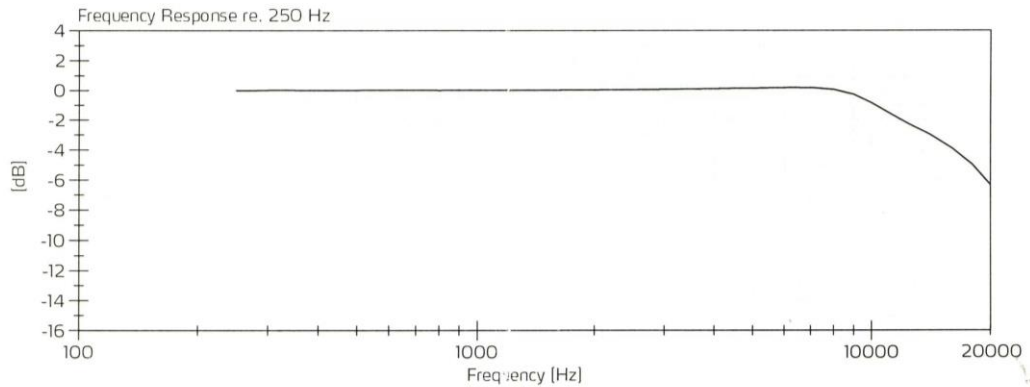
½" Prepolarized Pressure Microphone
Type 40AD

Serial No. 145170
Mic # 12

Frequency response
The graph shows the frequency response of the microphone. The response is recorded by elecrostatic actuator and is measured relative to 250 Hz.
(See back for more information)

G.R.A.S.
SOUND & VIBRATION

Skovlytoften 33 · 2840 Holte · Denmark
E-mail: gras@gras.dk · www.gras.dk

40AD ½" Prepolarized Pressure Microphone

The 40AD is a ½" prepolarized pressure microphone for general purpose acoustic measurements in couplers, at boundaries etc. The microphone complies with the requirements in IEC Standard 61094 part 4.

The pressure microphone is designed to measure the sound pressure at the diaphragm. It has a flat pressure frequency response in its entire frequency range.
At higher frequencies the presence of the microphone itself in the sound field will change the sound pressure.

In general the sound pressure around the microphone cartridge will increase due to reflections and diffraction. The pressure microphone is designed so that it measures the pressure on the diaphragm, including the influence of the microphone on the sound field.

Specifications

Nominal Open Circuit Sensitivity :			Sensitivity to Vibrations:	
at 250Hz	50 mV/Pa		Equiv. SPL for 1m/s^2 perpendicular to diaphragm 62 dB re. 20μPa	
Frequency Response:				
±2 dB	3.15Hz-10kHz		Temperature Range:	
±1 dB	12.5Hz-7.5kHz			-40 to +150°C
Polarization Voltage:			Mean Temperature Coefficient:	
	0V		-10 to +50°C	0.01dB/°C
Upper Limit of Dynamic Range:			Length:	
3% Distortion	148dB re. 20μPa		With Protection Grid	16.2mm
Lower Limit of Dynamic Range:			Diameter:	
Thermal noise	16dBA re. 20μPa		With Protection Grid	13.2mm
			Without Protection Grid	12.7mm
Nominal Cartridge Capacitance:				
Polarized	20pF		Thread:	
			Protection Grid	12.7mm 60 UNS
Resonance Frequency:			Preamplifier	11.7mm 60 UNS
90° Phase shift	14kHz			
			Weight:	
Effective Front Volume:				9g
Nominal at 250Hz	50mm^3			
Static Pressure Coefficient:				
250Hz at 25°C	-0.008 dB/kPa			

C.2   Microphone Pre-amplifier Typical Datasheet

Calibration Chart
½" CCP Preamplifier
Type 26CA

G.R.A.S.
SOUND & VIBRATION

Preamplifier Type 26CA:	Serial No. 144421

Calibration Date: 26. mar 2011
Operator: CP

Noise floor (w. 20 pF input adapter)

Linear Noise 20Hz - 20kHz [µV]	A-Weighted Noise [µV]
3.48	2.15

Description
The 26CA is a Constant Current Powered (CCP) general purpose ½" preamplifier, with integrated BNC connector. It is ICP® compatible, and can also be used with G.R.A.S. ¼" microphones, using the adaptor RA0019. The 26CA supports TEDS (Transducer Electronic Data Sheet) according to IEEE 1451.4.

(ICP is a trademark of PCB Piezotronics Inc.)

Specifications:

Frequency Range (±0.2 dB) (cable load 4.7 nF):
  2.5 Hz - 100 kHz

Input Impedance:
  20 GΩ, 0.4pF

Output Impedance (Cs = 20 pF, f=1000Hz):
  25 Ω typical

Output Voltage Swing (Peak):
  ±8 V

Noise (measured with 20 pF ½" dummy mic.):
  A-weighted: < 2.5 µV
  Linear (20Hz - 20kHz):   < 6 µV

Gain:
  Typical -0.30 dB

Power Supply:
  2 - 20 mA (4 mA typical)

Temperature:
  Operation: -30° - +70°C
  Storage: -40° - +85°C

Relative Humidity:
  Operation: 0 - 95%
  Storage: 0 - 95%

Dimensions:
  Diameter: 12.7 mm   (0.5")
  Length: 73 mm   (2.85")
  Weight: 26 g   (0.9 oz)

½" CCP Preamplifier
Type 26CA

Serial No. 144421

Preamp # 12

G.R.A.S.
SOUND & VIBRATION

Skovlytoften 33 · 2840 Holte · Denmark
E-mail: gras@gras.dk · www.gras.dk

C.3   Microphone Nose Cone Datasheet

Calibration Certificate

1/2" Nose Cone RA0020

G.R.A.S.
SOUND & VIBRATION

Description:

The RA0020 is a ½" Nose Cone to be mounted on ½" measurement microphones instead of the normal protection grid. The nose cone reduces the aerodynamically induced noise when measuring in high speed laminar flows, as for example in wind tunnels. The Nose Cone should be pointed in the direction towards the wind flow.
The nose cone has been designed in accordance with specifications in NLR TP 96320 with a special aerodynamic shape to minimize the pressure gradient at the screen position and maximize the boundary layer stability.

Ref. : Nationaal Lucht- en Ruimtevaartlaboratorium, "Design and Testing of a Low Self-noise Aerodynamic Microphone Forebody", T. Dassen, H. Holthusen and M. Beukema, NLR TP 96320 L, Netherlands.
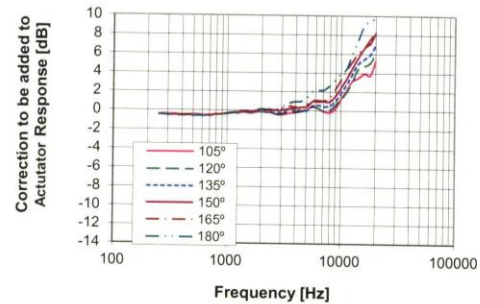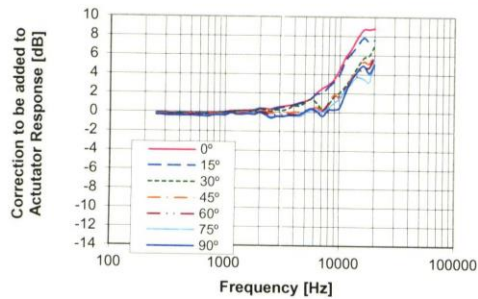
Specifications:

Frequency Range :
  Up to 20 kHz

Dimensions:
  Diameter: 13.0mm
  Length: 54.0mm
  Weight: 45g

Free Field Correction for ½" Free Field microphone Type 40AF fitted with Nose Cone RA0020

1/2" Nose Cone
RA0020

G.R.A.S.
SOUND & VIBRATION

Skovlytoften 33 · 2840 Holte · Denmark
E-mail: gras@gras.dk · www.gras.dk

NI USB-443*x* Specifications

Français	Deutsch	日本語	한국어	简体中文
		ni.com/manuals		

This document lists specifications for the NI USB-443*x* devices. The specifications apply to both the NI USB-4431 and NI USB-4432 unless otherwise noted. These specifications are typical at 25 °C unless otherwise stated. All specifications are subject to change without notice. Visit ni.com/manuals for the most current specifications and product documentation.

⚠ **Caution** The inputs of this sensitive test and measurement product are not protected for electromagnetic interference for functional reasons. As a result, this product may experience reduced measurement accuracy or other temporary performance degradation when cables are attached in an environment with electromagnetic interference present. Refer to the Declaration of Conformity (DoC) of this product for details of the standards applied to assess electromagnetic compatibility performance. To obtain the DoC, visit ni.com/certification, search by model number or product line, and click the appropriate link in the Certification column.

⚠ **Caution** To ensure the specified EMC performance, operate this product only with shielded cables and accessories.

Analog Input

Input channels
    NI USB-4431 4
    NI USB-4432 5

Input connector ....1 BNC per channel

PC communication...USB 2.0

Power consumption...2.5 W max

ADC resolution ....24 bits

ADC type ....Delta-sigma

Sampling mode ....Simultaneous

Sample rates (f_s)
    Range ....1 kS/s to 102.4 kS/s
    Resolution[1]...≤2.10 mS/s

Internal frequency timebase accuracy....................±100 ppm max

---

[1] Depends on the sample rate. Refer to the *Sample Rate and Update Rate, Accuracy and Coercion* section of the *NI Dynamic Signal Acquisition User Manual* for more information.

Input range

    NI USB-4431 .... ±10 V$_{pk}$

    NI USB-4432 .... ±40 V$_{pk}$

FIFO buffer size .... 1,023 samples (shared between all channels)

Input coupling .... AC or DC, each channel independently software selectable

Input Impedance

Terminal	NI USB-4431 Input Impedance	NI USB-4432 Input Impedance
Between positive input and negative input	200 kΩ ‖ 130 pF	800 kΩ ‖ 120 pF
Between negative input and chassis ground	1 kΩ	1 kΩ

Absolute Maximum Input Voltage

Input	Voltage (V$_{pk}$)*
Positive terminal (+)	±60
Negative terminal (–)	±10

Notes: Voltages above those listed in this table may cause permanent damage to the device.

This is a stress rating only; specifications for the device are only valid when it is operated within its listed input range.

* Voltages with respect to chassis ground.

AI Gain Accuracy (NI USB-4431)

Temperature Range	Amplitude Accuracy (AC at 1 kHz)*[†]	Amplitude Accuracy (DC)*
10 °C to 40 °C	±0.025 dB typ	±0.15% typ
	±0.032 dB max	±0.3% max
–30 °C to 70 °C	±0.052 dB max	±0.5% max

* For sample rates lower than 40 kS/s, add 0.01 dB of AC error and 0.1% of DC error to both typical and maximum specifications.

[†] Applies to both AC and DC coupling.

AI Gain Accuracy (NI USB-4432)

Temperature Range	Amplitude Accuracy (AC at 1 kHz)*	Amplitude Accuracy (DC)*
10 °C to 40 °C	±0.025 dB typ	±0.25% typ
	±0.035 dB max	±0.35% max
–30 °C to 70 °C	±0.055 dB max	±0.65% max
* For sample rates lower than 40 kS/s, add 0.06 dB of AC error and 0.25% of DC error to both typical and maximum specifications.		

AI interchannel gain mismatch (–30 °C to 70 °C)
    NI USB-4431 ....0.01 dB at 1 kHz
    NI USB-4432 ....0.015 dB at 1 kHz

AI Offset

Temperature Range	NI USB-4431 Offset*	NI USB-4432 Offset*
10 °C to 40 °C	±750 µV typ	±2.6 mV typ
	±2.25 mV max	±7 mV max
–30 °C to 70 °C	±6.25 mV max	±17 mV max
* Source impedance ≤1 Ω. Offsets apply for both AC and DC coupling settings.		

AI Frequency Response

AI Amplitude Flatness

Input Signal Frequency (f_{in})	Flatness*
20 Hz to 20 kHz	±0.01 dB typ
	±0.02 dB max
20 Hz to 46.4 kHz	±0.02 dB typ
	±0.05 dB max
* Relative to 1 kHz	

AI phase linearity
    f_{in} = 20 Hz to 20 kHz ....±0.01°
    f_{in} = 20 Hz to 46.4 kHz ....±0.05°

AI interchannel phase mismatch
    (f_{in} ≥100 Hz)...0.02°/kHz · f_{in} typ, 0.04°/kHz · f_{in} max

–3 dB bandwidth...0.49 · f_s

AC coupling
    NI USB-4431
        –3 dB cutoff frequency ....0.8 Hz
        –0.1 dB cutoff frequency ....6 Hz

NI USB-4432

 −3 dB cutoff frequency ....0.1 Hz

 −0.1 dB cutoff frequency ....0.7 Hz

ADC filter delay (nominal)...................................39 samples

AI Distortion Plus Noise (NI USB-4431)

Input Signal Frequency (f_{in})	THD*	THD+N*
20 Hz to 20 kHz	−99 dB typ	−90 dB typ
	−93 dB max	−84 dB max
20 Hz to 46.4 kHz	−93 dB typ	−86 dB typ
	−87 dB max	−80 dB max
* V_{in} = 8.9 V_{pk}		

AI Distortion Plus Noise (NI USB-4432)

Input Signal Frequency (f_{in})	THD*	THD+N*
20 Hz to 20 kHz	−97 dB typ	−92 dB typ
	−91 dB max	−86 dB max
20 Hz to 46.4 kHz	−95 dB typ	−91 dB typ
	−89 dB max	−85 dB max
* V_{in} = 8.9 V_{pk}		

AI dynamic range (−60 dBFS, 1 kHz tone; f_s = 102.4 kS/s)

 NI USB-4431 ....100 dB typ, 98 dB min

 NI USB-4432 ....101 dB typ, 99 dB min

AI spurious free dynamic range (SFDR)

 (−1 dBFS, 1 kHz tone; f_s = 102.4 kS/s)...........104 dB

AI non-harmonic SFDR

 (−1 dBFS, 1 kHz tone; f_s = 102.4 kS/s)...........110 dB

AI intermodulation distortion (IMD)

 (CCIF 11 kHz + 12 kHz, 1:1, −6 dBFS)........−100 dB

AI Noise

Measurement Bandwidth	NI USB-4431 Noise	NI USB-4432 Noise
20 kHz	55 μV_{rms} typ	200 μV_{rms} typ
	75 μV_{rms} max	240 μV_{rms} max
46.4 kHz	75 μV_{rms} typ	250 μV_{rms} typ
	100 μV_{rms} max	300 μV_{rms} max

124

AI Common-Mode Rejection Ratio (CMRR)

AI CMRR (f_{in} = 20 Hz to 1 kHz)

NI USB-4431 .... 55 dB

NI USB-4432 .... 45 dB

AI Crosstalk

f_{in}	NI USB-4431*	NI USB-4432*
1 kHz	−110 dB	−105 dB
46.4 kHz	−90 dB	−80 dB
* Source impedance ≤50 Ω		

IEPE Excitation

Channels AI0, AI1, AI2, AI3

Current .... 0 or 2.1 mA, each channel independently software selectable

Compliance voltage .... 20 V min

Output impedance .... 200 kΩ at 1 kHz

Current noise density .... 25 pA/$\sqrt{\text{Hz}}$ at 10 kHz

Fault detection

Thresholds .... <1.5 V (short), >19.5 V (open)

Indication .... Software, per channel

Transducer Electronic Data Sheet (TEDS) Support

Analog inputs AI<0..3> support Transducer Electronic Data Sheet (TEDS) according to the IEEE 1451 Standard.

For more information about TEDS, go to ni.com/info and enter the Info Code rdteds.

Maximum cable length .... 100 ft

Tachometer Inputs

You can use any analog input channel as a tachometer input.

Analog Output (NI USB-4431)

Output channels 1

AO signal connection .... BNC

AO frequency range .... DC to 43.5 kHz

Internal frequency timebase accuracy .... ±100 ppm max

DAC resolution .... 24 bits

DAC type .... Delta-sigma

Output signal range .... ±3.5 V_{pk}

Output coupling ....DC

Short circuit protection ....Indefinite

Minimum working load ....1 kΩ

Output impedance..50 Ω

DAC filter delay[1]...63.3 samples max

FIFO buffer size ....4,095 samples

AO Update Rates

Available rates are expressed by the following equation:

$$f_M/n$$

where

$f_M = \{51.2 \text{ kS/s}, 80 \text{ kS/s}, 96 \text{ kS/s}\}$, and

$n = \{1, 2, 4, 8, 16, 32, 64\}$

n	51.2 kS/s	80 kS/s	96 kS/s
1	51.2 kS/s	80 kS/s	96 kS/s
2	25.6 kS/s	40 kS/s	48 kS/s
4	12.8 kS/s	20 kS/s	24 kS/s
8	6.4 kS/s	10 kS/s	12 kS/s
16	3.2 kS/s	5 kS/s	6 kS/s
32	1.6 kS/s	2.5 kS/s	3 kS/s
64	800 S/s	1.25 kS/s	1.5 kS/s

AO Gain Accuracy

Temperature Range	Amplitude Accuracy (AC at 1 kHz)	Amplitude Accuracy (DC)
10 °C to 40 °C	±0.025 dB typ	±0.2% typ
	±0.045 dB max	±0.4% max
–30 °C to 70 °C	±0.1 dB max	±1.1% max

AO Offset

Temperature Range	Offset (DC)
10 °C to 40 °C	±700 µV typ
	±2 mV max
–30 °C to 70 °C	±6.5 mV max

---

[1] Refer to the *Filter Delay* section of the *NI Dynamic Signal Acquisition User Manual* for more information.

AO Frequency Response

AO phase linearity

f_{out} = DC to 20 kHz ....±0.25°

f_{out} = DC to 43.5 kHz ....±2.5°

AO Amplitude Flatness

Output Signal Frequency (f_{out})	Flatness*
DC to 20 kHz	±0.05 dB typ
	±0.09 dB max
DC to 43.5 kHz	±0.3 dB typ
	±0.4 dB max

* Relative to 1 kHz

AO Distortion and Noise

Note Specifications for the listed update rates also apply to their respective derivative rates as listed in the *AO Update Rates* section.

AO Distortion

Update Rate*	THD[†] (1 kHz)	THD[†] (20 Hz to 20 kHz)
51.2 kS/s	−100 dB typ	−89 dB max
80 kS/s	−97 dB typ	−86 dB max
96 kS/s	−95 dB typ	−85 dB max

Note: The measurement bandwidth is 0 Hz to 0.453 × the Update Rate.

* Refer to the note under the *AO Distortion and Noise* section for applicability to other update rates.

[†] V_{out} = 3.1 V_{pk}

AO Distortion Plus Noise

Update Rate*	THD+N[†] (1 kHz)	THD+N[†] (20 Hz to 20 kHz)
51.2 kS/s	−92 dB typ	−86 dB max
80 kS/s	−91 dB typ	−84 dB max
96 kS/s	−90 dB typ	−82 dB max

Note: The measurement bandwidth is 0 Hz to 0.453 × the Update Rate.

* Refer to the note under the *AO Distortion and Noise* section for applicability to other update rates.

[†] V_{out} = 3.1 V_{pk}

AO Noise

Update Rate*	Noise
51.2 kS/s	90 μV_{rms} typ
	120 μV_{rms} max
80 kS/s	100 μV_{rms} typ
	150 μV_{rms} max
96 kS/s	120 μV_{rms} typ
	200 μV_{rms} max

Note: The measurement bandwidth is 0 Hz to 0.453 × the Update Rate.

* Refer to the note under the *AO Distortion and Noise* section for applicability to other update rates.

AO Spurious Free Dynamic Range (Includes Harmonics)

Update Rate*	SFDR (–1 dBFS, 1 kHz)
51.2 kS/s	102 dB
80 kS/s	98 dB
96 kS/s	96 dB

Note: The measurement bandwidth is 0 Hz to 0.453 × the Update Rate.

* Refer to the note under the *AO Distortion and Noise* section for applicability to other update rates.

AO Dynamic Range

Update Rate*	Dynamic Range†
51.2 kS/s	89 dB typ
	86 dB min
80 kS/s	88 dB typ
	84 dB min
96 kS/s	86 dB typ
	82 dB min

Note: The measurement bandwidth is 0 Hz to 0.453 × the Update Rate.

* Refer to the note under the *AO Distortion and Noise* section for applicability to other update rates.

† V_{out} = –60 dBFS, 1 kHz

AO intermodulation distortion
(CCIF 11 kHz + 12 kHz, 1:1, –6 dBFS) ....–96 dB

AO Transients

The following actions will result in a transient on the analog output:

- Powering up the NI USB-4431
- Changing between AO rates in different columns of the table in the *AO Update Rates* section
- Changing the AI sample rate

Digital I/O Lines

Power-up mode .... Inputs pulled low

Input protection .... +5.6 V/–0.5 V

Purpose .... Start or reference trigger (importing only)

Source .... PFI<0..7>

Compatibility .... Transistor-transistor logic (5V TTL)

Polarity .... Rising or falling edge

Environment Specifications

Pollution degree 2

Maximum altitude .... 2,000 m

Indoor use only.

Operating Environment

Operating temperature .... –30 °C to 70 °C
(Tested in accordance with IEC-60068-2-1 and IEC-60068-2-2.)

Relative humidity range .... 0% to 95% RH, non-condensing
(Tested in accordance with IEC-60068-2-56.)

Storage Environment

Ambient temperature range .... –30 °C to 70 °C
(Tested in accordance with IEC-60068-2-1 and IEC-60068-2-2.)

Calibration

External calibration interval .... 1 year

Warm-up time .... 15 minutes to rated specifications

General Specifications

Physical

Dimensions .... 142 mm × 180 mm × 38 mm
(5.6 in. × 7.1 in. × 1.5 in.)

Weight .... 675 g (1.5 lbs)

Safety

This product meets the requirements of the following standards of safety for electrical equipment for measurement, control, and laboratory use:

- IEC 61010-1, EN 61010-1
- UL 61010-1, CSA 61010-1

Note For UL and other safety certifications, refer to the product label or the *Online Product Certification* section.

Electromagnetic Compatibility

This product meets the requirements of the following EMC standards for electrical equipment for measurement, control, and laboratory use:

- EN 61326-2-1 (IEC 61326-2-1): Class A emissions; Basic immunity
- EN 55011 (CISPR 11): Group 1, Class A emissions
- AS/NZS CISPR 11: Group 1, Class A emissions
- FCC 47 CFR Part 15B: Class A emissions
- ICES-001: Class A emissions

Note In the United States (per FCC 47 CFR), Class A equipment is intended for use in commercial, light-industrial, and heavy-industrial locations. In Europe, Canada, Australia and New Zealand (per CISPR 11) Class A equipment is intended for use only in heavy-industrial locations.

Note Group 1 equipment (per CISPR 11) is any industrial, scientific, or medical equipment that does not intentionally generates radio frequency energy for the treatment of material or inspection/analysis purposes.

Note For EMC declarations and certifications, and additional information, refer to the *Online Product Certification* section.

CE Compliance $\mathnormal{C}\mathnormal{E}$

This product meets the essential requirements of applicable European Directives as follows:

- 2006/95/EC; Low-Voltage Directive (safety)
- 2004/108/EC; Electromagnetic Compatibility Directive (EMC)

Online Product Certification

Refer to the product Declaration of Conformity (DoC) for additional regulatory compliance information. To obtain product certifications and the DoC for this product, visit ni.com/certification, search by model number or product line, and click the appropriate link in the Certification column.

Environmental Management

NI is committed to designing and manufacturing products in an environmentally responsible manner. NI recognizes that eliminating certain hazardous substances from our products is beneficial to the environment and to NI customers.

For additional environmental information, refer to the *NI and the Environment* Web page at ni.com/environment. This page contains the environmental regulations and directives with which NI complies, as well as other environmental information not included in this document.

Waste Electrical and Electronic Equipment (WEEE)

EU Customers At the end of the product life cycle, all products *must* be sent to a WEEE recycling center. For more information about WEEE recycling centers, National Instruments WEEE initiatives, and compliance with WEEE Directive 2002/96/EC on Waste and Electronic Equipment, visit ni.com/environment/weee.

电子信息产品污染控制管理办法 （中国 RoHS）

中国客户 National Instruments 符合中国电子信息产品中限制使用某些有害物质指令 (RoHS)。关于 National Instruments 中国 RoHS 合规性信息，请登录 ni.com/environment/rohs_china。(For information about China RoHS compliance, go to ni.com/environment/rohs_china.)

Appendix D: Wind Tunnel Source Speaker information

KICKER® DSC Coaxial Speakers

Package Contents:

- (2) DSC Coaxial Speakers
- (8) Mounting screws and speed clips
- (2) Positive–Negative lead wires
- (4) Wire caps

Model:	DSC693
Speaker Design	3 - Way
Woofer (in, mm)	6x8, 160x230
Mid (in, mm)	2, 50
Tweeter (in, mm)	1/2, 13
Rated Impedance (Ω)	4
Peak Power Handling (Watts)	360
Continuous Power Handling (Watts RMS)	90
Sensitivity (1W, 1m)	90
Frequency Response (Hz)	30-20k
Mounting Hole Diameter (in, mm)	5-5/8 x 8-7/16, 14.3x215
Top Mount Depth (in, mm)	7/10, 12
Bottom Mount Depth (in, mm)	3-3/16, 81
Tweeter Protrusion (in, mm)	1/10, 1
Grilles	Yes
Tweeter Magnet Material	Neodymium
Tweeter Dome Material	PEI (polyether imide)
Tweeter Design	Balanced dome
Woofer Cone Material	Polypropylene
Woofer Surround Material	Polyester foam

KICKER products are warranted against defects. Duration and terms of warranty depend on the laws in the country in which it was purchased. For details see your local KICKER Dealer or www.kicker.com/warranty.

Our goods come with guarantees that cannot be excluded under the **Australian Consumer Law**. You are entitled to a replacement or refund for a major failure and for compensation for any other reasonably foreseeable loss or damage. You are also entitled to have the goods repaired or replaced if the goods fail to be of acceptable quality and the failure does not amount to a major failure.

Appendix E: Boundary Layer Survey Results

Reference Section 3.4.6 for boundary layer survey discussion and methodology.

Free Stream Velocity: 36.5 ft/s

Free Stream Velocity: 36.5 ft/s
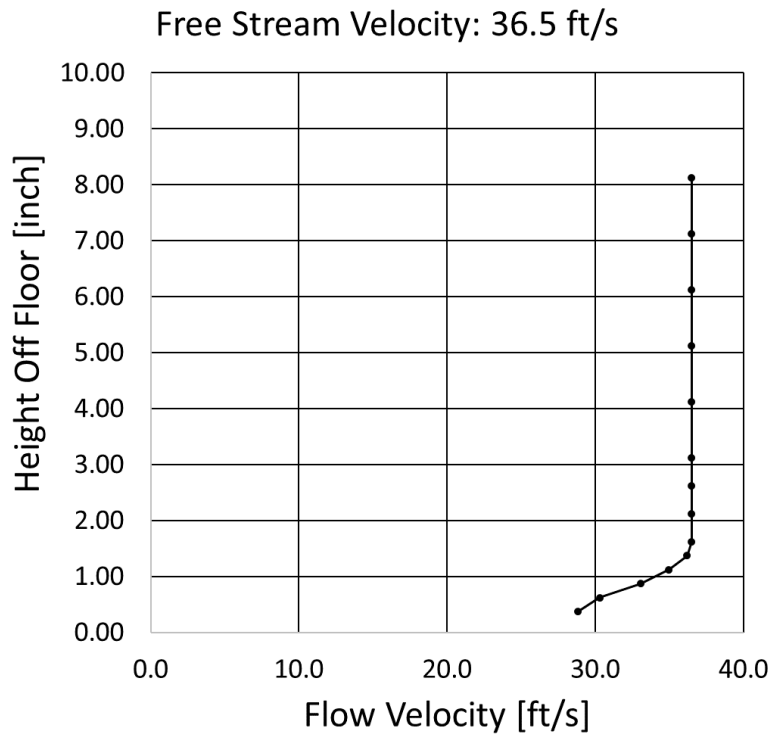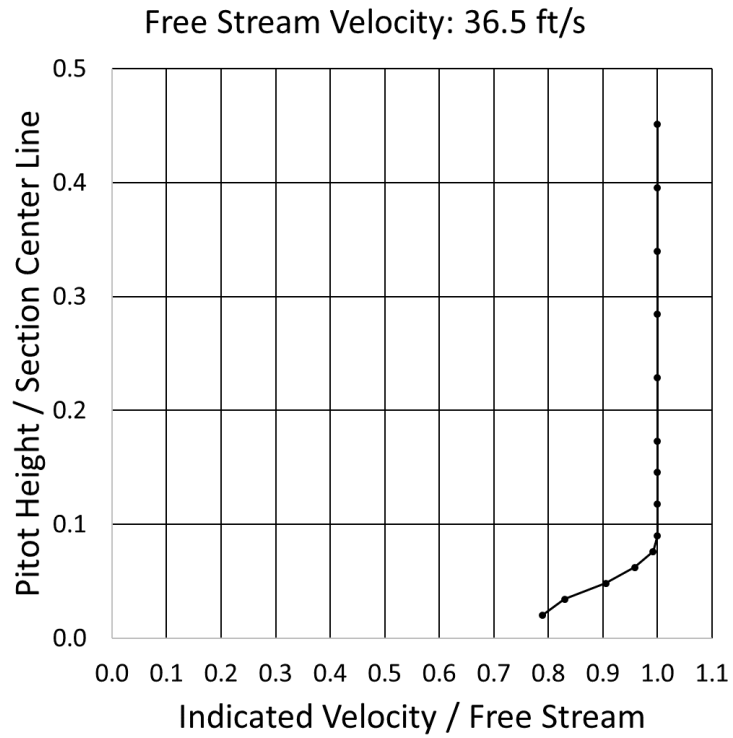
Free Stream Velocity: 41.3 ft/s
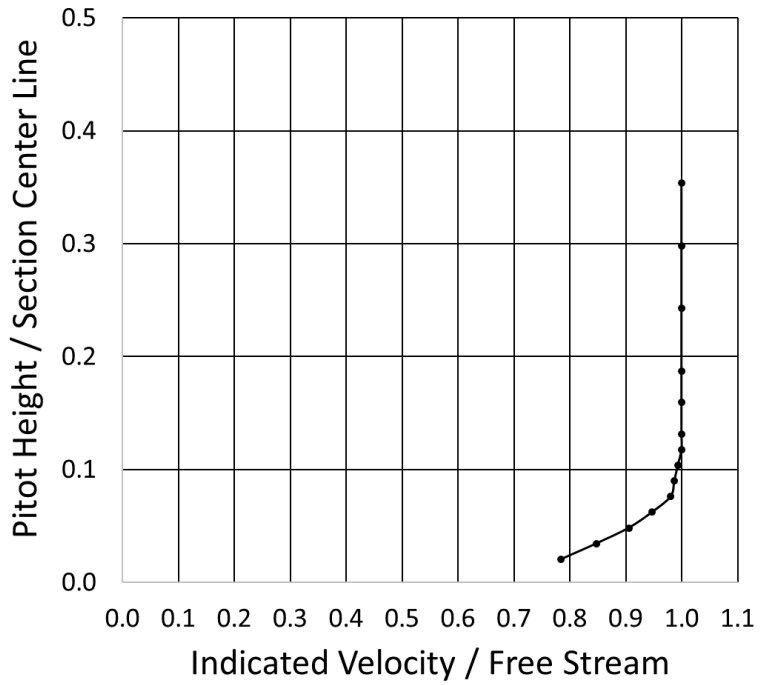
Free Stream Velocity: 41.3 ft/s
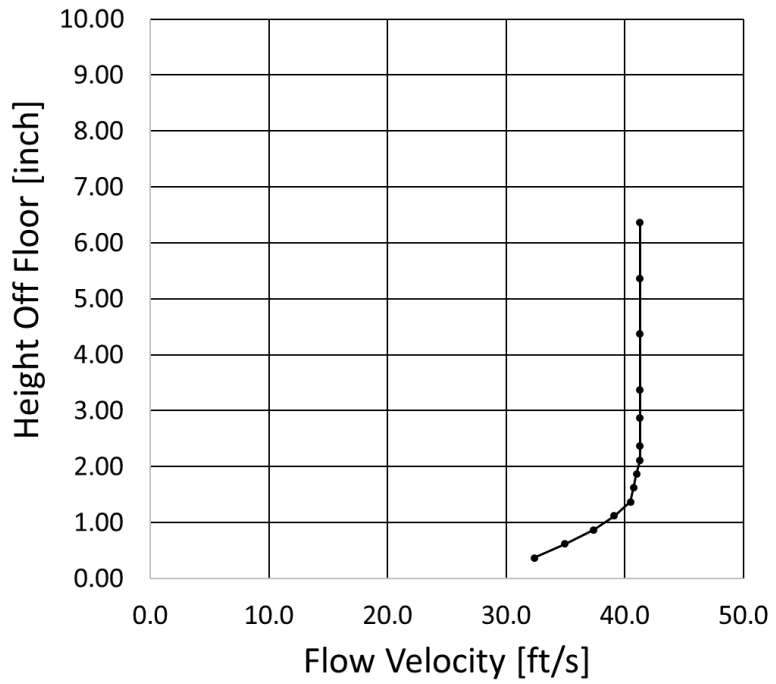
Free Stream Velocity: 46.7 ft/s
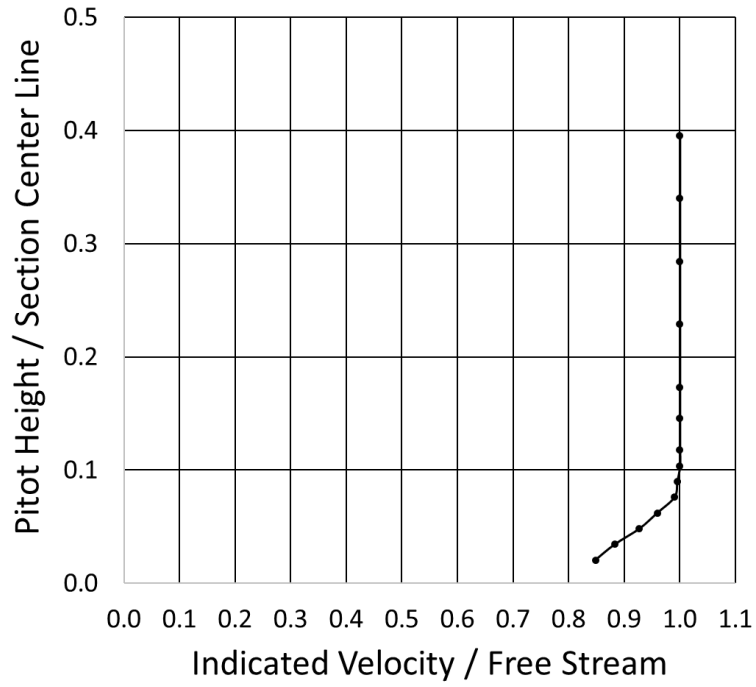
Free Stream Velocity: 46.7 ft/s
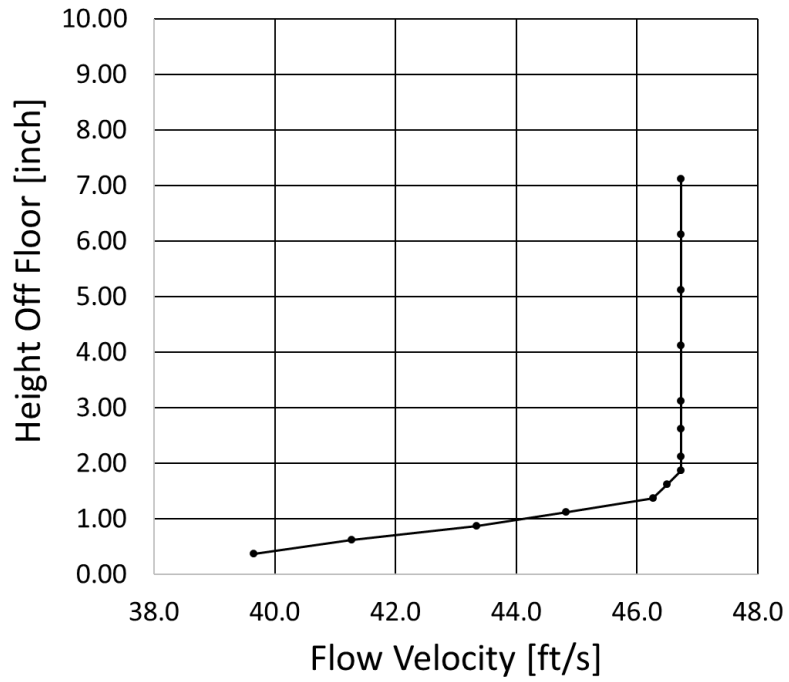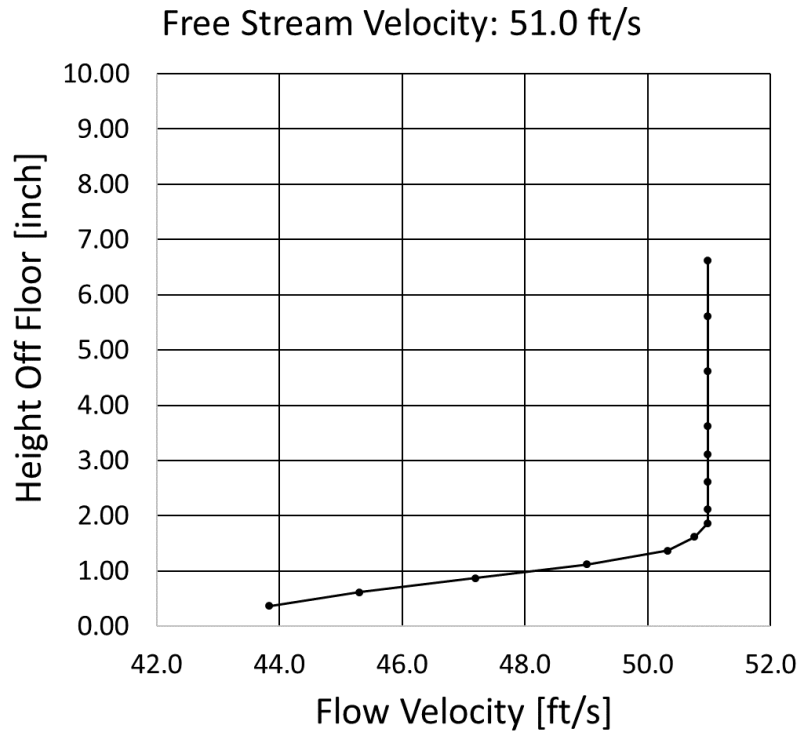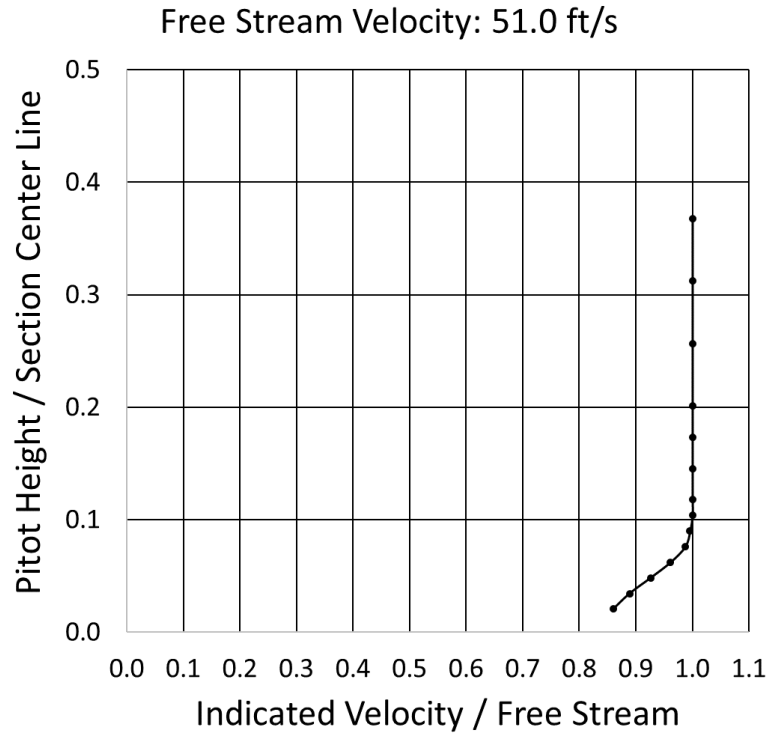
Figure 64. Boundary layer velocity profiles at all flow speeds measured with 1/4-inch traversing pitot probe connected to high precision water manometer

Appendix F: Acoustic Test Data

F.1   Flow-off White Noise STL Data
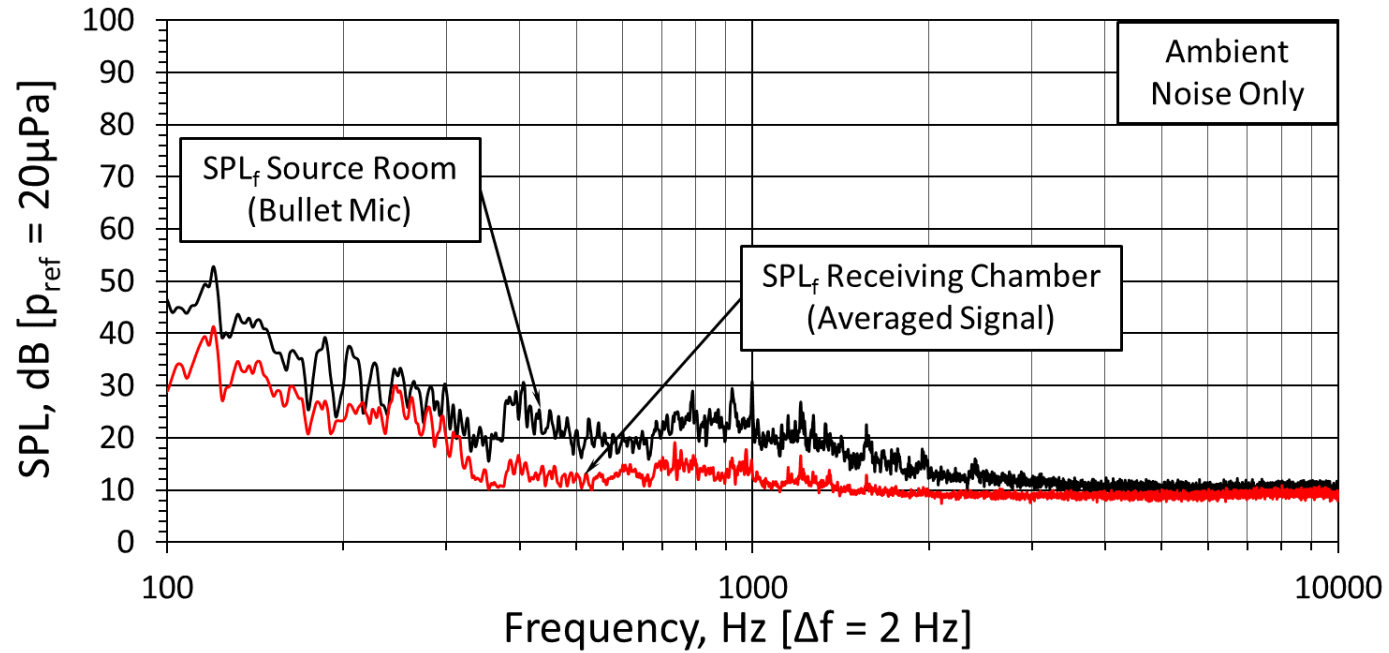
Figure 65. Tunnel specturm for specimen door configuration with ambient noise-only measured by bullet mic and quiet box spectrum averaged signal with flow off
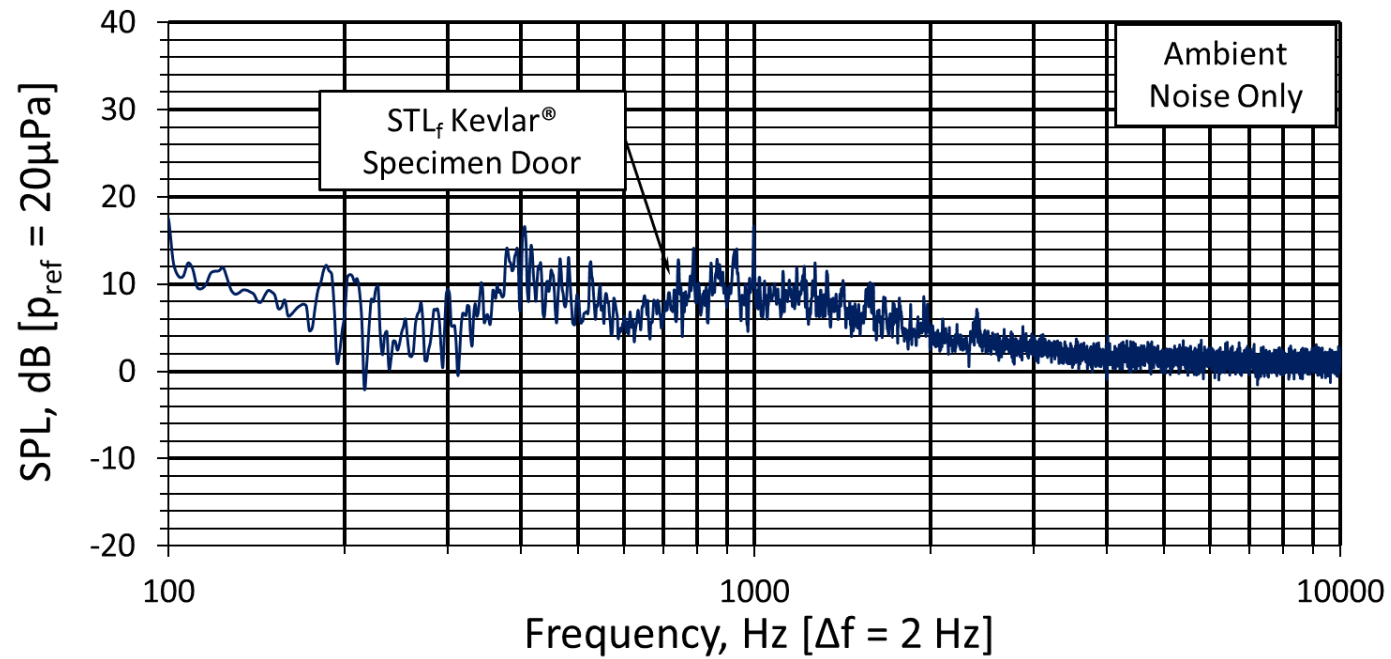
Figure 66. Tensioned Kevlar® validation specimen STL_f with ambient noise-only measured by bullet mic and quiet box spectrum averaged signal with flow off
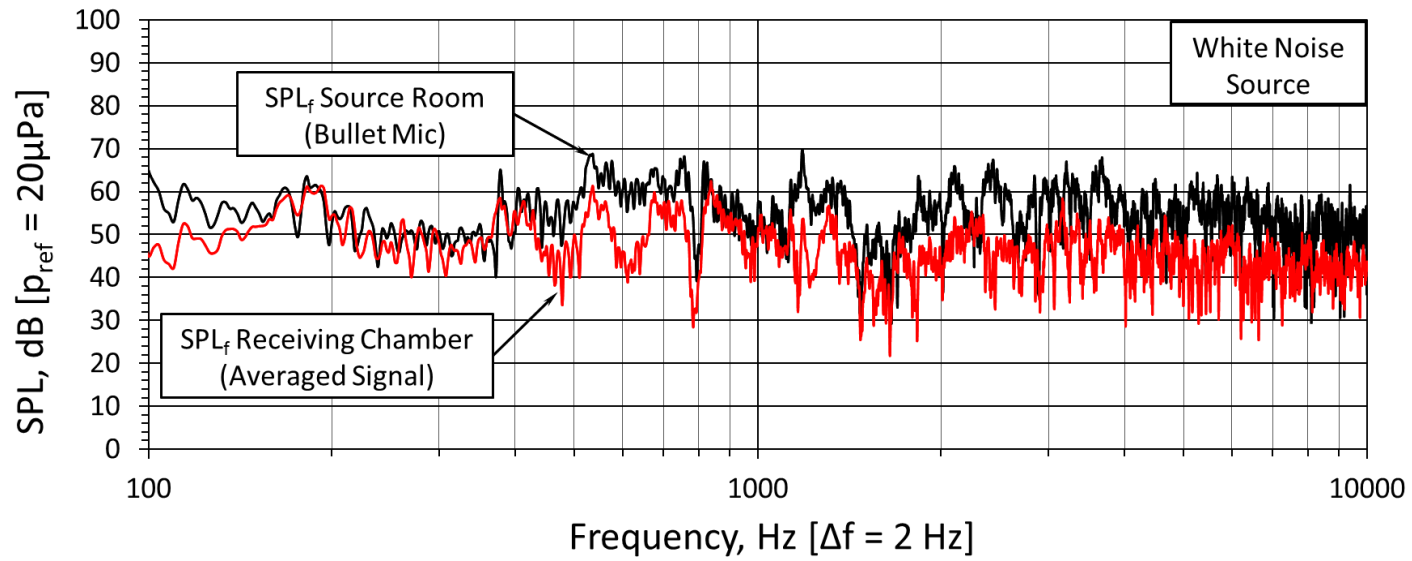
Figure 67. Tunnel specturm for specimen door configuration with white noise source measured by bullet mic and quiet box spectrum averaged signal with flow off
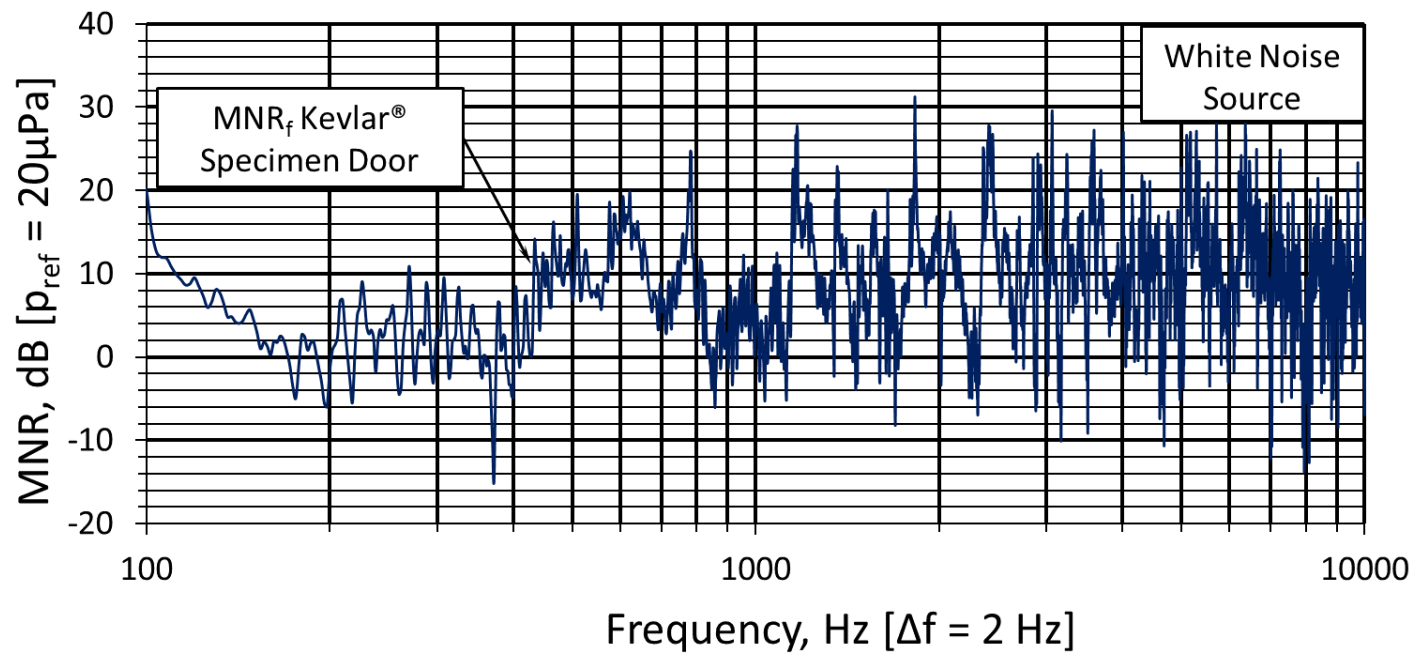
Figure 68. Tensioned Kevlar® validation specimen STL$_f$ with white noise source measured by bullet mic and quiet box spectrum averaged signal with flow off

F.2 Flow-on Tone Source STL Data
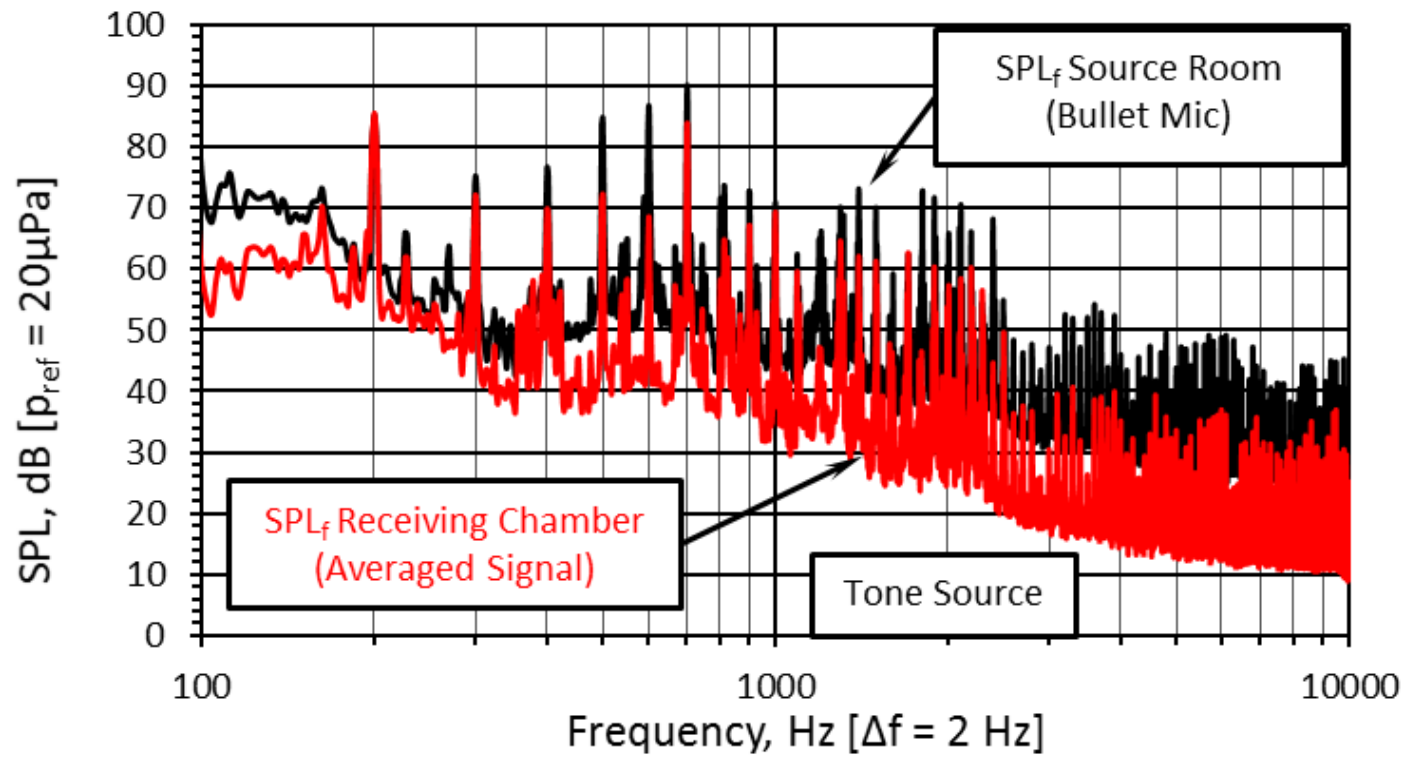
Figure 69. Tunnel specturm measured by bullet mic and quiet box spectrum averaged signal for flow speed of 36.3 ft/s
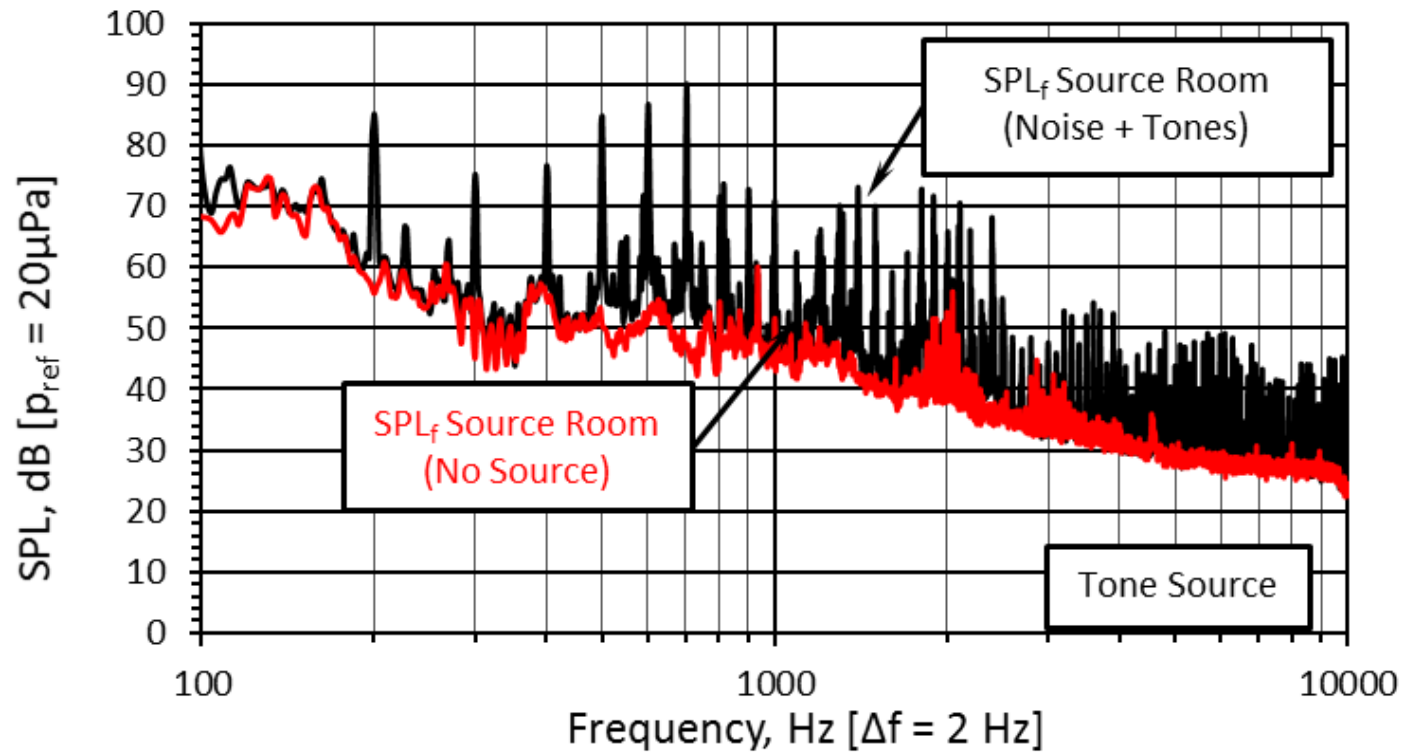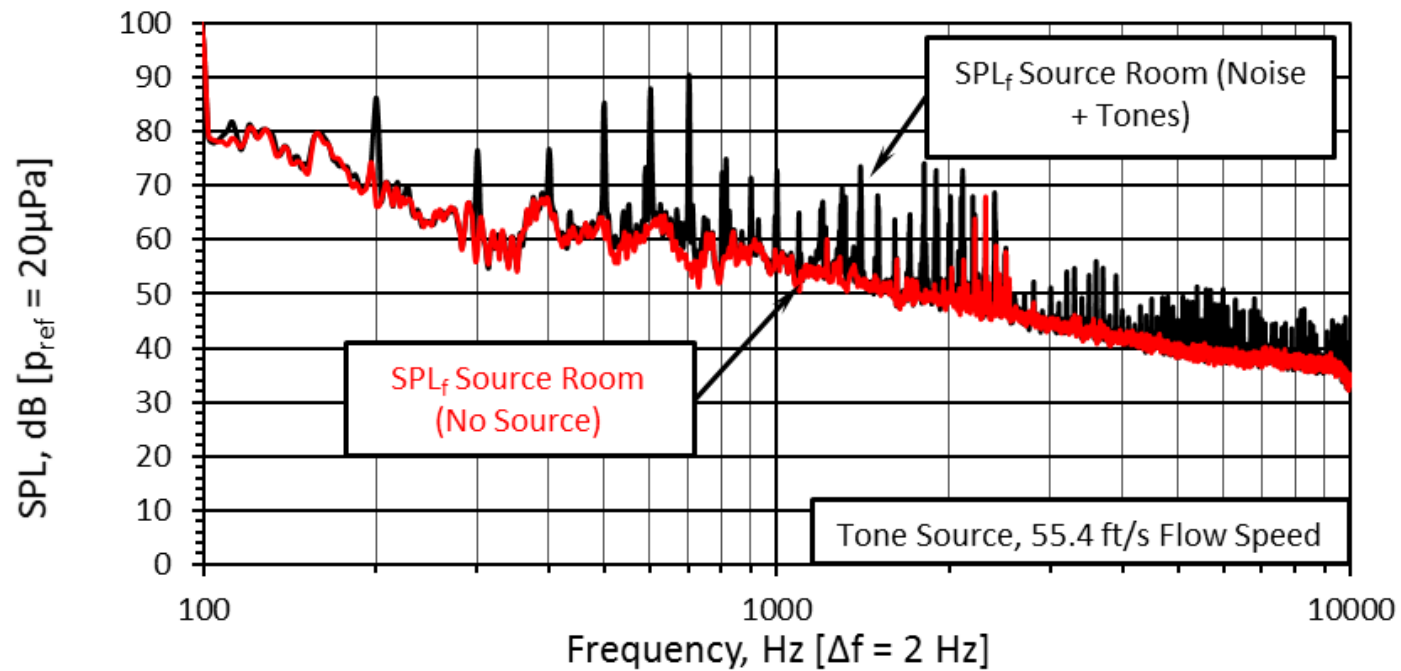
Figure 70. Tunnel specturm for background noise only and background noise + tone signal measured by bullet mic for flow speed of 36.3 ft/s
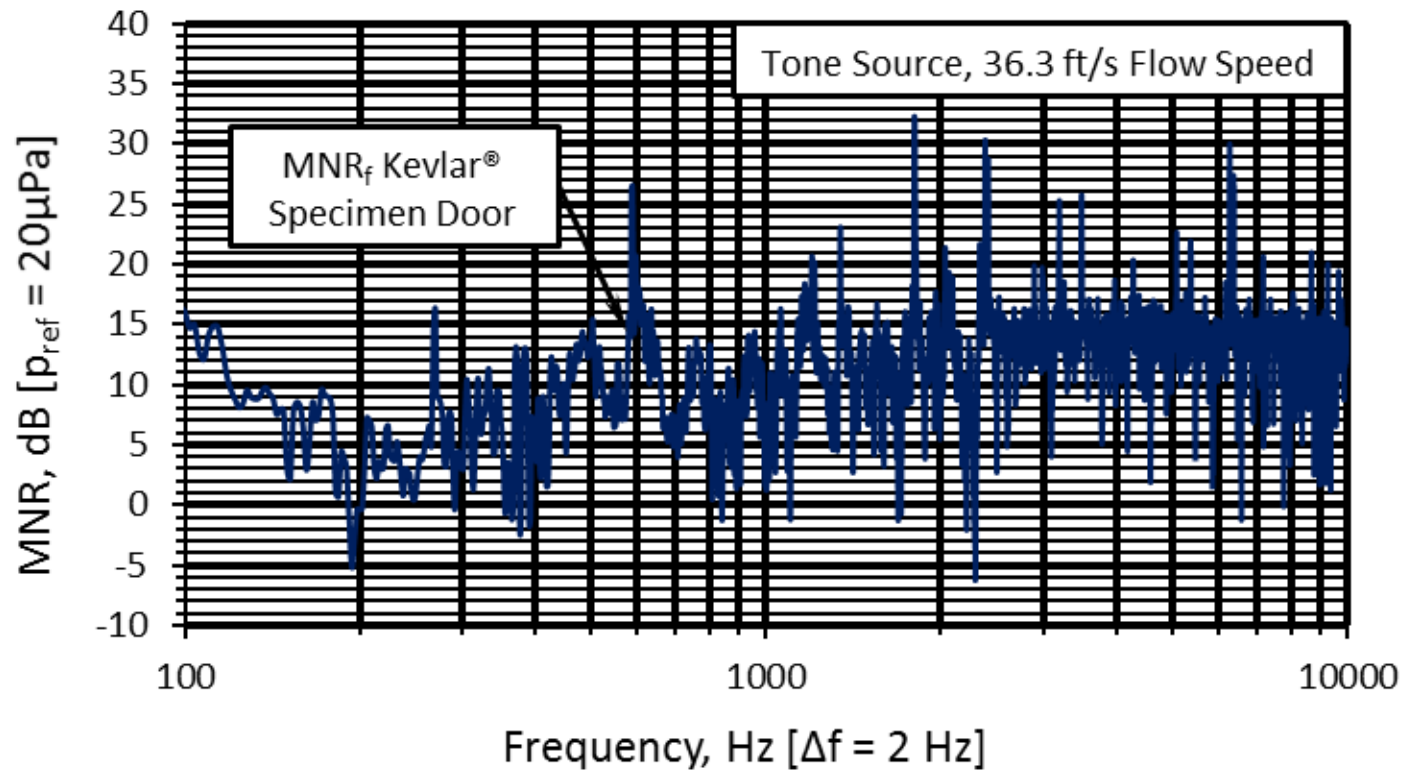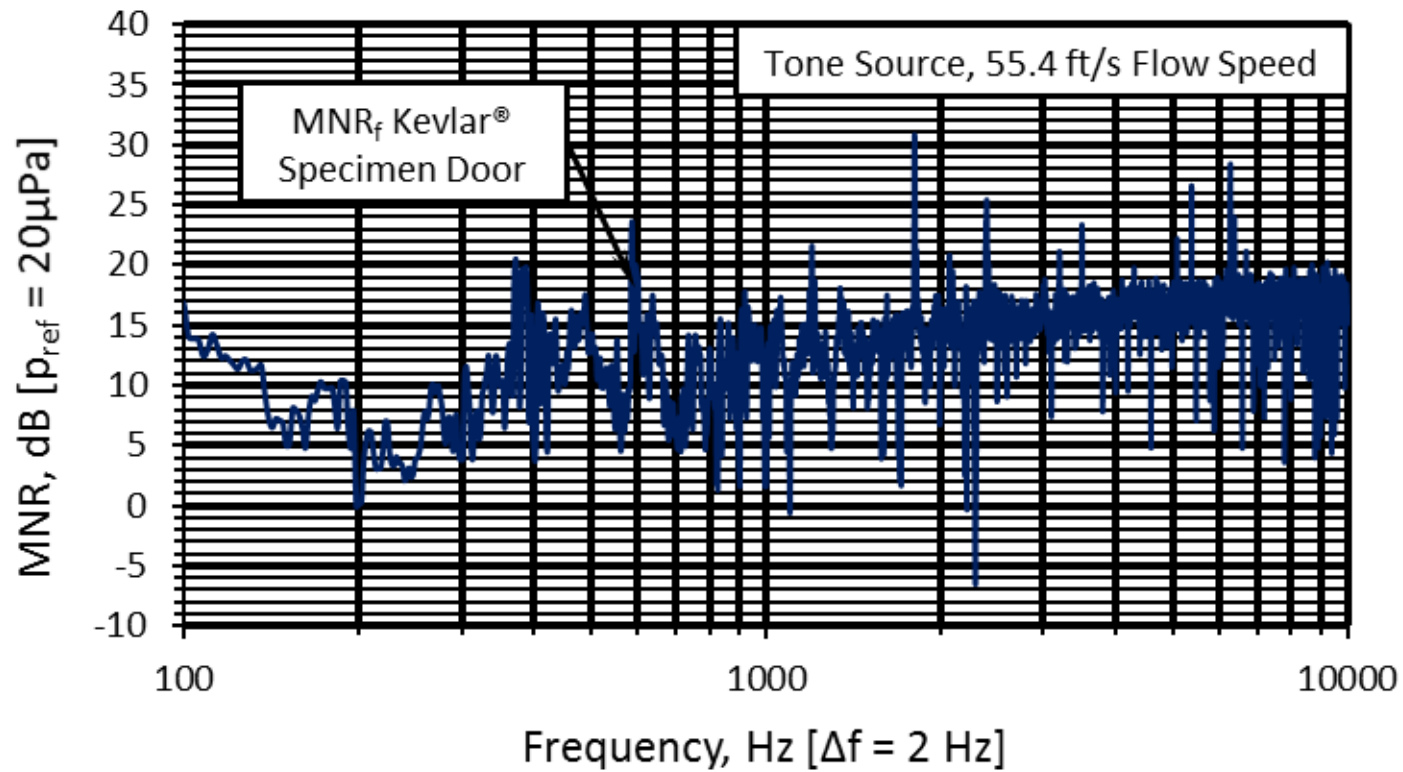
Figure 71. Flow noise + source tones Measured Noise Reduction specturm (MNR$_f$) measured by correcting for background noise then subtracting receiving chamber SPL$_f$ from source room SPL$_f$ for flow speed of 36.3 ft/s
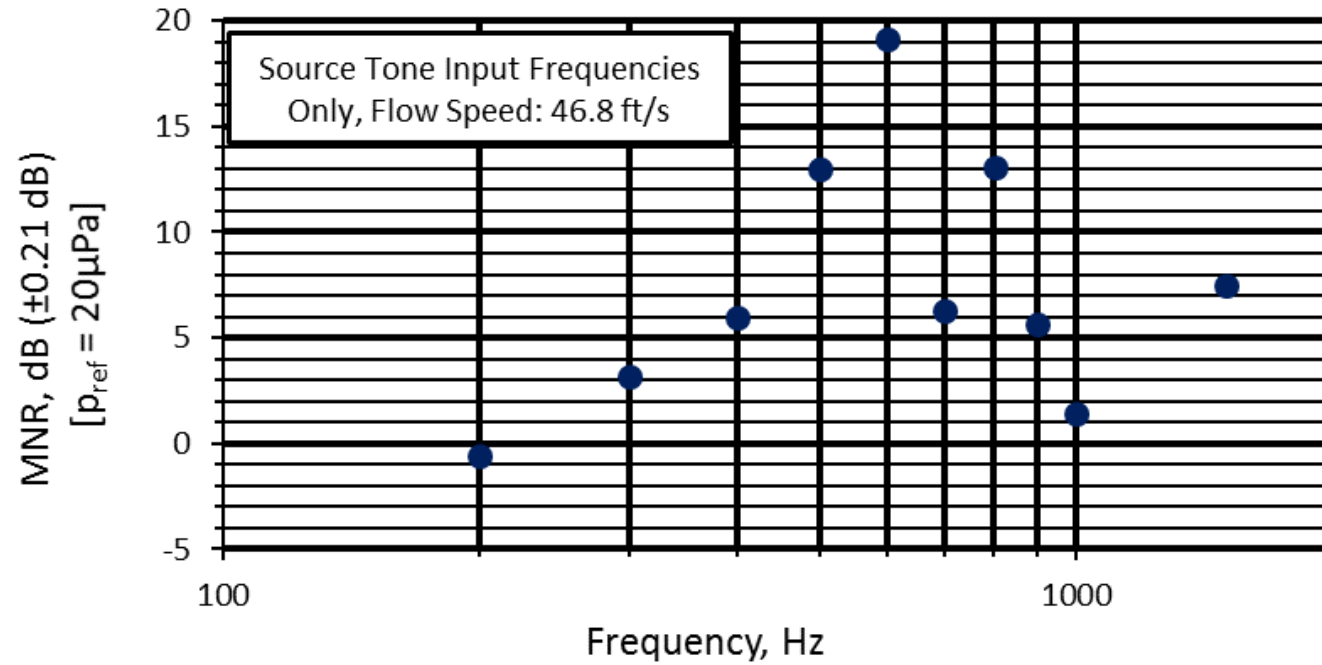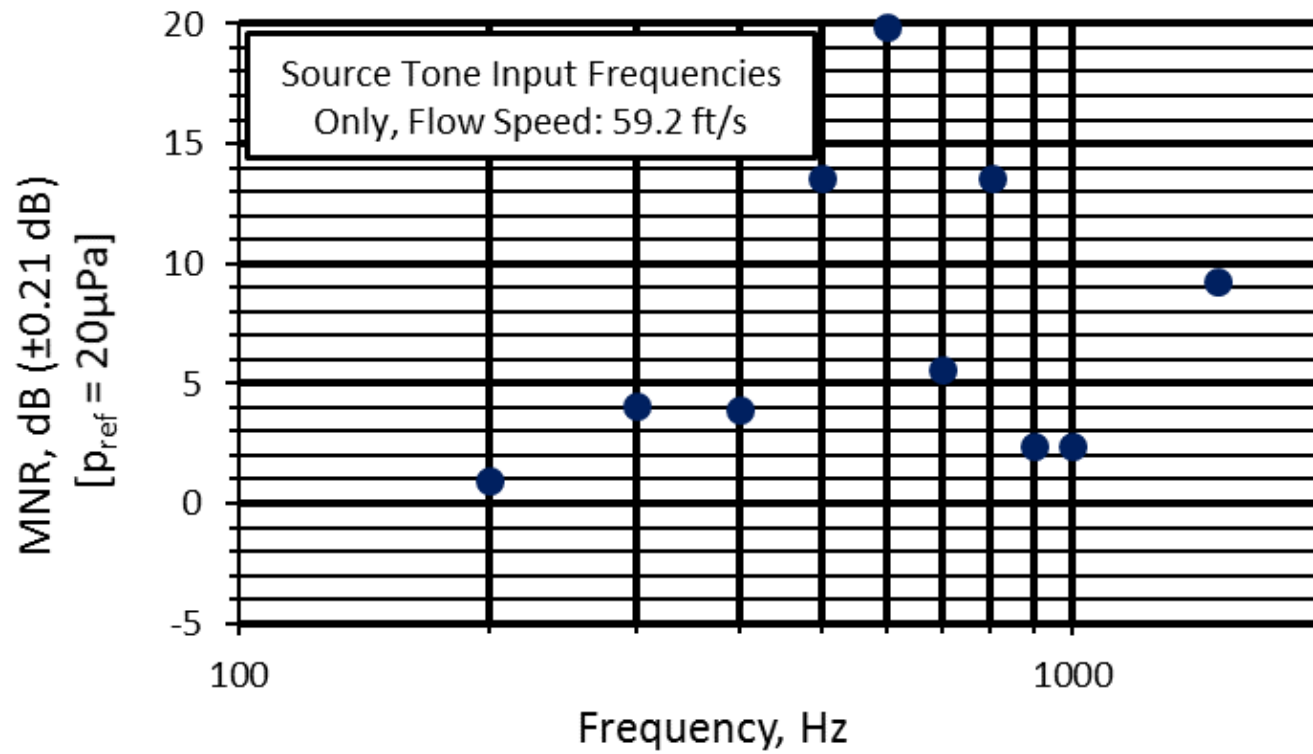
Figure 72. Source tone only Measured Noise Reduction specturm (MNR_f) measured by correcting for background noise then subtracting receiving chamber SPL_f from source room SPL_f for flow speed of 36.3 ft/s
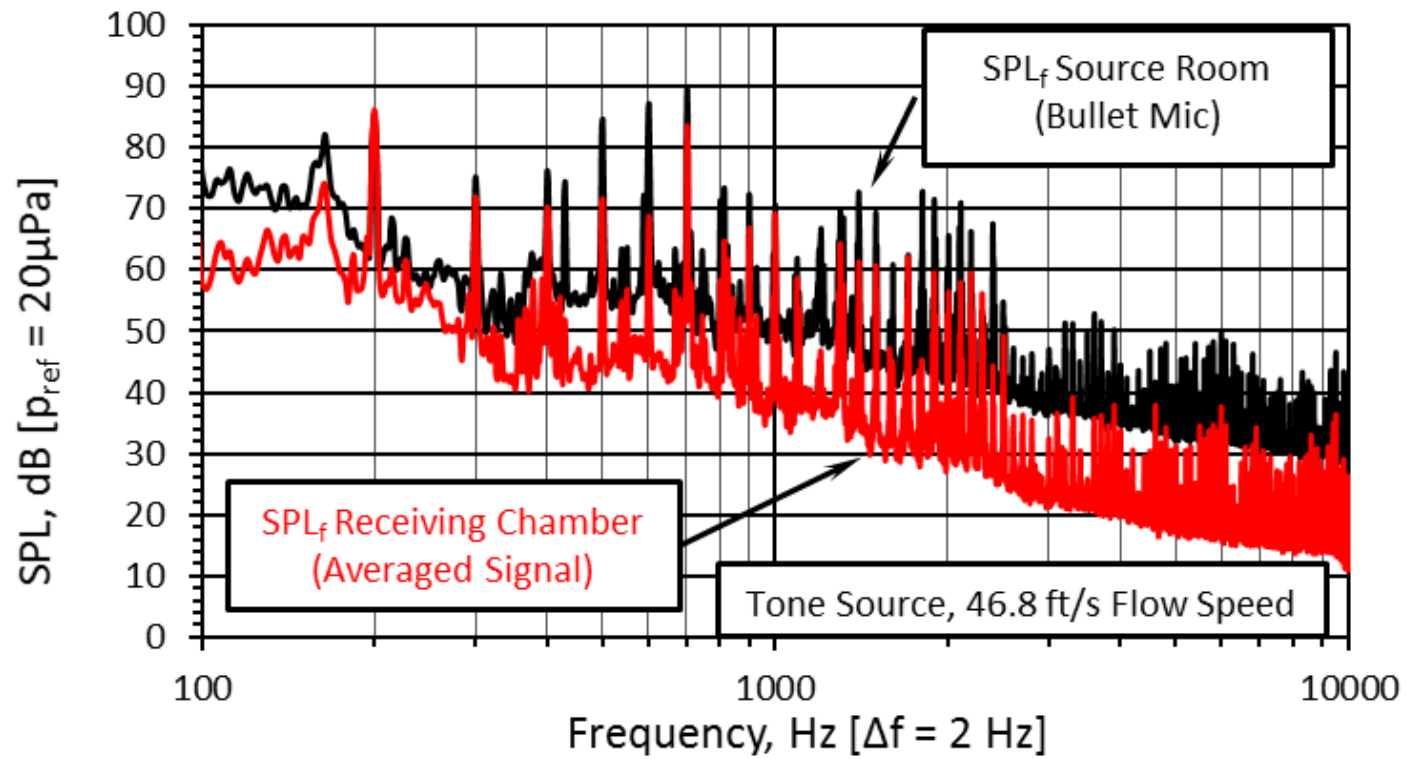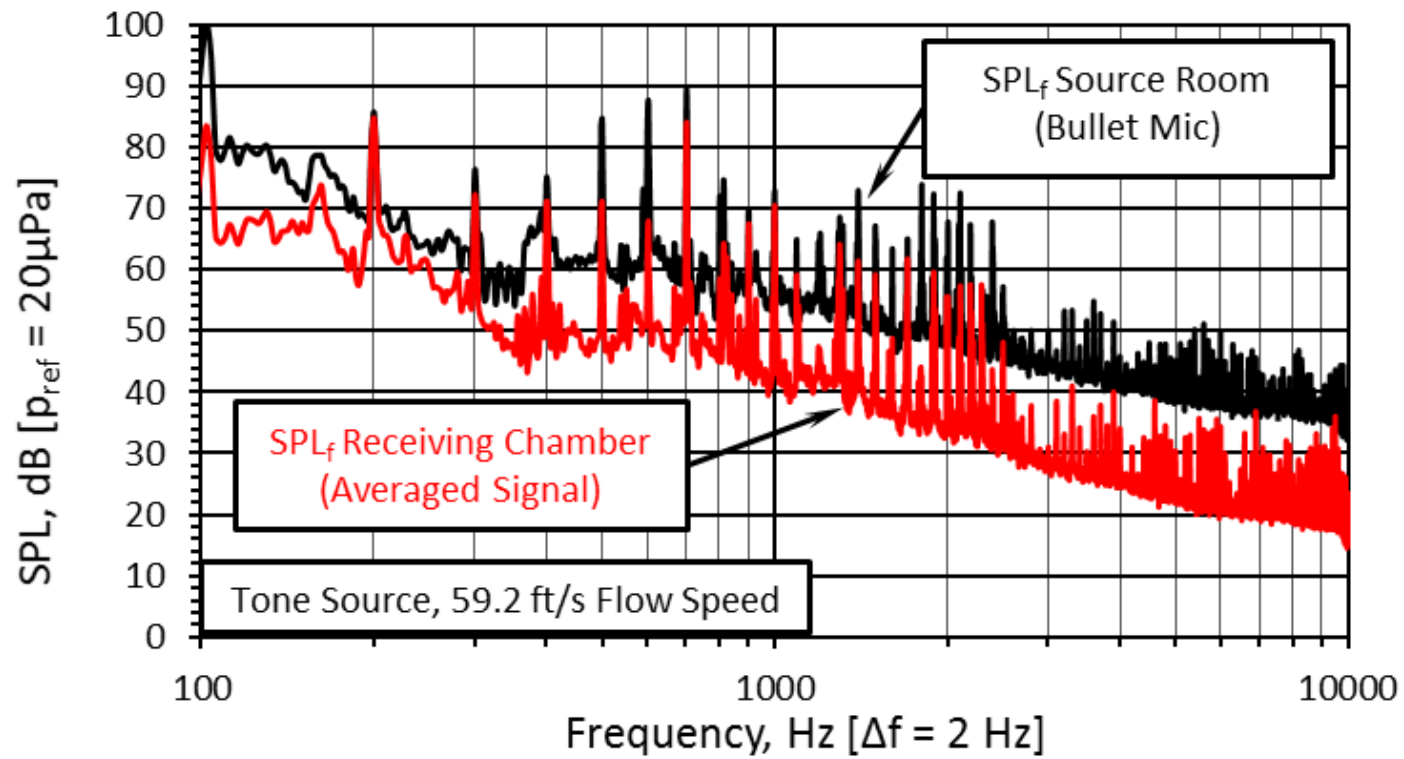
Figure 73. Tunnel specturm measured by bullet mic and quiet box spectrum averaged signal for flow speed of 46.8 ft/s
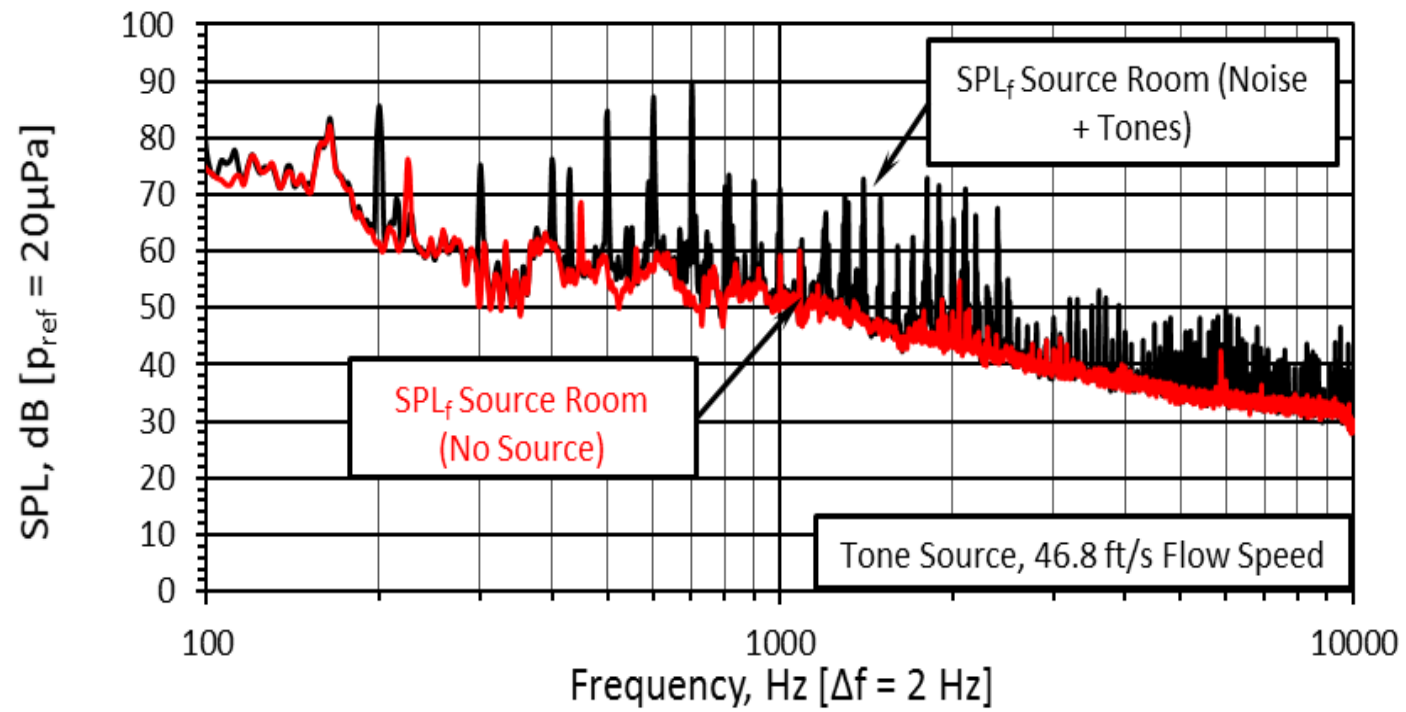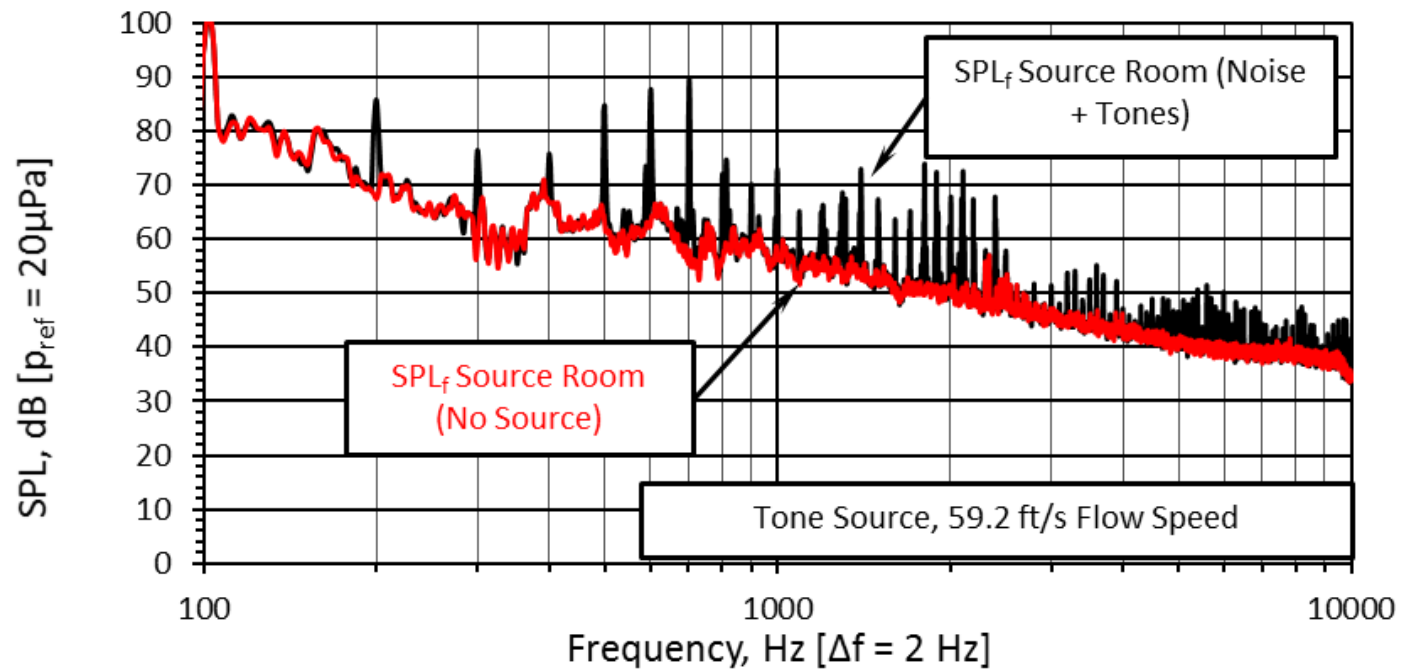
Figure 74. Tunnel specturm for background noise only and background noise + tone signal measured by bullet mic for flow speed of 46.8 ft/s
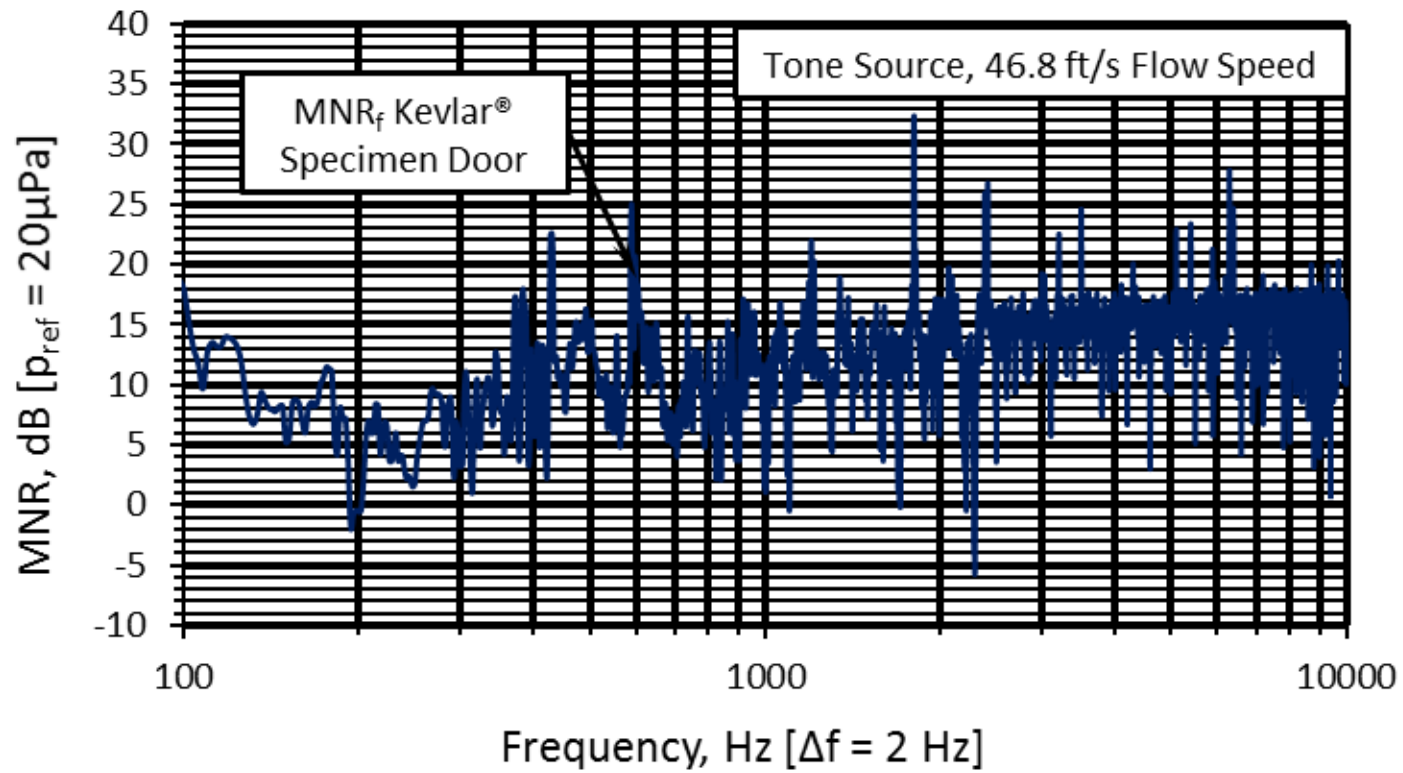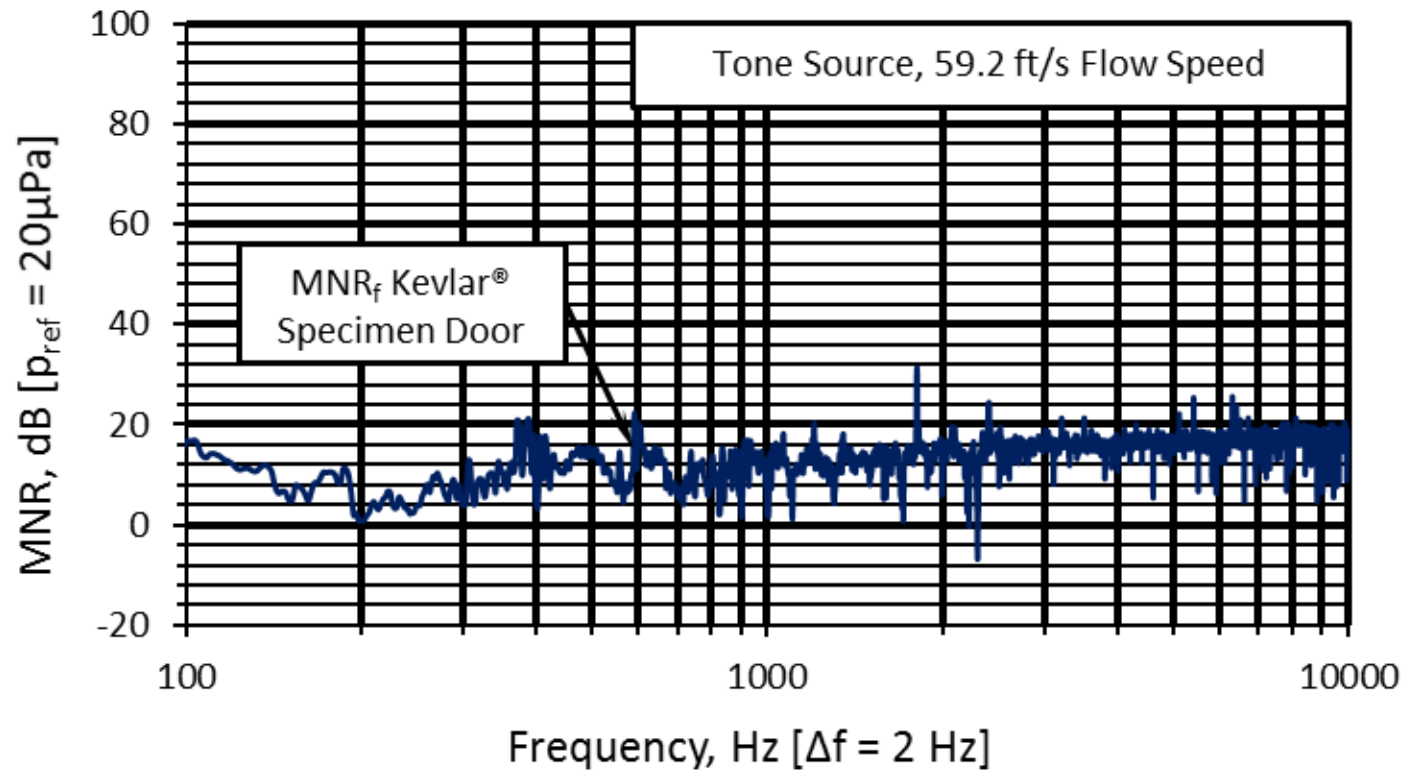
Figure 75. Flow noise + source tones Measured Noise Reduction specturm (MNR$_f$) measured by correcting for background noise then subtracting receiving chamber SPL$_f$ from source room SPL$_f$ for flow speed of 46.8 ft/s
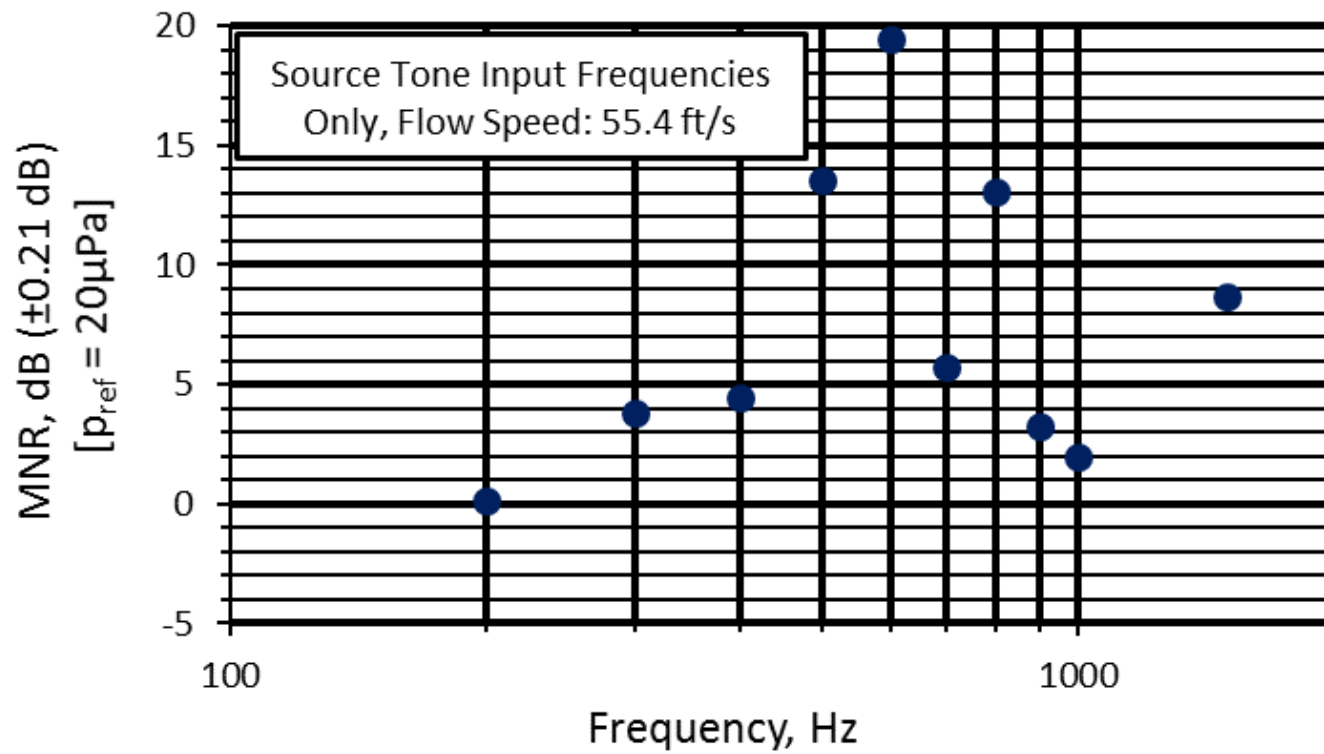
Figure 76. Source tone only Measured Noise Reduction specturm (MNR$_f$) measured by correcting for background noise then subtracting receiving chamber SPL$_f$ from source room SPL$_f$ for flow speed of 46.8 ft/s
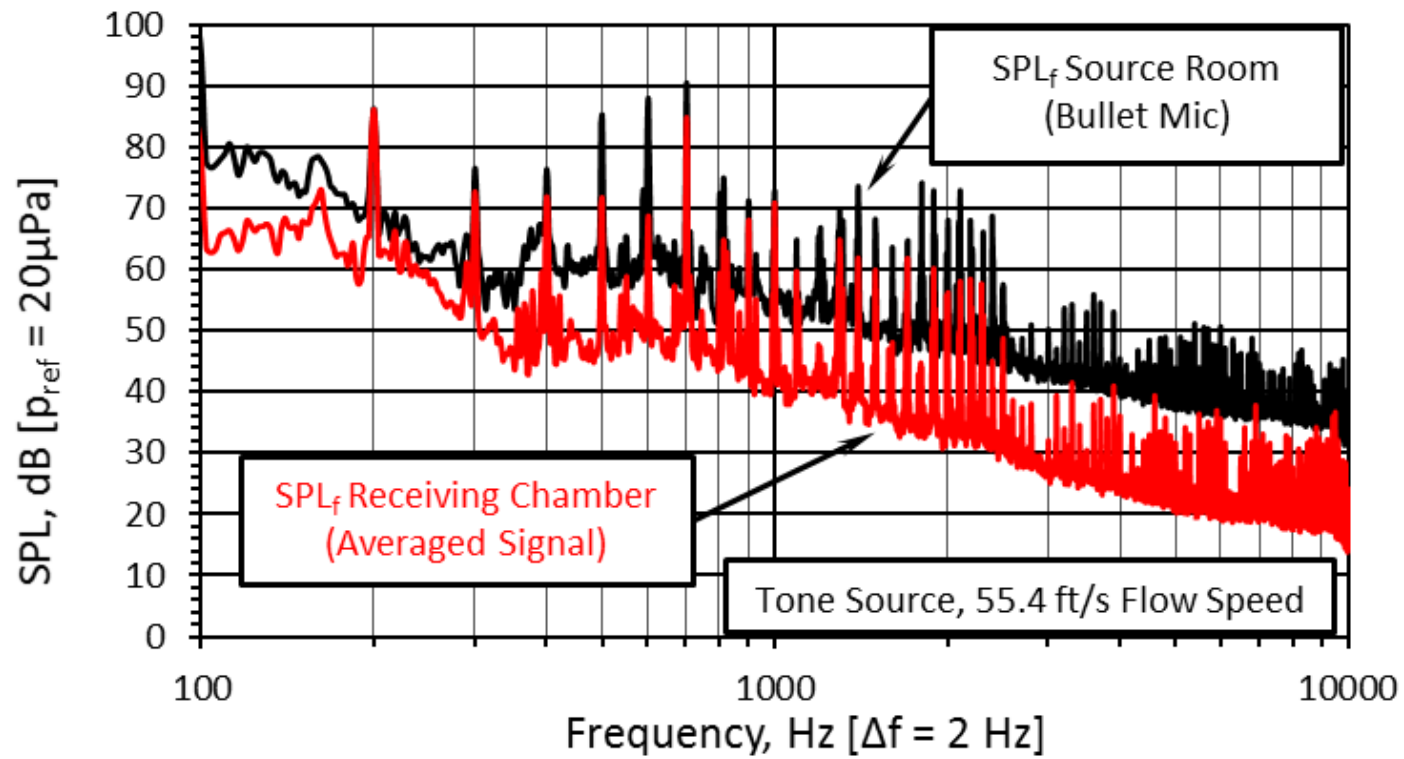
Figure 77. Tunnel specturm measured by bullet mic and quiet box spectrum averaged signal for flow speed of 55.4 ft/s

Figure 78. Tunnel specturm for background noise only and background noise + tone signal measured by bullet mic for flow speed of 55.4 ft/s

Figure 79. Flow noise + source tones Measured Noise Reduction specturm (MNR$_f$) measured by correcting for background noise then subtracting receiving chamber SPL$_f$ from source room SPL$_f$ for flow speed of 55.4 ft/s
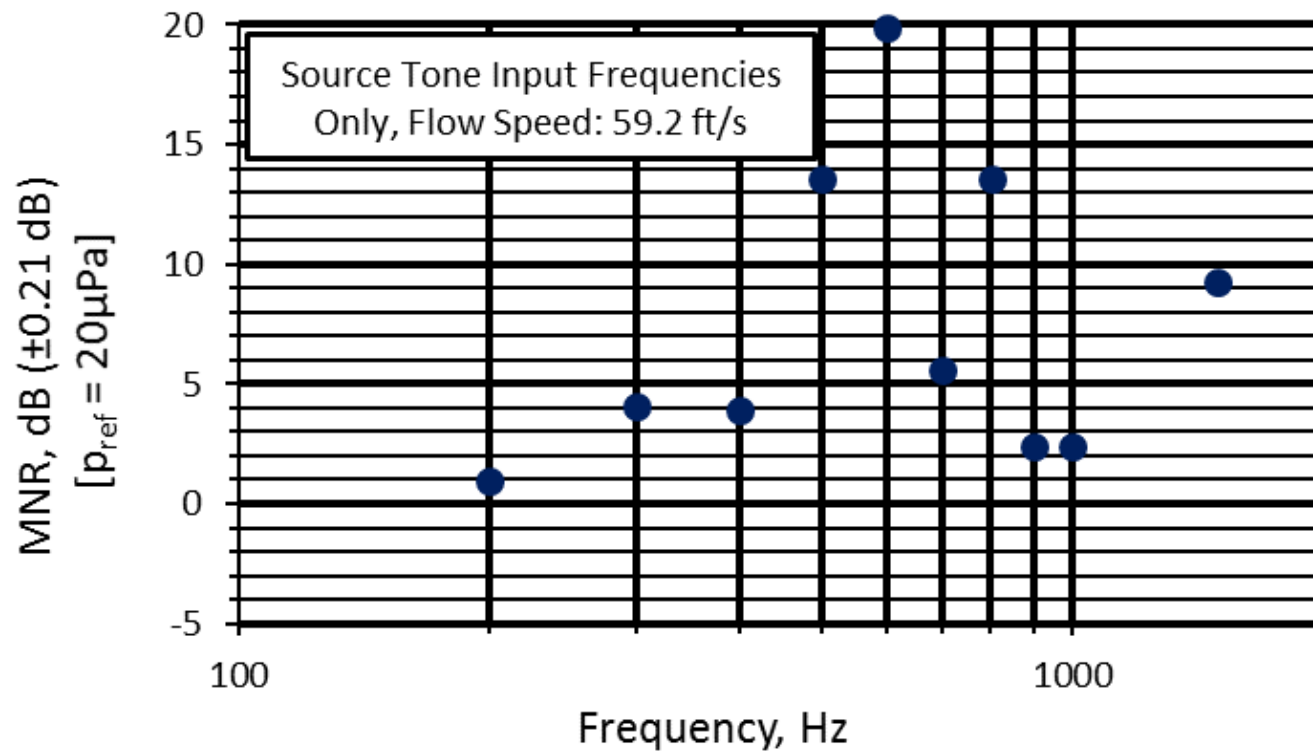
Figure 80. Source tone only Measured Noise Reduction specturm (MNR$_f$) measured by correcting for background noise then subtracting receiving chamber SPL$_f$ from source room SPL$_f$ for flow speed of 55.4 ft/s

Figure 81. Tunnel specturm measured by bullet mic and quiet box spectrum averaged signal for flow speed of 59.2 ft/s

Figure 82. Tunnel specturm for background noise only and background noise + tone signal measured by bullet mic for flow speed of 59.2 ft/s

Figure 83. Flow noise + source tones Measured Noise Reduction specturm (MNR_f) measured by correcting for background noise then subtracting receiving chamber SPL_f from source room SPL_f for flow speed of 59.2 ft/s

Figure 84. Source tone only Measured Noise Reduction specturm (MNR$_f$) measured by correcting for background noise then subtracting receiving chamber SPL$_f$ from source room SPL$_f$ for flow speed of 59.2 ft/s

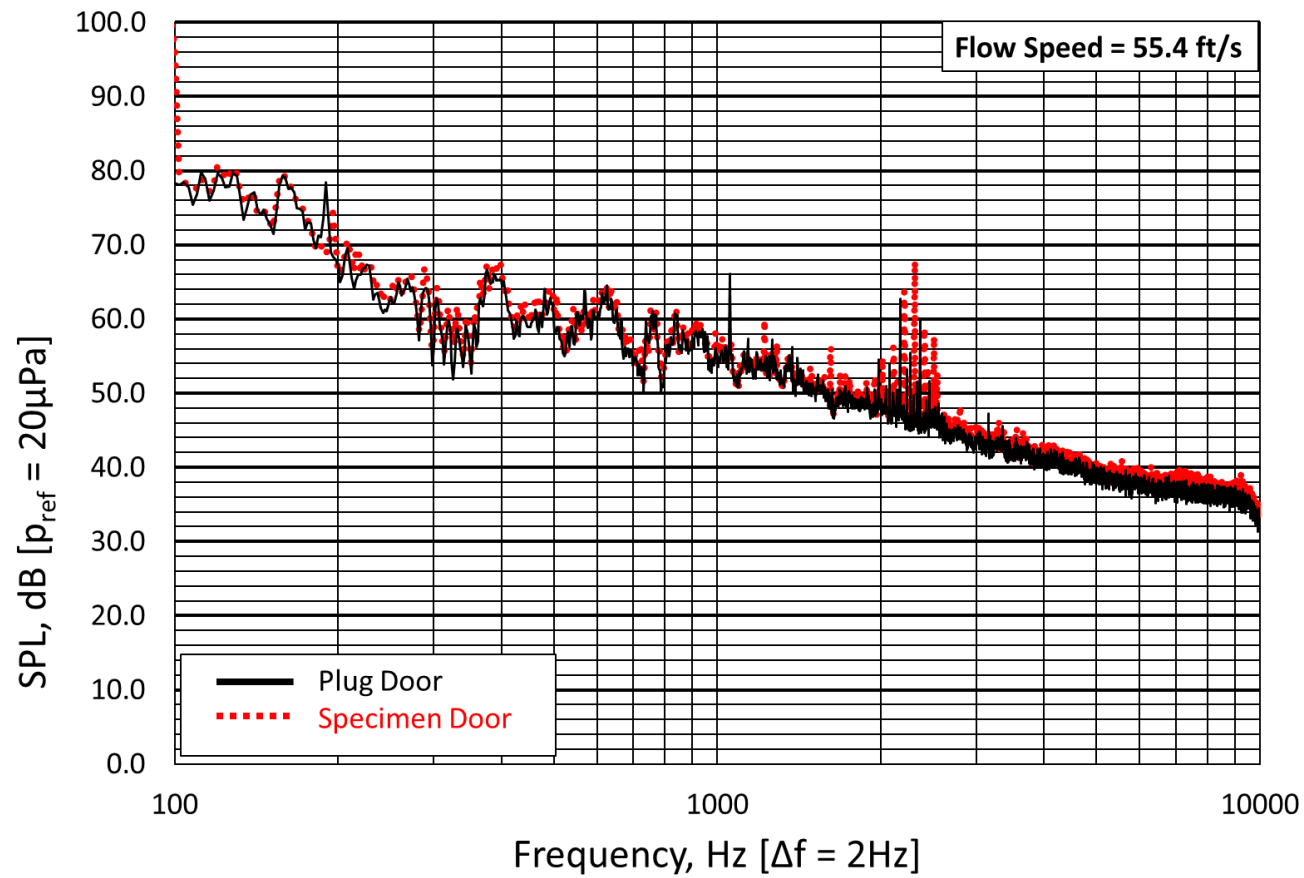**F.3** In-flow Bullet Microphone Method for Noise Increase Measurement
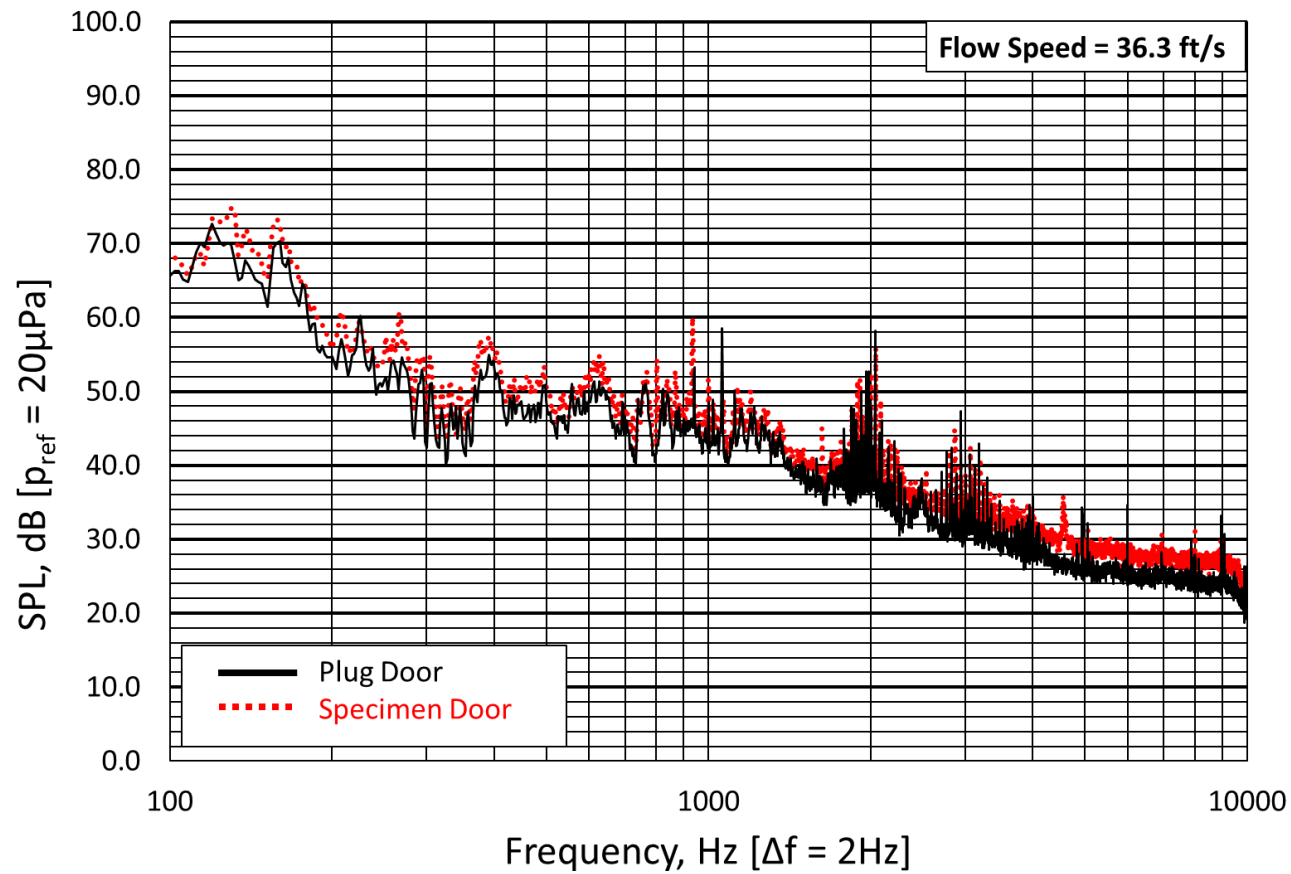
Figure 85. *Tunnel specturm measured by bullet microphone comparing plug door and specimen door configurations for flow speed of 36.3 ft/s*
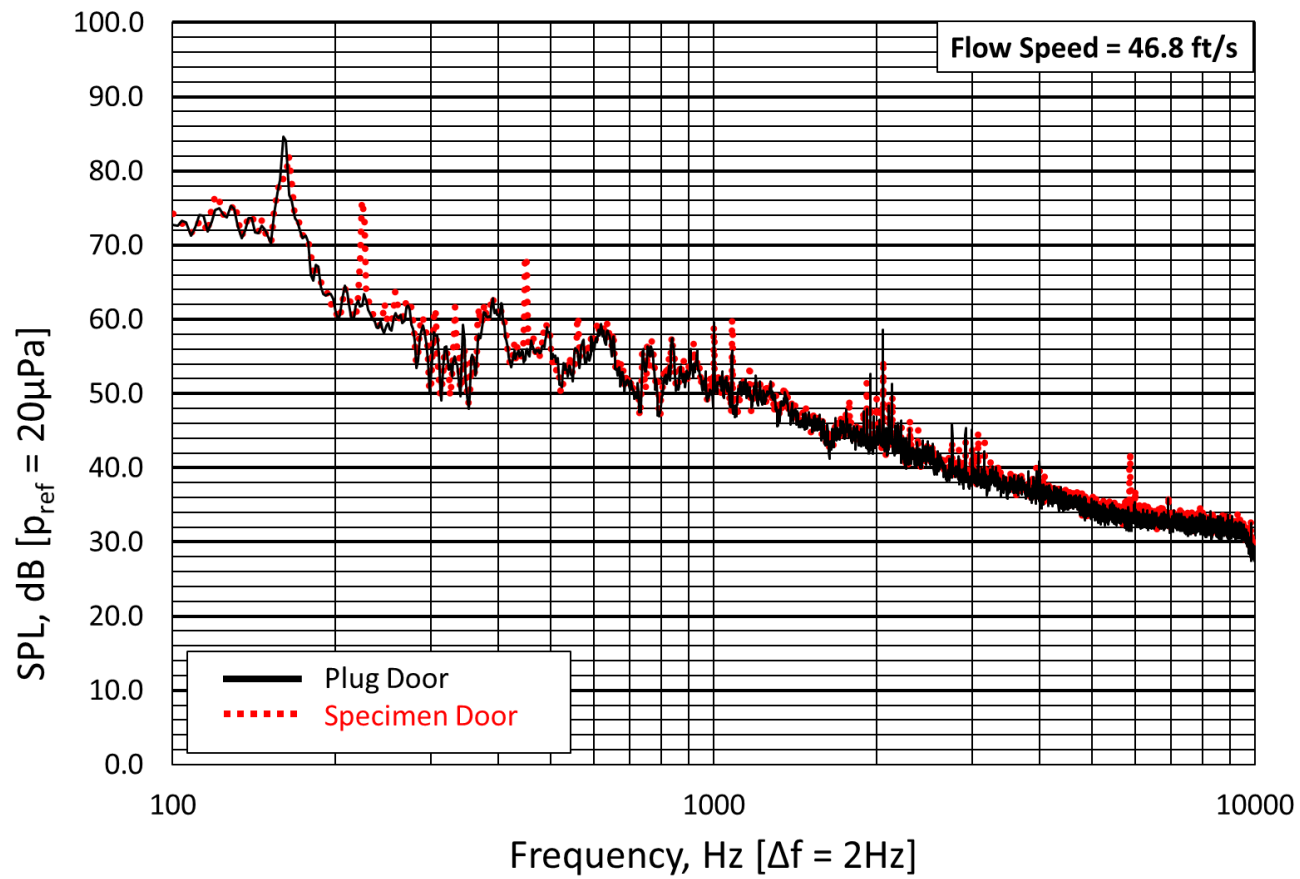
Figure 86. Tunnel specturm measured by bullet microphone comparing plug door and specimen door configurations for flow speed of 46.8 ft/s
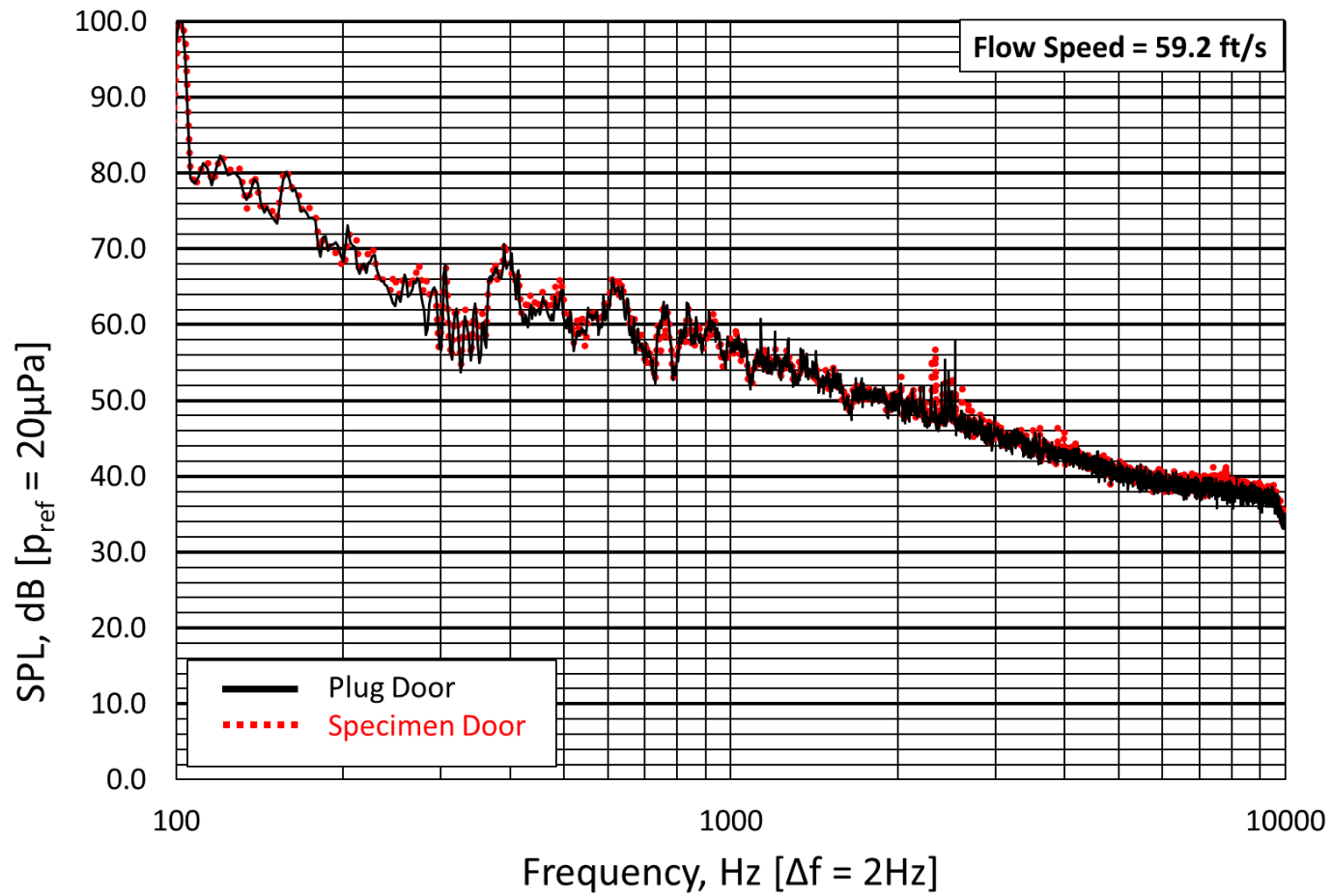
Figure 87. Tunnel specturm measured by bullet microphone comparing plug door and specimen door configurations for flow speed of 55.4 ft/s

Figure 88. Tunnel specturm measured by bullet microphone comparing plug door and specimen door configurations for flow speed of 59.2 ft/s

A7.5   In-flow Flush Mount Microphone Method for Noise Increase Measurement
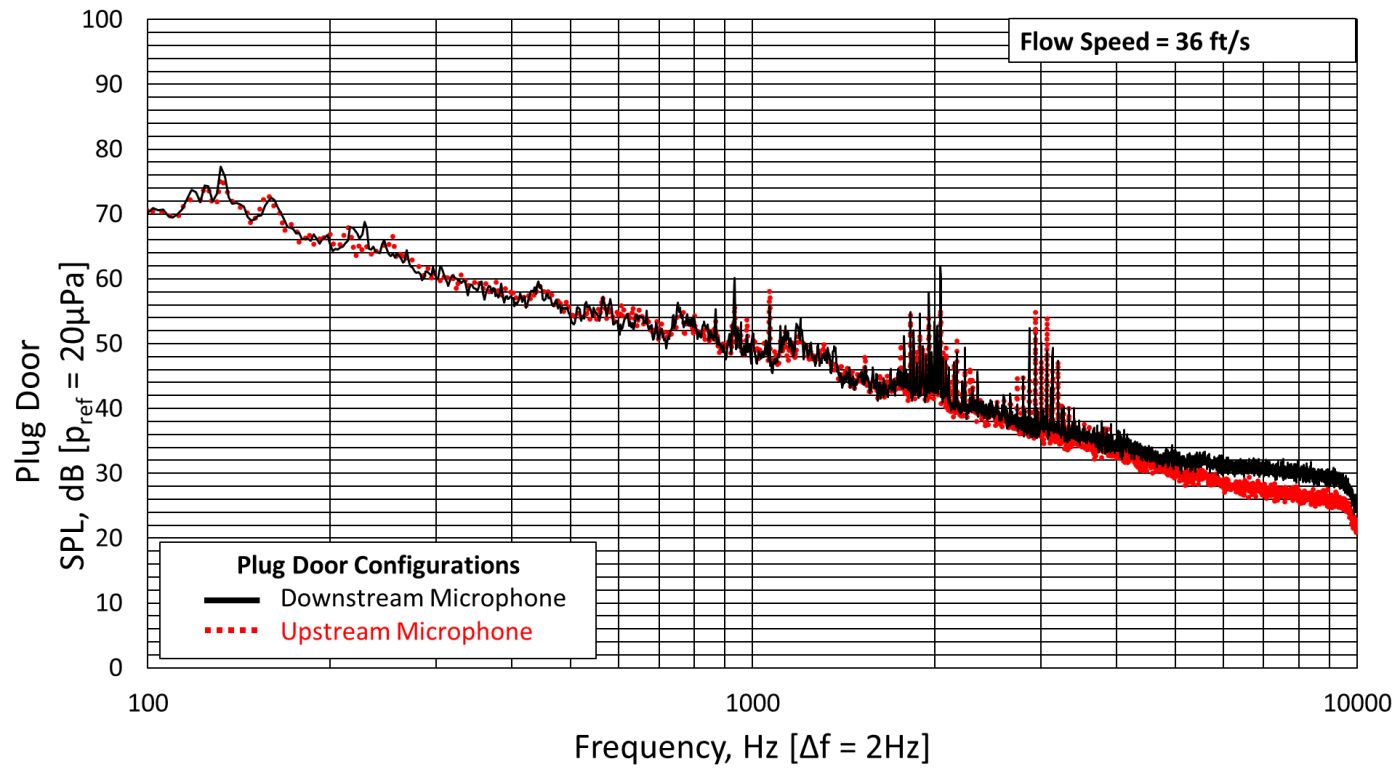

Figure 89. Tunnel specturm measured by flush mounted upstream and downstream microphones for plug door configuration for flow speed of 36 ft/s
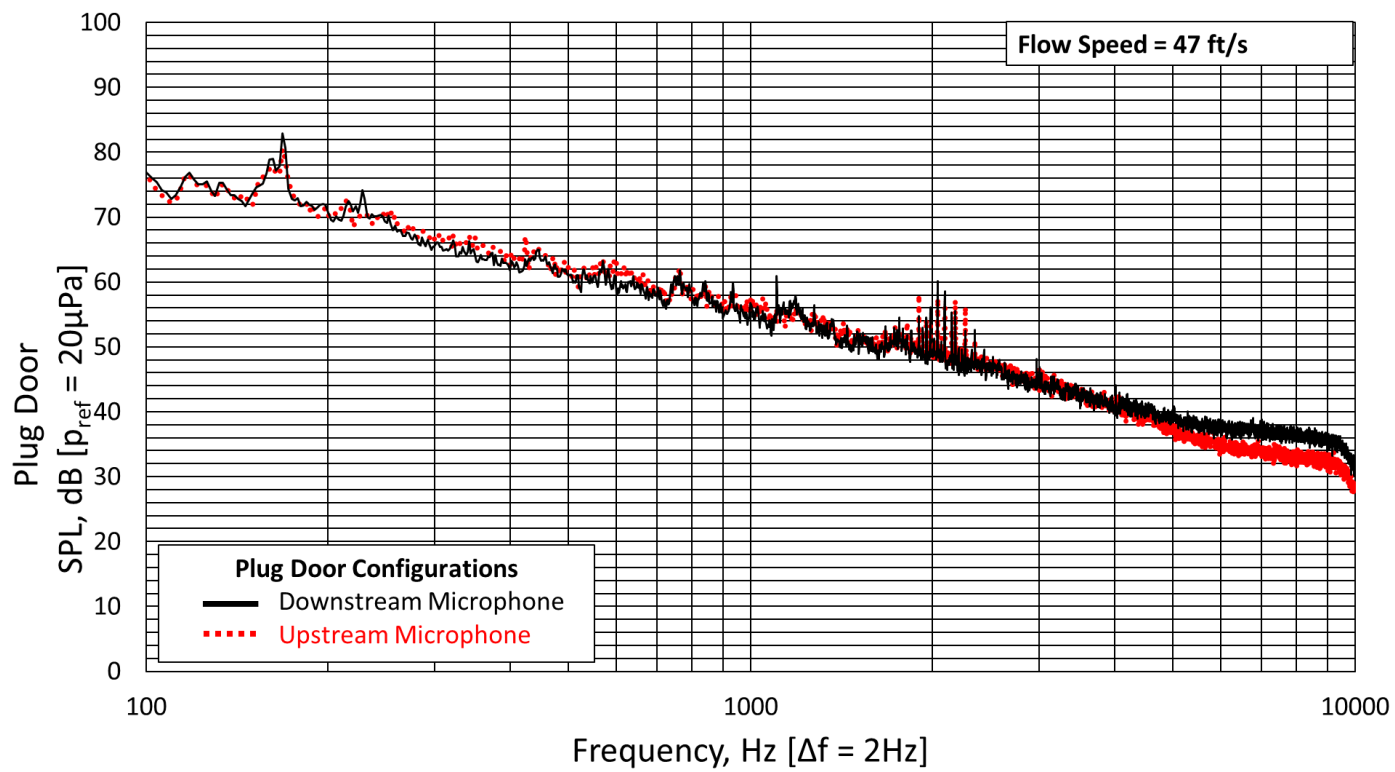
Figure 90. Tunnel specturm measured by flush mounted upstream and downstream microphones for plug door configuration for flow speed of 47 ft/s
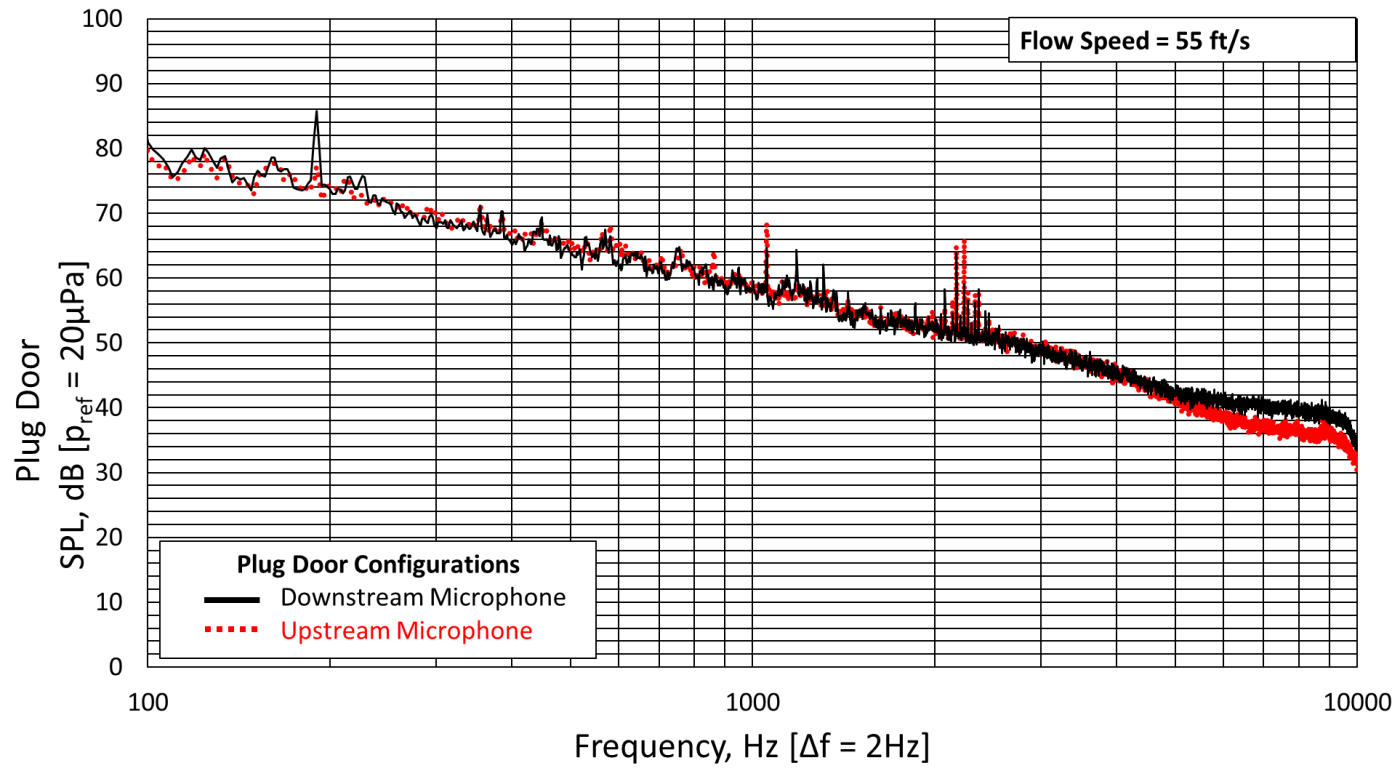
162

Figure 91. Tunnel specturm measured by flush mounted upstream and downstream microphones for plug door configuration for flow speed of 55 ft/s
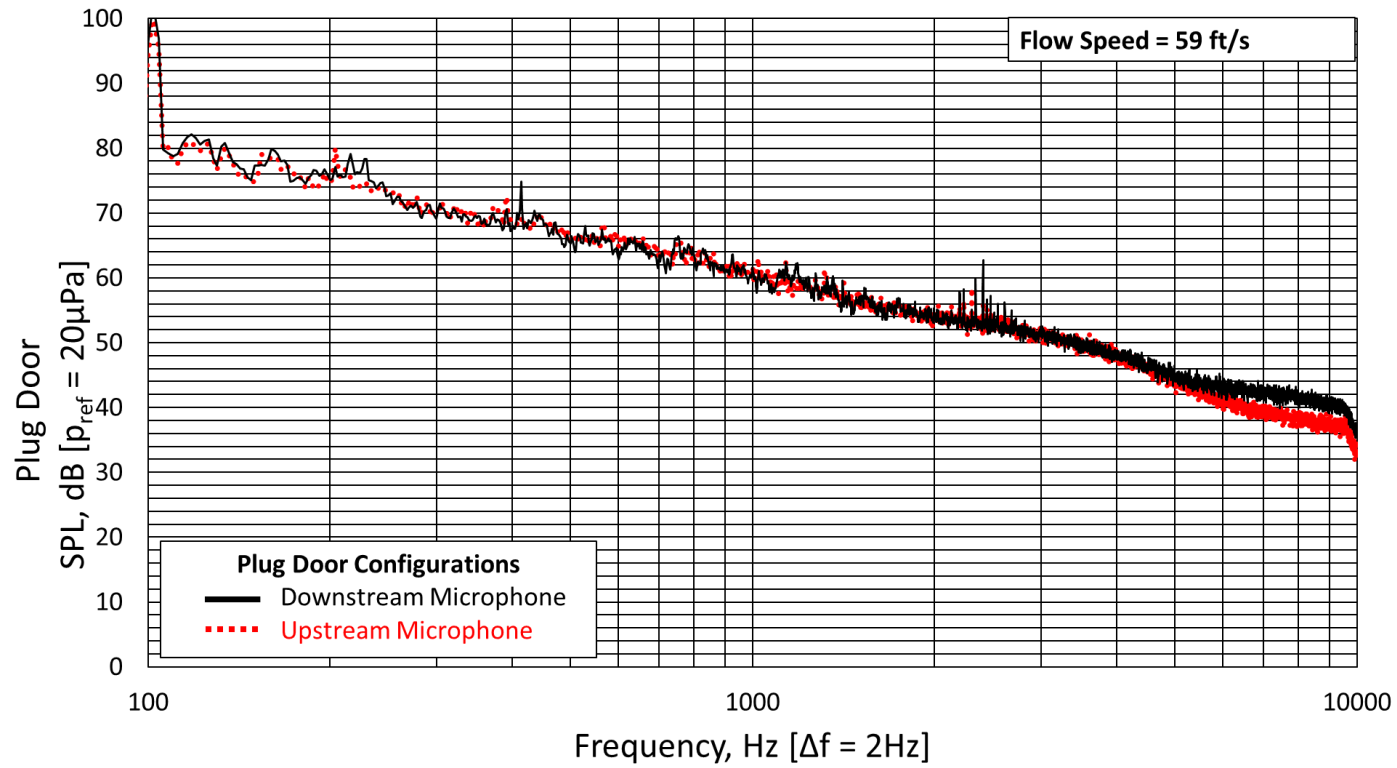
Figure 92. Tunnel specturm measured by flush mounted upstream and downstream microphones for plug door configuration for flow speed of 59 ft/s
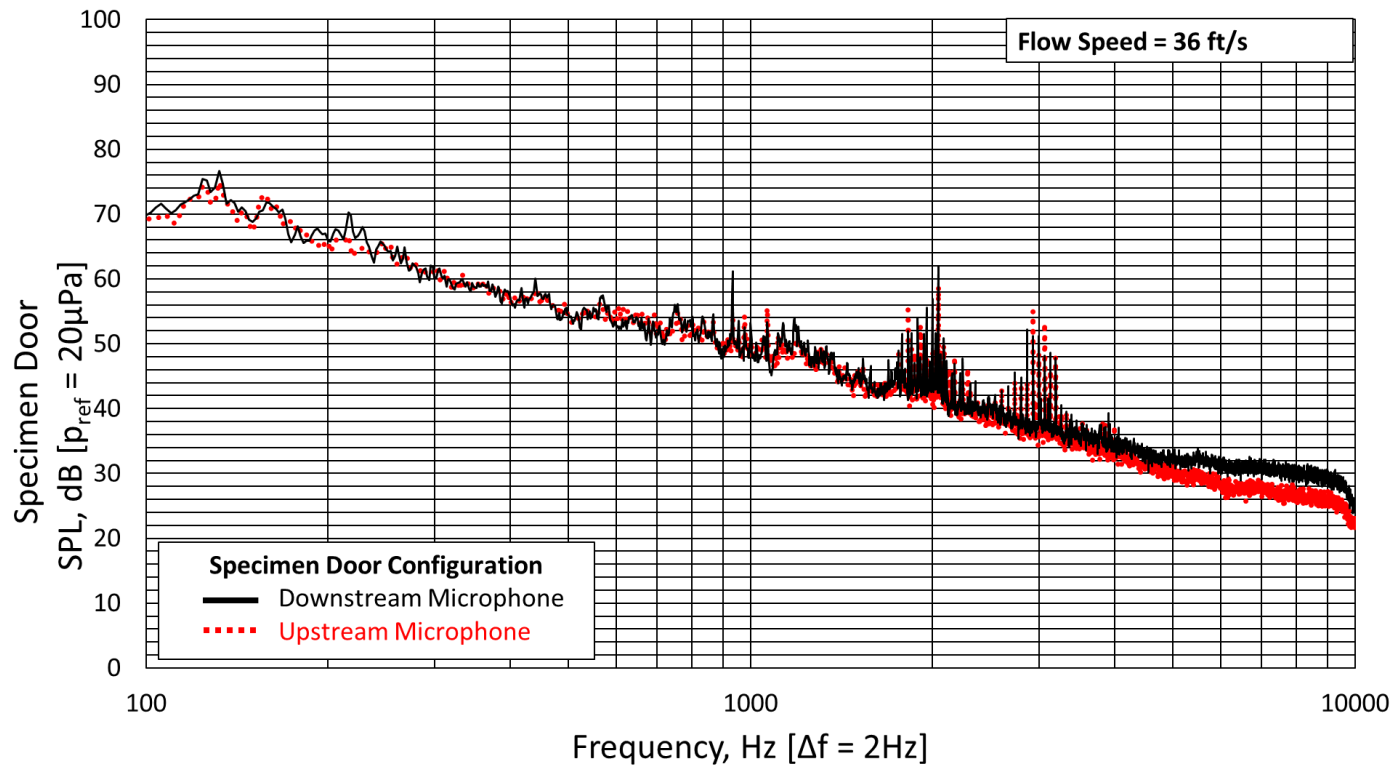
Figure 93. Tunnel specturm measured by flush mounted upstream and downstream microphones for specimen door configuration for flow speed of 36 ft/s

Figure 94. Tunnel specturm measured by flush mounted upstream and downstream microphones for specimen door configuration for flow speed of 47 ft/s

166

Figure 95. Tunnel specturm measured by flush mounted upstream and downstream microphones for specimen door configuration for flow speed of 55 ft/s
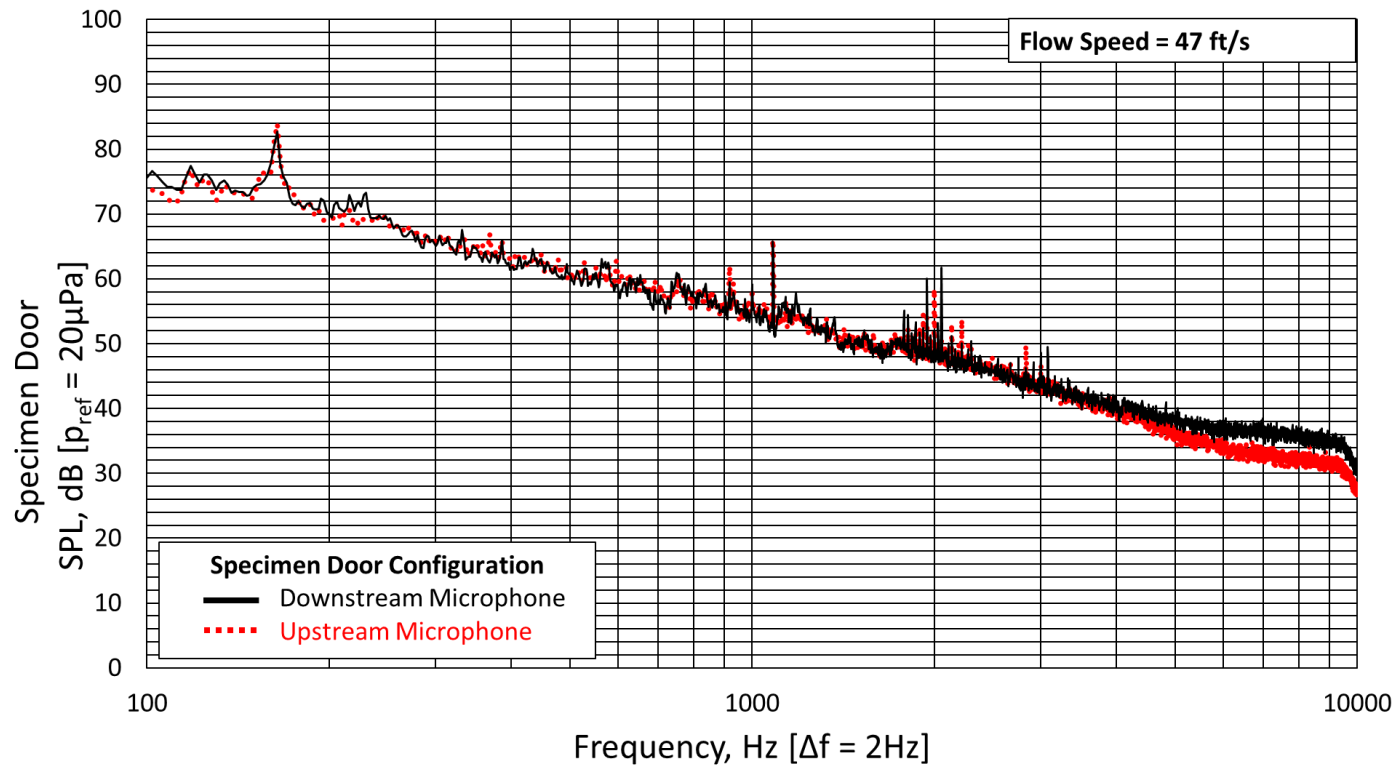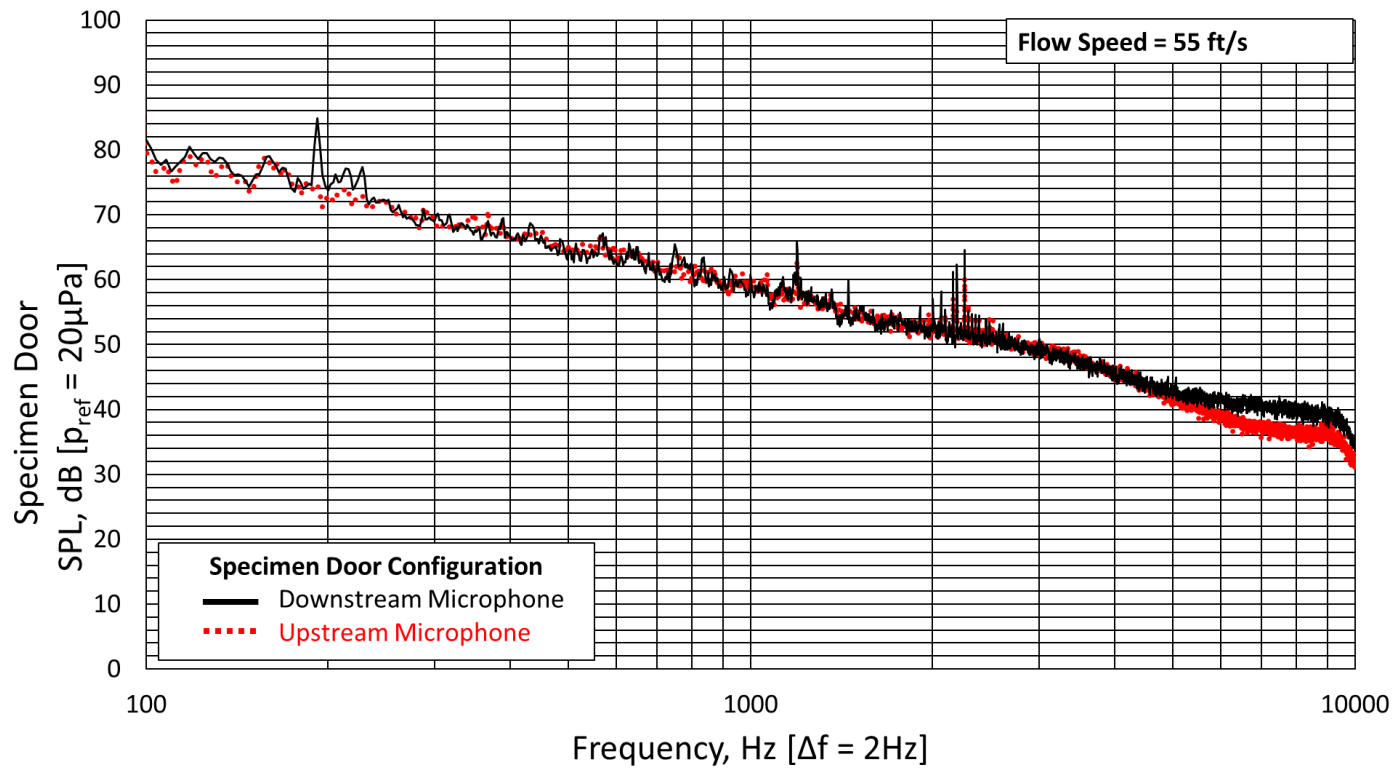
Figure 96. Tunnel specturm measured by flush mounted upstream and downstream microphones for specimen door configuration for flow speed of 59 ft/s

Figure 97. Downstream microphone – upstream microphone specturm measured by flush mounteds for plug door and specimen door configurations for flow speed of 36 ft/s
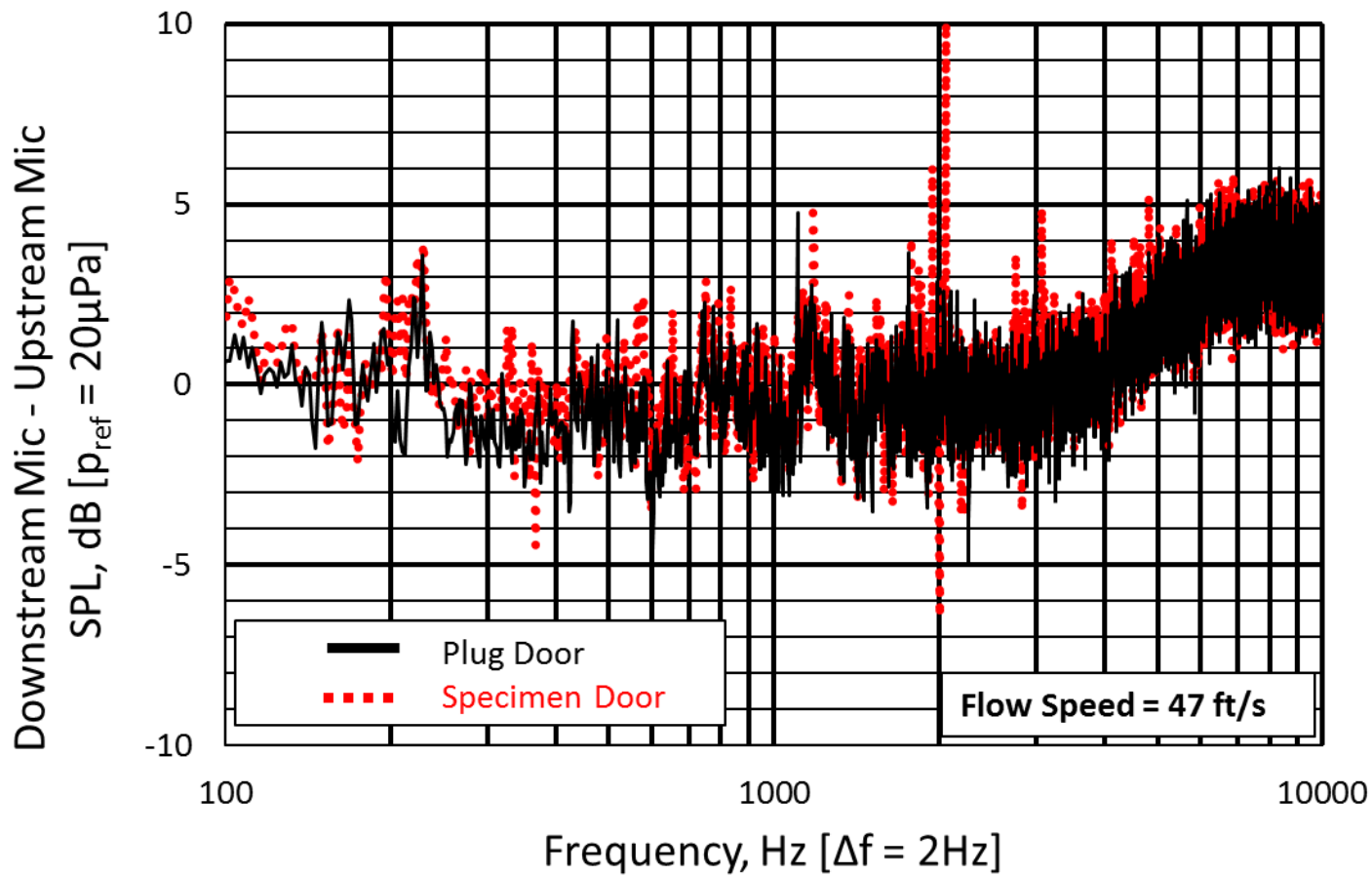
Figure 98. Downstream microphone – upstream microphone specturm measured by flush mounteds for plug door and specimen door configurations for flow speed of 47 ft/s
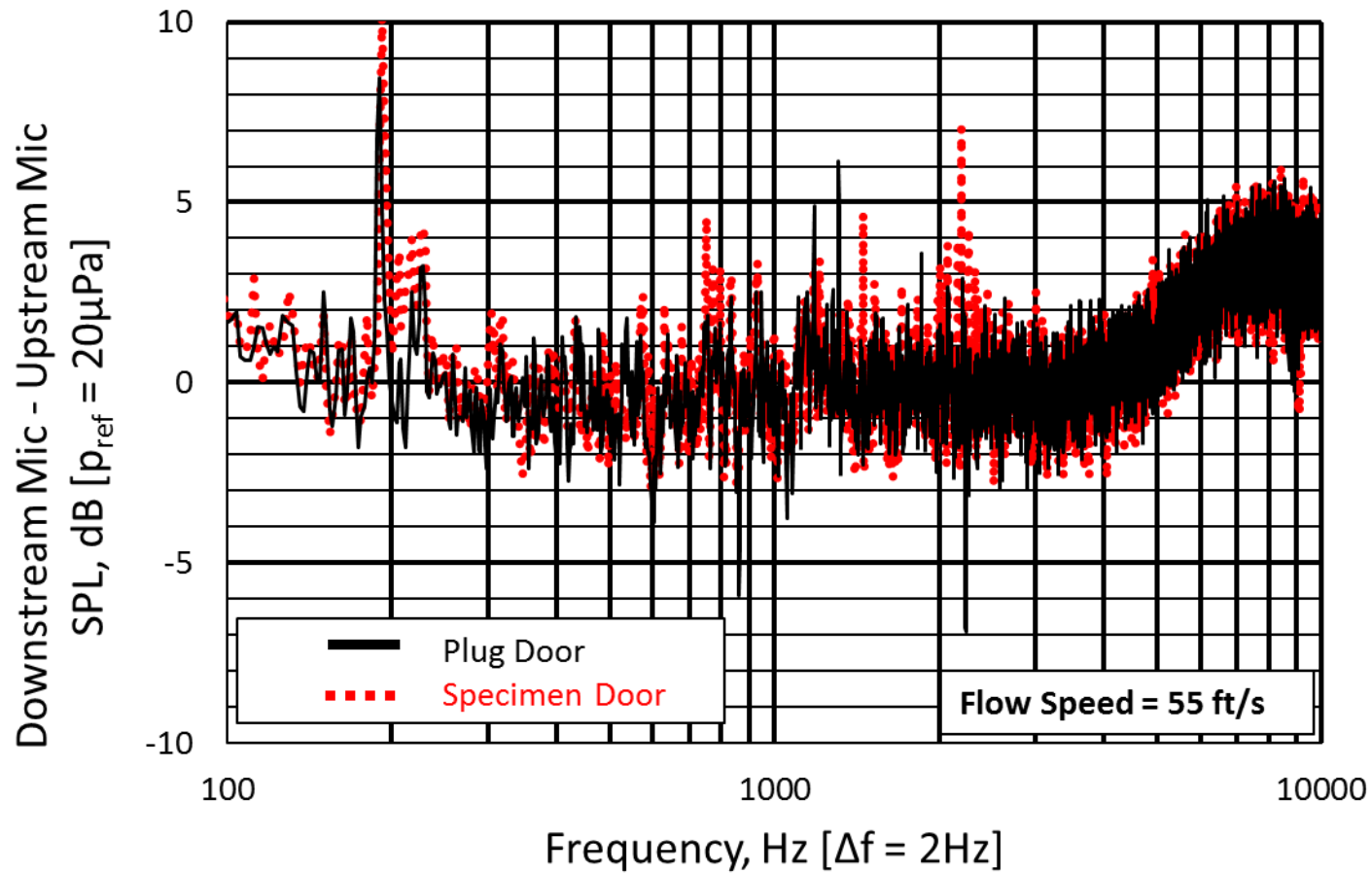
Figure 99. Downstream microphone – upstream microphone specturm measured by flush mounteds for plug door and specimen door configurations for flow speed of 55 ft/s
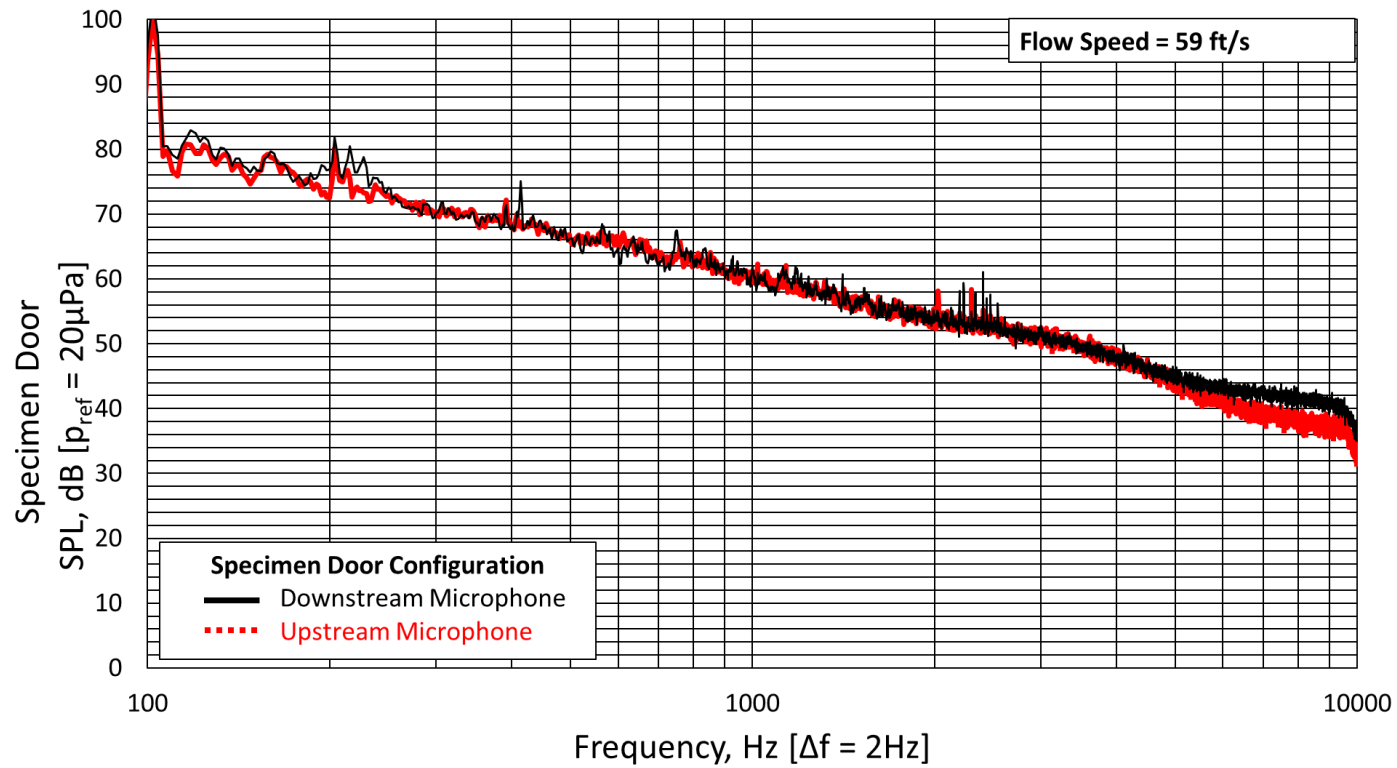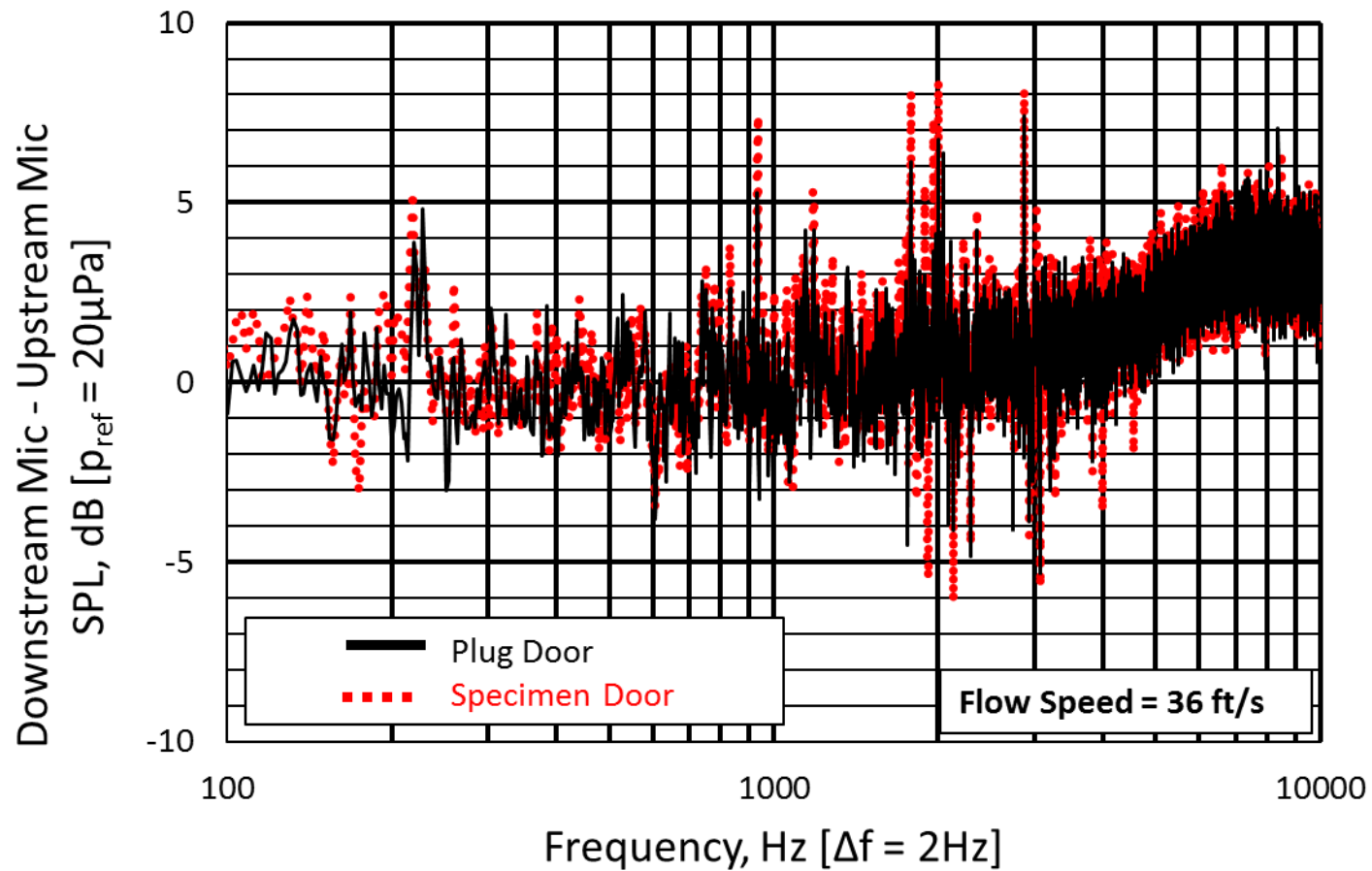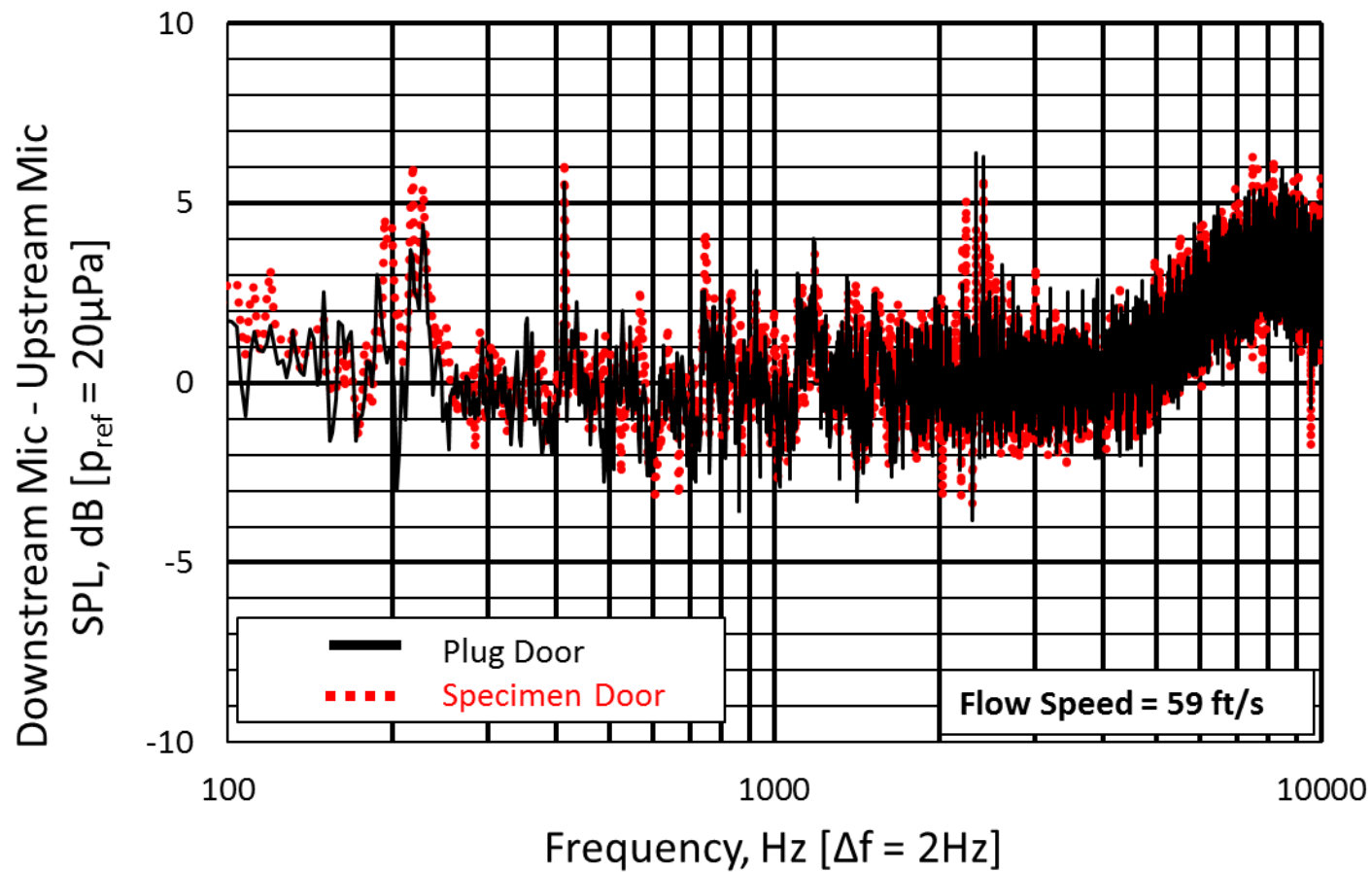
Figure 100. Tunnel specturm measured by flush mounted upstream and downstream microphones for specimen door configuration for flow speed of 59 ft/s
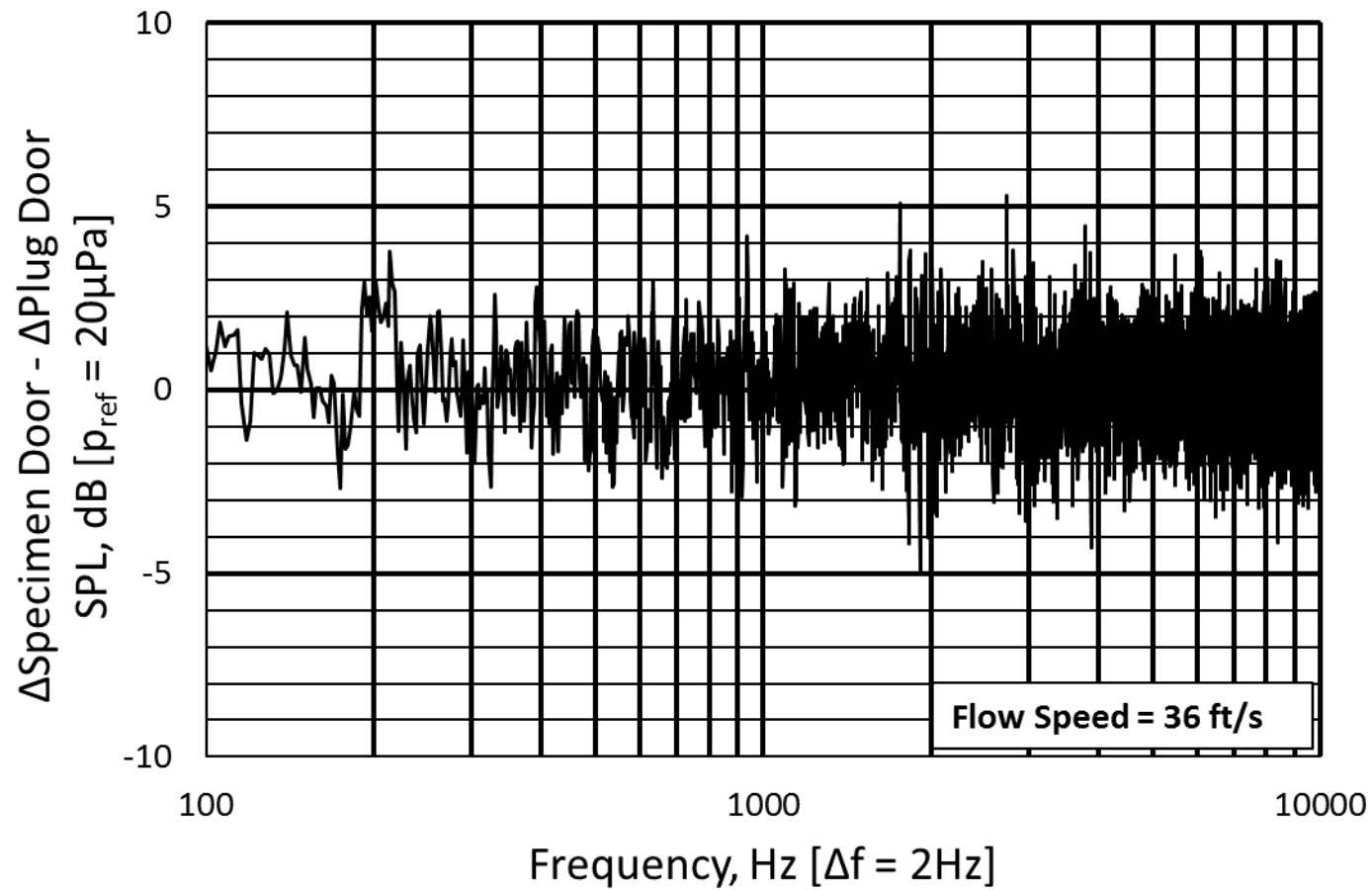
Figure 101. Downstream – upstream microphones for specimen door configuration subtracted from downstream – upstream microphones for plug door configuration for flow speed of 36 ft/s
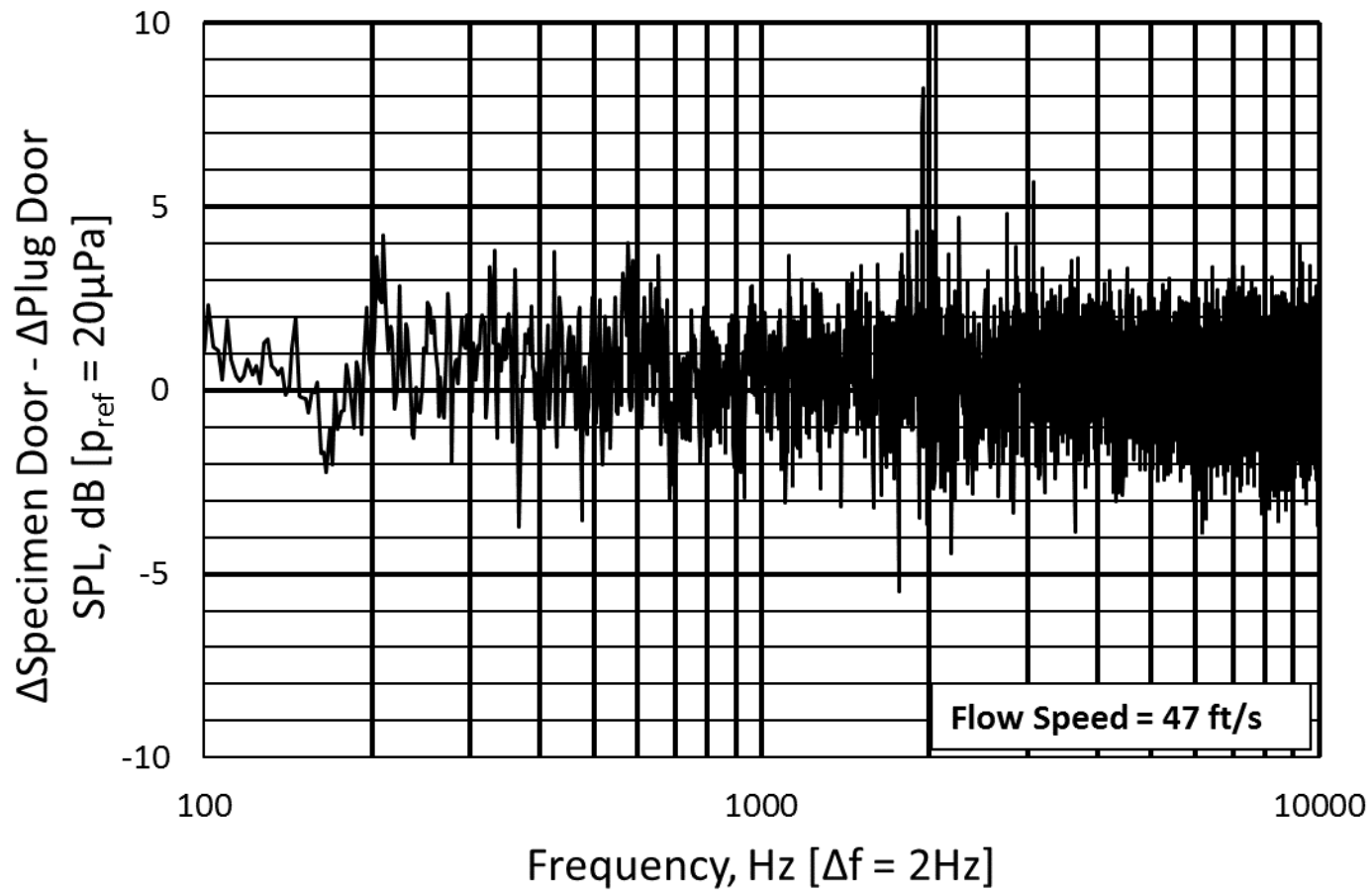
Figure 102. Downstream – upstream microphones for specimen door configuration subtracted from downstream – upstream microphones for plug door configuration for flow speed of 47 ft/s

Figure 103. Downstream – upstream microphones for specimen door configuration subtracted from downstream – upstream microphones for plug door configuration for flow speed of 55 ft/s
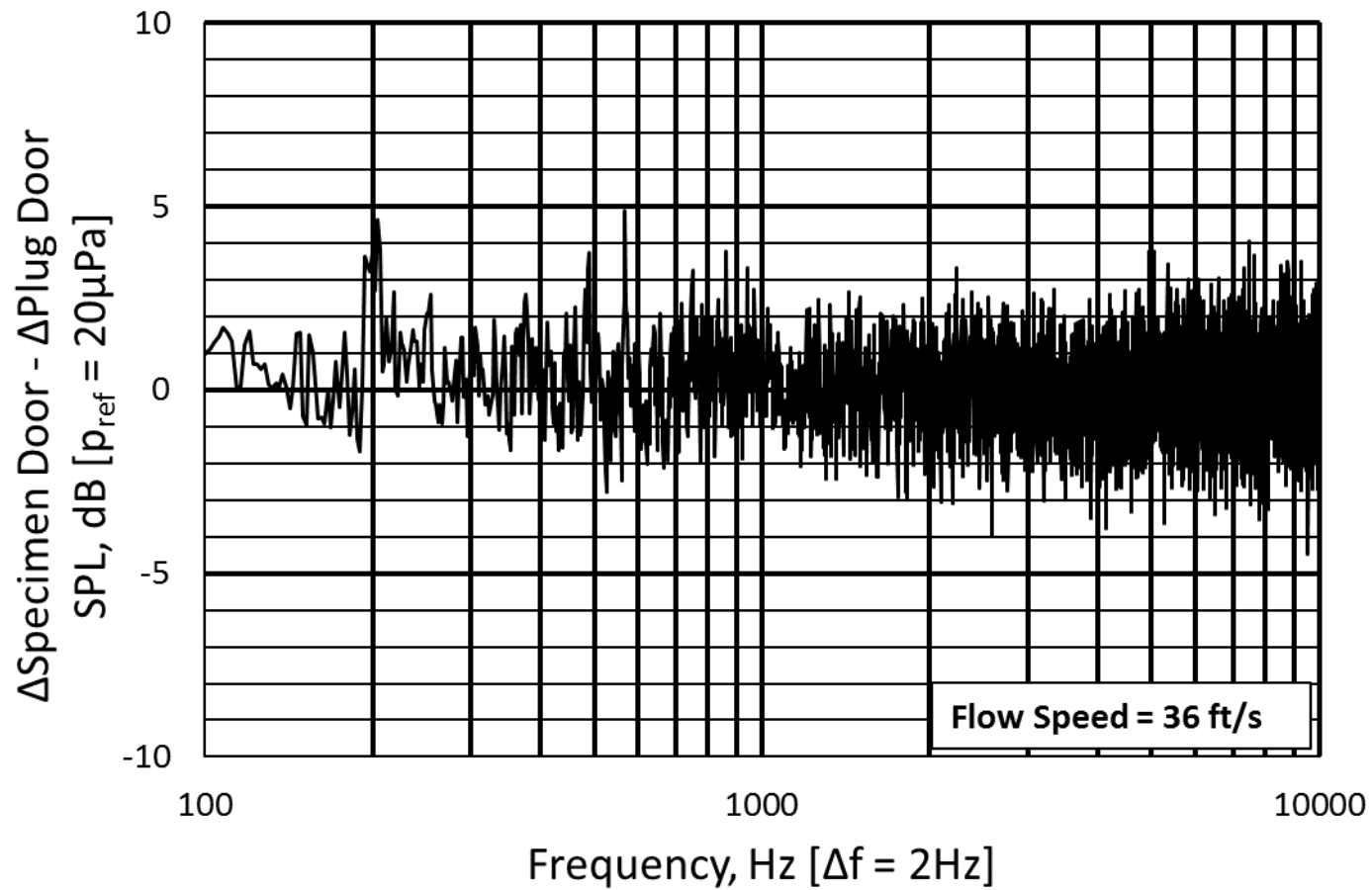
Figure 104. Downstream – upstream microphones for specimen door configuration subtracted from downstream – upstream microphones for plug door configuration for flow speed of 59 ft/s

Appendix G: Tone Generation MATLAB Code

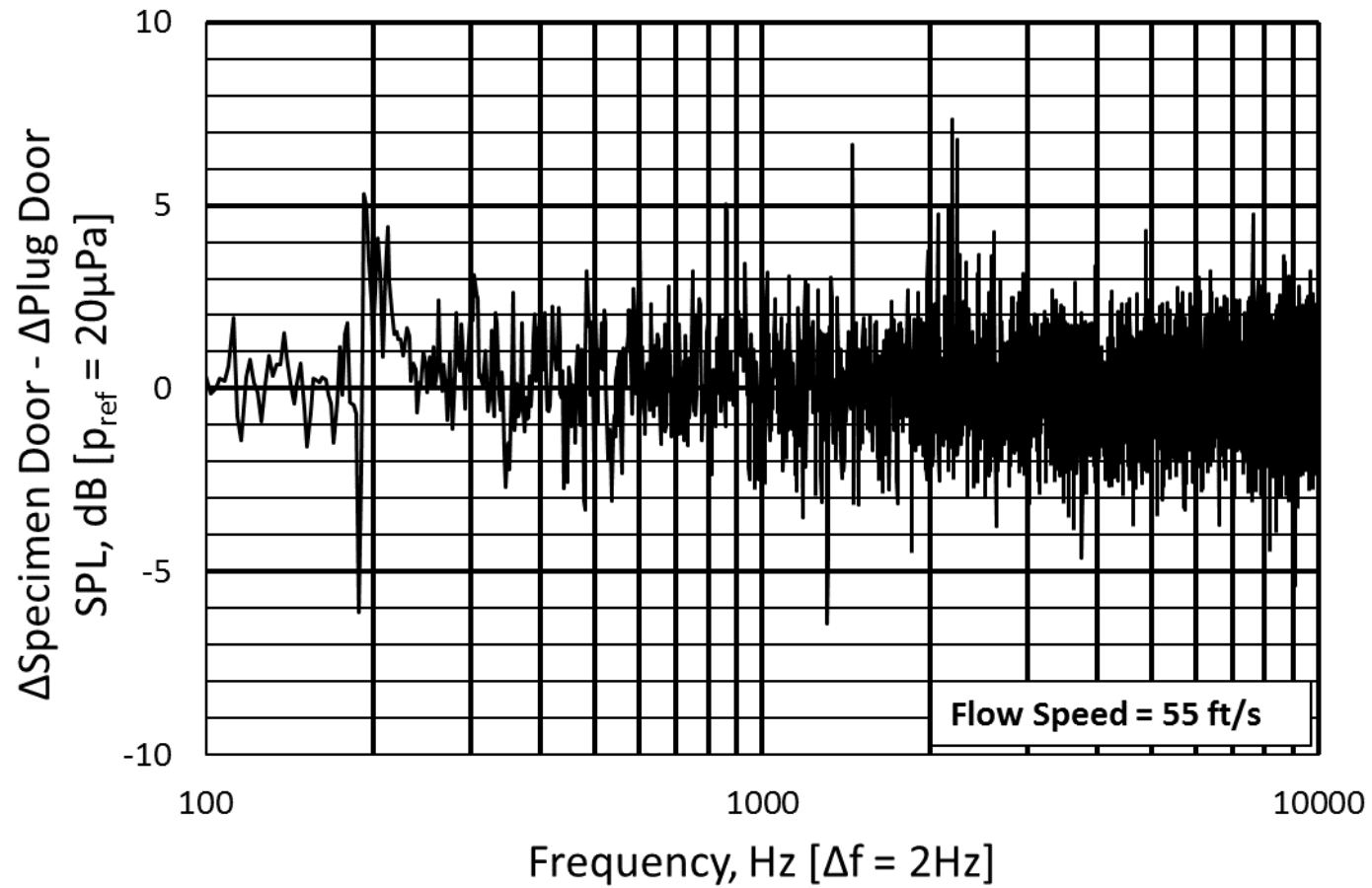

```matlab
% Tone generation code for use in transmission loss tesing
%J. A. Banks, 2017

clear all
fs=4000; %2x fmax to avoid niquest condition
T=60;
amp=[10,3, .5, 10, 10, 8, 15, 20, 100, 100]% amplitude matrix
f=[200, 300, 400, 500, 600, 700, 800, 900, 1000, 1500];%Frequency matrix
F_Shift = -5;
t=1:(1/fs):T;%time from 1 to 10 by 1/sampling frequency

a=amp(1)*sin(2*pi*(F_Shift+ f(1))*t);
b=amp(2)*sin(2*pi*(F_Shift-2+ f(2))*t);
c=amp(3)*sin(2*pi*(F_Shift-4 +f(3))*t);
d=amp(4)*sin(2*pi*(F_Shift- 8+f(4))*t);
e=amp(5)*sin(2*pi*(F_Shift-8 +f(5))*t);
f=amp(6)*sin(2*pi*(F_Shift-10 +f(6))*t);
g=amp(7)*sin(2*pi*(F_Shift-28 +f(7))*t);
h=amp(8)*sin(2*pi*(F_Shift - 12+f(8))*t);
i=amp(9)*sin(2*pi*(F_Shift- 8+ f(9))*t);
j=amp(10)*sin(2*pi*(F_Shift- 14+f(10))*t);

sound(a,fs); %plays sound signal
sound(b,fs);
sound(c,fs);
sound(d,fs);
sound(e,fs);
sound(f,fs);
sound(g,fs);
sound(h,fs);
sound(i,fs);
sound(j,fs);
```

Appendix H: Impedance Tube Transfer Matrix Method MATLAB Code

(Developed by J. Callicoat[10])

```matlab
% File 'TL.m' rev. 140418 jrcalli
%------------------------------------------------------------------------
% This program implements the calculations described in ASTM E2611-09 to
% compute the normal-incidence transmission loss and other acoustic
% properties using the 4-microphone method.
%------------------------------------------------------------------------

function TL(TL_file)        %input is Excel acoustic data file

% input parameters (do not change)
sheet = 1;
startRow = 23;                      %first line of TL input data
endRow = 1372;                      %last line of TL input data

disp('Working...')
% read in input data
[num,txt,raw] = xlsread(TL_file,sheet,'B5:B5');
cal_file = char(txt);               %calibration input file (.mat)
str = fprintf('Loading calibration factors from file: %s \n', cal_file);
load(cal_file, 'frequency','H21_correction','H31_correction','H41_correction');

str = fprintf('Reading acoustic test data for sample: %s \n', TL_file);
T = xlsread(TL_file,sheet,'B6:B6');           %room temperature (degC)
P = xlsread(TL_file,sheet,'B7:B7');           %atmospheric pressure (kPa)
d = xlsread(TL_file,sheet,'B8:B8');           %thickness of sample (inches) ==> spacing
between tubes
numLoads = xlsread(TL_file,sheet,'B9:B9');  %qty of termination cases used (1 or 2)
surf_den = xlsread(TL_file,sheet,'B10:B10');   %surface density of sample (g/ft^2)

frequency2 = xlsread(TL_file,sheet,sprintf('A%d:A%d',startRow,endRow));

Hbar11a_Re = xlsread(TL_file,sheet,sprintf('B%d:B%d',startRow,endRow));
Hbar21a_Re = xlsread(TL_file,sheet,sprintf('C%d:C%d',startRow,endRow));
Hbar31a_Re = xlsread(TL_file,sheet,sprintf('D%d:D%d',startRow,endRow));
Hbar41a_Re = xlsread(TL_file,sheet,sprintf('E%d:E%d',startRow,endRow));

Hbar11a_Im = xlsread(TL_file,sheet,sprintf('I%d:I%d',startRow,endRow));
Hbar21a_Im = xlsread(TL_file,sheet,sprintf('J%d:J%d',startRow,endRow));
Hbar31a_Im = xlsread(TL_file,sheet,sprintf('K%d:K%d',startRow,endRow));
Hbar41a_Im = xlsread(TL_file,sheet,sprintf('L%d:L%d',startRow,endRow));

% form the complex FRF functions
Hbar11a = Hbar11a_Re + i*Hbar11a_Im;
Hbar21a = Hbar21a_Re + i*Hbar21a_Im;
Hbar31a = Hbar31a_Re + i*Hbar31a_Im;
Hbar41a = Hbar41a_Re + i*Hbar41a_Im;

% correct for mismatches arising from the mic amplitude & phase responses
H11a = Hbar11a;
H21a = Hbar21a ./ H21_correction;
H31a = Hbar31a ./ H31_correction;
```

178

```
H41a = Hbar41a ./ H41_correction;

% display message
if numLoads==1
    disp('Executing one-load method...')
end

% calculations
L1 = 3.5 * 0.0254;      %distance from ref plane to nearest upstream mic (m)
s1 = 2.0 * 0.0254;         %spacing between upstream mics (m)
L2 = (3.5 + d) * 0.0254;    %distance from ref plane to nearest downstream mic (m)
s2 = 2.0 * 0.0254;             %spacing between downstream mics (m)

c = 20.047*sqrt(273.15+T);          %speed of sound (m/s)
k = 2*pi*frequency2/c;                %wave number in air (1/m)
rho = 1.290*(P/101.325)*(273.15/(273.15+T));   %air density (kg/m^3)

Aa = 1i * ((H11a.*exp(-1i*k*L1)) - (H21a.*exp(-1i*k*(L1+s1)))) ./ (2*sin(k*s1));
Ba = 1i * ((H21a.*exp(1i*k*(L1+s1))) - (H11a.*exp(1i*k*L1))) ./ (2*sin(k*s1));
Ca = 1i * ((H31a.*exp(1i*k*(L2+s2))) - (H41a.*exp(1i*k*L2))) ./ (2*sin(k*s2));
Da = 1i * ((H41a.*exp(-1i*k*L2)) - (H31a.*exp(-1i*k*(L2+s2)))) ./ (2*sin(k*s2));

p0a = Aa + Ba;
pda = Ca.*exp(-1i*k*d) + Da.*exp(1i*k*d);
u0a = (Aa-Ba) ./ (rho*c);
uda = (Ca.*exp(-1i*k*d) - Da.*exp(1i*k*d)) ./ (rho*c);

T11 = (pda.*uda + p0a.*u0a) ./ (p0a.*uda + pda.*u0a);
T12 = (p0a.^2 - pda.^2) ./ (p0a.*uda + pda.*u0a);
T21 = (u0a.^2 - uda.^2) ./ (p0a.*uda + pda.*u0a);
T22 = (pda.*uda + p0a.*u0a) ./ (p0a.*uda + pda.*u0a);

% for SECOND load case (if applicable)...
if numLoads==2
    disp('Executing two-load method...')

    % read in additional input data
    Hbar11b_Re = xlsread(TL_file,sheet,sprintf('P%d:P%d',startRow,endRow));
    Hbar21b_Re = xlsread(TL_file,sheet,sprintf('Q%d:Q%d',startRow,endRow));
    Hbar31b_Re = xlsread(TL_file,sheet,sprintf('R%d:R%d',startRow,endRow));
    Hbar41b_Re = xlsread(TL_file,sheet,sprintf('S%d:S%d',startRow,endRow));

    Hbar11b_Im = xlsread(TL_file,sheet,sprintf('W%d:W%d',startRow,endRow));
    Hbar21b_Im = xlsread(TL_file,sheet,sprintf('X%d:X%d',startRow,endRow));
    Hbar31b_Im = xlsread(TL_file,sheet,sprintf('Y%d:Y%d',startRow,endRow));
    Hbar41b_Im = xlsread(TL_file,sheet,sprintf('Z%d:Z%d',startRow,endRow));

    % form the complex FRF functions
    Hbar11b = Hbar11b_Re + i*Hbar11b_Im;
    Hbar21b = Hbar21b_Re + i*Hbar21b_Im;
    Hbar31b = Hbar31b_Re + i*Hbar31b_Im;
```

179

```
    Hbar41b = Hbar41b_Re + i*Hbar41b_Im;

    % correct for mismatches arising from the mic amplitude & phase responses.
    H11b = Hbar11b;
    H21b = Hbar21b ./ H21_correction;
    H31b = Hbar31b ./ H31_correction;
    H41b = Hbar41b ./ H41_correction;

    % calculations
    Ab = 1i * ((H11b.*exp(-1i*k*L1)) - (H21b.*exp(-1i*k*(L1+s1)))) ./ (2*sin(k*s1));
    Bb = 1i * ((H21b.*exp(1i*k*(L1+s1))) - (H11b.*exp(1i*k*L1))) ./ (2*sin(k*s1));
    Cb = 1i * ((H31b.*exp(1i*k*(L2+s2))) - (H41b.*exp(1i*k*L2))) ./ (2*sin(k*s2));
    Db = 1i * ((H41b.*exp(-1i*k*L2)) - (H31b.*exp(-1i*k*(L2+s2)))) ./ (2*sin(k*s2));

    p0b = Ab + Bb;
    pdb = Cb.*exp(-1i*k*d) + Db.*exp(1i*k*d);
    u0b = (Ab-Bb) ./ (rho*c);
    udb = (Cb.*exp(-1i*k*d) - Db.*exp(1i*k*d)) ./ (rho*c);

    T11 = (p0a.*udb - p0b.*uda) ./ (pda.*udb - pdb.*uda);
    T12 = (p0b.*pda - p0a.*pdb) ./ (pda.*udb - pdb.*uda);
    T21 = (u0a.*udb - u0b.*uda) ./ (pda.*udb - pdb.*uda);
    T22 = (pda.*u0b - pdb.*u0a) ./ (pda.*udb - pdb.*uda);

end

% Transmission coefficient (anechoic-backed)
t = 2*exp(1i*k*d) ./ (T11 + (T12/(rho*c)) + rho*c*T21 + T22);

% Normal incidence transmission loss
TL_n = 20*log10(abs(1./t));


% Reflection coefficient (hard-backed)
R = (T11-rho*c*T21) ./ (T11+rho*c*T21);

% Absorption coefficient (hard-backed)
alpha = 1 - (abs(R)).^2;
save alpha.txt frequency2 alpha

% Propagation wavenumber in material
k_prop = (1/d) * acos(T11);

% Characteristic impedance in material
z = sqrt(T12./T21);

%Addition to write The alpha and Frequency2 data to Notepad File
filename = 'testdata.xlsx';
sheet=1;
xlswrite(filename,frequency2,sheet);
sheet=1;
```

180

```matlab
xlRange = 'B1';
xlswrite(filename,alpha,sheet,xlRange);

% plot the acoustic coefficient values
figure1 = figure;
axes1 = axes('Parent',figure1,...
    'YTickLabel',{'-0.1','0','0.2','0.4','0.6','0.8','1','1.1'},...
    'YTick',[-0.1 0 0.2 0.4 0.6 0.8 1 1.1],...
    'YGrid','on',...
    'XTickLabel',{'60','500','1000','1500','2000','2500'},...
    'XTick',[60 500 1000 1500 2000 2500],...
    'XGrid','on');
xlim(axes1,[60 2700]);
ylim(axes1,[-0.1 1.1]);
box(axes1,'on')
hold(axes1,'all')
title('Reflection, Absorption, and Transmission Coefficients');
xlabel('Frequency, Hz');
ylabel('Magnitude');
plot1 = plot(frequency2,abs(R), frequency2,alpha, frequency2,abs(t),'Parent',axes1);
set(plot1(1),'DisplayName','reflection coeff.');
set(plot1(2),'DisplayName','absorption coeff.');
set(plot1(3),'DisplayName','transmission coeff.');
legend(axes1,'show');

% plot the propagation wave number in the material
figure2 = figure;
axes2 = axes('Parent',figure2,...
    'YGrid','on',...
    'XTickLabel',{'60','500','1000','1500','2000','2500'},...
    'XTick',[60 500 1000 1500 2000 2500],...
    'XGrid','on');
xlim(axes2,[60 2700]);
%%ylim(axes2,[-0.1 1.1]);
box(axes2,'on')
hold(axes2,'all')
title('Propagation wave number in material');
xlabel('Frequency, Hz');
ylabel('Wave number, 1/m');
plot2 = plot(frequency2,abs(k_prop),'Parent',axes2);

% plot the characteristic impedance in the material
figure3 = figure;
axes3 = axes('Parent',figure3,...
    'YGrid','on',...
    'XTickLabel',{'60','500','1000','1500','2000','2500'},...
    'XTick',[60 500 1000 1500 2000 2500],...
    'XGrid','on');
xlim(axes3,[60 2700]);
%%ylim(axes3,[-0.1 1.1]);
box(axes3,'on')
```

181

```matlab
hold(axes3,'all')
title('Characteristic impedance in material');
xlabel('Frequency, Hz');
ylabel('Impedance, Rayls');
plot3 = plot(frequency2,real(z), frequency2,imag(z),'Parent',axes3);
set(plot3(1),'DisplayName','real component');
set(plot3(2),'DisplayName','imaginary component');
legend(axes3,'show');

% plot the transmission loss
figure4 = figure;
axes4 = axes('Parent',figure4,...
    'YGrid','on',...
    'XTickLabel',{'60','500','1000','1500','2000','2500'},...
    'XTick',[60 500 1000 1500 2000 2500],...
    'XGrid','on');
xlim(axes4,[60 2700]);
%%ylim(axes4,[-0.1 1.1]);
box(axes4,'on')
hold(axes4,'all')
title('Normal incidence transmission loss');
xlabel('Frequency, Hz');
ylabel('Transmission loss, dB');
plot4 = plot(frequency2,TL_n, 'Parent',axes4);

% alert user if TL test frequencies not consistent with calibration frequencies
check = isequaln(frequency,frequency2);
if check == true
    disp('Done!')
    save(TL_file);      %save the .mat file
else
    disp('ERROR: TL frequencies NOT CONSISTENT with calibration frequencies!!!)'
    delete(figure1, figure2, figure3, figure4);
end
```

182

VITA

Joseph Andrew Banks

Candidate for the Degree of

Master of Science

Thesis: HIGH-GAIN AIRBORNE MICROPHONE WINDSCREEN
CHARACTERIZATION METHOD USING MODIFIED RESEARCH WIND
TUNNEL

Major Field: Mechanical and Aerospace Engineering

Biographical:

Education:

Completed the requirements for the Master of Science in Mechanical and
Aerospace Engineering at Oklahoma State University, Stillwater, Oklahoma in
May, 2017.

Completed the requirements for the Bachelor of Science in Mechanical and
Aerospace Engineering at Oklahoma State University, Stillwater, Oklahoma in
May 2014.